

AD-A104 660

NEW MEXICO ENGINEERING RESEARCH INST ALBUQUERQUE
DESIGN OF AIRPORT PAVEMENTS FOR EXPANSIVE SOILS.(U)

F/6 8/13

JAN 81 R G McKEEN

F29601-76-C-0015

UNCLASSIFIED

NMERRI-AP-37

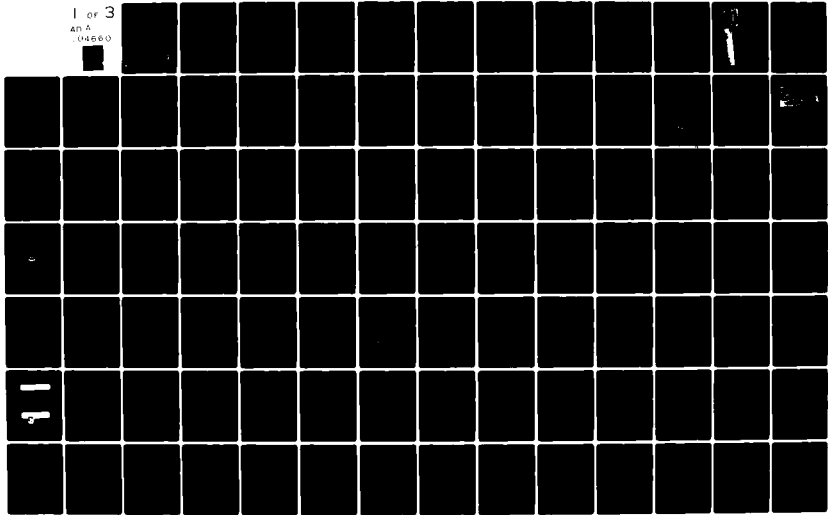
FAA/RD-A1/25

NL

1 or 3

An A

04660



7

LEVEL

12

DOT/FAA/RD-81/25

Systems Research &
Development Service
Washington, D.C. 20590

Design of Airport Pavements for Expansive Soils

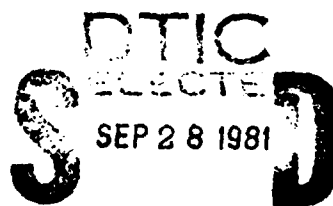
R. Gordon McKeen
New Mexico Engineering Research Institute
University of New Mexico
University Station Box 25
Albuquerque, New Mexico 87131

AD A104660

January 1981

Final Report

This document is available to the U.S. public
through the National Technical Information
Service, Springfield, Virginia 22161.



U.S. Department of Transportation
Federal Aviation Administration

81 9 28 140

DTIC FILE COPY

NOTICE

This document is disseminated under the sponsorship of
the Department of Transportation in the interest of
information exchange. The United States Government assumes
no liability for its contents or use thereof.

111

Technical Report Documentation Page

1. Report No. DOT/FAA/RD/81/25/	2. Government Accession No. AD-A104 660	3. Recipient's Catalog No. 111	
4. Title and Subtitle Design of Airport Pavements for Expansive Soils.		5. Report Date January 1981	
6. Performing Organization Code		8. Performing Organization Report No. NMERI-AP-37	
7. Author(s) R. Gordon McKeen		10. Work Unit No. (TRAIS)	
9. Performing Organization Name and Address New Mexico Engineering Research Institute University of New Mexico, Box 25 University Station, Albuquerque, New Mexico 87131		11. Contract or Grant No. F29601-76-C-0015 ✓	
12. Sponsoring Agency Name and Address US Department of Transportation Federal Aviation Administration Systems Research and Development Service Washington, DC 20590		13. Type of Report and Period Covered Final Report.	
15. Supplementary Notes		14. Sponsoring Agency Code FAA-ARD-830	
16. Abstract Expansive soil subgrades exhibit volume changes with variation in moisture condition. These changes result in differential movement of airport pavements resting on these soils. Special design procedures must be used to account for the expansive soil activity during equilibration. In addition, special precautions are required to protect the subgrade from moisture variation with climate. Measurement of soil suction is a key step in quantifying moisture-induced soil behavior. Procedures are outlined for suction characterization of the soil and for estimating the in situ differential movement likely to occur under the pavement. Once the wavelength and amplitude characteristics of the differential movement are obtained, design calculations to select the thickness and materials for the pavement may proceed.			
17. Key Words Pavement Roughness Expansive soils Thermocouple Gilgai psychrometer Soil suction Filter paper		18. Distribution Statement Document is available to the public through the National Technical Information Service, Springfield, VA, 22161	
19. Security Classif. (of this report) Unclassified	20. Security Classif. (of this page) Unclassified	21. No. of Pages 192	22. Price

111

METRIC CONVERSION FACTORS

Approximate Conversions to Metric Measures

Symbol	When You Know	Multiply by	To Find	Symbol	When You Know	Multiply by	To Find	Symbol
LENGTH								
in	feet	*2.5	centimeters	mm	in	0.04	inches	in
ft	30	centimeters	cm	in	0.4	inches	in	
yd	0.9	meters	m	in	3.3	feet	ft	
mi	1.6	kilometers	km	in	1.1	yards	yd	
AREA								
in ²	square inches	6.5	square centimeters	cm ²	in ²	0.16	square inches	in ²
ft ²	square feet	0.09	square meters	m ²	ft ²	1.2	square yards	yd ²
yd ²	square yards	0.8	square meters	m ²	yd ²	0.4	square miles	mi ²
mi ²	square miles	2.6	square kilometers	km ²	mi ²	2.5	acres	ac
MASS (weight)								
oz	ounces	28	grams	g	oz	0.035	ounces	oz
lb	pounds	0.45	kilograms	kg	lb	2.2	pounds	lb
	short tons (2000 lb)	0.9	tonnes	t		1.1	short tons	st
VOLUME								
ts	teaspoons	5	milliliters	ml	ts	0.03	fluid ounces	fl oz
Tbsp	tablespoons	15	milliliters	ml	Tbsp	2.1	pints	pt
fl oz	fluid ounces	30	milliliters	ml	fl oz	1.06	quarts	qt
c	cups	0.24	liters	l	c	0.26	gallons	gal
pt	pints	0.47	liters	l	pt	35	cubic feet	ft ³
qt	quarts	0.95	liters	l	qt	1.3	cubic meters	m ³
gal	gallons	3.8	cubic meters	m ³	gal			
ft ³	cubic feet	0.03	cubic meters	m ³	ft ³			
yd ³	cubic yards	0.76			yd ³			
TEMPERATURE (exact)								
°F	Fahrenheit temperature	5 after subtracting 32)	Celsius temperature	°C	°F	9/5 (then add 32)	Fahrenheit temperature	°F
					-40	32	32	212
					-20	40	40	200
					0	80	80	100
					40	120	120	160
					80	160	160	200
					120	200	200	240
					160	240	240	280
					200	280	280	320
					240	320	320	360
					280	360	360	400
					320	400	400	440

Approximate Conversions from Metric Measures

Symbol	When You Know	Multiply by	To Find	Symbol	When You Know	Multiply by	To Find	Symbol
LENGTH								
in	in	0.04	inches	in	in	0.4	inches	in
ft	ft	3.3	feet	ft	ft	1.1	feet	ft
yd	yd	1.1	yards	yd	yd	0.33	yards	yd
mi	mi	0.6	miles	mi	mi	0.6	miles	mi
AREA								
in ²	in ²	0.16	square inches	in ²	in ²	1.2	square inches	in ²
ft ²	ft ²	1.2	square feet	ft ²	ft ²	1.2	square yards	yd ²
yd ²	yd ²	1.2	square yards	yd ²	yd ²	1.2	square miles	mi ²
mi ²	mi ²	1.2	square miles	mi ²	mi ²	1.2	square kilometers	km ²
MASS (weight)								
oz	ounces	2.2	ounces	oz	oz	0.035	ounces	oz
lb	pounds	2.2	pounds	lb	lb	0.035	pounds	lb
	short tons	2.2	tonnes	t	t	0.035	tonnes	t
VOLUME								
ml	ml	0.03	fluid ounces	fl oz	ml	0.03	fluid ounces	fl oz
l	l	0.03	pints	pt	l	0.03	pints	pt
ml	ml	0.03	quarts	qt	ml	0.03	quarts	qt
l	l	0.03	gallons	gal	l	0.03	gallons	gal
ml	ml	0.03	cubic feet	ft ³	ml	0.03	cubic feet	ft ³
l	l	0.03	cubic meters	m ³	l	0.03	cubic meters	m ³
TEMPERATURE (exact)								
°C	Celsius temperature	9/5 (then add 32)	Fahrenheit temperature	°F	°C	9/5 (then add 32)	Fahrenheit temperature	°F
		32	32	°F		32	32	212
		40	40	°F		40	40	200
		80	80	°F		80	80	100
		120	120	°F		120	120	160
		160	160	°F		160	160	200
		200	200	°F		200	200	240
		240	240	°F		240	240	280
		280	280	°F		280	280	320
		320	320	°F		320	320	360

CONTENTS

<u>Section</u>		<u>Page</u>
I	INTRODUCTION	1
	The Problem	1
	Objectives and Scope	1
II	BACKGROUND: STATE OF THE ART	5
	Suction	5
	Soil Response to Suction Change	10
	The Gilgai Phenomenon	13
	Effects of Pavement on Soils	18
	Summary	18
III	SITES STUDIED	21
	Gallup Airport Site	22
	Jackson Airport Site	24
	Dallas/Fort Worth Airport Site	29
IV	SUCTION STUDIES	33
	Test Methods	33
	Comparison of FP and TCP Measurements	53
	Results	64
	Suction Conclusions	83
V	ELEVATION STUDIES	87
	Elevation Data Gathering	87
	Soil Surface Elevations	91
	Pavement Surface Data Analysis	101
VI	AIRCRAFT SIMULATIONS	109
	Taxi Computer Code	109
	Results of Simulations	110
VII	ANALYSIS AND CONCLUSIONS	115
	Heave Prediction	115
	Prediction of Weighted Amplitude	116
	Wavelength and Roughness	118
	Acceptability Criteria	125

CONTENTS (Continued)

<u>Section</u>	<u>Page</u>
VIII RECOMMENDATIONS	129
Indicator Test	129
Soil Characterization	129
Soil-Pavement Interaction Model	132
Expansive Soil Design Procedure	139
Limitations and Recommendations	146
REFERENCES	148
SYMBOLS AND ABBREVIATIONS	153
APPENDIX A: ELEVATION PROFILES	155
APPENDIX B: FREQUENCY DOMAIN DATA	175
APPENDIX C: CALCULATED PROFILE CHARACTERISTICS	177
APPENDIX D: AIRCRAFT DATA FOR TAXI SIMULATION	183
APPENDIX E: CLOD TEST PROCEDURE	191

Accession For	
NTIS GRA&I	<input checked="" type="checkbox"/>
DTIC TAB	<input type="checkbox"/>
Unannounced	<input type="checkbox"/>
Justification	
By	
Distribution/	
Availability Codes	
Avail and/or	
Dist	

A

LIST OF FIGURES

<u>Figure</u>		<u>Page</u>
1-1	Pavement surface distorted by soil behavior	2
1-2	Recommended design procedure	3
2-1	Schematic diagrams and properties of clay minerals	6
2-2	Water content-free energy relationships	9
2-3	Consolidation data	11
2-4	Load-suction-volume surface for swelling soils	14
2-5	Stages of genesis of normal gilgai	15
2-6	Gilgai structure in undisturbed soils	17
3-1	Thornthwaite data for Gallup airport	25
3-2	Thornthwaite data for Jackson airport	28
3-3	Thornthwaite data for Dallas/Fort Worth	31
4-1	A Peltier thermocouple psychrometer	34
4-2	Typical thermocouple psychrometer output, high range	40
4-3	Typical thermocouple psychrometer output, low range	41
4-4	Calibration variation with cooling period	42
4-5	Calibration variation with ambient temperature	43
4-6	Filter paper calibration relationships	51
4-7	Hydraulic tensiometer configuration	54
4-8	Laboratory comparison - same sample	55
4-9	Laboratory comparison - WES study	56
4-10	Illustration of TCP equilibration time	58
4-11	Filter paper and thermocouple psychrometer profiles at DFW	60
4-12	Shelby tube samples with sand seams	61
4-13	Field-laboratory data comparison	63
4-14	TCP suction profiles for GAL	65
4-15	TCP suction profiles for DFW	66
4-16	TCP suction profiles for JSN	66
4-17	Comparison of TCP and FP suction profiles at DFW	68
4-18	Variation of suction during recharge at DFW	69
4-19	Comparison of TCP and FP suction profiles at GAL	70
4-20	Comparison of TCP and FP suction profiles at JSN	72

LIST OF FIGURES (Continued)

<u>Figure</u>		<u>Page</u>
4-21	Results of suction measurements on boring samples at JSN	73
4-22	Moisture suction data for DFW	74
4-23	Moisture suction data for GAL	75
4-24	Moisture suction data for JSN	76
4-25	Suction compressibility from COLE tests	79
4-26	Suction compressibility from clod tests	81
4-27	Chart for suction compressibility prediction	83
5-1	Dallas/Fort Worth Regional Airport site layout	88
5-2	Gallup Municipal Airport site layout	89
5-3	Jackson Municipal Airport site layout	90
5-4	Elevations on soil surface at GAL	92
5-5	Elevations on soil surface at DFW	93
5-6	Elevations on soil surface at JSN	94
5-7	Range of elevation changes at DFW and GAL	95
5-8	Evidence of soil differential response at GAL	96
5-9	Correlation of elevation and suction changes	98
5-10	Soil subsidence as a result of wetting	99
5-11	Crack subsidence problem	100
5-12	Illustration of Fourier transformation of a profile	104
7-1	Characterization of soil behavior for pavement design	117
7-2	Depth-wavelength relationships at DFW, NAS, GAL	124
7-3	Depth-wavelength relationships at JSN	124
7-4	Acceptability of pavements for the B727-200 and B727-100	127
7-5	Acceptability of pavements for the DC-9-40 and the TriJet Composite	128
8-1	Estimation of soil wavelength	131
8-2	Prediction of \bar{A} from γ_h and its variation	133
8-3	Beam on deformed elastic foundation problem	134
8-4	Solution to pavement model equation	138
8-5	Revised design procedure	140

LIST OF TABLES

<u>Table</u>		<u>Page</u>
2-1	Gilgai characteristics	16
3-1	Gallup boring logs	23
3-2	Jackson boring logs	26
3-3	Dallas/Fort Worth boring logs	30
4-1	Regression models	44
4-2	Instrumentation at GAL	46
4-3	Instrumentation at DFW	47
4-4	Instrumentation at JSN	48
4-5	Effects of sample variation and equilibrium time	57
4-6	Region mineralogical composition	82
5-1	Rough pavements surveyed	87
5-2	Cracking characteristics compared	101
5-3	Velasco's independent variables	107
5-4	Additional profile characteristics	108
6-1	Results of aircraft simulations	111
7-1	Amplitude-wavelength for soil surfaces	119
7-2	Amplitude-wavelength for DFW pavements	120
7-3	Amplitude-wavelength for JSN and GAL	121
7-4	Amplitude-wavelength for rough pavements	122
7-5	Pavement effective depth	123
8-1	Results of soil characterization	143
8-2	Results of interaction study	144
8-3	Alternative pavement designs for JSN	146

1. INTRODUCTION

THE PROBLEM

Pavement surfaces for runways, taxiways, and aprons of modern airports play an important part in the overall performance of the facility. Pavement design, construction, and maintenance are important in providing acceptable surfaces at reasonable overall cost. Experience has shown that pavements on expansive soils often require rehabilitation at an early stage of pavement life.

Expansive soils are clayey soils which exhibit significant volume changes as a result of soil moisture variations. Problems with airport pavements are caused by this kind of volume change in the underlying soil. These changes produce unacceptable differential movements in the pavement surface, causing surface roughness and cracking. An example of a pavement surface distorted by expansive soil behavior is shown in Figure 1-1. The pavement shown is capable of supporting the load it was designed to carry. However, as an aircraft travels across the surface, the roughness excites the airplane, inducing unacceptable vertical accelerations in the aircraft. When these accelerations reach a certain level, pilots are unable to safely negotiate the aircraft on the pavement, passengers are uncomfortable, and damage to the aircraft or cargo may occur.

The behavior of expansive soils influences the performance of pavement structures founded on these soils. Therefore, understanding the properties that make a soil expansive or not expansive aids in evaluating specific soils for pavement design. The objectives of pavement design are to incorporate methods in the construction process that prevent or reduce the effects of soil volume changes.

OBJECTIVES AND SCOPE

The Systems Research and Development Service of the Federal Aviation Administration initiated a study of expansive soils in 1975. In Phase I of the study, the New Mexico Engineering Research Institute (NMERI) used the technical literature to update airport pavement design procedures. The proposed design method which resulted from the literature review is shown in Figure 1-2. NMERI began a program to develop this method in February 1977.

FIGURE 1-1. PAVEMENT SURFACE DISTORTED BY SOIL BEHAVIOR.



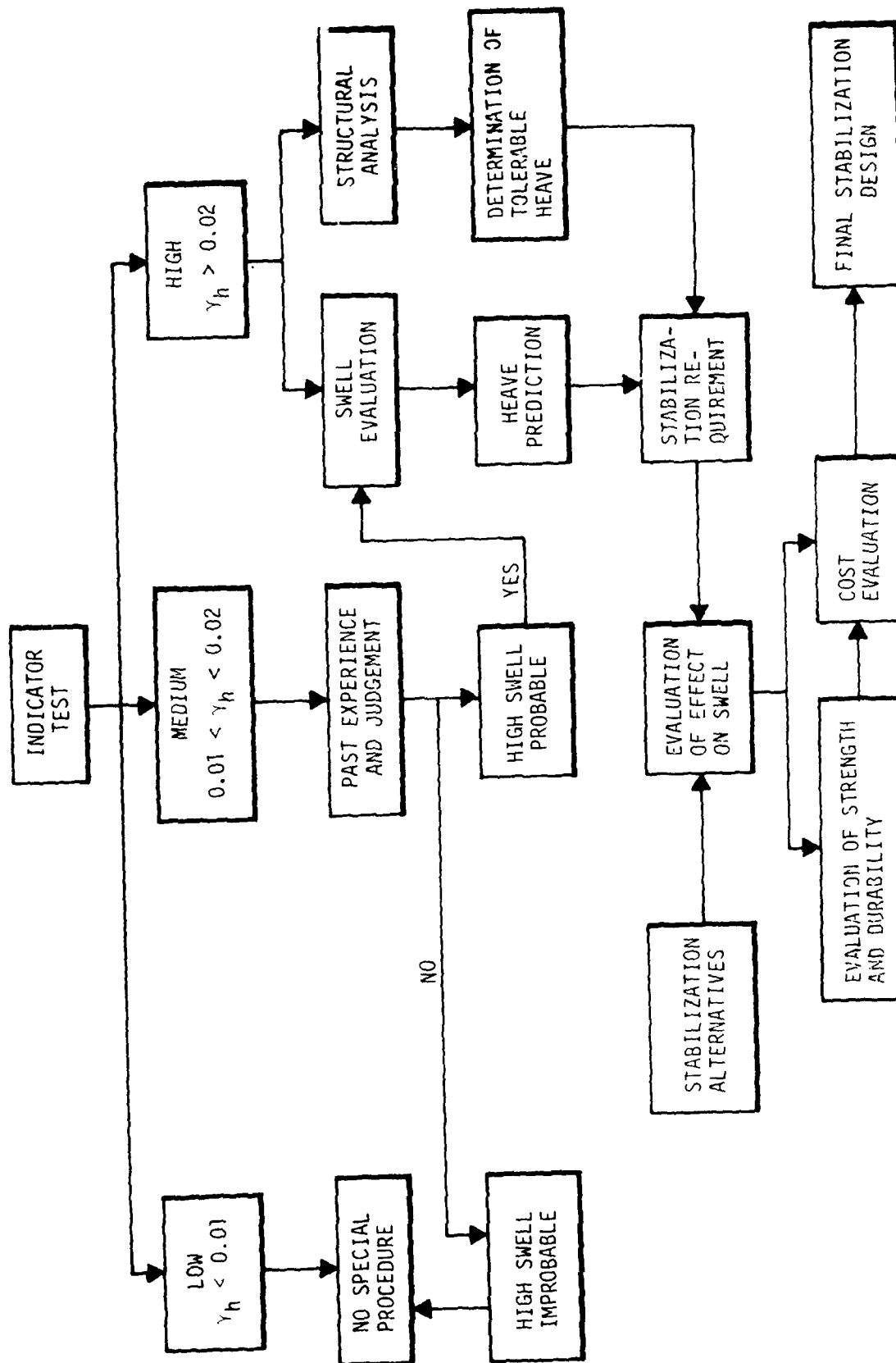


FIGURE 1-2. RECOMMENDED DESIGN PROCEDURE.

Phase II was a laboratory study of soil characterization methods. Phase III was a field study of airport pavement and in situ soil behavior at three sites with distinctly different climates. Phase IV consisted of analysis and design recommendations. The results of Phases I and II are reported in McKeen (1976) and McKeen and Nielsen (1978). Phase III and Phase IV are the subject of this report.

McKeen, R. G., (1976) *Design and Construction of Airport Pavements on Expansive Soils*, FAA-RD-76-66, Federal Aviation Administration, Washington, DC.

McKeen, R. G. and Nielsen, J. P., (1978) *Characterizing Expansive Soils for Airport Pavement Design*, FAA-RD-78-59, Federal Aviation Administration, Washington, DC.

II. BACKGROUND: STATE OF THE ART

During the past twenty years significant research efforts around the world have been devoted to the study of expansive soil interaction with structures. Costly structures and equipment are damaged by expansive soil behavior, and the standard methods in soil mechanics are not capable of describing the phenomena adequately for proper design. The results of much of this research have been available in the technical literature for several years. It remains to apply these evolving theories to practical problems and present design methods that are implementable.

SUCTION

Expansive soils cause problems beneath structures because they change volume. The soils may swell with great force, lifting a structure, or shrink away from it, removing support altogether. Only two causes of these volume changes are involved in most problems: changes in load and changes in moisture condition. The response of soils to loads has been a part of soil mechanics since its beginning. In contrast, the volume changes accompanying variation in moisture condition have only recently been studied. Soil volume changes caused by moisture variation are the predominant factor involved in pavement design on expansive soils.

The potential of a soil to undergo volume change because of moisture variation is determined by the type of clay contained in the soil and the amount present. Soils that do not contain clay (particles less than $0.002 \mu\text{m}$ in size) do not exhibit expansive soil behavior. In addition, the type of clay minerals in the soil is important. In engineering work, three groups of clay minerals are identified. In descending order of volumetric activity, these are the smectite, illite, and kaolinite groups. These minerals are composed of layers of silica tetrahedra and gibbsite stacked in various configurations (Figure 2-1). Naturally occurring soils are invariably composed of mixtures of these groups plus other, less common, varieties.

Volume changes of these minerals result from adsorbed water layers attached to the clay mineral surfaces. Water molecules are dipolar and are attracted to the surfaces by unbalanced negative charges. The imbalance is

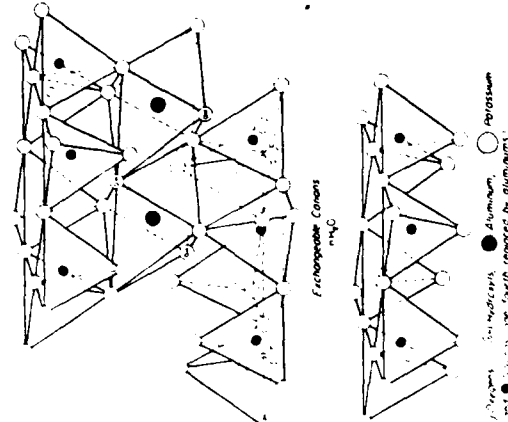
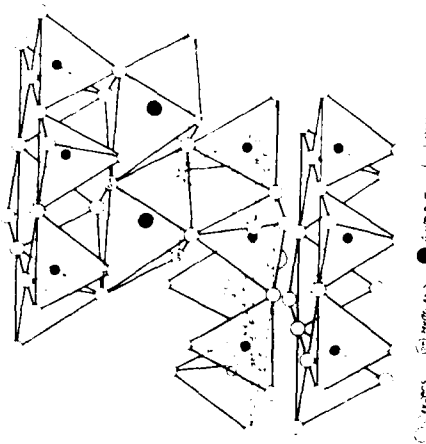
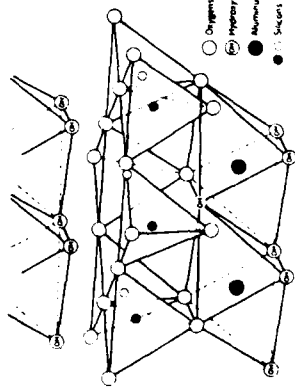
SCHEMATIC STRUCTURE OF CLAY MINERALS		SMECTITE	ILLITE	KAOLINITE
				
PARTICLE THICKNESS		0.003 to 0.1 μm	$> 9.5 \text{ \AA}$	0.5 to 2 μm
SPECIFIC SURFACE, m^2/g^2		65 to 180	50 to 840	10 to 20
CATION EXCHANGE CAPACITY, MILLEQUIVALENTS/100 g		3 to 15	10 to 40	80 to 150

FIGURE 2-1. SCHEMATIC DIAGRAMS AND PROPERTIES OF CLAY MINERALS.

created by isomorphous substitution of metallic ions in the clay mineral lattice systems. Large surface areas and charge densities require large quantities of water to satisfy the imbalance. As large amounts of water are adsorbed, the clay platelets are forced apart, occupying a larger volume.

Soil moisture suction is defined as a macroscopic property of the soil which indicates the intensity with which a soil will attract water. Suction is normally defined as a negative gage pressure (energy : volume = units of force per unit area), but it should not be confused with pore water pressure. Pore water pressure is normally associated with the density of a liquid, distance from a free water surface, and surface tension forces. Suction results from (a) the interplay of attraction and repulsion forces of charged clay particles and polar water molecules, (b) surface tension forces of water, (c) solution potentials caused by dissolved ions, and (d) gravity potential. The representation of suction, the sum of all these forces, as an equivalent height of water has been called the *capillary model*. This model was controversial until 1960 when substantial agreement was reached on its validity (Aitchison, 1961).

In engineering problems, soil moisture suction is considered to be composed of matrix suction and osmotic (or solute) suction. Matrix suction is the negative pressure which will hold soil water in equilibrium through a porous membrane with the same soil water within a sample of the soil. Matrix suction results from surface adsorption and capillary forces. Osmotic or solute suction is a negative gage pressure which will hold pure water in equilibrium with soil water through a membrane which allows only water molecules to pass. Osmotic suction results from variation in ion concentration in the pore fluid. Matrix suction is directly influenced by mechanical loads and water content whereas osmotic suction is not.

Two independent stress variables have been used to describe the state of stress in unsaturated soils. The preferable stress state variables are $(\sigma - U_a)$ and $(U_a - U_w)$ where σ = total stress, U_a = pore air pressure, and U_w = pore water pressure. The term $(\sigma - U_a)$ is called the *total stress term*, and $(U_a - U_w)$ is called the *matrix suction term*. This combination of stress

Aitchison, G. D., (1961) "Relationships of Moisture Stress and Effective Stress Functions in Unsaturated Soils," in *Pore Pressure and Suction in Soils*, Butterworths, London.

state variables is most satisfactory because the effects of environmental variables can be readily separated in terms of stress changes. This approach assumes that U_a is approximately atmospheric and that the osmotic component of suction remains constant. These assumptions are adequate for many engineering problems.

The logarithmic unit pF is used to measure suction in the present paper, along with units of pressure in kPa. pF is defined as

$$pF = \log_{10} (\text{pressure in cm of water}) \quad (2-1)$$

Figure 2-2 illustrates the suction phenomenon. The vertical axis represents suction (free energy) of the water. Also on the vertical axis is a scale representing molecular layers of adsorbed water, taken from Michurin and Lytayev (1967). An explicit relationship between water layers and suction is indicated. Data for several materials were used to illustrate that all porous hygroscopic materials exhibit similar adsorption of water. Curves for portland cement concrete (McKeen, 1969), lumber (ASCE, 1975), filter paper (McQueen and Miller, 1977), clay minerals, and real soils are illustrated. For practical use, these relationships may be represented as linear. Note the influence of the surface areas indicated in Figure 2-2 for the clays and soils.

The range shown in Figure 2-2 is the adsorbed water range (2.5 to 6.25 pF). Below 2.5 pF, additional large quantities of water are held in the capillary range. Above 6.25 pF, water molecules intimately associated with crystalline structures of minerals are mobilized. The volume changes of interest in studying pavement behavior on expansive soils occur in the range of adsorbed water from 2.5 to 5.5 pF (McKeen and Nielsen, 1978).

ASCE, (1975) *Wood Structures, A Design Guide and Commentary*, Structural Division, 1975.

McKeen, R. G., (1969) "Shrinkage-Cracking Characteristics of Structural Light-weight Concrete," Thesis, Texas A & M University, College Station, Texas.

McQueen, I. S., and Miller, R. F., (1977) "The Wide-Range (Filter Paper) Method for Measuring the Forces of Moisture Retention," personal correspondence.

Michurin, B. N., and Lytayev, I. A., (1967) "Relationship between Moisture Content, Moisture Tension, and Specific Surface Area in Soil," *Soviet Soil Science*, Vol. 8, pp. 1093-1103.

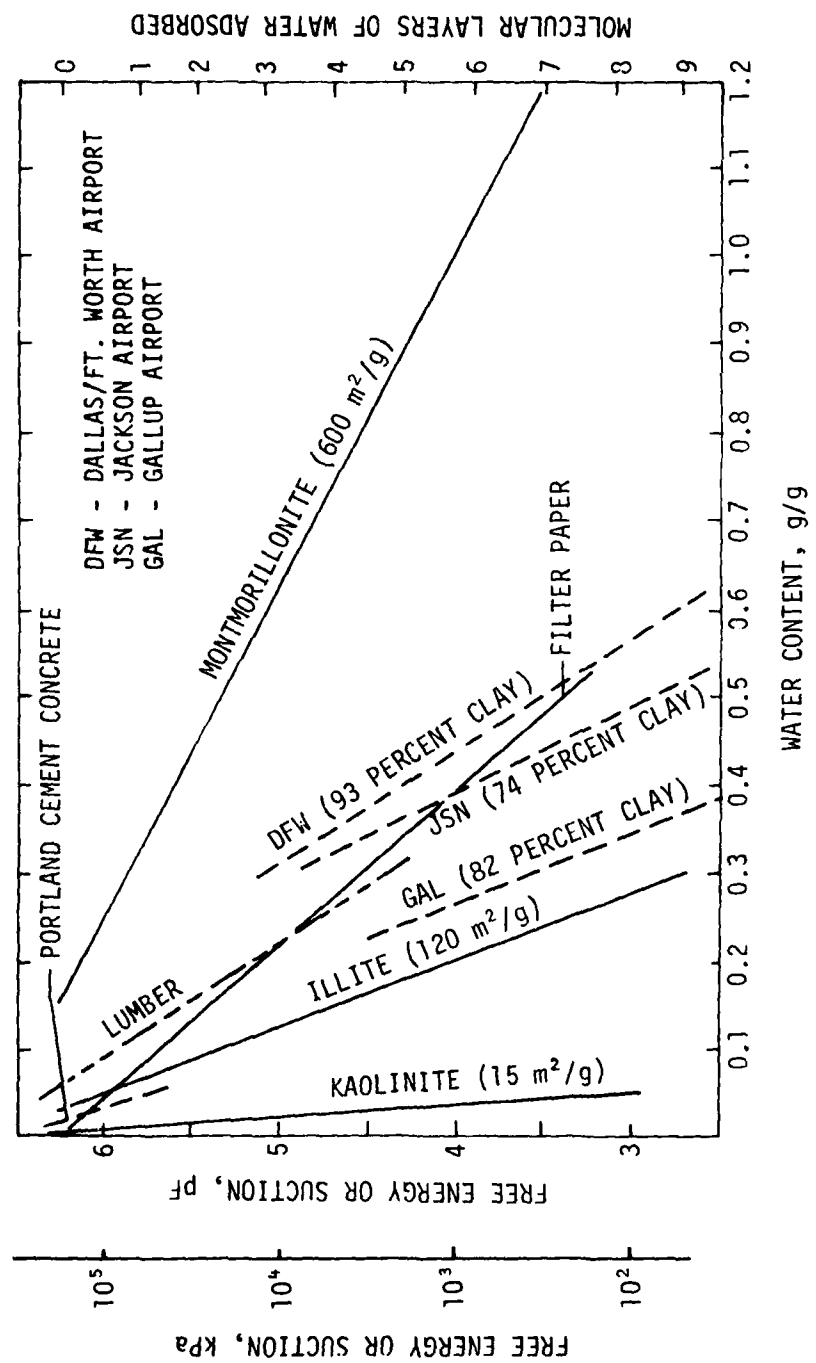


FIGURE 2-2. WATER CONTENT-FREE ENERGY RELATIONSHIPS.

SOIL RESPONSE TO SUCTION CHANGE

The response of soil volume to suction changes may be studied in much the same manner as soil consolidation in response to applied load changes (Aitchison and Woodburn, 1969; McKeen and Nielsen, 1978; Escario, 1969; Lytton, 1977; Compton, 1970; Fredlund and Morgenstern, 1977). However, some basic differences must be recognized. Figure 2-3 shows consolidation data for tests on a sample of expansive soil. Curve A is the result of a conventional one-dimensional consolidation test. Curve B is the result of a hydrostatic consolidation test. Curve C represents consolidation resulting from suction induced by drying samples to various moisture conditions. In all cases the stresses are effective stresses. The effective stresses for the suction curve were computed using an equation presented by Aitchison (1961):

$$\sigma'' = \frac{1}{100} (S + p'') + \sum_0^{\infty} 0.3p'' \cdot \Delta S \quad (2-2)$$

σ'' = effective stress component caused by p''

S = degree of saturation

$\Delta S = 100 - S$

p'' = pressure deficiency, kg/cm²

An important difference between suction (Curve C) and the conventional test (Curve A) is that suction changes are not one-dimensional. The suction forces on a soil element are body forces rather than externally applied forces

Aitchison, G. D., and Woodburn, J. A., (1969) "Soil Suction in Foundation Design," *Proceedings*, 7th International Conference on Soil Mechanics and Foundation Engineering, Mexico City, Vol. 21, pp.1-8.

Compton, Phil V., (1970) *A Study of the Swelling Behavior of an Expansive Clay as Influenced by the Clay Microstructure, Soil Suction, and External Loading*, AFWL-TR-70-26, Air Force Weapons Laboratory, Kirtland Air Force Base, New Mexico.

Escario, Ventura, (1969) "Swelling of Soils in Contact with Water at a Negative Pressure," *Proceedings*, 2nd International Research and Engineering Conference on Expansive Clay Soils, College Station, Texas, pp. 207-217.

Fredlund, D. G., and Morgenstern, N. R., (1977) "Stress State Variables for Unsaturated Soils," *Journal of the Geotechnical Engineering Division*, ASCE, Vol. 103, No. GT5, pp. 447-466.

Lytton, R. L., (1977) "The Characterization of Expansive Soils in Engineering," presentation at the Symposium on Water Movement and Equilibrium in Swelling Soils, American Geophysical Union, San Francisco, California. (unpublished)

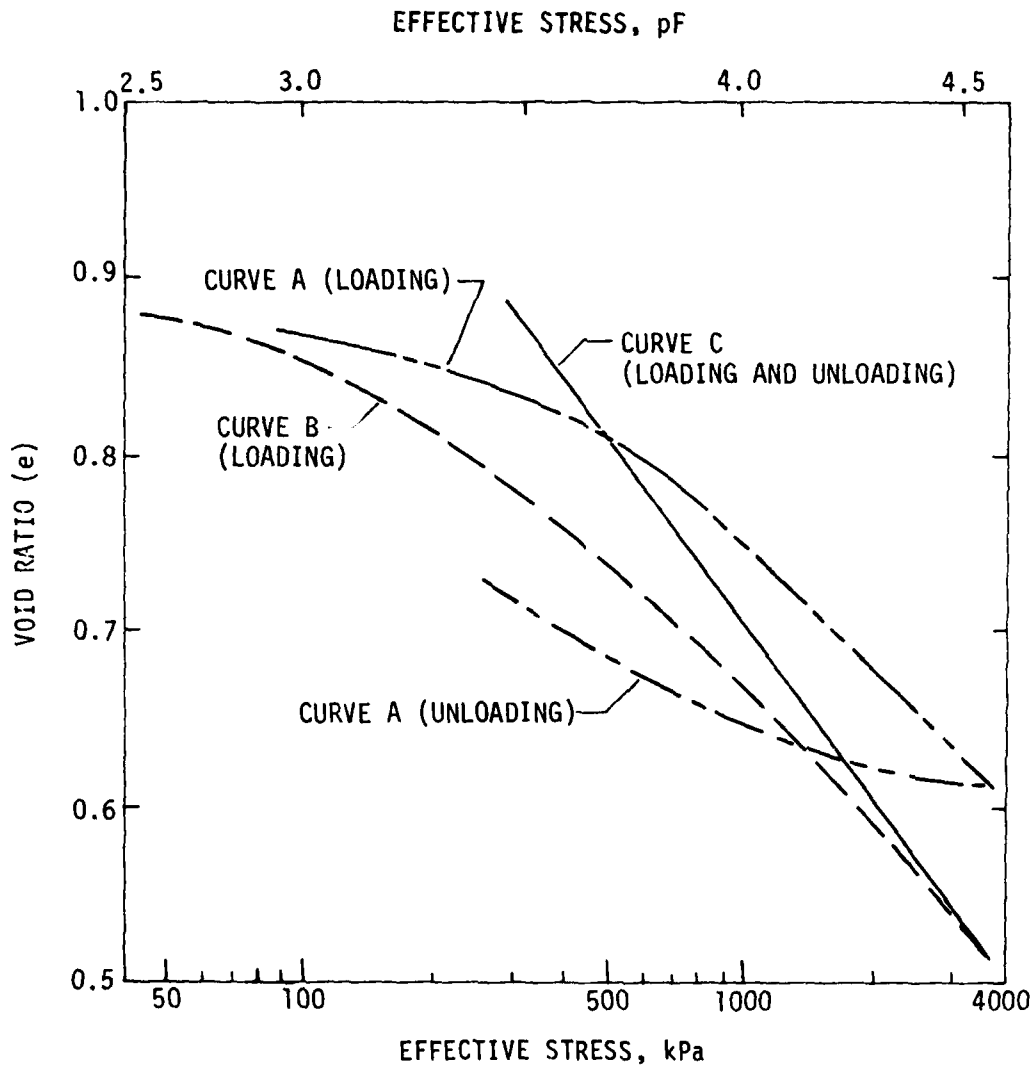


FIGURE 2-3. CONSOLIDATION DATA.

at the surface of the element. Suction forces yield a single curve for a soil, regardless of whether it is wetting or drying. When the effective stress is reduced, the relieved body forces remold the soil. In the case of applied loads at the surface, this remolding does not occur; therefore the rebound curves from mechanical loading are different from the loading curves.

Because suction stresses are largely effective stresses applied directly to the soil skeleton as body forces, volume change studies may be made using total suction values. In practical engineering problems, it is the slope of the volume change versus suction curve that quantifies soil response to moisture changes. Thus the suction compression index, γ_h , is defined as the slope of the volume-total suction curve (Lytton, 1977). No constraint on the manner in which the volume change is determined is specified here. The importance of this aspect is discussed later.

$$\gamma_h = \frac{\Delta V/V_i}{\log_{10} \frac{h_f}{h_i}} \quad (2-3)$$

where

γ_h = suction compression index

$\Delta V/V_i$ = change of volume with respect to initial volume

h_f, h_i = final and initial total suction, arithmetic units

Values of γ_h may be determined by several testing methods. A measured volume change and suction change are required, and these data must cover the range of moisture suction applicable to the problem under study. The volume measurement may be made in a conventional oedometer which constrains the sample to one-dimensional volume change. Another test, the COLE (coefficient of linear extensibility) test, measures unrestrained three-dimensional volume change (McKeen and Nielsen, 1978). Natural soils will experience lateral restraint conditions that vary between the two conditions represented in these tests. A dry, cracked clay soil profile will approach the COLE condition; an uncracked clay will approach the fully restrained condition. The selection of a proper γ_h value requires some knowledge of the lateral restraint experienced by the soil.

Another factor to consider in arriving at γ_h values is the effect of applied loads in reducing the soil swell. The compression index for load changes is determined as follows (Lytton, 1977):

$$\gamma_{\sigma} = \frac{\Delta V/V_i}{\log \frac{\sigma_f}{\sigma_i}} \quad (2-4)$$

where

γ_{σ} = total stress compression index

$\Delta V/V_i$ = change of volume with respect to initial volume

σ_f , σ_i = final and initial total stress

The two compression indexes, γ_h and γ_{σ} , may be combined into an incremental volume strain equation for the soil (Lytton et al, 1976; McKeen and Nielsen, 1978):

$$\frac{\Delta V}{V} = -\gamma_h \frac{\Delta h}{h_i} = -\gamma_{\sigma} \frac{\Delta \sigma}{\sigma_i} \quad (2-5)$$

Evaluation of these expressions reveals the surface, describing soil behavior in response to load and suction changes. This surface is illustrated in Figure 2-4.

THE GILGAI PHENOMENON

A natural clay soil left to interact with climatic forces will develop an irregular surface microrelief pattern. As illustrated in Figure 2-5 (from Spotts, 1974), the pattern develops in seven stages. First, sedimentary clay is deposited. Following deposition, drying occurs, producing surface shrinkage cracks. Further desiccation results in the formation of major cracks penetrating far into the clay. The extent of penetration and spacing are determined

Lytton, R. L., Boggess, R. L., and Spotts, J. W., (1976) "Characteristics of Expansive Clay Roughness of Pavements," *Swelling Soils*, Transportation Research Record No. 568, Washington, DC, pp. 9-23.

Spotts, J. W., (1974) "The Role of Water in Gilgai Formation," Dissertation, Texas A & M University, College Station, Texas.

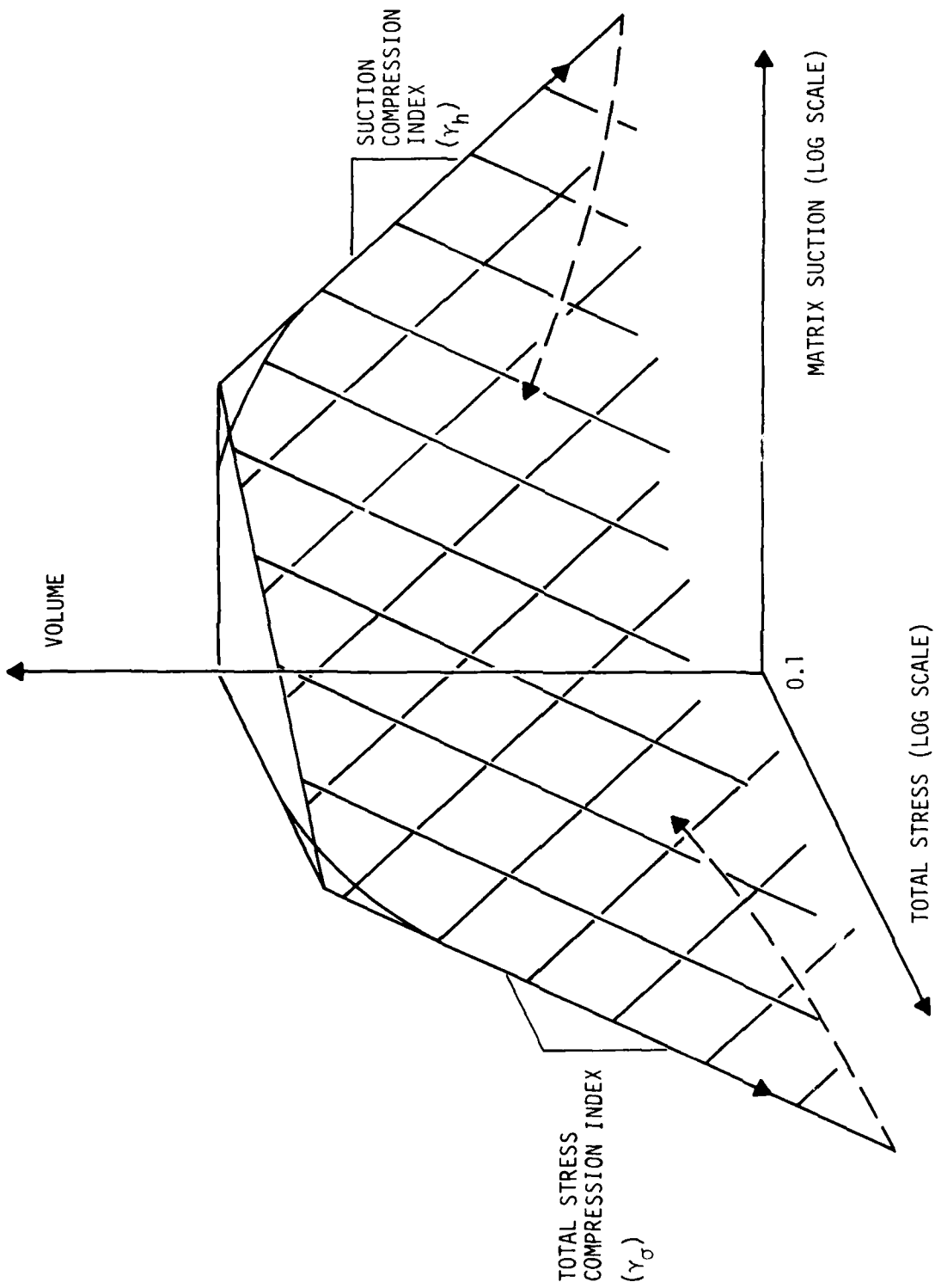
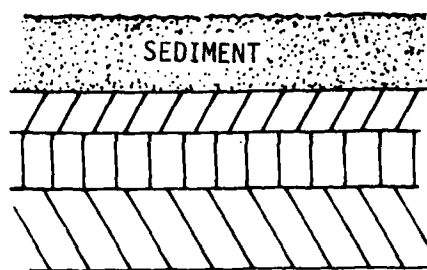
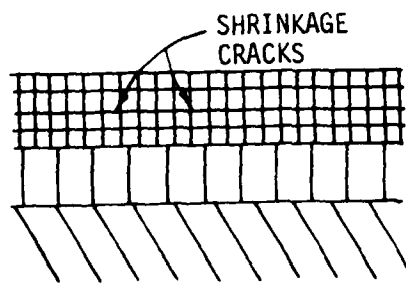


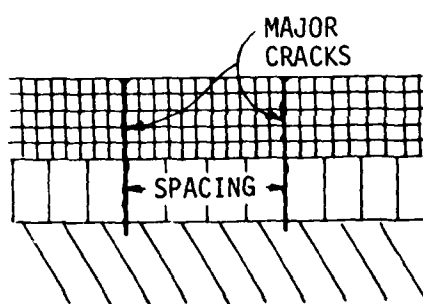
FIGURE 2-4. LOAD-SUCTION-VOLUME SURFACE FOR SWELLING SOILS.



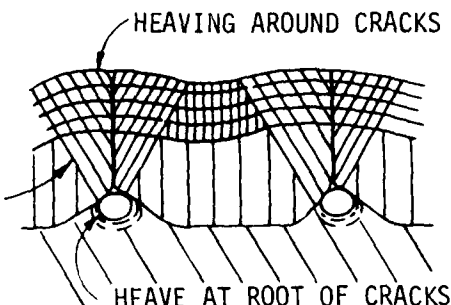
STAGE 1. DEPOSITION



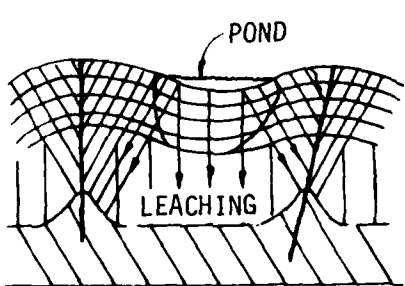
STAGE 2. DRYING



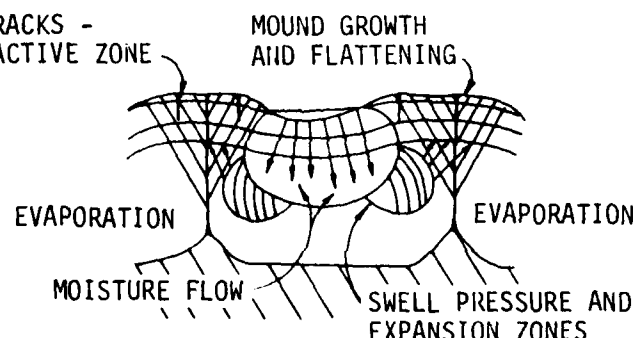
STAGE 3. MAJOR SHRINKAGE CRACKS FORM



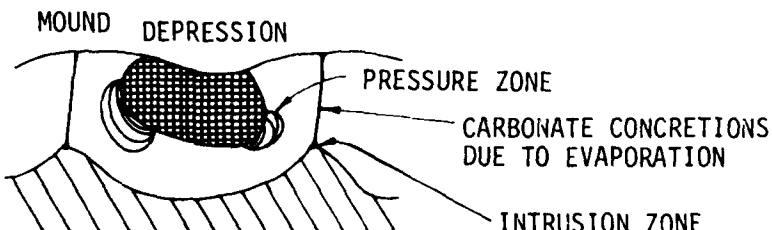
STAGE 4. HEAVE AROUND MAJOR CRACKS



STAGE 5. INFILTRATION AND LEACHING



STAGE 6. PRESSURE ZONES FORM EVAPORATION



STAGE 7. MATURE GILGAI PROFILE

FIGURE 2-5. STAGES OF GENESIS OF NORMAL GILGAI. (FROM SPOTTS, 1974)

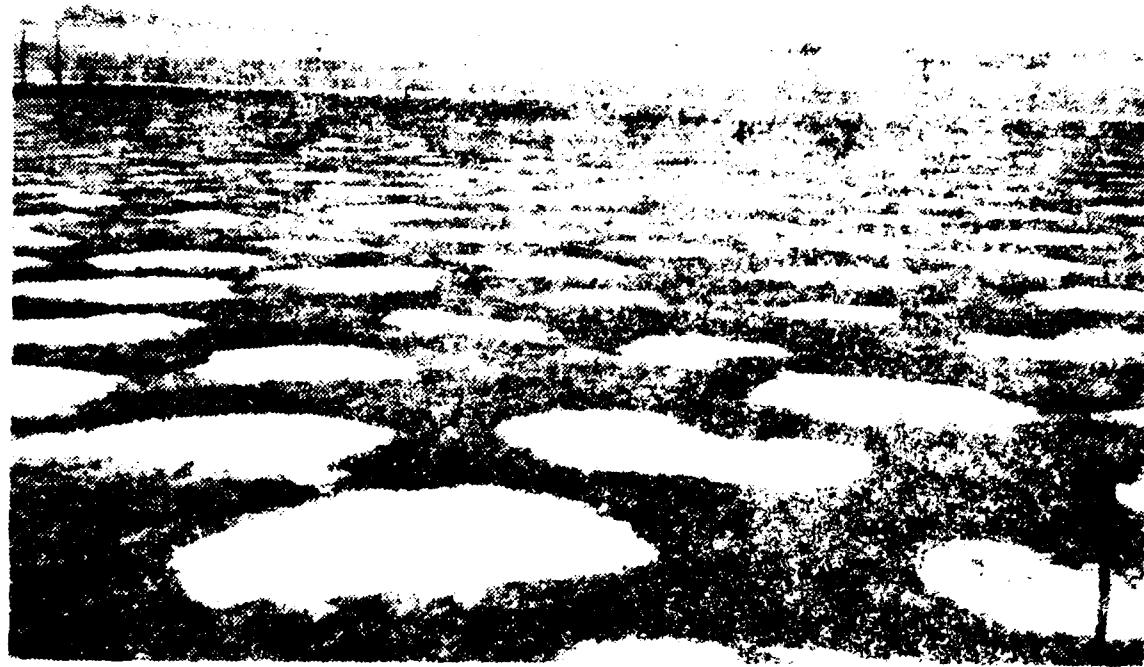
by a number of factors of which the degree and rate of drying and the clay type are the most significant. Subsequent development of microrelief occurs as the clay is wetted and dried by cyclic variation of the climate. Because water penetrates deeper at the major cracks, greater swell occurs. As the next cycle of drying proceeds, the higher areas dry first, causing the major cracks to reappear in approximately the same locations. Thus, over a period of several years, an undulating surface pattern called *gilgai* develops on the soil surface. Characteristics of some gilgai surfaces found in the United States are shown in Table 2-1.

TABLE 2-1. GILGAI CHARACTERISTICS

Soil - Location	Dominant wavelengths, m (ft)	Maximum amplitude, m (ft)
Burleson-Texas	4.5 (15) to 9.0 (30)	0.12 (0.4)
Houston Black-Texas	4.0 (13) to 9.0 (30)	0.16 (0.5)
Puerco-New Mexico	1.5 (5)	0.60 (2.0)
Denhawk-Texas	4.5 (15) to 9.0 (30)	0.46 (1.5)

The gilgai structure extends through the depth of soil that interacts with the climate, the *active zone* of the soil profile. Gilgai structural development begins when the soil is deposited. The depth of actual gilgai occurrence depends on the most extreme climate in the soil history and may not represent current active zone depth. Also, because of successive deposition cycles, some gilgai may be buried beneath more recent deposits (O'Neill and Ghazzaly, 1977). Gilgai structure in soil profiles causes soil response to environmental change to vary depending on position within the structure. The variation is produced by soil leaching, deposition of dissolved salts by evaporating water, development of internal drainage paths, and infiltration of surface material via cracks. Gilgai structure is most evident where soil surfaces are left undisturbed for long periods of time (Figure 2-6). Thus, an expansive soil profile will respond differentially from point to point when subjected to an environmental change.

O'Neill, Michael W., and Ghazzaly, Osman I., (1977) "Swell Potential Related to Building Performance," *Journal of the Geotechnical Engineering Division*, ASCE, Vol. 103, No. GT 12, pp. 1363-1379.



EFFECTS OF PAVEMENT ON SOILS

When an airport pavement is constructed on an expansive clay soil, the environment to which the soil is exposed changes dramatically. The pavement structure serves as a barrier to moisture exchange with the atmosphere. This barrier usually causes the active zone soil to exchange moisture with the soil beneath it until an equilibrium condition is approached. The ability of moisture to move through a soil profile via fissures, seams, and so on, may interrupt the equilibration process or prevent it entirely. If an area contains numerous routes for water movement in the soil, a large area may heave, altering the pavement profile by displacing sections of pavement. Examples of this alteration are given in the elevation profiles in Appendix A. Once the soil attains an equilibrium condition beneath the pavement, the edges will still be subjected to seasonal variations.

The initial equilibration of the soil may produce differential vertical movement in the pavement profile. Additional disturbance of the equilibrated soil will occur if cracks, joints, or other pavement surface characteristics permit infiltration of surface water into the subgrade. Usually this kind of distress is localized about a specific moisture source. Both initial equilibration and subsequent infiltration involve suction changes, and both result in unacceptable profile characteristics. These two mechanisms are the major cause of difficulties in the maintenance of airport pavements on expansive soils.

A significant factor contributing to pavement profile deterioration is the pavement response to aircraft loads. The loads produce permanent deformation in the subgrade which accumulates with repetition. In addition, any differential support beneath the pavement structure caused by differential movement in the soil will be enhanced by the aircraft loads. Thus the two processes of pavement deterioration complement one another.

SUMMARY

The problem at hand is to develop design methods to prevent the rapid development of excessively rough surfaces on airport pavements built on expansive clays. The roughness exhibited by such pavements is the result of normal soil behavior in response to the conditions imposed by pavement construction.

Once the pavement imposes a change in the environment, considerable time may be required to reestablish moisture equilibrium in the soil. The literature in this field indicates that soil characterization using suction is the best approach to understanding equilibrium.

Three mechanisms may cause distress when airport pavements are founded on expansive soils. First, normal soil equilibration with the boundary conditions imposed by pavement construction may produce differential surface movement. Second, soil beneath pavement edges swells and shrinks in response to normal climate cycling. This behavior is strongly affected by shoulder and drainage design. Third, the infiltration routes through the pavement (e.g., cracks and joints) result in localized heave near the point of infiltration. The first two mechanisms are considered design problems while the third is primarily a maintenance problem.

III. SITES STUDIED

Three sites were selected for the Phase III field study portion of this investigation: Gallup Municipal Airport, New Mexico; Dallas/Fort Worth Regional Airport, Texas; and Jackson Municipal Airport, Mississippi. The bases of the selections were (1) previous expansive soil problems in the area, (2) existing pavement structures, and (3) variation in climate types among the three sites. The following paragraphs briefly describe the geology, climate, and soil properties of the three sites.

Geological information was extracted from the literature. Soil properties were determined from reports written during the construction of pavements at the airports and from borings made at the sites. Specific references are given in the discussion of the sites. Borings were made to a depth of 6 m (20 ft) at each site. Most of the data discussed here were taken from one borehole at each site. Samples taken from the boreholes were subjected to standard engineering tests in the laboratory. Properties investigated were clay content (C), liquid limit (LL), plasticity index (PI), and water content (w).

The climate for each site is categorized using a procedure developed by Thornthwaite (1948). The climate cycle is described by balancing the rainfall (R), potential evapotranspiration (PE), and soil water holding capacity (HC). In this method the cycle is divided into periods as follows:

- Depletion (DP) $PE > R$, soil drying
- Deficit (DF) $PE > R$, soil moisture depleted
- Recharge (RC) $PE < R$, soil wetting
- Surplus (S) $PE < R$, water drains away

The Thornthwaite Index (TI) is derived as follows:

$$TI = \frac{100S - 60DF}{PE}$$

The TI provides an indication of PE and R balance on an annual basis. Negative values indicate dry climates, and positive values mean wetter climates.

Thornthwaite, C. W., (1948) "An Approach Toward a Rational Classification of Climate," *Geographical Review*, Vol. 38, No. 1, pp. 54-94.

GALLUP AIRPORT SITE

The Gallup airport site (GAL) is located in the city of Gallup, New Mexico, in the northwestern part of the state. The surface soil consists of a lacustrine deposit of recent origin. The clay layer is estimated to be approximately 91 m (300 ft) thick. Very little information is available on the specific deposit on which the airport is constructed. However, the material is derived by erosion from Mancos Shale in the surrounding area. An in-progress study of Mancos-derived soils over a four-state area has yielded some information applicable to the site (Potter et al, 1979):

As a result of its formation in a marine environment, the Mancos has a high content of sodium and sulfate. The influence of variable amounts of organic matter and calcium carbonate affect the weathering pattern of exposed shale and the physical and chemical make-up of shale-derived soils. Mancos soils have a high clay content, generally including a high percentage of expandable clays. The soils swell on wetting and often exhibit poor water penetration. High concentrations of sodium in the crystal lattice exaggerate this condition.

The X-ray studies of clays from shale samples show that the typical mineralogy consists of small amounts of kaolinite and illite, and larger amounts of interstratified illite-smectite, the smectite composed principally of montmorillonite. Except for a few localities near igneous intrusions, the interstratified species is approximately 50% illite [I]--50% smectic [S]. The range observed is 60I - 40S to 40I - 60S, with majority near 50 - 50.

The main modification to the materials at the Gallup site has been the leaching associated with erosion and lacustrine deposition. A boring log is shown in Table 3-1 along with information from other investigations. Initial suction tests reveal a very uniform profile, indicating that the moisture is in equilibrium.

The present runway and taxiway pavements were constructed of 229 mm (9 in) of compacted subgrade, 152 mm (6 in) of lime-stabilized subgrade, 229 mm (9 in) of cement-treated base, prime coat, and 51 mm (2 in) of bituminous surface course; critical areas had a 76-mm (3-in) surface course and a 279-mm (11-in) base. The cement-treated base consists of pulverized reclaimed

Potter, Loren D., Reynolds, Robert C., and Louderbough, Ellen T., (1979)
Properties of Shale Soils and their Effects on Plant Communities, Final Report, U.S. Forest Service, Contract No. 16-729-GR, University of New Mexico, February 1979.

TABLE 3-1. GALLUP BORING LOGS.

Depth, m (ft)	Construction testing	NMERI Boring No. 1	Laboratory test data			
			C	LL	PI	W
0			28	49	23	21
(2)	Red-brown clay very stiff to hard	Surface contains sand and fine gravel	81	95	58	18
1			75	51	35	
(4)			82			
(5)						
2		Red-brown clay, dry, very uniform	85			
3						
(10)						
4			87			
(15)						
5			53			
6			72			
(20)			75	79	49	23

C = clay content
 LL = liquid limit
 PI = plasticity index
 W = water content

asphaltic pavement, red dog (a local burned clay), old base materials, and approximately 4 percent cement. The pavements were repaired in 1972 with deep patching and an overlay of 114 mm (4.5 in) of dense-graded bituminous surface. An open-graded porous friction course (PFC) was then placed. Shoulders were constructed on both the runway and taxiway. The shoulders were 3 m (10 ft) wide and consisted of 127 mm (5 in) of crusher fines and a double surface treatment with cover aggregate.

Weather at the site is dry with cold winters. The precipitation and potential evapotranspiration are shown in Figure 3-1a. Note the absence of surplus at anytime during the year. A large moisture deficit is apparent during the summer months. These factors combine to produce very dry soil conditions. The actual weather during the experiment, shown in Figure 3-1b, included an extremely wet winter followed by normal weather.

JACKSON AIRPORT SITE

The Jackson airport site (JSN) is located southeast of the city of Jackson, Mississippi. Within the airport boundaries, surface soils consist of weathered Yazoo clay and alluvium. Boring logs for this test program (NMERI Nos. 1 and 2) and a log of a nearby boring made during construction of the airport are shown in Table 3-2.

Baughman described the Yazoo clay as follows (Baughman, 1971):

The unweathered Yazoo clay is a more or less homogeneous unit of blue-green, blue-gray, and gray calcareous clay with occasional pyrite, many thin soft fossils and fossiliferous zones, foraminifera, occasionally slightly sandy and usually limy near the base. Some thin beds of soft marly limestone are often present in the upper portion of the formation.

Yazoo clay is greenish yellow-tan. On the surface it is usually blocky and crumbly when dry with much black staining which is due to the presence of manganese. Calcareous nodules on weathered surfaces of the clay are common in some areas. Pyrite is not found in weathered Yazoo. Gypsum is present in the weathered zone in the form of selenite crystals. These crystals are a weathering phenomenon and do not appear below the weathered zone, which is normally 27 to 31 feet.

Baughman, Wilbur T., (1971) "Rankin County Geology and Mineral Resources," *Mississippi Geological, Economic, and Topographic Survey*, Jackson, Mississippi.

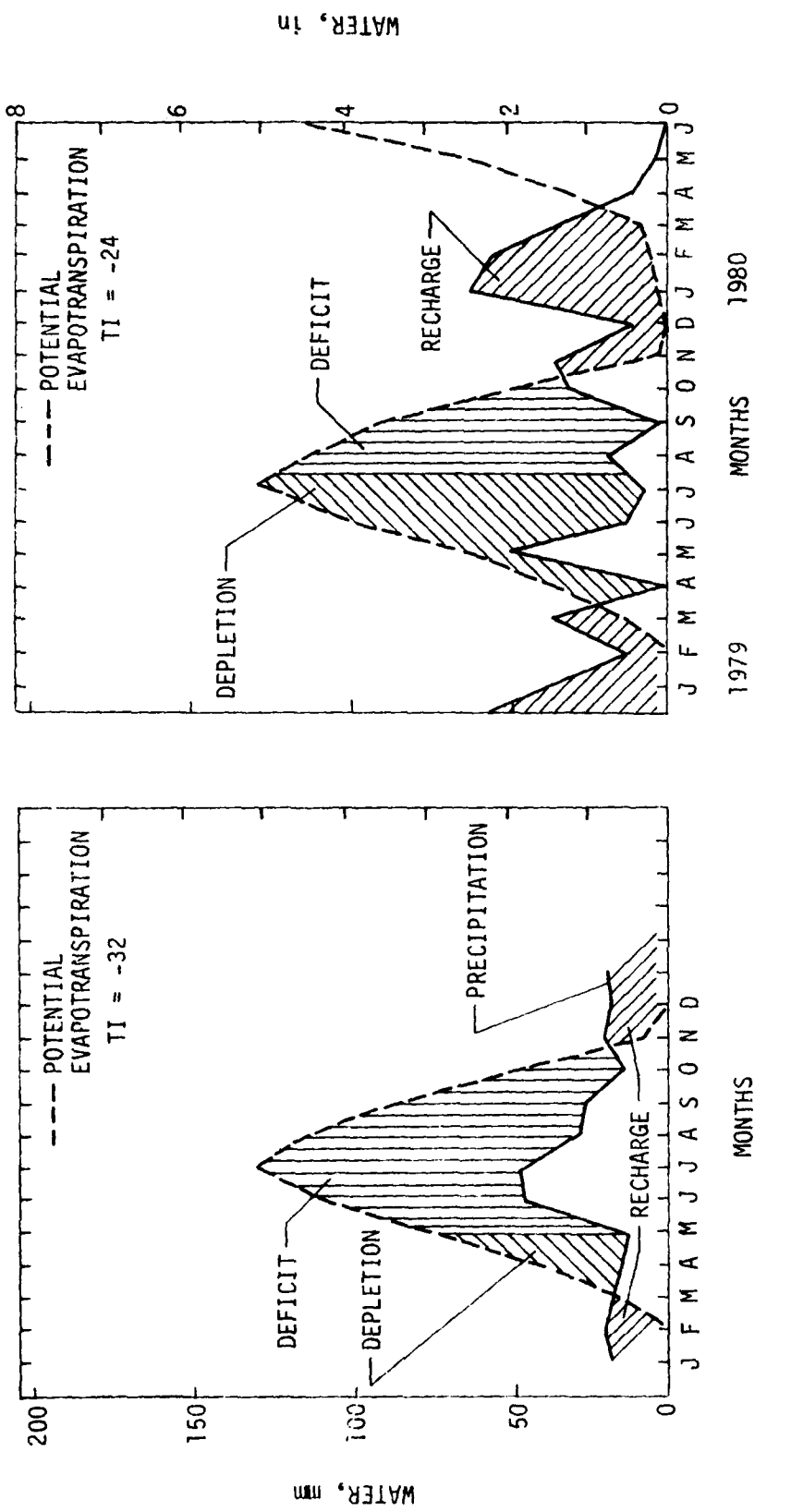


FIGURE 3-1. THORNTONLAITE DATA FOR GALLUP.

a. NORMAL WEATHER CYCLE.

b. ACTUAL WEATHER CYCLE.

TABLE 3-2. JACKSON BORING LOGS

Depth, m (ft)	Construction testing	NMERI Borings No. 1 and 2	Laboratory test data			
			C	LL	PI	W
0	Pavement, base, and fill	Gray silty clay (alluvium fill)				
1			20	36	14	26
(5)	Stiff brown and gray silty clay (weathered Yazoo)	Very stiff gray and tan clay (weathered Yazoo)	40	64	42	25
2						
3	Stiff tan and gray (weathered Yazoo)	Tan and light gray clay (weathered Yazoo)				
(10)			55	76	47	28
4						
(15)		Light gray and tan clay with oxidized seams (weathered Yazoo)	72	114	77	39
5						
6						
(20)						

C = clay content

LL = liquid limit

PI = plasticity index

w = water content

The Yazoo clay varies from approximately 340 to 460 feet thick in Rankin County. The average thickness of the Yazoo in Rankin County is approximately 375 feet.

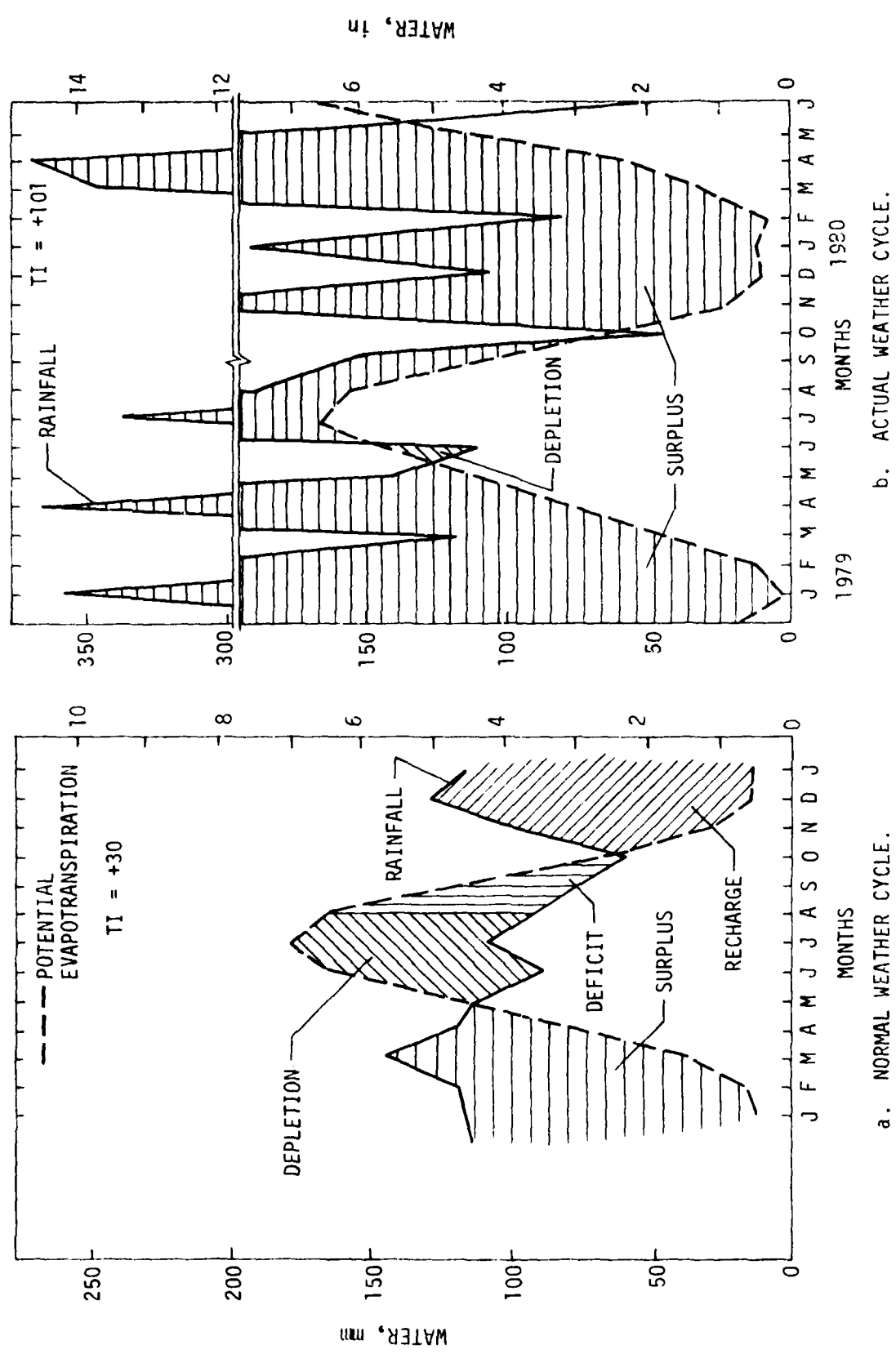
Further information is provided from the results of a Mississippi Highway Department study (Teng et al, 1972). Findings significant to the present work were as follows:

1. Mineralogical analysis: smectite, 65 percent; kaolinite, 20 percent; mica, 10 percent; quartz, 5 percent.
2. Horizontal and vertical particle orientations are not significantly different.
3. Because of small seams of sand in the clay, no moisture change occurs as a result of capillary rise. The only mechanism by which moisture changes occur is surface runoff.
4. The field coefficient of permeability is extremely low for remolded Yazoo clay.
5. The most severe pavement maintenance problem is the occurrence of fissures caused by desiccation and their subsequent filling with water.

The present pavement at the Jackson airport consists of varying amounts of medium-dense clayey, fine sand fill, generally ranging from 203 to 381 mm (8 to 15 in) thick. The fill is overlain by 152 mm (6 in) of cement-treated base, and 229 to 356 mm (9 to 14 in) of portland cement concrete pavement. The east runway and east parallel taxiway have been overlaid with varying amounts of asphaltic concrete, 152 to 203 mm (6 to 8 in) thick in most areas. A considerable amount of distress has been produced in the pavement by swelling soil behavior.

Figure 3-2a illustrates a normal weather cycle for the Jackson airport site. The dry hot summers and wet winters which normally occur in Jackson are the factors producing a large swing in soil moisture conditions. However, because of an unusually wet cycle, as shown in Figure 3-2b, the soil was saturated (surplus condition) throughout the field experiment.

Teng, T. C. Paul, Mattox, Robert M., and Clisby, M. Barrett, (1972) *A Study of Active Clays in Relation to Highway Design*, Final Report, MSHD-RD-72-045, Vol. 1 and Vol. 2, Mississippi State Highway Department, Jackson, Mississippi.



DALLAS/FORT WORTH AIRPORT SITE

The Dallas/Fort Worth airport site (DFW) is located between the cities of Dallas and Fort Worth, Texas. The site is in the Gulf Coastal Plain physiographic province. Formations outcropping on the airport are the Woodbine and Eagleford. All work in the present study involved soils derived from the Upper Cretaceous Eagleford Formation. The Eagleford Formation has been subdivided into a number of members at various locations. At the study site, the parent material has weathered to a heavy black clay at the surface [0 to 1.2 m (4 ft)]. Below this material is a tan gray, fissured, heavy clay containing numerous seams filled with sand. Typical logs of borings are shown in Table 3-3. X-ray diffraction testing indicates that the clays are dominantly montmorillonite with smaller amounts of illite and kaolinite. The area is widely known for problems encountered in construction and performance of engineering structures on these soils.

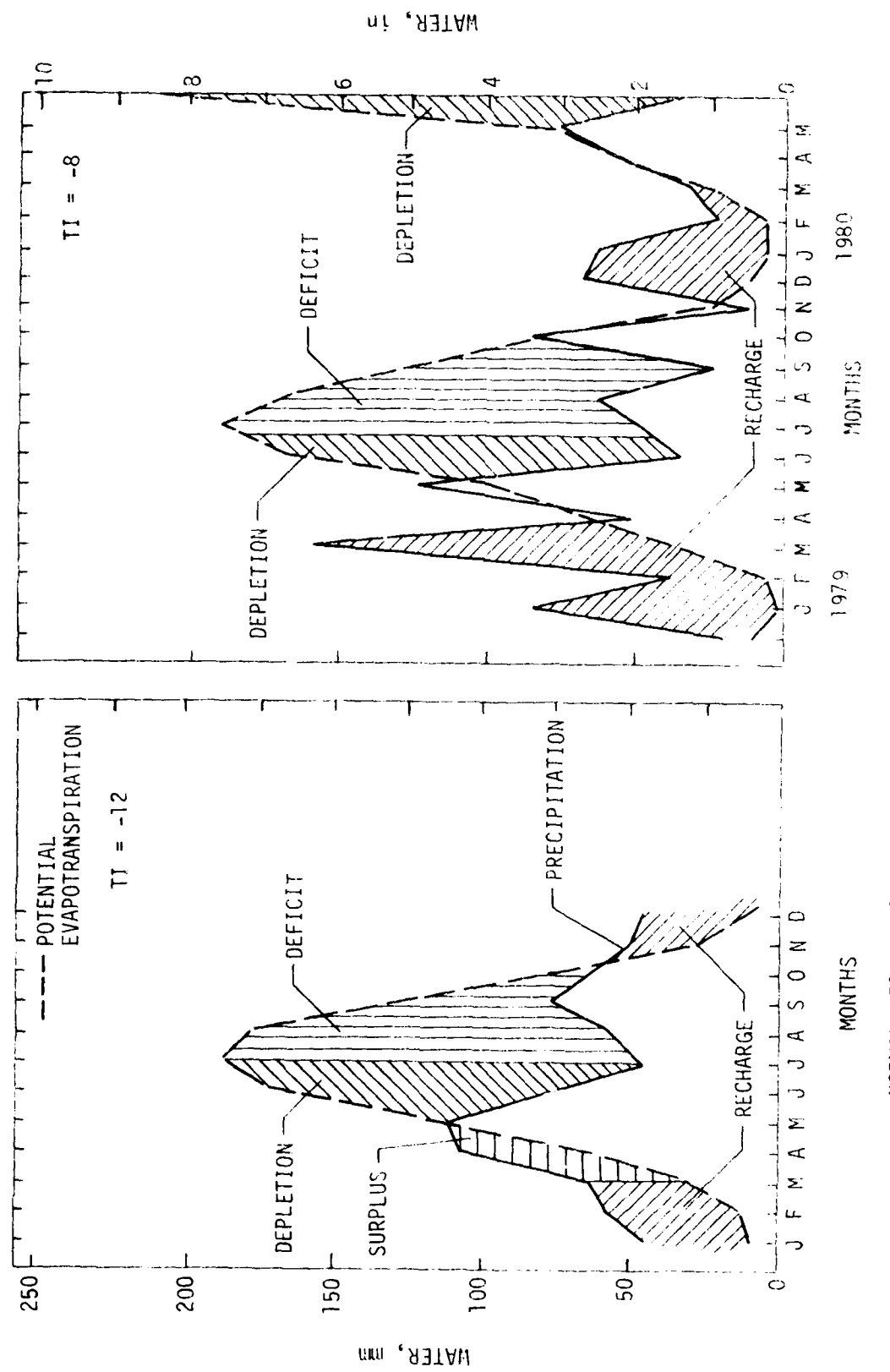
The present pavement at the DFW Regional Airport was constructed in the early 1970's after substantial testing of materials and test sections and a great amount of analysis and study. The taxiway section studied in the present work consisted of 229 mm (9 in) of lime-stabilized subgrade, 229 mm (9 in) of cement-treated base, and 381 mm (15 in) of portland cement concrete pavement. The lime-stabilized subgrade was constructed using 6 to 7 percent lime. The subgrade was covered with about 1.8 L/m² (0.4 gal/yd²) of asphalt emulsion to form a seal. The sealed subgrade was then left undisturbed for at least 75 days, permitting equilibrium of the soil moisture conditions. As of the present report, the pavements have performed well and exhibit no distress.

The normal weather cycle for the DFW Regional Airport is shown in Figure 3-3a. The cycle shows both deficit and surplus areas, indicating that the normal climatic cycle will produce large variations in the soil moisture condition. Departures from the normal cycle will result in prolonged deficit or surplus conditions. Figure 3-3b, the actual weather during the investigation, reveals a nearly normal weather cycle for the DFW site during the field experiment.

TABLE 3-3. DALLAS/FORT WORTH BORING LOGS

Depth, m (ft)	Airmail Facility Boring TB3 (Nov 71)		NMERI Boring No. 4 (Oct 78)				
			C	LL	PI	W	
0	Fill						
1	Dark brown clay		Heavy dark brown clay	56	70	44	20
(5)	Tan brown clay			55	76	50	28
2				67	73	46	25
3			Weathered shale tan and light gray with sand seams				
(10)							
4	Light tan and gray clay with sand seams and bentonite seams			64	68	43	28
5							
6							
(20)							
7							
(30)	Dark blue shale (weathered)						
8							
9	Dark blue shale						
(40)							

C = clay content
 LL = liquid limit
 PI = plasticity index
 W = water content



a. NORMAL WEATHER CYCLE.

FIGURE 3-3. THORNTWTAITE DATA FOR DALLAS/FORT WORTH.

IV. SUCTION STUDIES

The present state of the art (Lyton, 1977; Fredlund and Morgenstern, 1977; Aitchison and Woodburn, 1969; Fredlund et al, 1980) for characterizing expansive soils shows that volume changes result directly from changes in applied load and changes in suction. Soil response to suction changes is the volume change of interest in problems with pavements on expansive soils. The following paragraphs describe the methods used in studying suction, some results of laboratory and field measurements, and the soil properties obtained with suction-based testing.

TEST METHODS

Thermocouple Psychrometers

The idea of inferring suction values from thermocouple psychrometer (TCP) measurements of relative humidity was introduced by Spanner (1951). Numerous researchers have worked toward the improvement of equipment and procedures for use of suction in various research fields. Through the expenditure of a great effort primarily at the U.S. Salinity Laboratory (Riverside, California), Utah State University, and the U.S. Forest Service (Logan, Utah), many variables have been studied. The diversity of applications has ranged from studies of plant growth to irrigation, forest hydrology, soil mechanical behavior, and dust emissions from roadways. Much can be learned from the wealth of documented studies involving these instruments. The intention here is to familiarize the reader with the instrument and some of the precautions necessary for proper usage.

Principles involved--A psychrometer (Figure 4-1) is defined as two similar thermometers with the bulb of one being kept wet so that the cooling that results from evaporation makes it register a lower temperature than the dry one; the difference between the readings represents a measure of the dryness of the atmosphere.

Fredlund, D. G., Hasan, J. U., and Filson, H. L., (1980) "The Prediction of Total Heave," *Proceedings, 4th International Conference on Expansive Soils*, Vol. 1, ASCE, pp. 1-17.

Spanner, D. C., (1951) "The Peltier Effect and Its Use in the Measurement of Suction Pressure," *Journal of Experimental Botany*, Vol. 11, pp. 145-168.

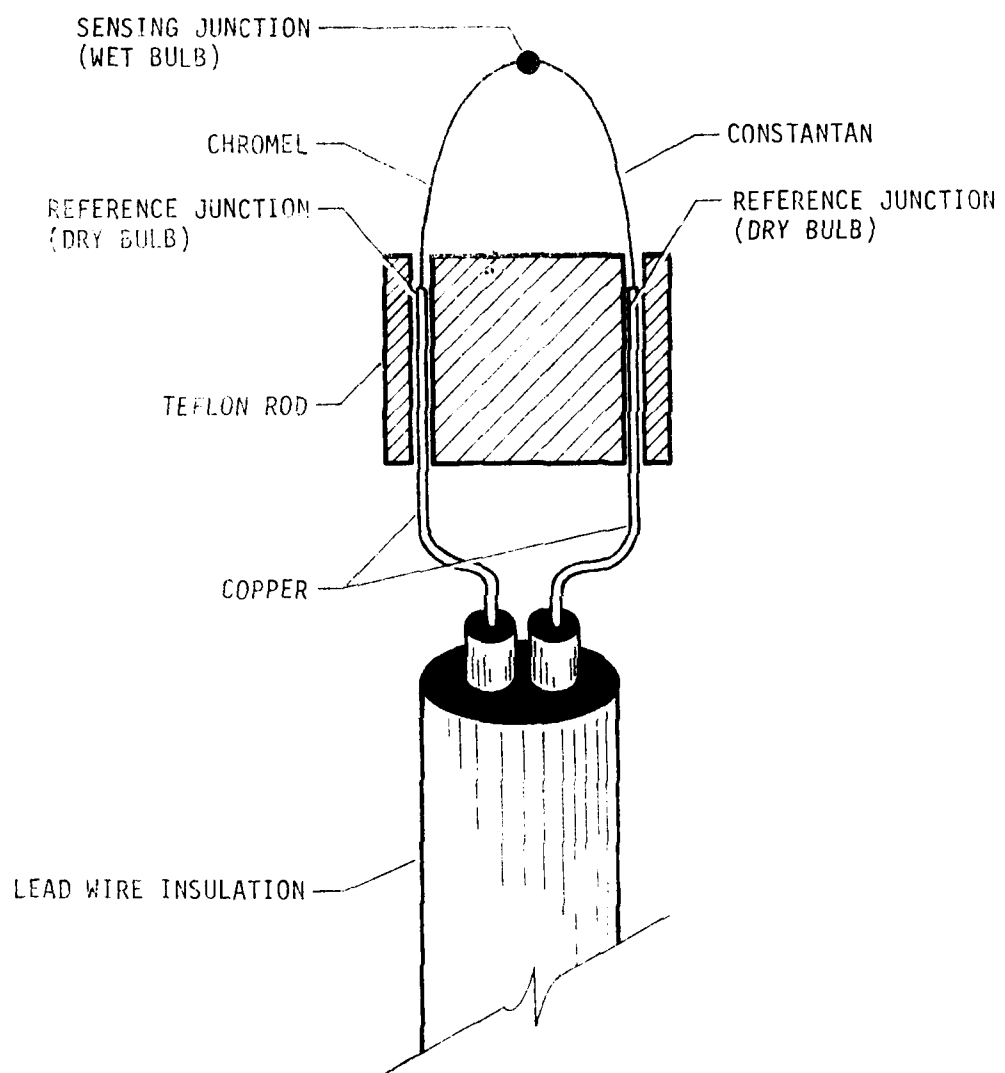


FIGURE 4-1. A PELTIER THERMOCOUPLE PSYCHROMETER.

The difference between the two readings is called the *wet bulb depression*. For a known wet bulb depression and dry bulb temperature, the ratio of the water vapor pressure in the air to that of pure free water at the same temperature and pressure can be computed. This ratio is the relative humidity.

Psychrometers have been used for many years in studying the environment. One essential feature of conventional instruments is that the psychrometer is ventilated in order to yield valid measurements. Traditionally the ventilation rate was a critical factor involved in psychrometry. Spanner (1951) demonstrated that, by reducing the size of the wet bulb, the psychrometer could be used in static air.

Once the ventilation requirement is waived, a procedure for measuring wet bulb depression is necessary. Spanner employed two principles of thermoelectricity, the Peltier effect and the Seebeck effect. The Seebeck effect states that a current will flow around a loop of two dissimilar metals if the two junctions are kept at different temperatures. The Peltier effect states that, if a small current is passed through a thermocouple sensing junction (wet bulb) in the proper direction, cooling of the junction occurs; and an exactly equal amount of heating occurs at the reference junction (dry bulb). Once the temperature of the sensing junction drops below the dew point of the atmosphere to which it is exposed, water will condense on the junction. The maximum attainable cooling is theoretically about 1.8°C (Verbrugge, 1974). At this point, the temperature of the sensing junction has been dropped, and the temperature of the reference junction has been raised. In order to use the technique, Spanner constructed massive heat sinks at the reference junction. The design was intended to reduce the temperature change at the reference junction to 10^{-3} to 10^{-4}°C . In this way the reference junction could be assumed not to change and to be equal to the temperature of the water bath in which the entire apparatus was immersed. Thus, the dry bulb temperature is known.

When the cooling current is stopped, water condensed on the sensing junction begins to evaporate, maintaining a lower temperature at the sensing junction than at the reference junction. The wet bulb depression maintained is,

Verbrugge, J. C., (1974) "Contribution A La Mesure De La Suction Et De La Pression Interstitielle Dans Les Sols Non Satures," Brussels Free University, School of Applied Sciences, Jacques Verdeyen Laboratory. (USACCRREL, Draft Translation No. 529).

as in conventional psychrometers, a function of the relative humidity. As long as this temperature difference exists, an electromotive force (emf) is produced between the leads, in accordance with the Seebeck effect. Thus, the sensor output is a function of wet bulb depression at the sensing junction with respect to the reference junction. The thermocouple output resulting from the Seebeck effect reflects the temperature difference between the sensing and reference junctions regardless of the cause, e.g., evaporative cooling, initial temperature difference, heating caused by the Peltier current. Determining the cause of the temperature difference is a major problem in using the sensors for studying water potential in soil systems.

The relationship between the wet bulb depression and the water vapor pressure in the air is affected by a number of factors. In the theoretical treatment presented by Rawlins (1966) these include

1. Radii of wet junction, equilibration chamber, and thermocouple wire
2. Thermal conductivities of wire and air
3. Diffusivity of water vapor in air
4. Latent heat of vaporization of water
5. Saturation specific humidity
6. Temperature

Most researchers have been more concerned with the emf output as a function of water potential than with the wet bulb depression; therefore the Peltier and Seebeck coefficients of the metals involved must enter into the relationships. Although the theoretical treatments have provided insights into the response of the instrument to various design factors, they are of minor interest in applications. The complexities are overcome through calibration with salt solutions of known water potential. However, the use of calibration does not eliminate all pitfalls in the use of TCP.

Present usage--A variety of instruments are presently being used for studies involving TCPs. These are of two types generally. One (Spanner, 1951) depends on Peltier cooling to condense a water droplet on the wet junction;

Rawlins, S. L., (1966) "Theory for Thermocouple Psychrometers Used to Measure Water Potential in Soil and Plant Samples," *Agricultural Meteorology*, Vol. 3, pp. 293-310.

the other (Richards and Ogata, 1958) requires manual placement of a water drop on the wet junction. The Peltier cooled instrument was best suited for the present study because the other cannot be used for field measurements.

Several varieties of the Peltier instrument exist. In some cases, additional terminals are installed in the measuring chamber to provide a means of temperature compensation or to avoid heating at the reference junction when the Peltier current is flowing. These types may mask errors that result from temperature gradients. Another type has a single sensing junction enclosed in a protective chamber. An additional temperature-sensing thermocouple is provided as well. This instrument was selected for the present work as the best compromise of capability and simplicity. Therefore, this variety, shown in Figure 4-1, is the TCP discussed in this paper.

The TCP may be operated in either a psychrometric or hygrometric mode. In both modes, a drop of water is condensed on a sensing junction by passing a cooling current through it. The hygrometric mode uses an electric circuit to cool the junction periodically by pulses in the proper direction. The length of the cooling period is adjusted according to the TCP output. By entering a gain in the system (obtained by calibration), the circuit can maintain the drop of water and thus measure the emf resulting from keeping the wet junction at the dew point. Although this instrument has been used in field environments, it was not suitable for the present study because of very little experience in field applications.

In the psychrometric mode the sensing junction is cooled by passing a current through it in the proper direction. Once the cooling is finished, the current is stopped, and the emf output measured. After a certain period (usually 2 to 5 s) has elapsed, the emf is recorded. As the water drop evaporates, the wet junction is held at the dew point. When evaporative cooling drops off, the emf decays back to a zero reading if there is no temperature difference between the reference and sensing junctions. By comparing this emf to the calibration curve, a value of water potential may be obtained.

Richards, L. A., and Ogata, G., (1958) "Thermocouple for Vapor Pressure Measurement in Biological and Soil Systems at High Humidity," *J. Am. Soc. Agron.* 50:1089-1090.

Readout procedures--In order to operate TCPs, several procedures are required. A cooling current must be applied in the proper direction to cool the sensing junction. When it is stopped, a voltmeter in the range of 1 to 30 μ V is required to measure the TCP emf output. Most researchers agree that, in order to develop meaningful procedures using TCPs, an X-Y plotter or strip chart recorder should be used to study the emf versus time data for the psychrometers. Once some experience is gained, the necessity of plotting these outputs diminishes.

For this study, an MJ-55 thermocouple microvoltmeter was used, a Keithly Model 155 Microvoltmeter modified and sold by Wescor, Inc. Modifications include a cooling current circuit and manual switch, a 0°C thermocouple reference junction, and connectors for use with Wescor instruments. The emf-time data were plotted using a Hewlett-Packard Model 7046A X-Y recorder. The time was recorded at 10 s/in, and the output at 0.5 V/in. The MJ-55 provides a ± 1 -V output for full-scale positive or negative deflection at the terminal strip, through internal amplifiers, for driving the plotter.

The TCPs used were chromel-constantan thermocouples with a single sensing junction. The Wescor, Inc., model PT-51 and P51 instruments were used with lead wire lengths from 1.5 to 6.1 m (5 to 20 ft). The difference between these instruments is the addition of a copper-constantan thermocouple for temperature measurements on the PT model. These instruments are covered with a ceramic bulb that forms the sample chamber. Another type of TCP used was the No. 74-13 produced by J.R.D. Merrill Specialty Equipment. These are screen-covered instruments with a single sensing junction. An additional constantan wire is connected to one reference junction to provide temperature measuring capability. They are covered with a double stainless steel wire mesh.

The instruments were connected manually to the MJ-55. The meter was turned on and zeroed. (A large deflection of the meter indicates the lack of an equilibrium condition between the junctions.) The recorder was zeroed and started. The cooling current was applied using the manual switch on the MJ-55. After some experimenting, a 15-s cooling period was adopted as standard.

It is important to select a uniform procedure for reading the thermocouple output. Plots of output versus time were recorded and studied to select a method. Consistent results were obtained using a 2- to 5-s time delay. The delay begins when the cooling current is shut off and ends when the reading is made. Although a variety of output curve forms were observed, this procedure provided consistent results. Typical output plots are shown in Figure 4-2 and 4-3 for high- and low-range measurements respectively.

Calibration modeling--The present state of the art for using TCP sensors has been totally dependent on instrument calibration. Despite several attempts to theoretically predict the output, calibration is still an essential part of applications to real measurement problems. The emf will vary as the relative humidity changes. Normally the TCP output emf is plotted versus water potential. Figure 4-4 illustrates a typical calibration curve using several cooling periods (Bingham et al, 1972). Figure 4-5 illustrates calibration variation with ambient temperature (Meyn and White, 1972).

Because both water potential and emf output vary with temperature, it is necessary to evaluate the influence of temperature changes for all applications in which it is not closely controlled. Meyn and White (1972) have proposed a model for TCP calibration that accounts for the influence of temperature as follows:

$$Y = b_0x_0 + b_1x_1 + b_2x_2 + b_3x_1^2 + b_4x_2^2 + b_5x_1x_2 \quad (4-1)$$

where

Y = predicted water potential, bars

x_0 = dummy variable (1)

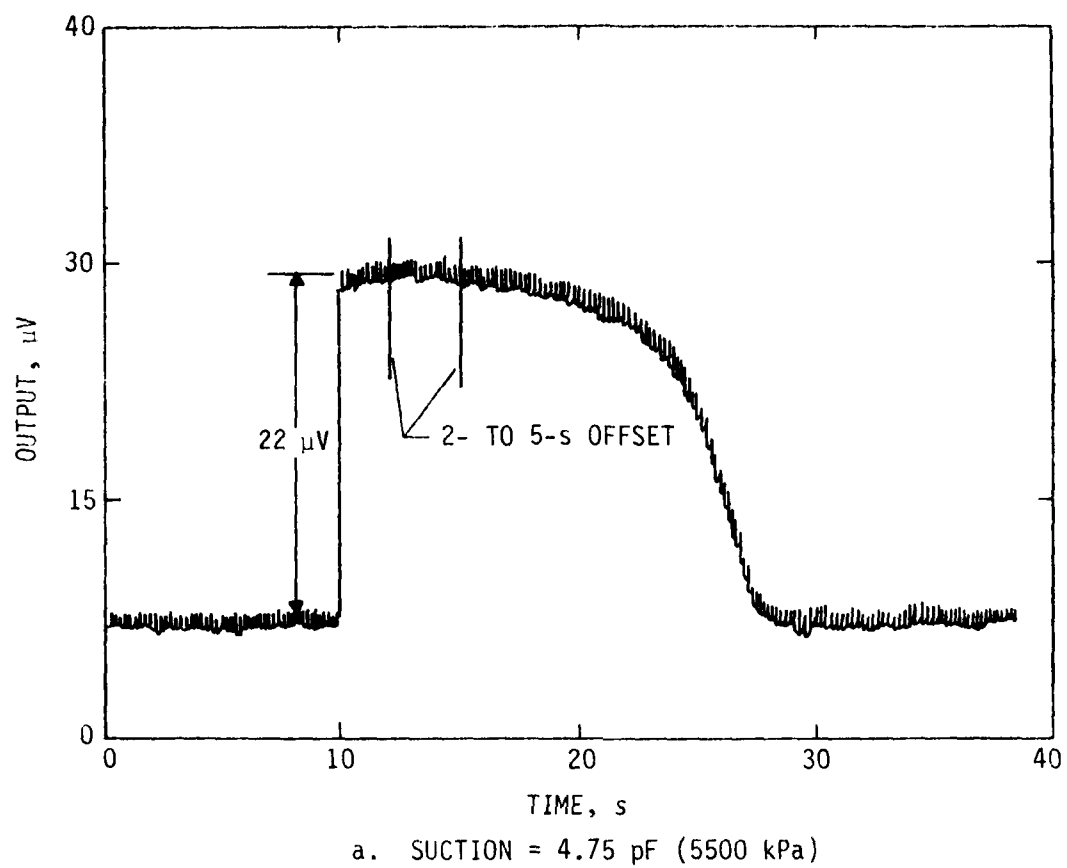
x_1 = emf, μV

x_2 = temperature, $^{\circ}\text{C}$

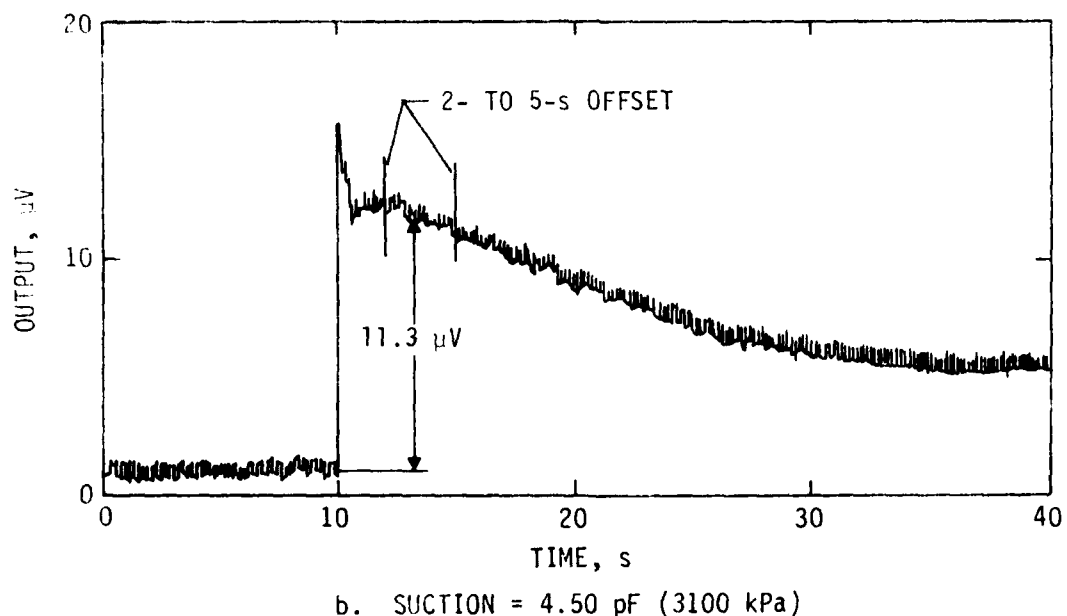
$b_0, b_1, b_2, b_3, b_4, b_5$ = regression constants

Bingham, G. E., Johnson, M. N., and Lemon, E. R., (1972) "Influence of Heat Sink Design on Thermocouple Psychrometer Response," in *Psychrometry in Water Relations Research*, Utah Agricultural Experiment Station, Utah State University, Logan, Utah.

Meyn, R. L. and White, R. S., (1972) "Calibration of Thermocouple Psychrometers: A Suggested Procedure for Development of a Reliable Predictive Model," in *Psychrometry in Water Relations Research*, Utah Agricultural Experiment Station, Utah State University, Logan, Utah, pp. 56-64.

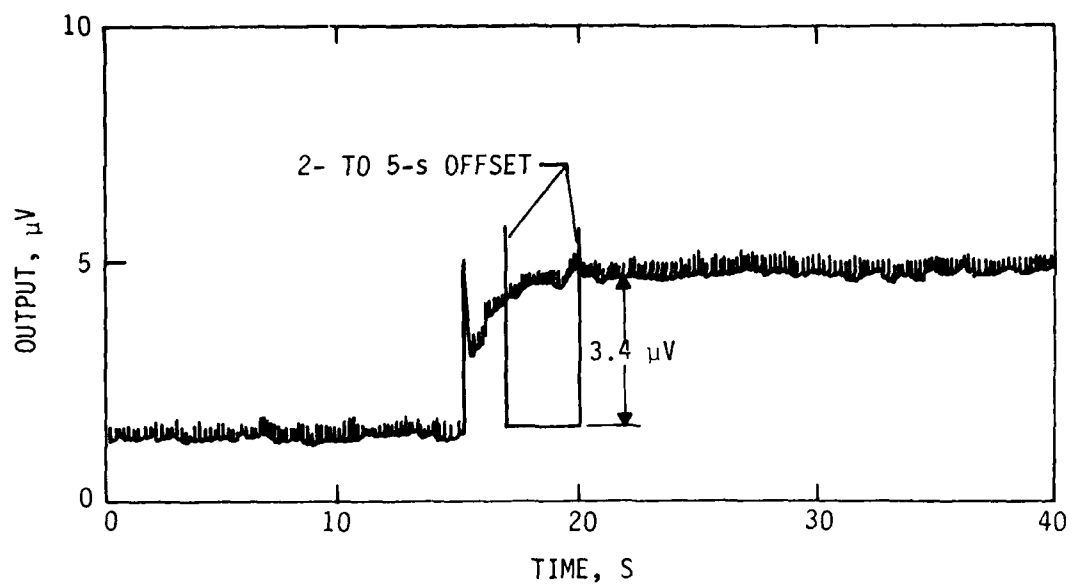


a. SUCTION = 4.75 pF (5500 kPa)

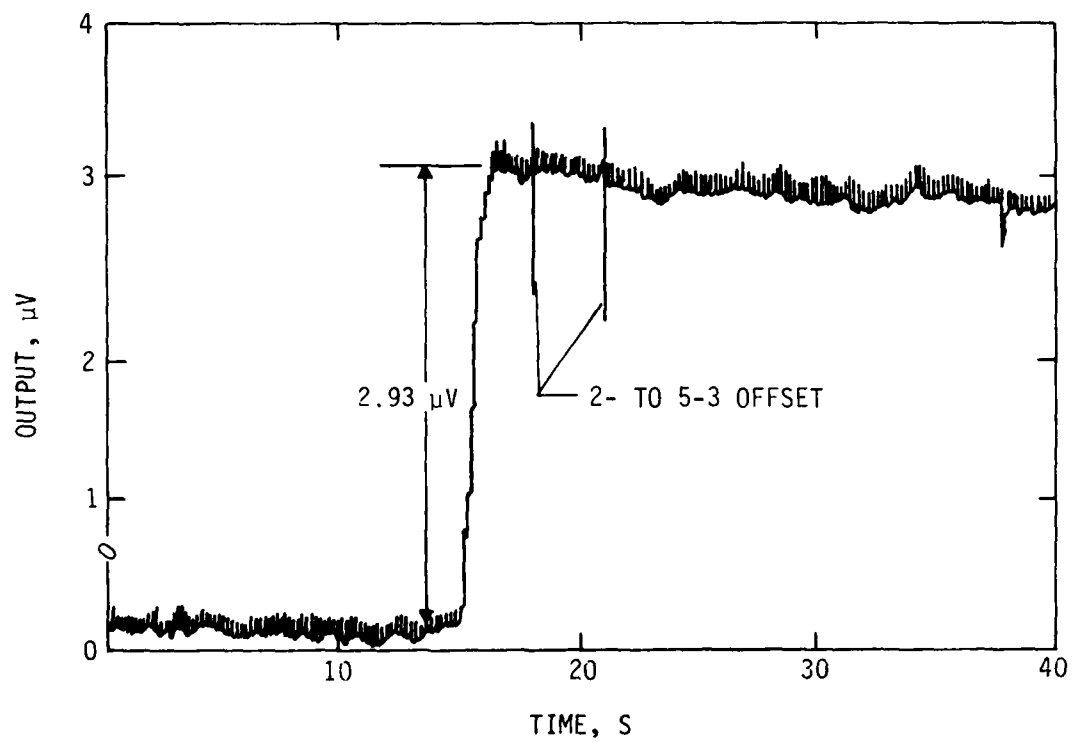


b. SUCTION = 4.50 pF (3100 kPa)

FIGURE 4-2. TYPICAL THERMOCOUPLE PSYCHROMETER OUTPUT, HIGH RANGE.



a. SUCTION = 3.90 pF (780 kPa)



b. SUCTION = 3.85 pF (700 kPa)

FIGURE 4-3. TYPICAL THERMOCOUPLE PSYCHROMETER OUTPUT, LOW RANGE.

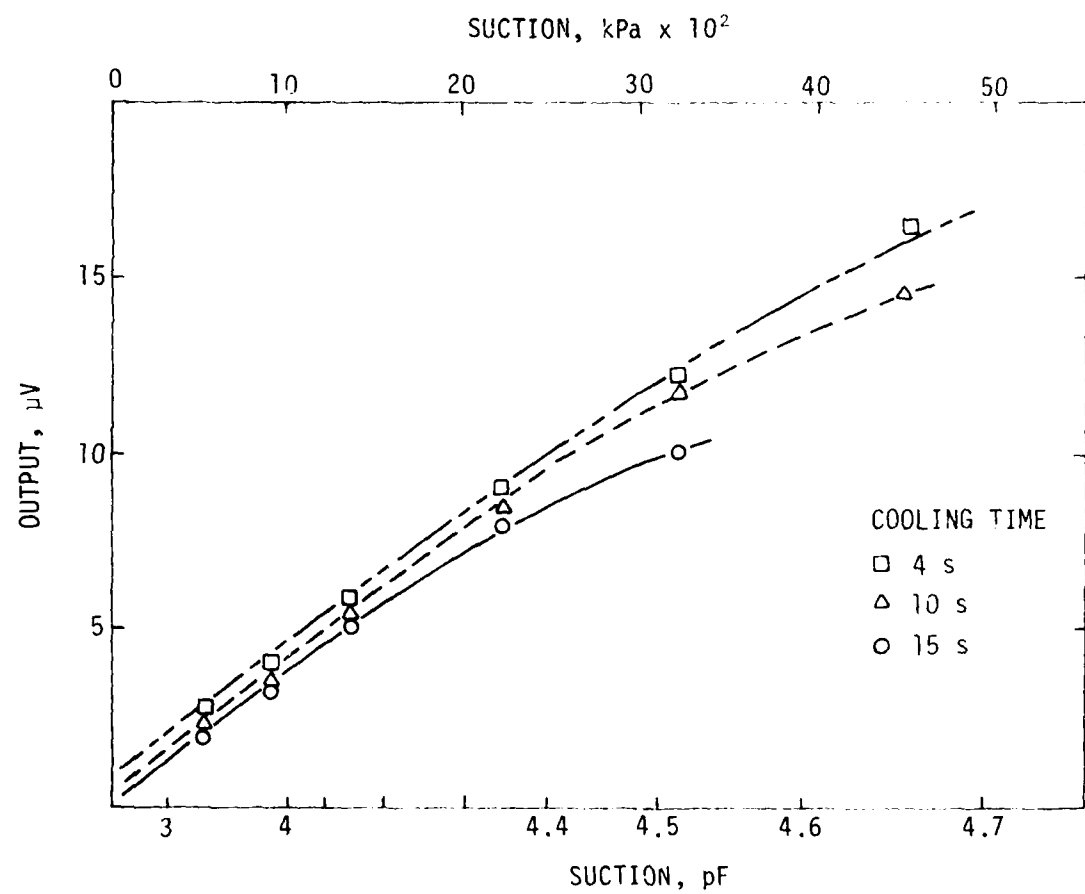


FIGURE 4-4. CALIBRATION VARIATION WITH COOLING PERIOD.
(AFTER BINGHAM ET AL, 1972)

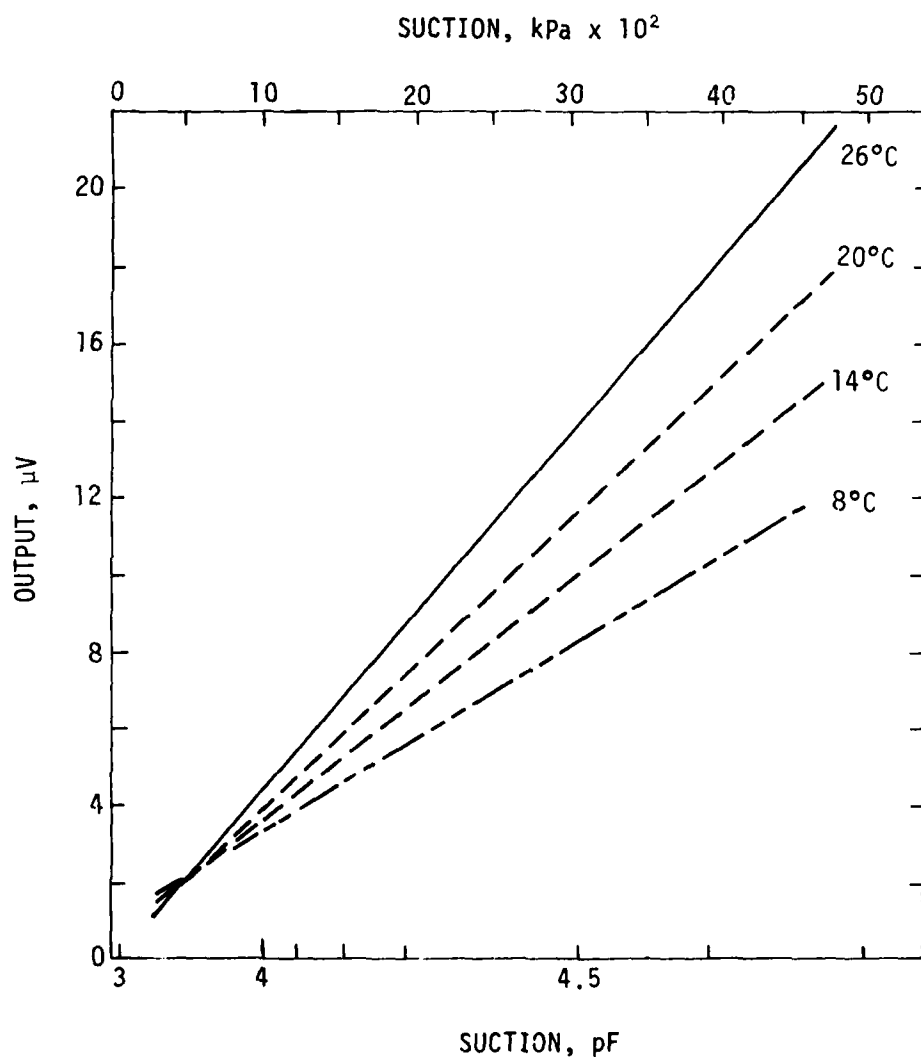


FIGURE 4-5. CALIBRATION VARIATION WITH AMBIENT TEMPERATURE.
(AFTER MEYN AND WHITE, 1972)

Slack (1975) and Riggle (1978) have followed the same approach. The results obtained by Riggle and Meyn and White, along with those of the present study, are shown in Table 4-1.

TABLE 4-1. REGRESSION MODELS

	Riggle (1978)	Meyn and White (1972)	NMERI
(dummy) b_0	2.292	0.10617	-16.4704
$(x_1) b_1$	-4.138	-4.6283	- 4.0883
$(x_2) b_2$	---	0.0778	1.6769
$(x_1)^2 b_3$	-0.0557	-0.0076	0
$(x_2)^2 b_4$	---	-0.0075	-0.0413
$(x_1x_2) b_5$	0.1110	0.1036	0.0728
coefficient (R^2) of determination	0.9756	0.9623	0.9630

In these experiments, a model involving fewer terms was developed in each case. Note that the calibration is valid only if the measurements are made in exactly the same manner as the calibrations.

Meyn and White developed their model for use with a large number of instruments whereas Riggle calibrated each instrument individually. In the NMERI calibrations, a single satisfactory model was sought. Development efforts commenced with the calibration of numerous instruments at ambient temperature in the laboratory. This was followed by additional calibrations in an environmental chamber at temperatures of roughly 10 and 15°C. These data were then evaluated using a stepwise multiple regression computer program. The form of the model was identical to those previously used.

Riggle, F. R., (1978) "Soil Water Potential Determinations with Thermocouple Psychrometers," Master of Agriculture Integrating Paper, University of Minnesota, St. Paul, Minnesota.

Slack, D. C., (1975) "Modeling the Uptake of Soil Water by Plants," Dissertation, University of Kentucky, Lexington, Kentucky.

Field installations--At the Gallup airport, two boreholes were made to a depth of 6.1 m (20 ft) for installation of the instruments. This depth was expected to include the soil active zone. On the recommendations of an expert on use of the instruments, redundancy was included to provide for failure of the units. Table 4-2 shows the instrumentation included in each borehole. Two types of instruments were used. The instruments with the model designation beginning with P were obtained from Wescor, Inc., in Logan, Utah. For these instruments, the P indicates psychrometer; T means that an additional temperature-measuring thermocouple is included; and numbers are the lead wire length in feet. The others, numbered in the 200's in Table 4-2, were obtained from the J.R.D. Merrill Specialty Co. in Logan, Utah. These instruments included a temperature-measuring thermocouple and a 3-m (9.8-ft) lead wire.

Initially two boreholes were drilled at the DFW airport (borings 5 and 6). Because of the poor performance of these instruments, five additional psychrometers were installed in another site (boring 8). Table 4-3 shows the instrumentation used.

Because of the climate at the Jackson airport, the equilibrium suction below the depth of the active zone was estimated to be too low for reliable performance at the depths used for DFW and GAL. Therefore, instruments were installed only to 1.5 m (5 ft) for measurements in the active zone of the soil (Table 4-4).

Instrument performance was monitored to evaluate the redundancy designed into the instrument configuration. The percentage of instruments doubled was as follows: DFW boring 5, 67; DFW boring 6, 57; DFW boring 8, 0; GAL boring 1, 50; GAL boring 2, 50; JSN boring 1, 0. The GAL installations were designed with less redundancy because of the dry climate and, therefore, favorable measurement conditions. More redundancy was used for the DFW sites because of wetter conditions and, therefore, more difficult operating environment. The instruments of JSN were not duplicated because of the ease of replacing instruments to a depth of 1.5 m (5 ft). The total percent of available instruments at each site was as follows: DFW boring 5, 83; DFW boring 6, 36; DFW boring 8, 100; GAL boring 1, 69; GAL boring 2, 81; JSN boring 1, 100.

TABLE 4-2. INSTRUMENTATION AT GAL

Boring 1			Boring 2		
Depth, m (ft)	Sensor number	Type	Depth, m (ft)	Sensor number	Type
0.61 (2.0)	8	PT51-05	0.5 (1.5)	3	PT51-05
0.61 (2.0)	2	PT51-05	0.5 (1.5)	4	PT51-05
1.2 (4.0)	22	PT51-10	1.1 (3.5)	24	PT51-10
1.2 (4.0)	203	74-13	1.1 (3.5)	204	74-13
1.8 (6.0)	21	PT51-10	1.7 (5.5)	23	PT51-10
1.8 (6.0)	25	PT51-10	1.7 (5.5)	27	PT51-10
2.1 (7.0)	201	74-13	2.0 (6.5)	203	74-13
2.4 (8.0)	108	PT51-16	2.3 (7.5)	109	PT51-16
3.0 (10.0)	110	P51-16	2.9 (9.5)	112	P51-16
3.0 (10.0)	111	PT51-16	2.9 (9.5)	107	PT51-16
3.7 (12.0)	115	PT51-16	3.5 (11.5)	113	P51-16
4.3 (14.0)	116	P51-16	4.1 (13.5)	114	PT51-16
4.9 (16.0)	101	PT51-20	4.7 (15.5)	103	PT51-20
4.9 (16.0)	104	P51-20	4.7 (15.5)	105	P51-20
5.5 (18.0)	102	P51-20	5.2 (17.5)	106	PT51-20

TABLE 4-3. INSTRUMENTATION AT DFW

Boring No. 5			Boring No. 6			Boring No. 8		
Depth, m (ft)	Sensor number	Type	Depth, m (ft)	Sensor number	Type	Depth, m (ft)	Sensor number	Type
0.3 (1.0)	5	PT51-05	0.3 (1.0)	11	PT51-05	0.3 (1.0)	36	PT51-05
0.3 (1.0)	6	PT51-05	0.3 (1.0)	12	PT51-05	0.6 (2.0)	51	P51-10
0.9 (3.0)	9	PT51-05	0.9 (3.0)	13	PT51-05	0.9 (3.0)	41	PT51-10
0.9 (3.0)	10	PT51-05	0.9 (3.0)	14	PT51-05	1.2 (4.0)	47	P51-10
1.5 (5.0)	28	PT51-10	1.5 (5.0)	31	PT51-10	1.5 (5.0)	42	PT51-10
1.5 (5.0)	205	74-13	1.5 (5.0)	207	74-13			
2.1 (7.0)	29	PT51-10	2.1 (7.0)	32	PT51-10			
2.1 (7.0)	206	74-13	2.1 (7.0)	210	74-13			
2.7 (9.0)	117	PT51-16	2.7 (9.0)	119	PT51-16			
3.4 (11.0)	127	P51-16	3.4 (11.0)	129	P51-16			
4.0 (13.0)	118	PT51-16	4.0 (13.0)	120	PT51-16			
4.0 (13.0)	128	P51-16						
4.6 (15.0)	121	P51-20						
5.2 (17.0)	122	P51-20						
5.2 (17.0)	125	PT51-20						

TABLE 4-4. INSTRUMENTATION AT JACKSON AIRPORT

Boring No. 3		
Depth, m (ft)	Sensor number	Type
0.3 (1.0)	1	PT51-05
0.6 (2.0)	33	PT51-10
0.9 (3.0)	130	PT51-16
1.2 (4.0)	38	PT51-10
1.5 (5.0)	39	PT51-10

The number available refers to the number of instruments in which the circuit was intact. However, the availability of an instrument did not guarantee that a measurement was made. In some cases, the soil was too wet for TCP operation. When the thermocouples corroded or otherwise failed, it was easily detected by measuring circuit resistance. Results of measurements using these instruments are discussed later in this section.

Filter Paper Method

Researchers in the field of soil science recognized that forces attracting water to paper could be used to estimate the magnitude of soil attraction for water. Hansen (1926) used blotting paper as a carrier for sugar solutions in work at the University of Copenhagen. Strips saturated with four different solutions were exposed to soils in closed containers. The one with the least moisture change at equilibrium was interpreted as being nearest the stress level of the soil. Stocker (1930) improved the accuracy of the method by employing more solutions. Another improvement was made by Gradmann (1934) who calibrated the blotting paper for weight versus stress after soaking in salt solutions. The sensors were then equilibrated with soil samples, and water

Gradmann, H., (1934) "Über die Messung von Bodensaughwerten" (About the measurement of soil suction), *Jh. Wiss Bot.* 80:92-111.

Hansen, H. C., (1926) "The Water Retaining Power of the Soil," *Journal of Ecology*, Vol. 14:111-119.

Stocker, O., (1930) "Über die Messungen von Bodensaughkräften und ihren Verhältnis zu den Wurzelsaugkräften," *Z. Bot.* 23:27-56.

contents were used to infer moisture stress. With some minor changes, Eckhardt (1960) used this method in France.

The first use of paper as a moisture stress sensor without a hygroscopic salt was reported by Gardner (1937). He used an ash-free quantitative filter paper (Schleicher and Schuell, No. 589, White Ribbon) calibrated for water content versus stress. From this beginning, numerous applications have followed, leading to the present method used extensively and routinely by the Water Resources Division of the U.S. Geological Survey (USGS). The first use of this method for civil engineering purposes was by McKeen (1977).

Calibration--Numerous calibrations have been made for different papers used in soil moisture studies. The calibration techniques have generally varied depending on the range of interest. Soil samples are prepared at a known moisture stress or suction level, then the filter paper is equilibrated with it for calibration. At the higher pressures, filter papers may be equilibrated on a pressure membrane or above salt or acid solutions of known concentration. In this way a full calibration curve can be developed.

McQueen and Miller (1974) found that a two-part relationship best fit their calibration data. They determined that the upper segment ($pF > 2.5$) represents moisture retained as film adsorbed to particle surfaces and that the lower segment ($pF < 2.5$) represents moisture retained by capillary or surface tension forces. It is no coincidence that this level (2.5 pF) of moisture stress corresponds to the field capacity of soils as found in the agricultural literature. In an extensive and thorough study by McQueen and Miller of calibration and factors influencing it, a range of calibration relationships was

Eckardt, F. E., (1960) "Eco-physiological Measuring Techniques Applied to Research on Water Relations of Plants in Arid and Semi-arid Regions, in *Arid Zone Res.*: XV. UNESCO.

Gardner, R. (1937), "A Method of Measuring the Capillary Tension of Soil Moisture over a Wide Moisture Range," *Soil Science*, Vol. 43:277-283.

McKeen, R. G., (1977) "Characterizing Expansive Soils for Design Purposes," presentation at the joint meeting of Texas, New Mexico, and Mexico sections, American Society of Civil Engineers, Albuquerque, New Mexico, October 6-8.

McQueen, I.S. and Miller, R. F., (1974) "Approximating Soil Moisture Characteristics from Limited Data: Empirical Evidence and Tentative Model," *Resources Research*, Vol. 10, No. 3:521-527.

defined (Figure 4-6). The calibrations for the USGS work and for the NMERI measurements are also shown in Figure 4-6. The NMERI curve falls lower than the USGS curve because the NMERI calibrations used salt solutions in the range of 3.0 to 4.7 pF. The calibration was intended for use with clay soils in this range of suctions and was therefore deemed satisfactory. Subsequent calibrations at the low end and communications with the developers of the USGS method substantiated the NMERI calibration relationship.*

Procedure--The method adopted for this study was essentially that published by McQueen and Miller (1968). The procedure uses filter paper discs 5 cm in diameter. In this study, Schleicher and Schuell No. 589 White Ribbon was used. As shown by McQueen and Miller (1977), virtually any uniform quality paper may be used. Air-dried filter papers were exposed to salt solutions (potassium chloride) for a period of seven days. The papers absorbed a small amount of water from the salt solution. The papers were quickly and carefully transferred into small aluminum weighing cans and weighed to the nearest 0.0001 g. The containers were opened and oven-dried overnight. The containers were then closed inside the oven, removed, and placed on an aluminum block to cool for 30 s. The filter paper was weighed to obtain the dry weight. In each case a separate tare weight was taken for both the wet and dry weighings. The moisture stress of the salt solution was plotted versus the filter paper water content.

Suction measurements on soil samples were made using filter paper from one lot. First, the sample was placed in a moisture can. Then two filter papers were placed directly on top of the soil sample. In most of the samples tested in this study, suctions were beyond the range of capillary water; therefore, the filter paper could not absorb water through capillary action. The moisture transferred by vapor diffusion and thus represents a total suction value. [For soils with suctions below the capillary limit (<2.5 pF), precautions are required to prevent capillary flow.] Following equilibration, both filter papers were removed and placed in separate moisture containers. Their respective water contents were determined. The water content of the bottom

McQueen, Irel S. and Miller, R. G., (1968) "Calibration and Evaluation of a Wide-Range Gravimetric Method for Measuring Moisture Stress," *Soil Science*, Vol. 106, No. 3:225-321.

*Personal communication from R. F. Miller to the author, 1977.

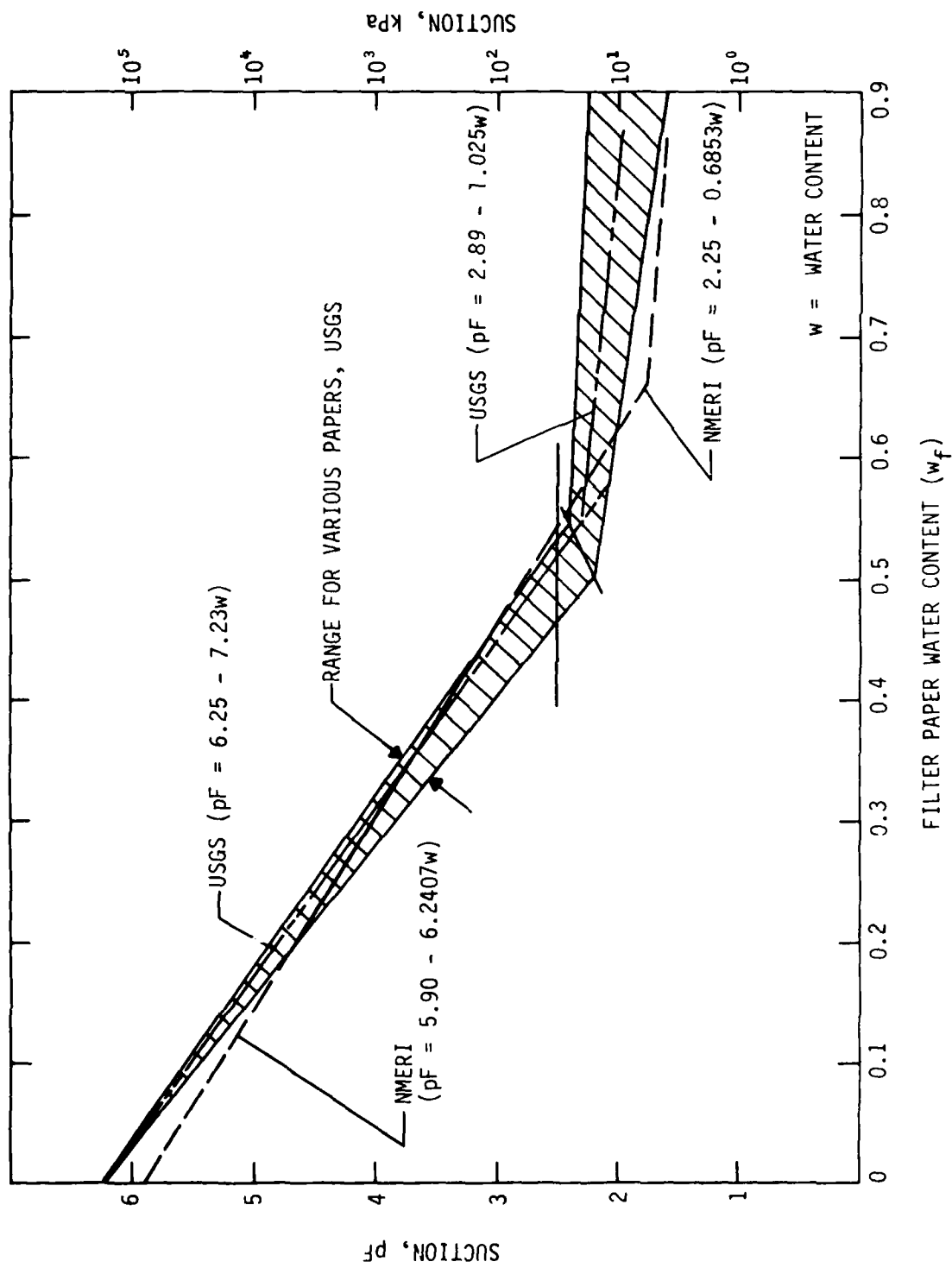


FIGURE 4-6. FILTER PAPER CALIBRATION RELATIONSHIPS.

filter paper (next to the top of the sample) was used as the measure of soil suction. The second filter paper measurement was used as a quality control check. If the upper paper was slightly drier than the bottom paper, normal equilibration occurred, and the measurement was good. Drastic differences (>0.5 pF) or a wetter top paper indicated an abnormal condition. Abnormal results were discarded.

Several things created problems in using the filter paper method. Occasionally, condensation occurs inside the container as a result of poor temperature control or very wet soil. If the filter paper contacts it, this moisture will be absorbed rapidly by capillary action. Great care in transferring filter papers is required. Dry laboratory air can drastically alter the moisture content of the filter paper sensor if exposed for a long time. Experience in this study indicates that technician training is very important. In most cases, errors result in extremely high or low water content of the sensors which yield improbable data. Thus an erroneous result is obvious when the data are examined.

Field measurements--In the field experiment, suction measurements were made regularly on soil samples removed near the locations of the *in situ* measurements. The samples were taken by pushing a small-diameter tube into the ground. The soil was removed and sealed with two filter papers in a moisture can. The containers were returned to the laboratory and equilibrated. The samples were obtained at 152-mm (6-in) intervals to a depth of 1.5 m (5 ft). When soil borings were taken with a truck-mounted drill rig, samples were also removed at intervals for suction determination. One advantage of the filter paper method is that large numbers of samples may be taken at very low cost.

In addition to the field samples, several sets of data were measured on soil samples in the laboratory for evaluation of the method and for comparison of procedures. Results are discussed later in this section of the report.

Hydraulic Tensiometers

Hydraulic tensiometers were installed to measure the low-suction (wet season) range of the field soils. Tensiometers were installed at the DFW and

JSN sites. It was anticipated that the weather conditions at the GAL site would be too dry for satisfactory operation of the instruments. Figure 4-7 illustrates the design of the instruments used. The ceramic bulbs were placed at depths of 0.3, 0.6, 0.9, 1.2, and 1.5 m (1.0, 2.0, 3.0, 4.0, and 5.0 ft) at the sites studied. A water-alcohol solution was used to provide a continuous liquid column from the bulb to the mercury container. The soil surrounding the ceramic bulb attracted water through the bulb by capillary action, pulling the mercury column up. With appropriate corrections for the liquid column lengths, a measurement of the suction in the soil was obtained. Because the ceramic bulb allows salts to pass through freely, this device measures only the matrix component of suction.

COMPARISON OF FP AND TCP MEASUREMENTS

Laboratory Comparison

The TCP and filter paper (FP) methods of suction measurement were compared and evaluated. Two comparisons were made using different procedures. First, TCPs and FP were exposed to the same soil sample in the same closed container. Four different groups of tests were performed, totaling thirty-one samples. The results are shown in Figure 4-8. The computation of the linear regression confirms that, under the conditions of this evaluation, the TCP and the FP methods yield the same results. The second comparison was made in an attempt to verify the procedures reported by Snethen and Johnson (1980) of Waterways Experiment Station (WES).

The results of the WES experiment indicate that FP provides lower values of suction than the TCP. This difference in results has been attributed to two specific reasons: the equilibrium period and the sampling technique. The procedure used by Snethen and Johnson assumes that the TCP equilibrates with the air above the soil sample in two days. Data to substantiate this time period selection are not evident in the literature. In the present study, the TCPs were allowed to equilibrate for seven days, the same period of time as the FP. Data from the WES report are plotted in Figure 4-9, along with the NMERI regression curve. It is apparent that, for low-range measurements, the

Snethen, D. R., and Johnson, L. D., (1980) *Evaluation of Soil Suction from Filter Paper*, Miscellaneous Paper GL-80-4, U.S. Army Waterways Experiment Station, Vicksburg, Mississippi.

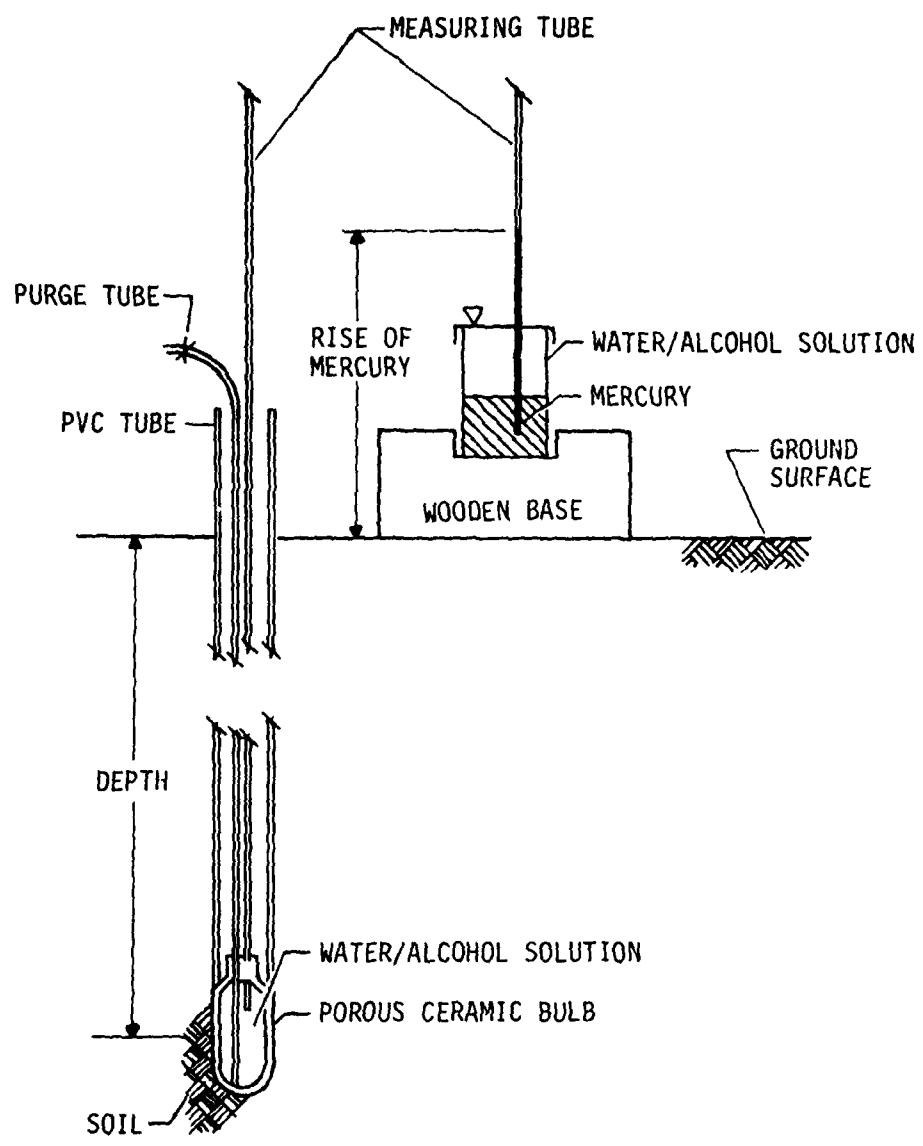
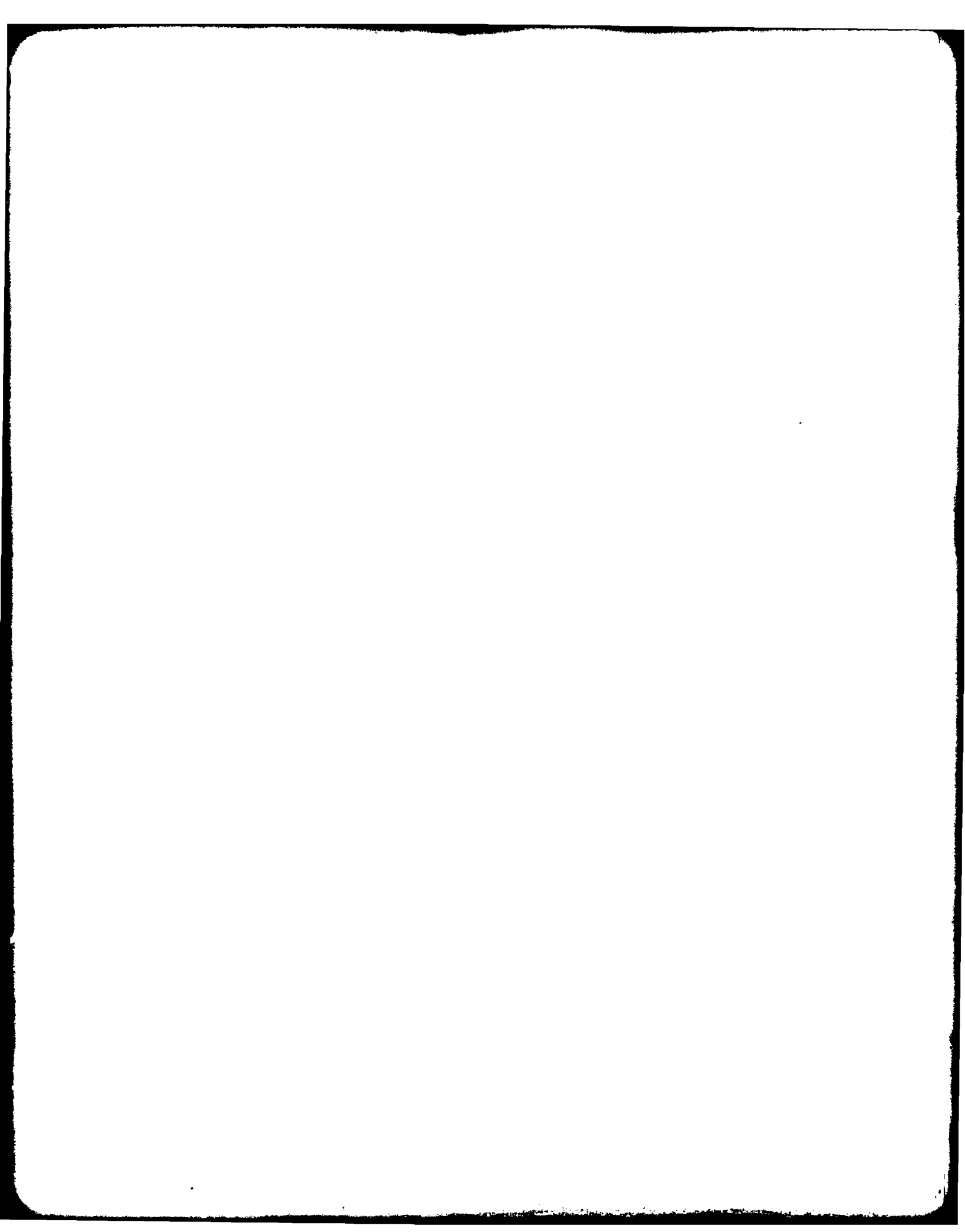
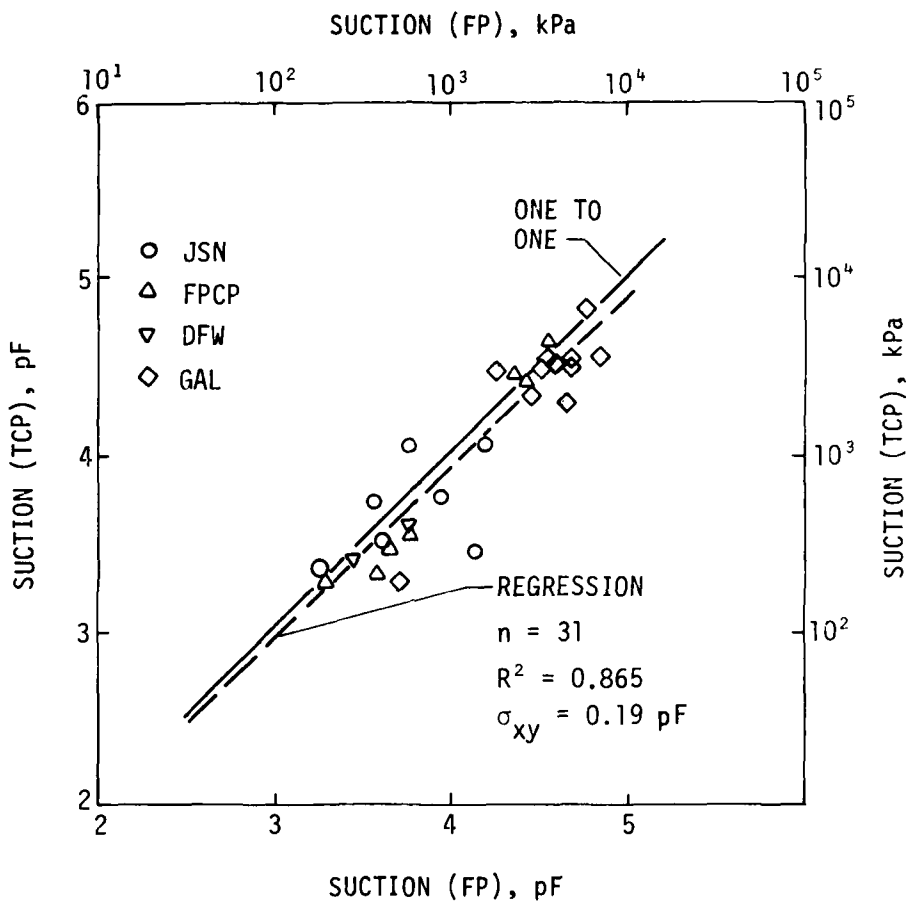


FIGURE 4-7. HYDRAULIC TENSIOMETER CONFIGURATION.





n = NUMBER OF POINTS
 R^2 = COEFFICIENT OF DETERMINATION
 σ = STANDARD ERROR

FIGURE 4-8. LABORATORY COMPARISON - SAME SAMPLE.

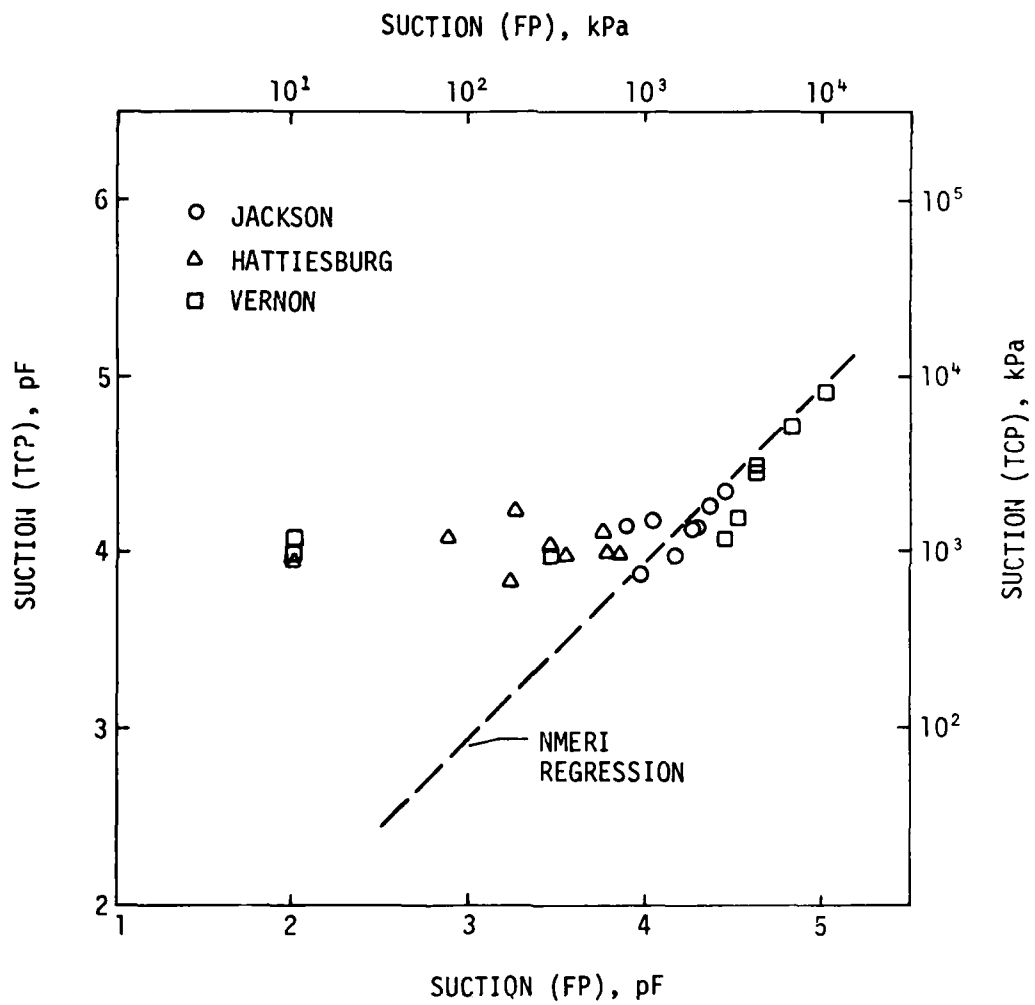


FIGURE 4-9. LABORATORY COMPARISON - WES STUDY.

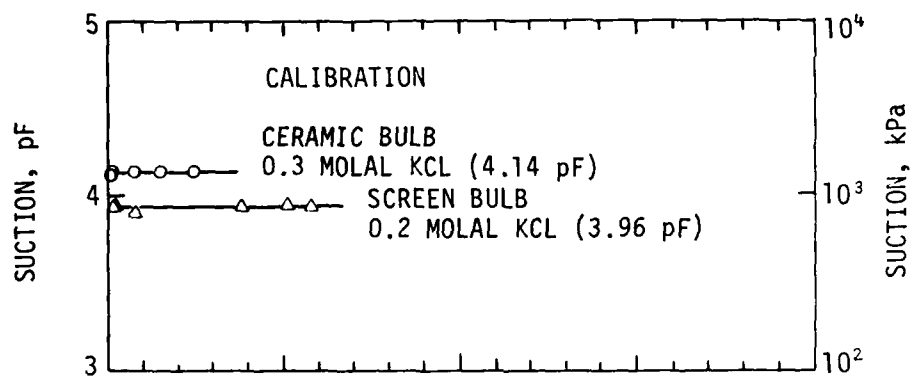
TCP instruments in the WES tests did not achieve vapor equilibrium with the soil samples. The porous ceramic protective cover on the TCP may not have been sufficiently permeable, at low pressure gradients, to allow equilibration in two days; or the covers may have been contaminated, preventing free diffusion of water vapor.

The interference of the ceramic cover with equilibration is called lag. Data were gathered in the laboratory to obtain an estimate of this lag. Figure 4-10a shows that equilibration is rapid in calibration solutions. In Figure 4-10b, equilibration is shown with a soil sample. The minimum equilibration time is about 6 days.

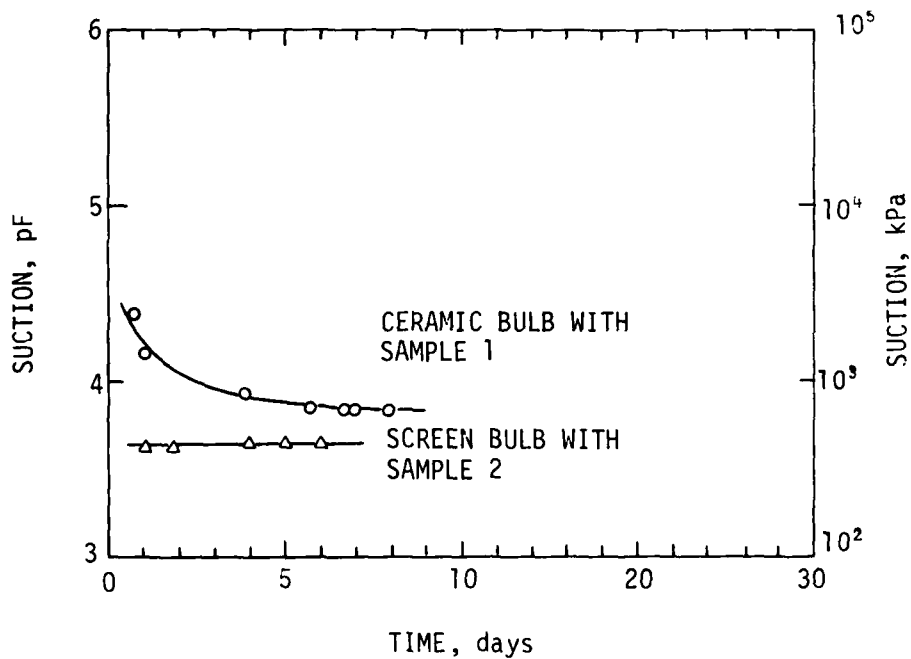
The WES sampling technique also differed from the NMERI procedures. In the WES technique, an undisturbed soil sample was divided into two pieces, one for each type of measurement. In the NMERI verification tests, the WES procedures of time and sampling were followed. Shelby tube samples were cut in slices approximately 25 mm (1 in) thick. These slices were then divided into two parts, one for suction measurement using FP, one for measurement using TCP. The samples were allowed to equilibrate for two days. The linear regression was computed and compared with the regression obtained with the NMERI procedures. The comparison is shown in Table 4-5. These data clearly show the dramatic influence of equilibration time period and sample variation, even though the samples were adjacent in the soil profile.

TABLE 4-5. EFFECTS OF SAMPLE VARIATION AND EQUILIBRATION TIME

Sampling method	Number of tests	Coefficient of determination	Standard error
Same sample for 7 days	31	0.865	0.19
Different samples for 2 days	53	0.624	0.45



a. CALIBRATION WITH SALT SOLUTION.



b. CALIBRATION WITH SOIL.

FIGURE 4-10. ILLUSTRATION OF TGP EQUILIBRIUM TIME.

From the present study it is concluded that, given full equilibration, no sample variance, and laboratory conditions, the FP and TCP methods are equivalent for the determination of soil moisture suction in the range 3.2 to 4.8 pF. Because this range covers most soils of interest in expansive soil studies, both methods can be applied to these studies. The choice of method should be based on other considerations; the precision appears to be equivalent. It is of primary importance that the TCPs be allowed to reach equilibrium.

Comparison of In Situ Samples

Borings to a depth of 6 m (20 ft) were made at each site to obtain samples for laboratory characterization studies. Suction profiles were measured with FP and TCP in each case. A total of six borings were made: three at DFW, two at JSN, and one at GAL.

The results of the FP and TCP measurements of the in situ suction profile from these borings are shown in Figure 4-11 for the DFW site. These data require some explanation. The ideas presented here evolved throughout the field experiment and should be placed in chronological order for clarity. Boring DFW 4 was made in October 1978 to determine the suitability of the site for the field experiment. Two suction profiles were measured in the laboratory on separate samples, one with TCP and one with FP. At that time the FP was being used on a trial basis. The TCP was considered a reliable method for suction determination. As shown in Figure 4-11, dramatic differences were noted between the two methods at depths below 1.8 m (6 ft). It was initially assumed that the FP data were erroneous. The TCP data indicated suctions above 3.4 pF, indicating no possibility of free water or a water table in the profile. The site was accepted as suitable for the field experiment.

Within about 30 days, borings were made for TCP installation. Before the installation could be completed, free water entered the borings and rose to within 1.8 to 2.4 m (6 to 8 ft) of the surface. The undisturbed tube samples from boring 4, as well as those for TCP installation (DFW 5 and 6), were thoroughly studied. The study revealed the presence of numerous sand seams in the profile (Figure 4-12). It was found that the FP suction measurements made on samples from DFW 4 had more accurately depicted the actual suction distribution in the profile. The TCPs evidently did not reach equilibrium.

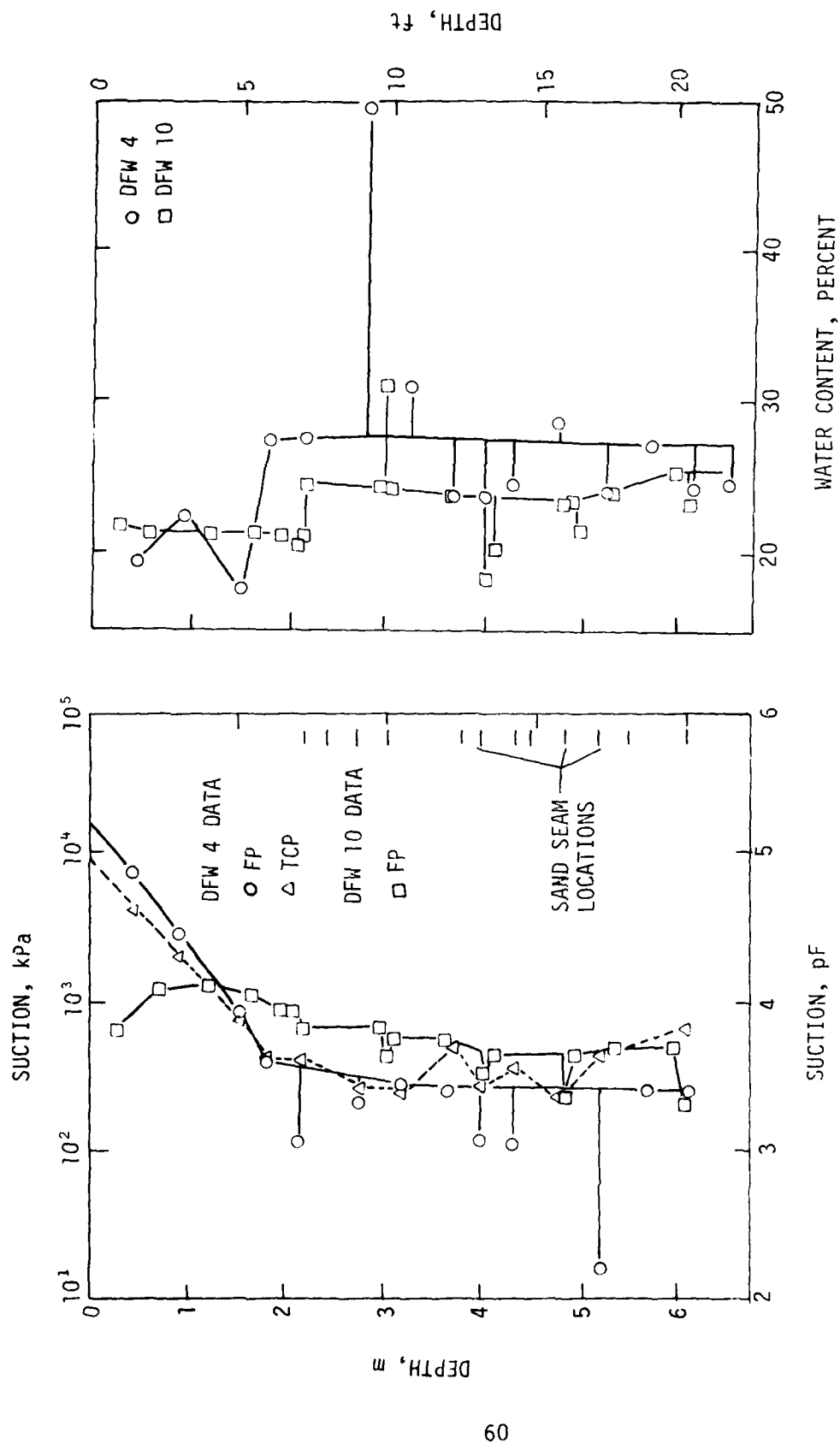


FIGURE 4-11. FILTER PAPER AND THERMOCOUPLE PSYCHROMETER PROFILES AT DFW.

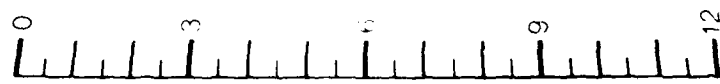


FIGURE 4-12. SHELBY TUBE SAMPLES WITH SAND SEAMS.

The results on samples from DFW 10 (Nov. 1979) confirm the sharp gradients in suction at several sand seams. During the sampling for DFW 10 there was no problem locating the sand seams. Suction samples were taken above, below, and within the seams at several points. It is clear that the water content in the profile gives virtually no information about moisture distribution and equilibrium in the soil profile, except in conjunction with suction measurements.

The water content profile from DFW 10 indicates that the sand seam at 2.1 m (7 ft) prevents water from below from moving up in the profile. The apparent dryness of DFW 10 data compared to DFW 4 is believed to be normal profile variation. The two borings were located about 15.2 m (50 ft) apart. The difference of 0.2 pF (3.7 to 3.5 pF) is well within the variation found for sample-to-sample differences.

A bentonite layer occurred at 3 m (9 ft) below the surface. Inspection of suction and water content at this depth clearly show that suction is an indicator of moisture condition whereas water content is not. The greater clay content (98 percent < 2 μm) of this layer requires a very high water content relative to surrounding clay.

Soil samples were removed at the time in situ TCP measurements were made at each site. These samples were sealed in the field into containers with FP sensors, transported to the laboratory, and equilibrated. Data showing in situ TCP measurements and FP measurements on samples from the same depth are plotted in Figure 4-13. A regression computed for these field-lab data and the regressions for the previous laboratory comparison are shown. Observations made from these data are as follows:

1. The standard deviation is less for these tests than for the laboratory tests on different samples (using WES procedure).
2. The deviation from a one-to-one slope again points to lower suctions for FP on the low end of the suction range measured.
3. FP measurements of suctions made in the laboratory on field samples are at least as accurate as in situ TCP measurements.

The slope of the field-lab regression line indicates a lower FP result as compared to the TCP on the low end of the range. Two causes are responsible for the discrepancy: lag caused by the ceramic cover, and installation

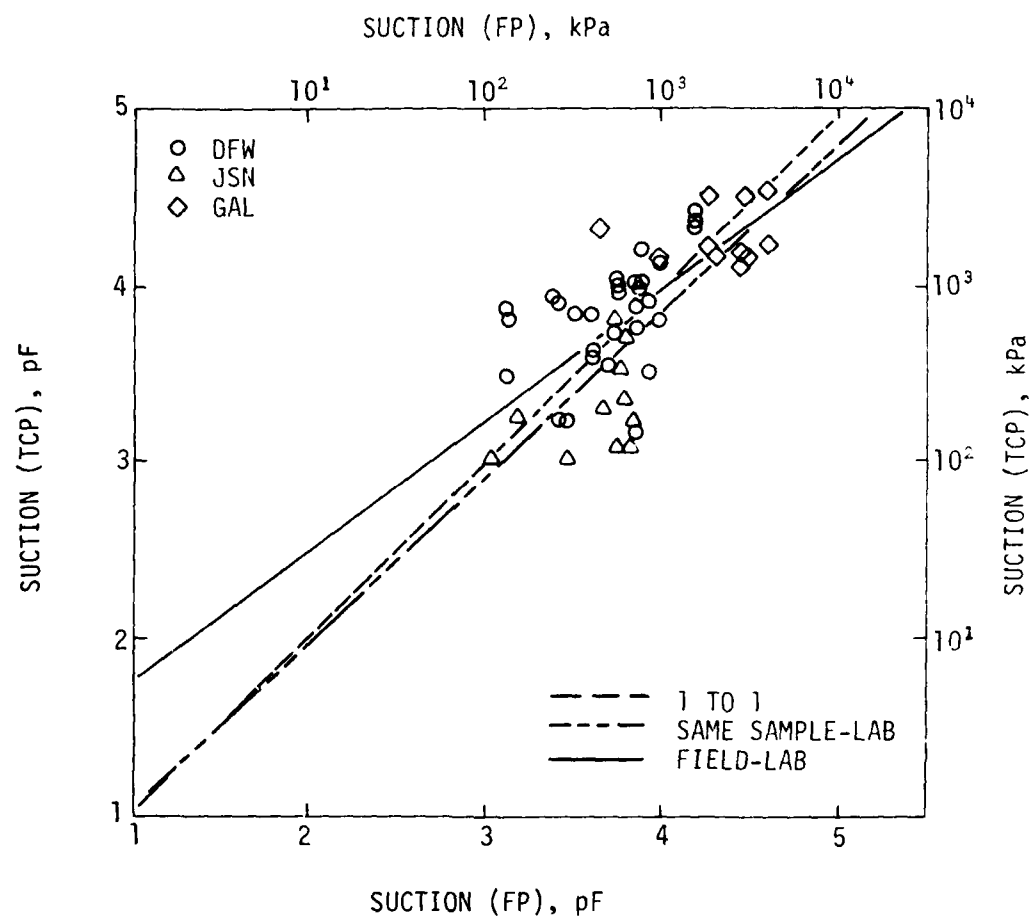


FIGURE 4-13. FIELD-LABORATORY DATA COMPARISON.

methods. The instruments were installed in the field by boring a hole, placing the instruments, and recompacting the soil. Thus, the field permeability was reduced at the point of measurement, resulting in increased lag time.

RESULTS

Field Profiles

In situ thermocouple psychrometers--TCPs were installed in boreholes at each site to measure in situ suction profiles. Two boreholes were instrumented at each of the GAL and DFW sites; a single installation was made at the JSN site. These TCPs were monitored periodically to obtain suction estimates throughout the year. The profiles are illustrated in Figures 4-14 to 4-16. Figure 4-14 shows that the suction at the GAL site is very stable below 1.5 m (5 ft). Water apparently seeped down the side of borehole 2, affecting measurements at 1.1 m (3.5 ft) and 1.7 m (5.5 ft).

The DFW data in Figure 4-15 shows evidence of seasonal effects to the 1.8-m (6-ft) depth. The presence of sand seams which periodically contained water at depths below 1.8 m (6 ft) produced an erratic suction profile. However, data obtained from this site with the FP method corroborated the TCP measurements. Most of the instrumentation at DFW was infiltrated when the sand seams filled with water. At DFW boring 5, for example, several instruments were operational, but conditions were too wet to allow a measurement. Apparently the relative humidity was too high, preventing evaporative cooling. In addition, the TCPs were too widely spaced to depict suction in a soil profile as discontinuous and complex as the DFW site.

The data for the JSN site, shown in Figure 4-16, were limited because of the range restrictions of the TCP. Although the instruments did not fail, the soil was too wet for reliable measurements by TCPs. The suitability of TCP for in situ measurements depends on the expected range of suction. Profiles that remain below 3.5 pF should not be instrumented. Profiles between 3.5 and 4.0 pF are satisfactory; those above 4.0 pF appear to be the optimum for TCP measurements.

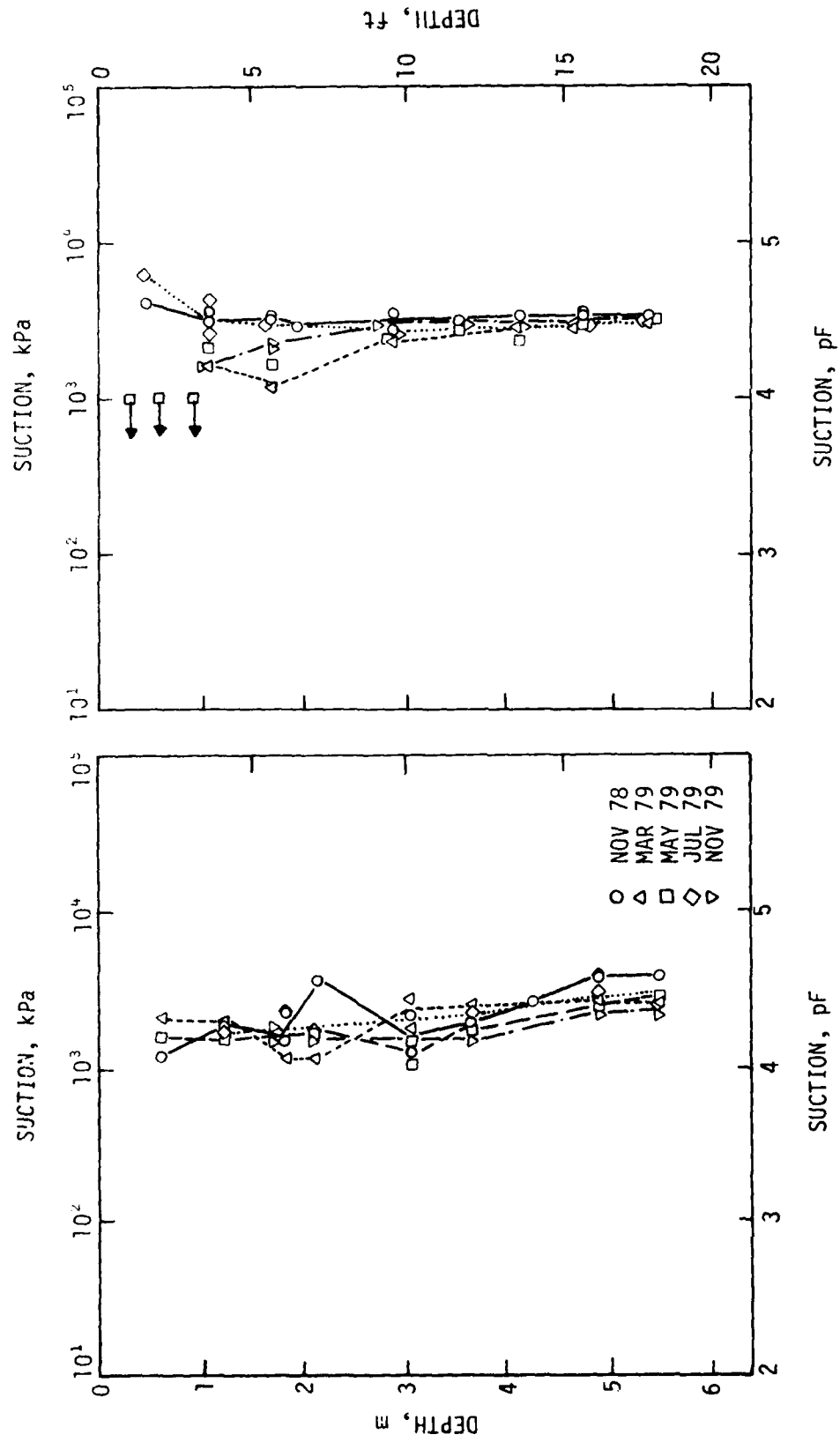


FIGURE 4-14. TCP SUCTION PROFILES FOR GAL.

a. BORING NO. 1.
b. BORING NO. 2.

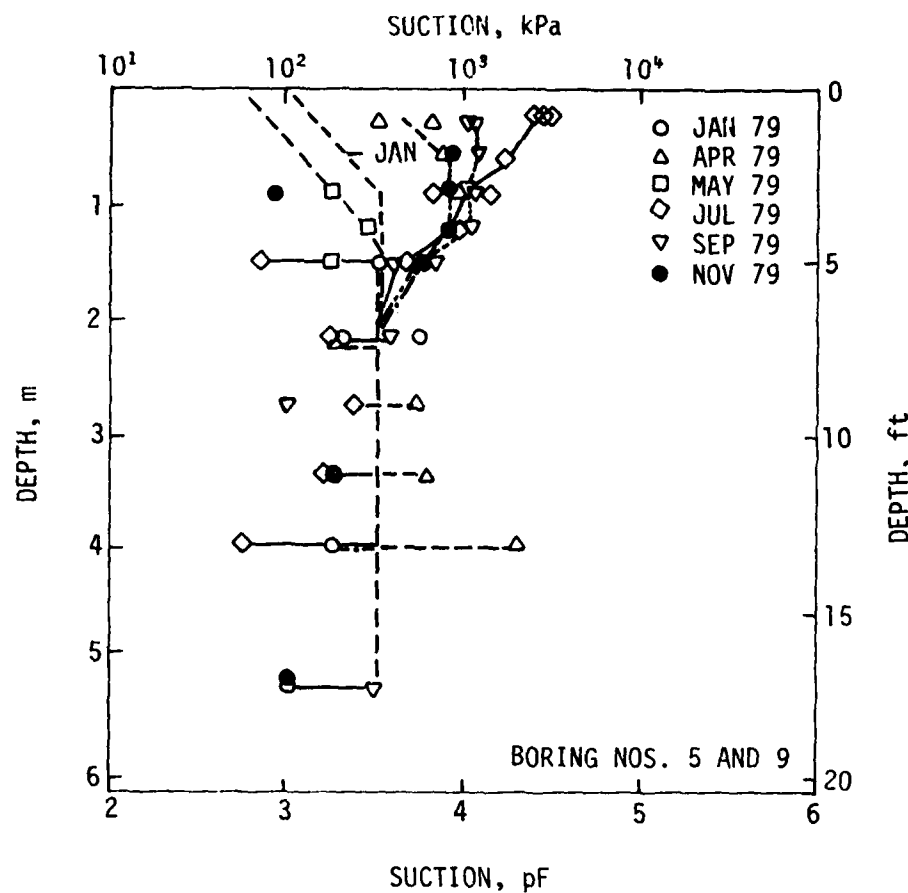


FIGURE 4-15. TCP SUCTION PROFILES FOR DFW.

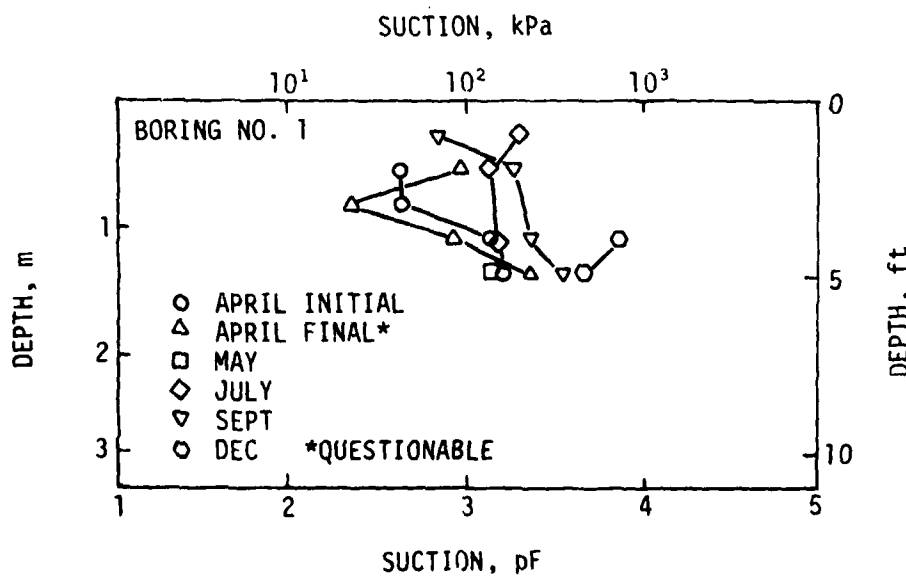


FIGURE 4-16. TCP SUCTION PROFILES FOR JSN.

Laboratory filter paper tests--Further descriptions of suction variation at DFW are shown in Figure 4-17. These profiles were determined in the laboratory using the FP method. The dashed lines represent the profiles determined from the TCPs as shown in Figure 4-15. The data for January indicate that the TCPs at 0.3 m (1 ft) and 0.9 m (3 ft) were too wet to respond. The results in April, September, and November show transition periods; May and July are at end points of the wet and dry cycle respectively. In the transition periods, water is either entering or leaving the profile. Because of variations in drainage of the water, suction variations are present; and TCP lag causes the discrepancy between TCP and FP measurements. As the wetting or drying influence persists, the soil approaches a uniform suction condition. In the May and July profiles this condition is clearly demonstrated.

Data in Figure 4-18 indicate the variety of suction profiles obtained during the transition period from dry to wet, the recharge period in the Thornthwaite system. The four plots represent suction versus depth at four different points horizontally separated by less than 15 m (50 ft). The rate of change of suction with elevation change is a good indicator of the rate of moisture movement into or out of the profile. Thus, the following observations can be made from Figure 4-18.

1. DFW sites 1, 2, and 4 were wetting at about the same rate.
2. At the zone for 0.6 to 0.9 m (2 to 3 ft) to 1.2 m (4 ft), all profiles show the effect of a prolonged wetting period. Weather data indicate that, 20 to 30 days before sampling, 8.6 cm (3.4 in) of rain occurred over a period of 15 days.
3. The field permeability and surface drainage characteristics are capable of producing dramatically different suction profiles over short horizontal distances during wetting or drying phases. Prolonged wetting or drying periods will produce more uniform suction conditions.

FP suction profiles for GAL are shown in Figure 4-19. The dashed line shows the TCP measurements (from Figure 4-14). As before, the data from May and July show good agreement, but the data for November '78, March '79, and November '79 do not agree well. Thus the data show the inability of the in situ TCP to track the changing suction profile.

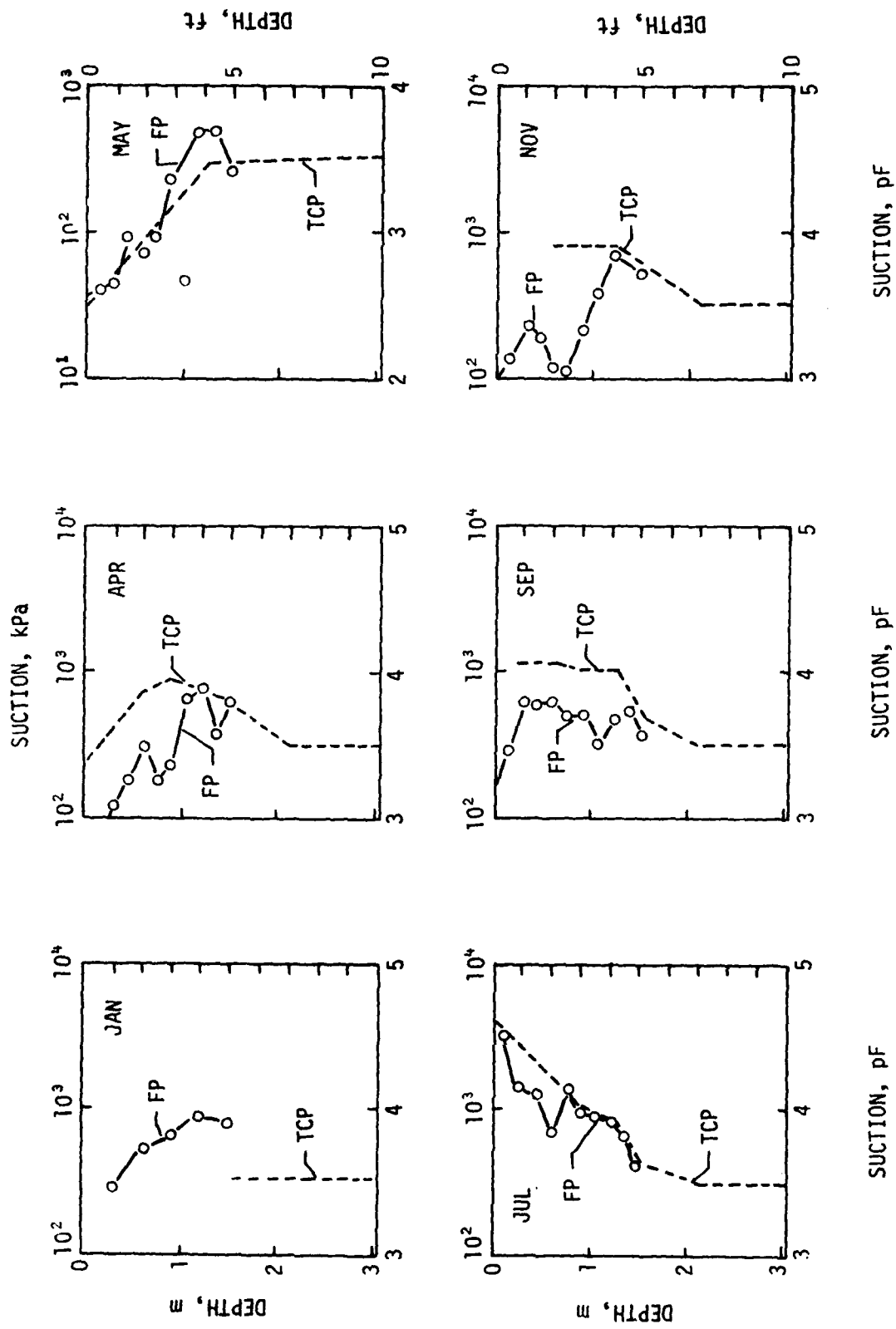


FIGURE 4-17. COMPARISON OF TCP AND FP SUCTION PROFILES AT DFN.

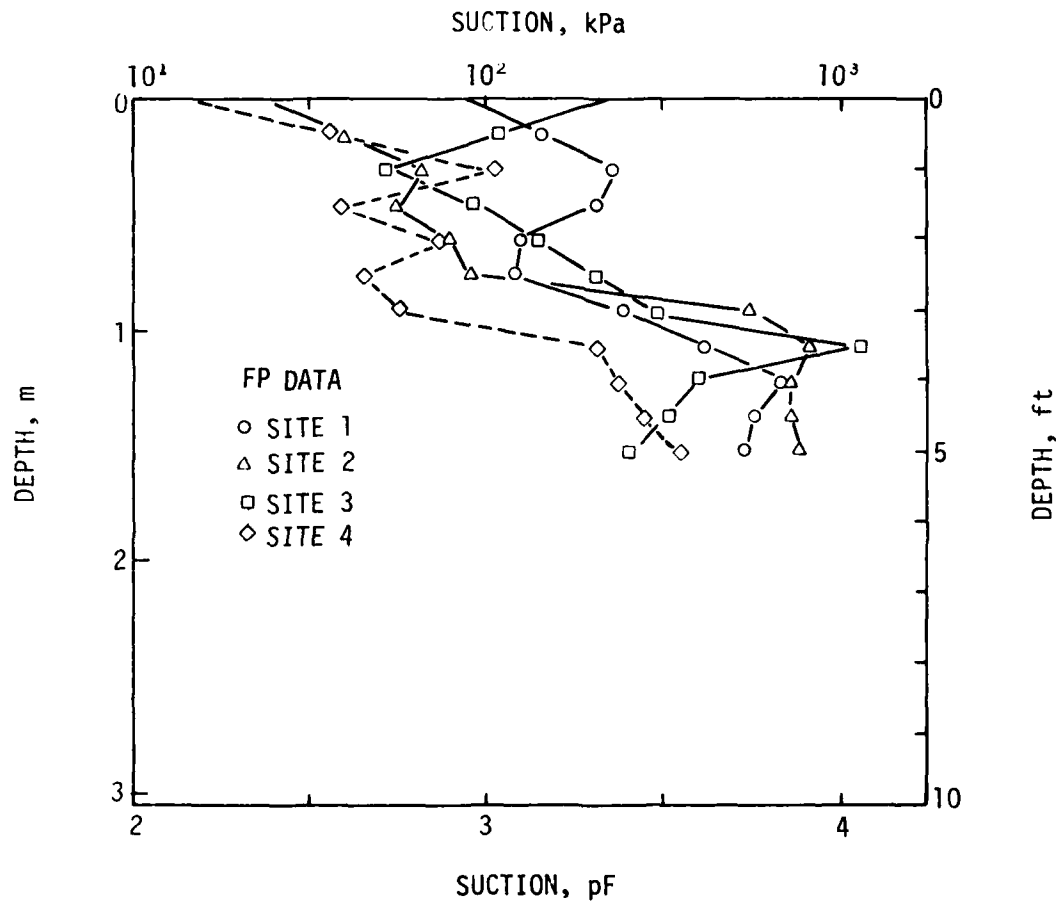


FIGURE 4-18. VARIATION OF SUCTION DURING RECHARGE AT DFW.

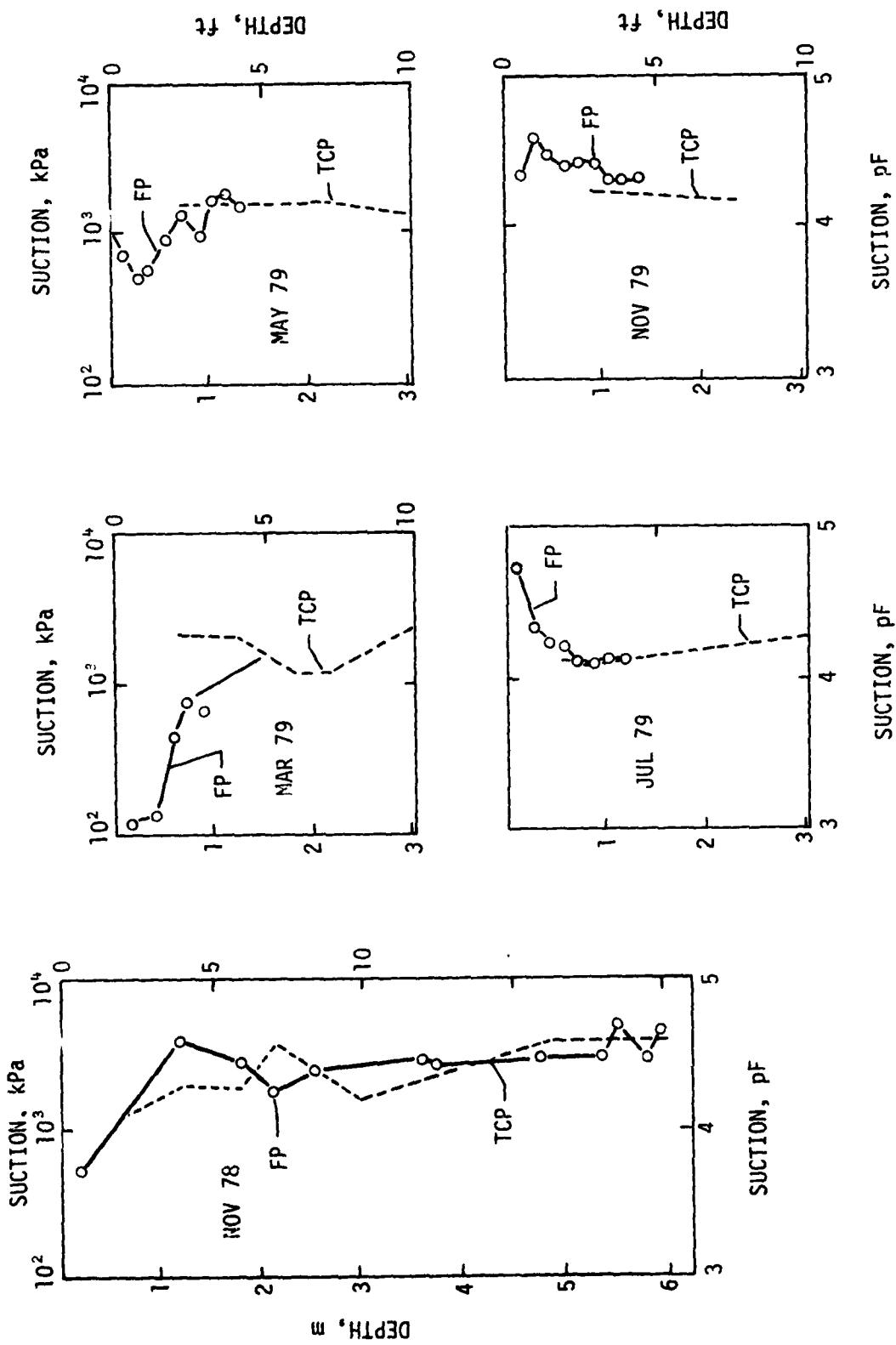


FIGURE 4-19. COMPARISON OF TCP AND FP SUCTION PROFILES AT GAL.

Results of measurements at the JSON site are shown in Figure 4-20. Note that most of the FP suction values are less than 3.0 pF in the top 0.76 m (2.5 ft) of the soil. Volume changes in soil at these levels of suction are not significant. It is also clear that the clay soil from about 0.76 m (2.5 ft) down remained at a stable suction between 3.0 and 4.0 pF throughout the observations.

Figure 4-21 shows FP data obtained from samples taken to the 6.1-m (20-ft) depth at JSON. The first boring (Jan. '79) was at a location about 91.5 m (100 yd) from the site because the site was inaccessible during rains. The profile shows ponding water at the surface resulting in wetting of the gray clay layer. However, once the wetting reached the interface with the next clay layer, the wetting effect disappears. The other 6.1-m (20-ft) boring (Dec. '79) was made near the site of the instrumentation. These data show no change with depth. The surface differences were caused by the elevation and drainage at the site.

It appears that the interface between clay layers affected the movement of water in the profile. Such features of the soil profile may provide access for water to infiltrate beneath pavements even when the pavement surface is properly maintained and provides a seal to moisture. The identification of these avenues of water movement must be a part of the investigation of the soil condition at a potential site.

Moisture Characteristics

The *soil moisture characteristic* defines the relationship between suction (or free energy of the soil water) and water content. Its value is largely a function of clay type and amount. Figures 4-22 to 4-24 show suction versus water content data for samples obtained in the field experiments at DFW, GAL, and JSON. These data are for samples taken in the top 1.5 m (5 ft) of the soil profile. In Figure 4-22, DFW data provide a moisture characteristic (m) of 0.082 for the central line shown. An abrupt change is apparent, beginning about 3.5 pF. At this point the soil response to water content changes is altered, and small increases produce relatively large reductions in suction. This aggregation behavior was discussed previously in McKeen and Nielsen (1978).

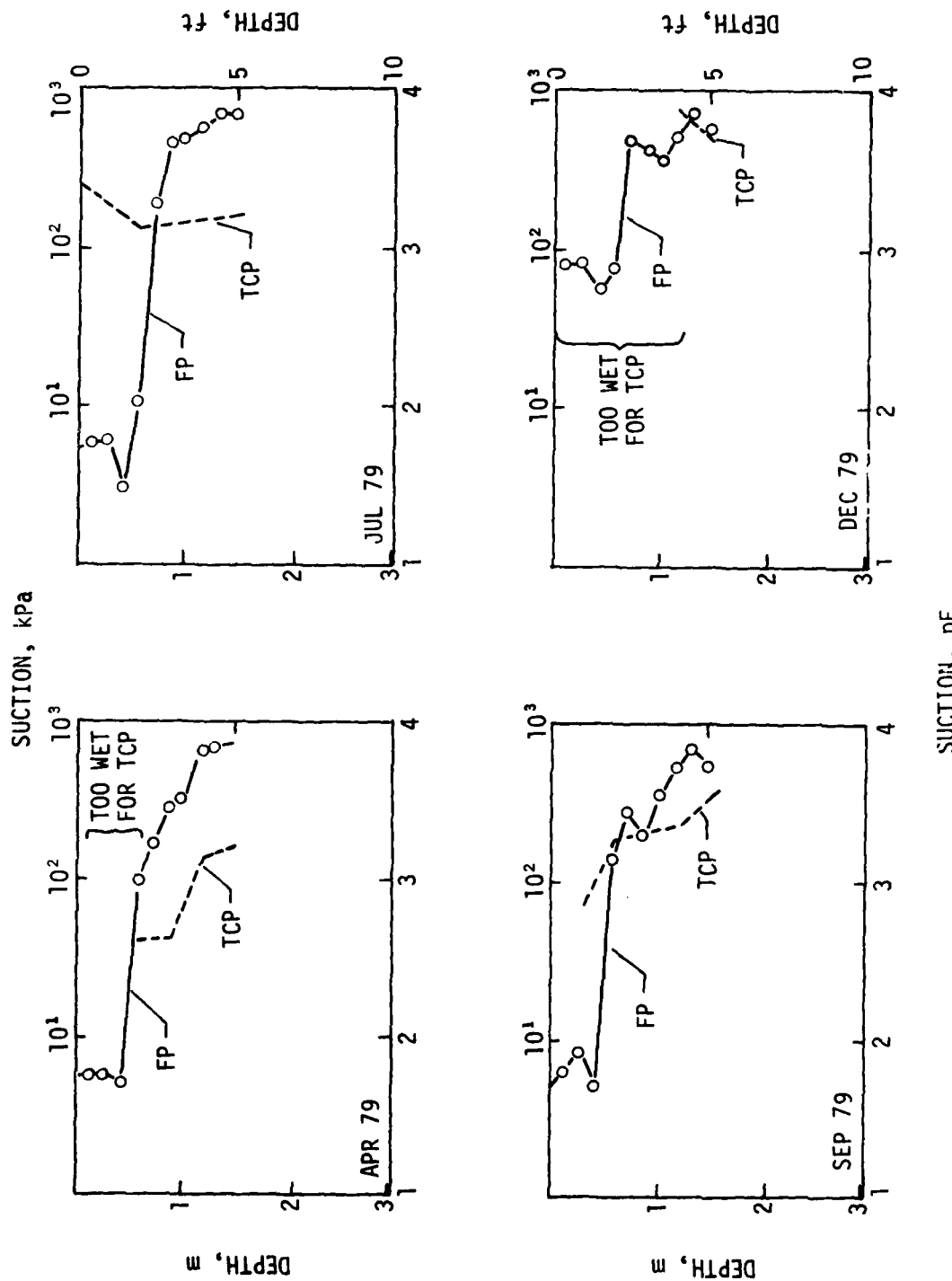


FIGURE 4-20. COMPARISON OF TCP AND FP SUCTION PROFILES AT JSN.

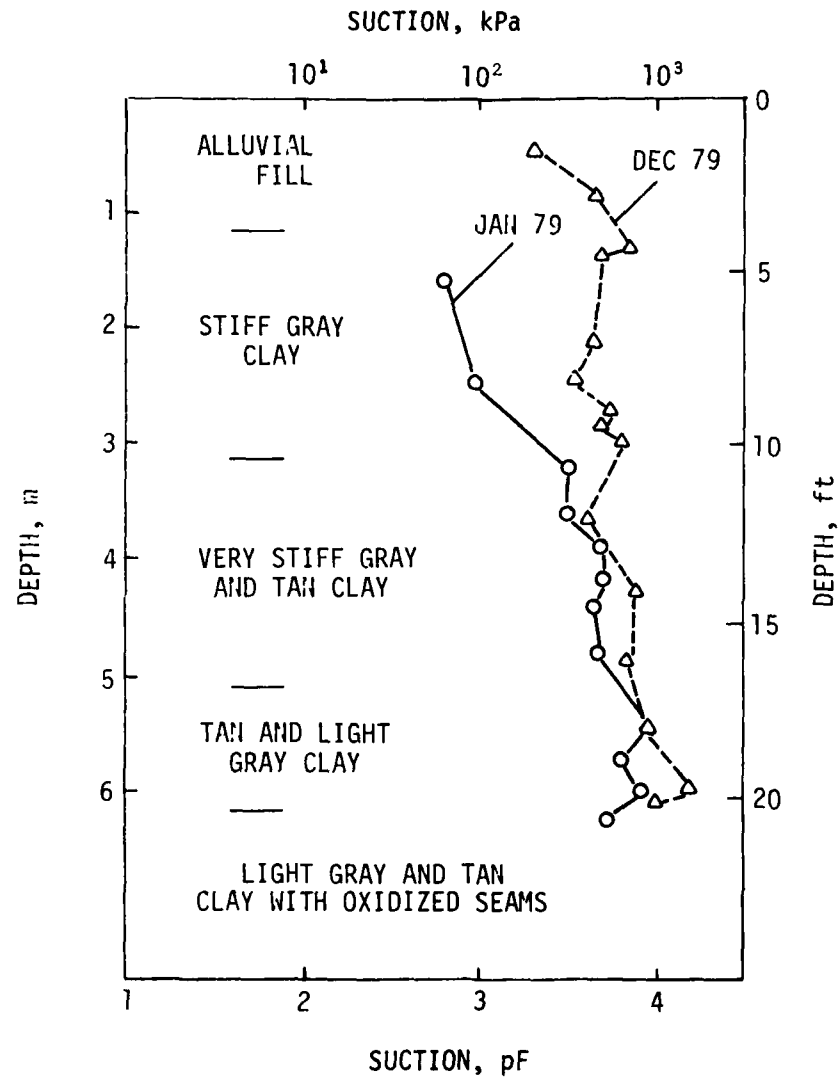


FIGURE 4-21. RESULTS OF FP SUCTION MEASUREMENTS ON BORING SAMPLE AT JSN.

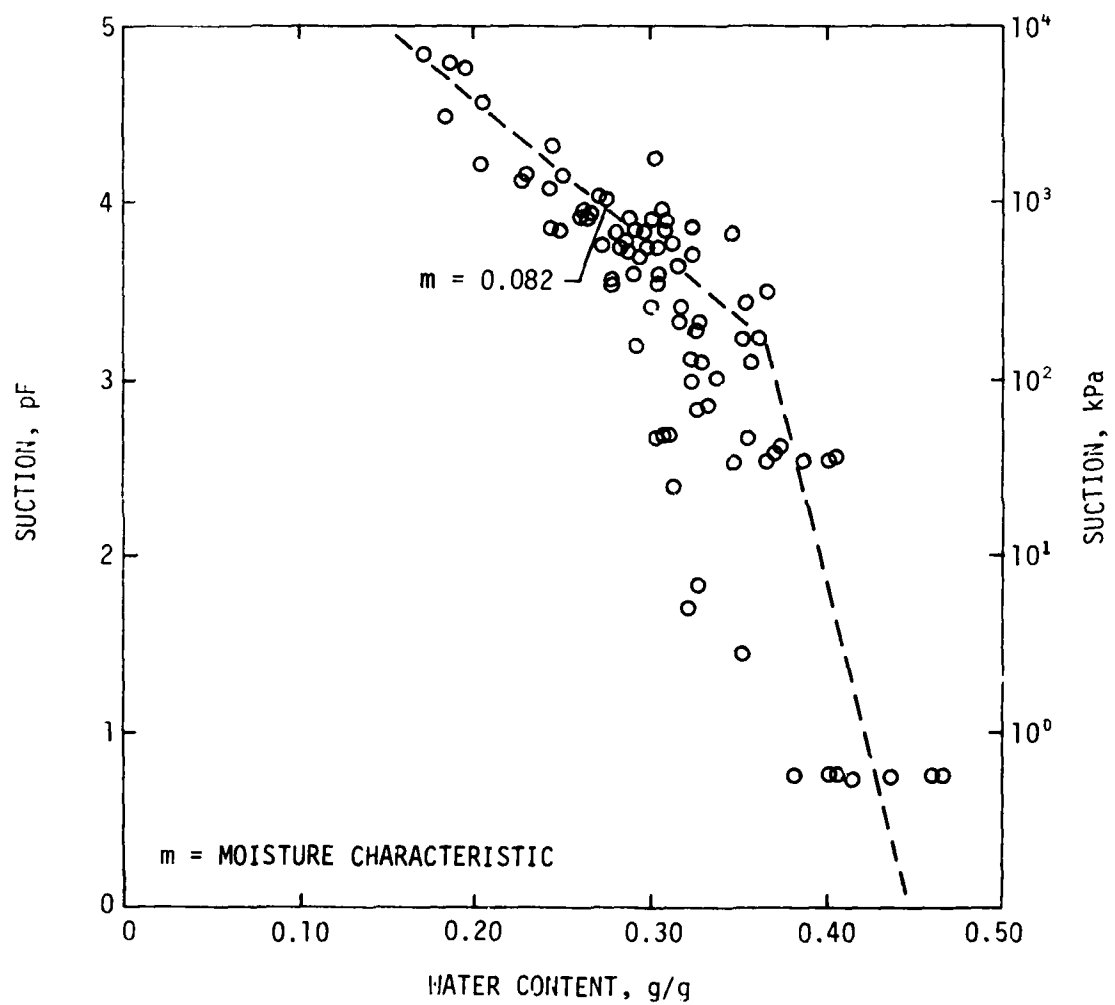


FIGURE 4-22. MOISTURE SUCTION DATA FOR DFW.

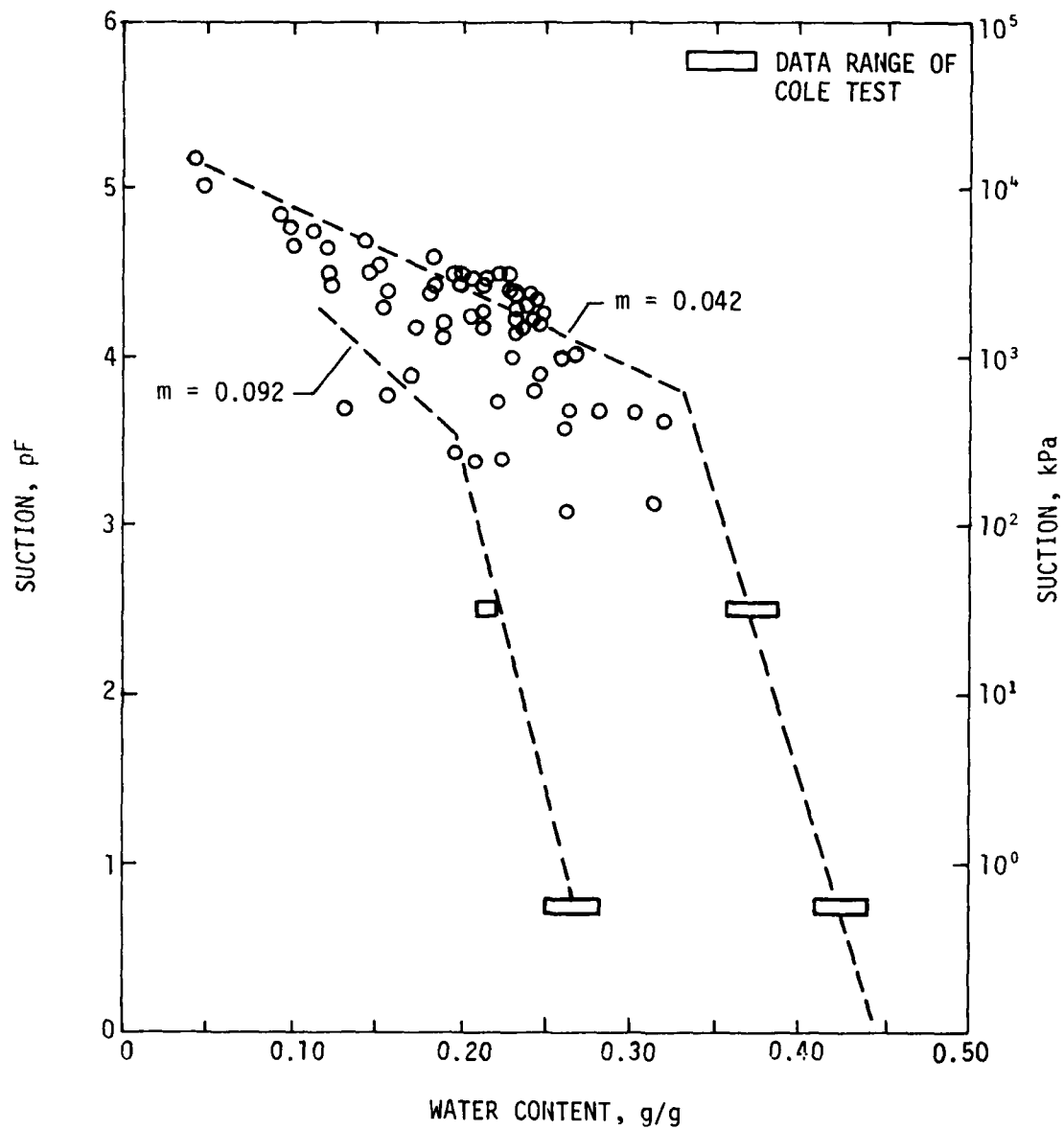


FIGURE 4-23. MOISTURE SUCTION DATA FOR GAL.

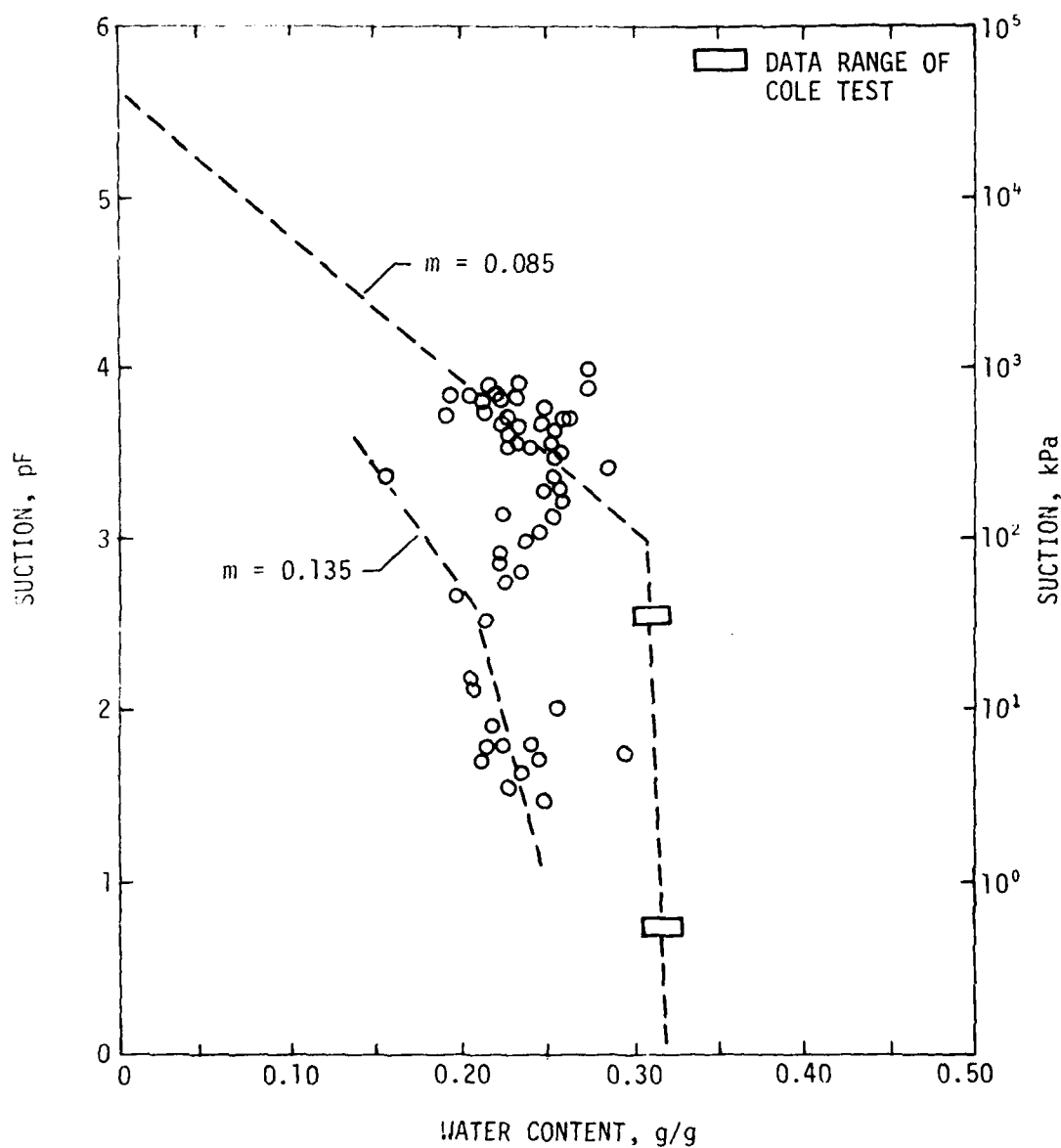


FIGURE 4-24. MOISTURE SUCTION DATA FOR JSN.

In Figure 4-23 the GAL data indicate a similar behavior, except that the surface material [top 15 cm (6 in)] is clearly different ($m = 0.092$) from the bulk of the soil ($m = 0.042$).

At JSN, a similar result was obtained because of the alluvial material at the surface. For the surface material, $m = 0.135$; the remainder of the profile is clay ($m = 0.085$). Transitions of samples from one group of data to the other were noted. The explanation for such occurrences is that the wetting phenomena reduces the suction. As suction is reduced, the soil structure is remolded and altered. Because of the structural alterations, the soil loses bearing capacity, exhibits lower density, and is not very responsive to further suction reduction. The soil will not swell under loads and may collapse or consolidate, driving out the capillary water which is at a much lower suction level. It is evident that field soils under overburden loads will not reach suctions as high as those of laboratory tests.

It is also apparent the field soils do not exhibit any significant hysteresis caused by the cycle of wetting and drying. At a given level of suction, there is little difference between water contents of the wetting and the drying soil. This lack of hysteresis contradicts a wealth of data in the literature. In all of the studies reporting hysteresis, the pressure membrane device and axis translation technique were used. All measurements made for the present study were at atmospheric pressure in contrast to the axis translational technique which raises the sample ambient pressure significantly in order to obtain measurements. Data in McKeen and Nielsen (1978) show no hysteresis. Therefore it is assumed that the suction-water content relationship is linear and nonhysteretic.

Suction Compressibility

Knowledge of suction changes must be combined with a measure of the soil response to unit suction change in order to solve engineering problems. As previously discussed, the suction compression index (the ratio of volume change to suction change) has been selected for use in this study. Some features of expansive soil behavior must be understood before proceeding further. Most expansive field soils exhibit in situ suctions between 2.5 pF and 5.0 pF. As noted in earlier work on this project (McKeen and Nielsen, 1978), soil volume response to suction changes in this range may be modeled as a linear relationship. For purposes of engineering analysis it may be assumed that swell ceases

at the capillary limit (2.53 pF) and at the shrinkage limit (5.5 to 6.0 pF). Several tests are discussed below which provide a measure of the slope of the volume-suction curve in this range.

COLE tests--The U.S. Soil Conservation Service uses the COLE test to rate soils as to their shrink-swell potential. The test was thoroughly evaluated in previous work (McKeen and Nielsen, 1978). The COLE is defined as

$$\text{COLE} = \frac{\Delta L}{L_d} = \left(\frac{\gamma_d}{\gamma_w} \right)^{1/3} - 1 = \left(\frac{\Delta V}{V_d} + 1 \right)^{1/3} - 1 \quad (4-2)$$

$\Delta L/L_d$ = linear strain relative to dry dimensions

γ_d = soil sample dry unit weight after oven drying

γ_w = soil sample dry unit weight at 2.53 pF

$\Delta V/V_d$ = volume change measured in the test

Several features of the COLE test should be noted:

1. A specific relationship between length change ($\Delta L/L_d$) and volume change ($\Delta V/V_d$) is explicitly assumed. The actual length-volume relationship in the analysis problem must be considered independently.
2. The volume change expression quantifies the response (ΔV) in relation to the oven-dry volume (V_d). Because real soils are wetter, usually between 3.0 and 4.0 pF, they fluctuate about a larger volume. Thus, COLE is probably a high estimate of volume response.
3. Standard COLE procedures report that volume change occurs between 2.53 pF and oven dry. If the shrinkage limit is assumed to occur at 5.5 pF, γ_h is obtained by dividing COLE volume change by 3.0 pF. This assumes that COLE is the change occurring over three orders of magnitude of suction change.
4. COLE procedures require coating the sample in its natural state with plastic resin. The sample is then allowed to absorb water and swell. The plastic coating restricts this volume change. For very wet samples little restriction occurs whereas considerable restriction is expected for dry samples. Previous work indicated that the plastic coating is equivalent to an average surcharge pressure of 10.3 kPa (1.5 lb/in²).

A number of COLE tests were performed on samples taken from each site under study. These data are shown in Figure 4-25. In each profile the soil

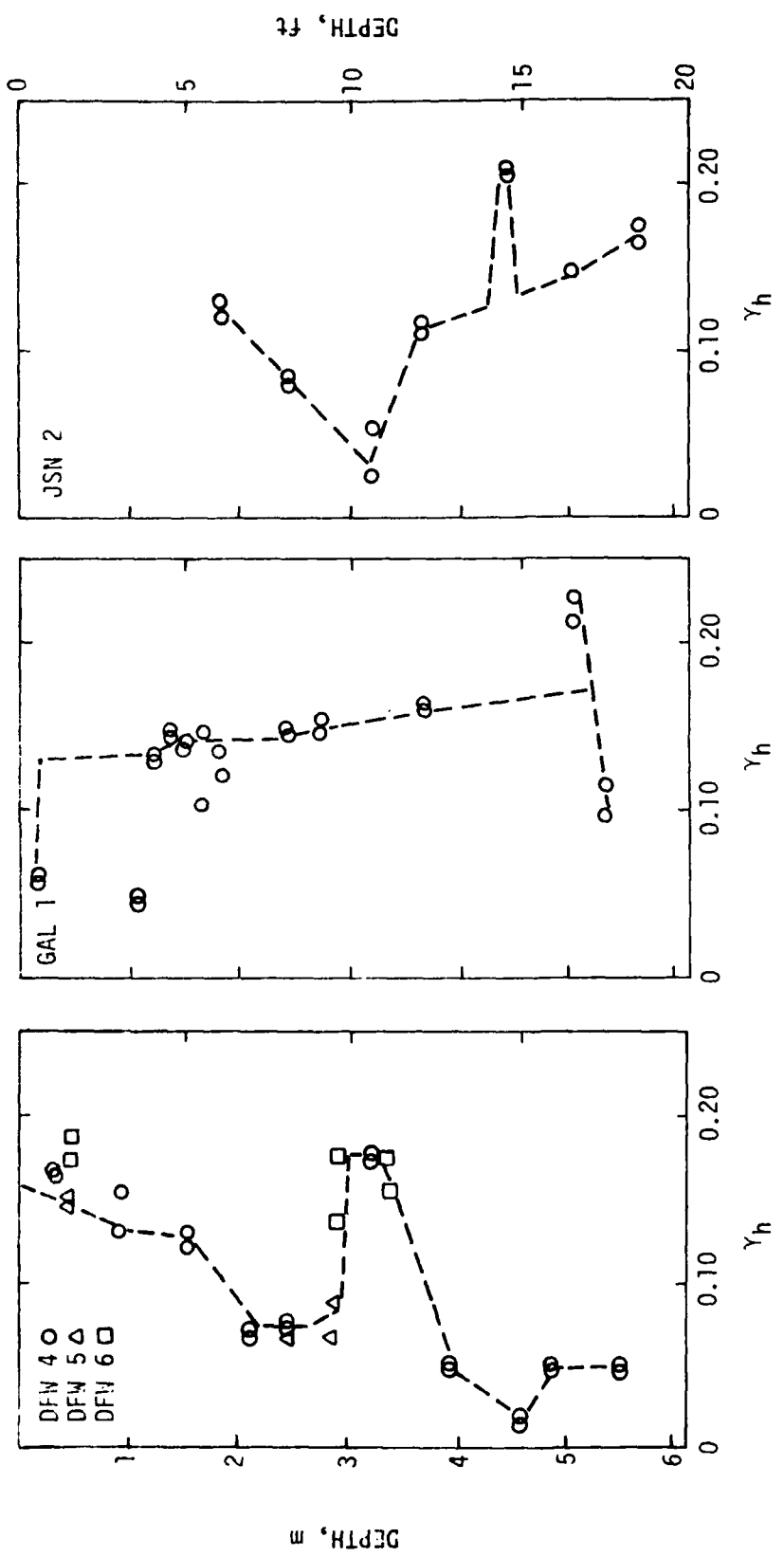


FIGURE 4-25. SUCTION COMPRESSIBILITY FROM COLE TESTS.

response varies dramatically from point to point. It is clear that any attempt to characterize these soils as isotropic homogeneous materials will require the determination of macroscopic soil parameters from a statistically sound sampling and testing program.

Clod tests--The suction compression index was also determined using the clod test, a modification of the COLE (McKeen and Nielsen, 1978). A variety of initial moisture conditions was used rather than a single starting point (2.53 pF in the COLE test). This modification allows a faster test and better description of the soil volume response. The values of the suction compression index determined from the clod tests are shown in Figure 4-26. The solid lines are the trends identified in the COLE data (Figure 4-25). The effect of the restrictions involved in the COLE test are evident in the lower γ_h values from COLE as compared to those determined from clod tests. The clod test better depicts the unrestrained response of the soil to suction variation. The COLE is perhaps better in depicting soil response under light loads; however, the actual load imposed in the test is unknown and cannot be measured. Appendix E gives the detailed procedures used in the clod test.

Chart method--The γ_h may also be determined using a chart method developed from data in the literature. Data published by the Soil Conservation Service were used as a source for COLE, percent clay, and cation exchange capacity for a large number of samples (Soil Surveys, 1973, 1974, 1976). Using a clay mineralogical classification system reported by Pearring (1968) and Holt (1969),

Holt, J. H., (1969) "A Study of Physico-Chemical, Mineralogical, and Engineering Index Properties of Fine-Grained Soils in Relation to Their Expansive Characteristics," Dissertation, Texas A & M University, College Station, Texas.

Pearring, J. R., (1968) "A Study of Basic Mineralogical Physical-Chemical, and Engineering Properties of Laterite Soils," Dissertation, Texas A & M University, College Station.

"Soil Survey Laboratory Data and Descriptions for Some Soils of Arizona," *Soil Survey Investigations Report No. 28*, (1974) Soil Conservation Service, U.S. Department of Agriculture, Washington, DC.

"Soil Survey Laboratory Data and Descriptions for Some Soils of California," *Soil Survey Investigations Report No. 24*, (June 1973) Soil Conservation Service, U.S. Department of Agriculture, Washington, DC.

"Soil Survey Laboratory Data and Description of Some Soils of Texas," *Soil Survey Investigations Report No. 30*, (January 1976) Soil Conservation Service, U. S. Department of Agriculture, Washington, DC.

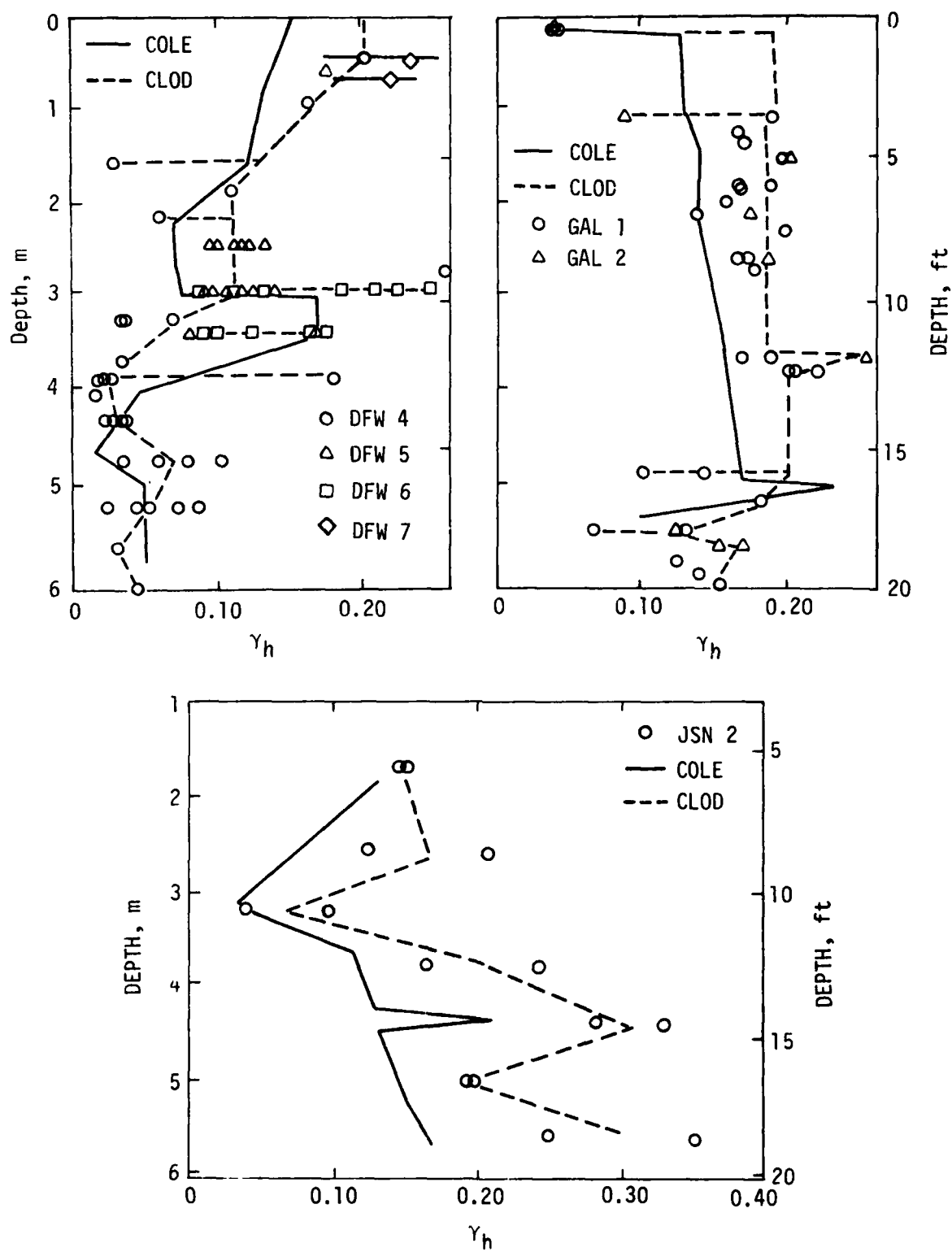


FIGURE 4-26. COMPARISON OF SUCTION COMPRESSIBILITY FROM CLOOD AND COLE TESTS.

NMERI produced a chart which gives values of γ_h without requiring suction tests. The Pearring-Holt system classified soils into mineralogical groups according to empirical relationships between mineralogy, plasticity index (PI), cation exchange capacity (CEC), and clay content (%C). CEC is measured in milliequivalents (me). Pearring and Holt segregated mineralogical groups according to clay activity (Ac) and cation exchange activity (CEAc) where

$$Ac = \frac{PI}{\%C}$$

and

$$CEAc = \frac{CEC}{\%C} \quad (4-3)$$

The NMERI chart carried this idea a step further by correlating COLE and mineralogical groups. About two hundred samples were used to develop the necessary regressions. Data were plotted on the CEAc - Ac chart. Boundaries were then established using mineralogy percentages, particularly the amount of smectite. Five regions were established, ranging from pure smectite to none. Table 4-6 shows the mineralogical makeup of the regions.

TABLE 4-6. REGION MINERALOGICAL COMPOSITION

Region	Smectite	Illite	Kaolinite	Vermiculite
I	>50	N	N	N
II	>50	Tr - 25	Tr - 25	N
IIIA	25 - 50	10 - 25	5 - 10	N
IIIB	5 - 50	5 - 25	Tr - 25	N
IVA	Tr - 10	5 - 25	5 - 50	N
IVB	Tr	10 - 25	5 - 50	N
VA	N	Tr - 25	5 - 50	Tr - 25
VB	N	N	10 - 25	Tr

All values expressed as percent of the clay fraction.

N = none

Tr = trace, <5 percent

With the regions identified, the γ_h for soils in each region were studied. Linear regressions were calculated for γ_h and percent clay in each region. All coefficients of determination were above 0.9. The γ_h values for a pure clay are shown on the chart Figure 4-27. The five regions are indicated by the Roman numerals given in Table 4-7. To obtain a γ_h value for a soil, the chart value is determined by plotting CEC versus Ac and multiplying the number obtained by the clay content as a decimal.

$$\text{Example: } \%C = 52$$

$$Ac = 0.981$$

$$PI = 51$$

$$CEAc = 0.610$$

$$CEC = 31.7 \text{ me/100 g}$$

$$\gamma_h = 0.52 (0.163) = 0.085$$

SUCTION CONCLUSIONS

The relationship of suction to water content depicts the most important feature of a clay: its ability to attract and hold water on the clay particle surfaces. It is this struggle for water between the soil and its surroundings that produces moisture movement which invariably is accompanied by volume change. As the suction goes below about 2.5 pF the principles of saturated

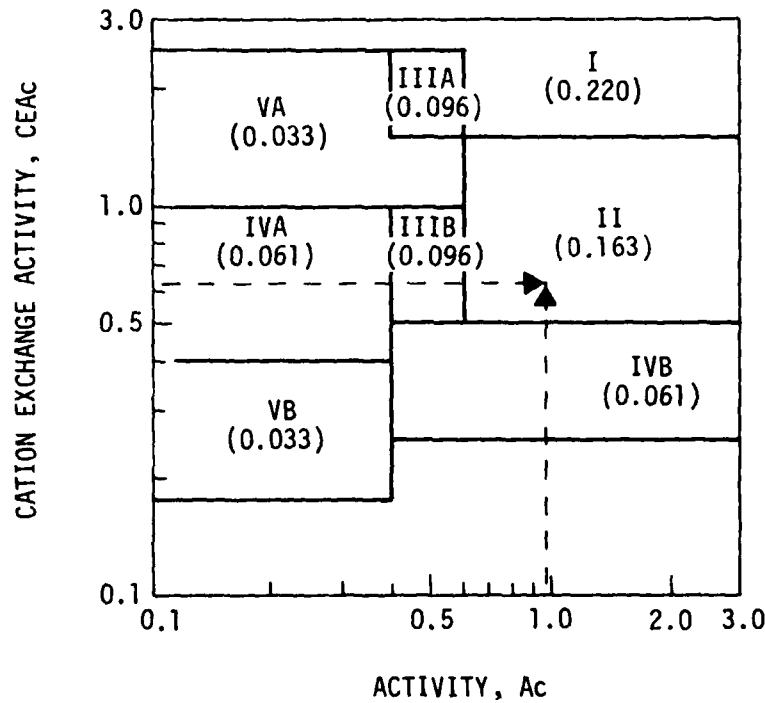


FIGURE 4-27. CHART FOR SUCTION COMPRESSIBILITY PREDICTION.

soil mechanics become increasingly accurate in modeling the soil behavior. Above about 5.5 pF the cohesion is so great that volume changes are of little consequence. The activity of importance in this study is between 2.5 and 5.5 pF, the range of activity of clay soils. The more water active in this range, the more potential for movement.

Both the TCP and FP methods of suction measurement can be used to measure soil suction. In the range of suction encountered in this study, laboratory measurements were good estimators of field suction. The FP has the advantage of a wider range than the TCP method. It is generally assumed that the TCP equilibrates faster than the FP; however, this study indicates that this is not true for ceramic-covered TCPs. Suction determinations should be made routinely on clay soils for any pavement project.

The γ_h varies dramatically within expansive soils. The variation is a natural result of the heterogeneous nature of the deposits. The characterization of such profiles must involve a large number of measurements and the determination of properties that will model the macroscopic response. The use of a few widely spaced samples is clearly a dangerous approach to soil characterization in expansive clays.

The γ_h determined from clod tests is a good measure of the unrestrained response of a soil to suction variation. Clod tests yield a better estimate of the soil behavior than the COLE test. In expansive soil profiles with wet densities of 1442 to 1762 kg/m³ (90 to 110 lb/ft³), the COLE models overburden loads to 0.61 to 0.73 m (2.0 to 2.4 ft) of overburden. Because swell reduction by loads is linear in the early stages, it is reasonable to assume that the COLE test can be used to characterize the top 1.5 to 1.8 m (5.0 to 6.0 ft) of a soil profile without making overburden load corrections to the swell predictions.

Clays which are cracked extensively are expected to swell three-dimensionally, approaching the COLE assumption. When the clay is wetter and does not contain cracks, it becomes confined by lateral soil pressure. Then virtually all volume change occurs in a vertical direction. Because of this single degree of freedom, internal shear stresses must increase significantly,

producing the slickenside feature found in active clays. The creation of these shear failures reduces the vertical swell below the total volume change that would have occurred in an unrestrained soil. This is an important consideration and virtually no information on it exists. Further consideration is given to this aspect in later parts of this report.

The presence of discontinuities in clay soil profiles has a profound influence on the in situ behavior. In the present study it was apparent that the interface between two clay layers may provide an avenue for water movement. Because of the very low permeability of intact clay, virtually all significant variation in moisture occurs by means of seams of more permeable material embedded in the clay or through fissures resulting from clay volume changes. The determination of the patterns of such features is essential to soil characterization.

V. ELEVATION STUDIES

ELEVATION DATA GATHERING

Soil and pavement profile characteristics were periodically observed by conventional rod and level surveying. Elevations were surveyed along three lines: Line 1, uncovered soil; Line 2, pavement edge; Line 3, pavement interior. Elevations were recorded at 0.6-m (2-ft) intervals, in most cases, over a horizontal distance of 40.6 m (130 ft). Several observations along these lines were made at 0.2-m (0.5-ft) intervals to study the suitability of the data for analysis using transform techniques. In addition to these observations, some measurements on rough pavements were made in June 1980 to provide a data base for the analysis. These measurements are described in Table 5-1. At each of the regular sites, a suitable bench mark was identified or constructed to serve as an elevation reference. Site layouts are illustrated in Figures 5-1 to 5-3.

TABLE 5-1. ROUGH PAVEMENTS SURVEYED

Location	Designation	Feature surveyed
Gallup Airport	GAL 4, 5, 6	Runway centerline
Jackson Airport	JSN 5, 6, 7, 8, 9	Taxiway
Jackson Airport	JSN 11, 12	Gate apron
Jackson Airport	JSN 4, 15, 16	General aviation apron
Clinton, Mississippi	JSN 10	Highway pavement
Dallas/Fort Worth Airport	DFW 7 to 12	Access roadway
Dallas Naval Air Station	NAS 1, 2	Apron/taxiway
Dallas Naval Air Station	NAS 3, 4	Taxiway
Greater Fort Worth (Amon Carter Field)	---	Visual survey and inspection of all pavements

TAXIWAY E31

38 cm (15 in) PORTLAND CEMENT CONCRETE
23 cm (9 in) CEMENT STAB BASE
23 cm (9 in) LIME STAB SOIL

PAVED SHOULDER

10 cm (4 in) ASPHALT CONCRETE
15 cm (6 in) LIME STAB SOIL

ACCESS ROAD

4 cm (1.5 in) ASPHALT CONCRETE
11 cm (4.5 in) ASPHALT CONCRETE DENSE GRADED
15 cm (6 in) LIME STAB AT 7 PERCENT
30 cm (12 in) LIME STAB AT 4 PERCENT

○ BORINGS
◊ INSTRUMENTATION SITE

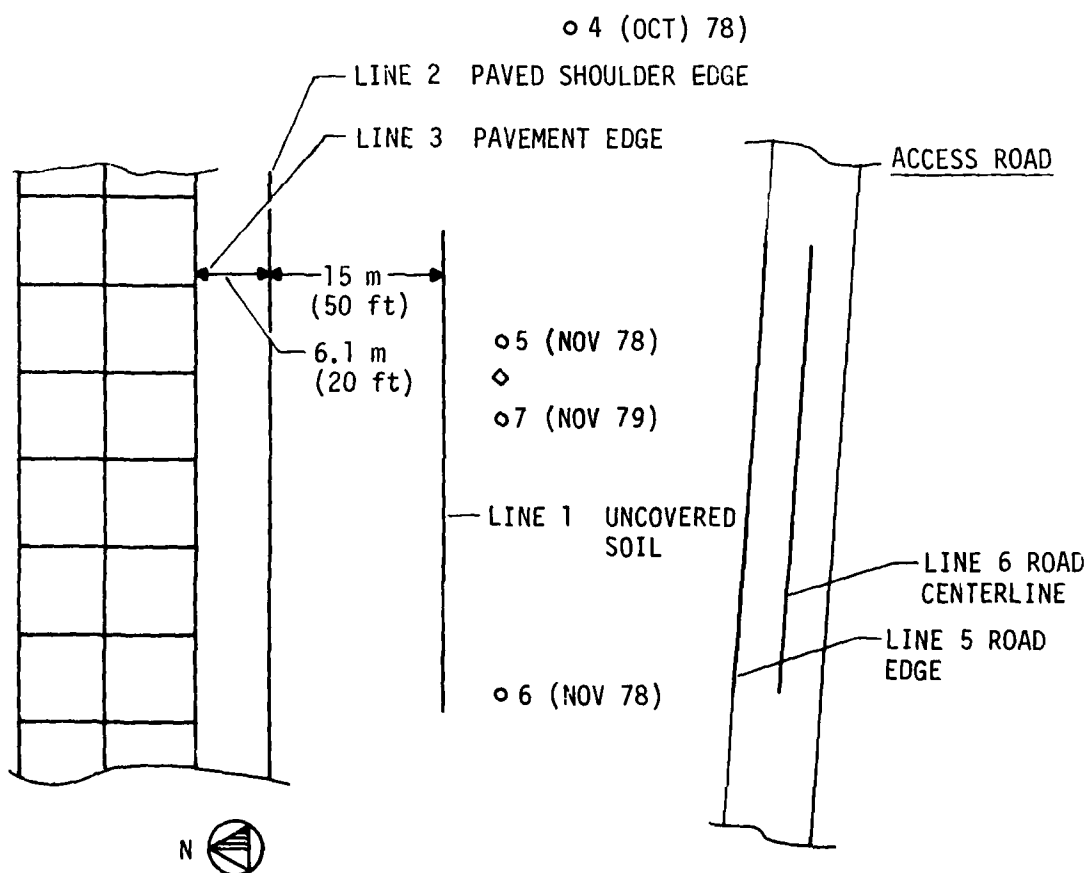


FIGURE 5-1. DALLAS/FORT WORTH REGIONAL AIRPORT SITE LAYOUT.

TAXIWAY

8 cm (3 in) BITUMINOUS SURFACE
28 cm (11 in) CEMENT TREATED BASE
15 cm (6 in) LIME TREATED SUBGRADE
22 cm (9 in) COMPAKTED SUBGRADE

SHOULDER

DOUBLE SURFACE TREATMENT
WITH COVER AGGREGATE
13 cm (5 in) SELECT BORROW
(CRUSHER FINES)

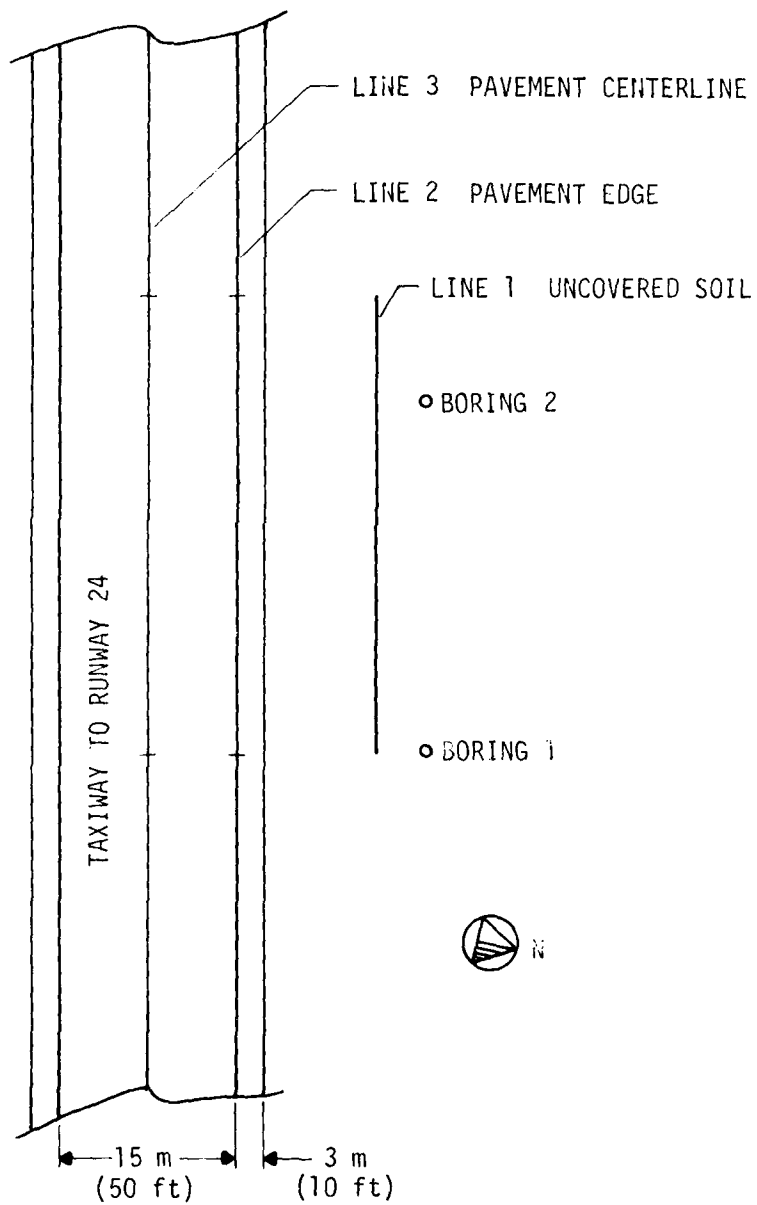


FIGURE 5-2. GALLUP MUNICIPAL AIRPORT SITE LAYOUT.

AD-A104 660

NEW MEXICO ENGINEERING RESEARCH INST ALBUQUERQUE
DESIGN OF AIRPORT PAVEMENTS FOR EXPANSIVE SOILS. (U)

F29601-76-C-0015

F/6 8/13

JAN 81 R G MCKEEN.

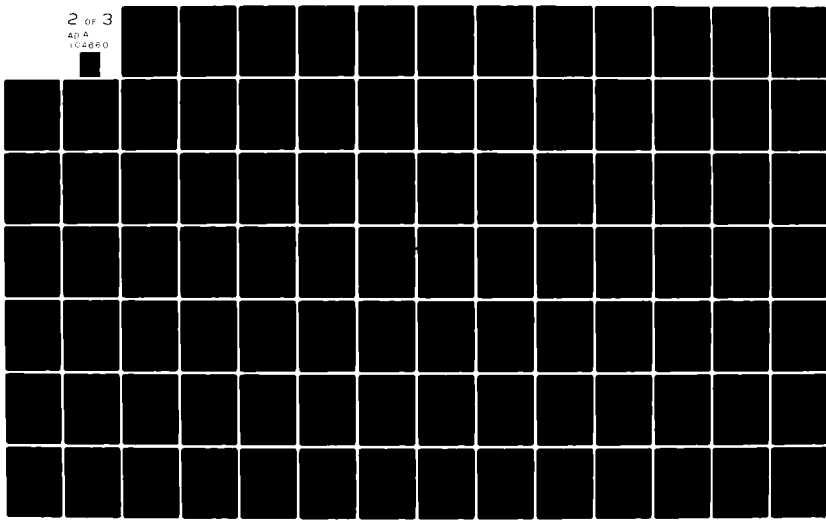
UNCLASSIFIED

NMERI-AP-37

FAA/RD-A1/25

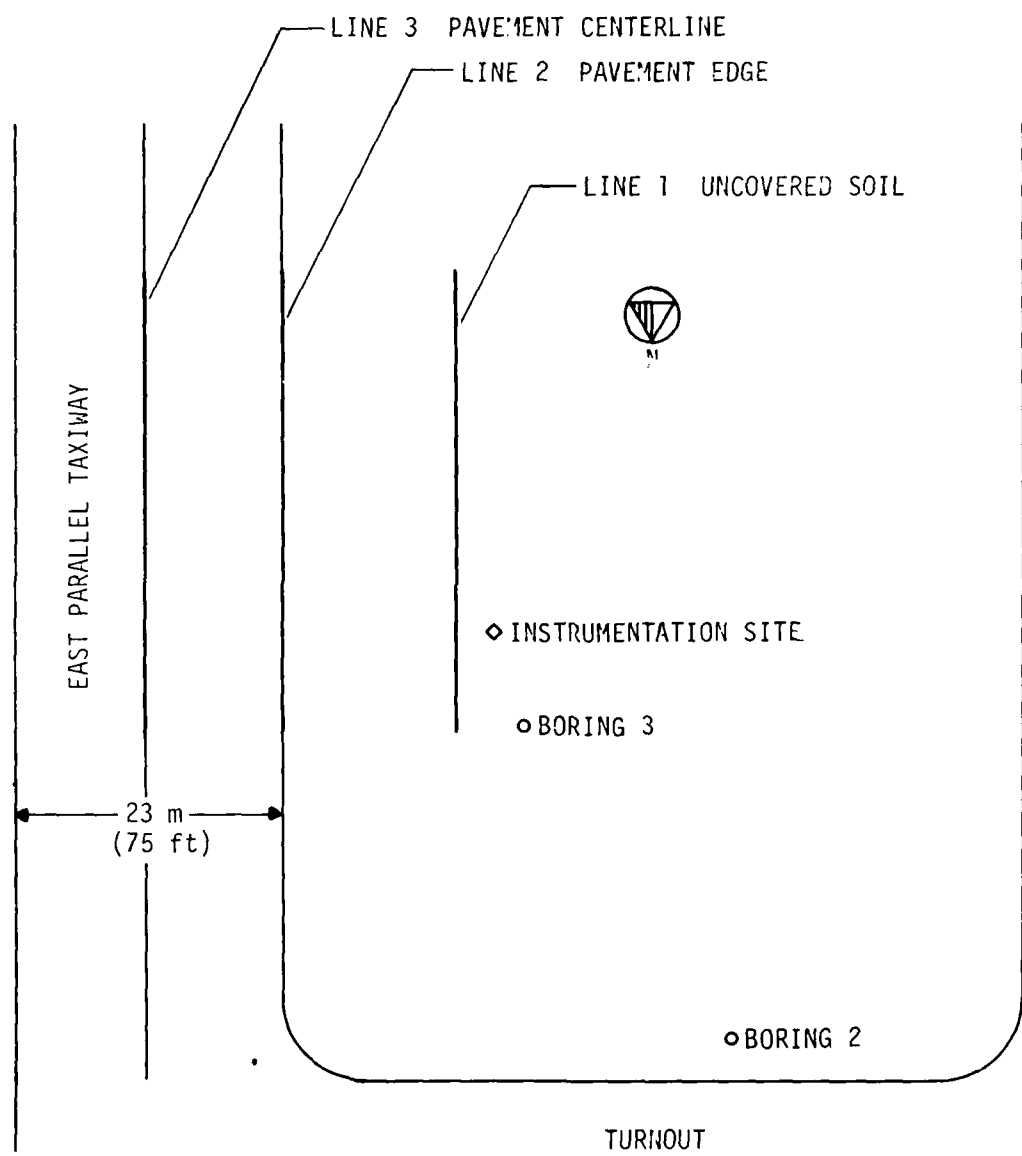
NL

2 OF 3
40 A
1C4860



EAST PARALLEL TAXIWAY

2.4 cm (6 in) ASPHALT CONCRETE OVERLAY
29.2 cm (11.5 in) PORTLAND CEMENT CONCRETE PAVEMENT
13 cm (5 in) SOIL CEMENT



GENERAL AVIATION PARKING APRON

FIGURE 5-3. JACKSON MUNICIPAL AIRPORT SITE LAYOUT.

SOIL SURFACE ELEVATIONS

Undisturbed soil profiles rise and fall with wetting and drying influences imposed by the environment. It was recognized early in the literature survey that understanding this *in situ* behavior was important. Therefore the natural soil surfaces adjacent to the pavements were observed. Figures 5-4 to 5-6 show typical data from the soil surface at each site. The GAL site is virtually flat; drainage is across Line 1 shown in Figure 5-2. At the DFW site the elevations are flat from 0 to 18 m (0 to 60 ft), then slope toward a culvert at about a 1-percent slope. Drainage is perpendicular to Line 1 shown in Figure 5-1 and toward the higher station numbers. The JSN site slopes for its entire length at about 0.5 percent. These areas were not prepared in any way.

Variations of the surface elevation were compared in several ways. In one method, the maximum elevation difference was determined at each point along a line. Results for DFW and GAL are illustrated in Figure 5-7. The DFW results reflect variation in the range of swell at regular intervals of between 3 and 6 m (10 and 26 ft). The dominant spacing is 5.5 m (18 ft). These observations are consistent with the characteristics of gilgai surfaces on clay soils. Data for the GAL site show about half as much vertical movement and no distinct pattern of response variation.

Another method of investigating the variation of soil response to environmental changes was inspection of individual profile plots for each observation date. The GAL data for June 1980 clearly indicate the varying response of the soil along the line (Figure 5-8). The elevations reflect differential soil response exhibiting a regular mound-depression pattern consistent with the gilgai model. The spacing of the mound-depression pattern is nearly 6 m (20 ft). Inspection of Figure 5-4 reveals no such distinct pattern for March 1979 (drying soil). This discrepancy leads to the conclusion that soil rate of drying varies, producing depressions where water moves out and evaporates faster. Likewise, mounds appear where water is moving out of the soil more slowly. Thus the development of differential surface features, as shown in Figure 5-8, is attributed to varying field soil permeability.

A third representation of the soil surface elevation was obtained with a fast Fourier transform to determine the amplitudes of discrete frequency components in the profile. The procedure used is explained in the next section.

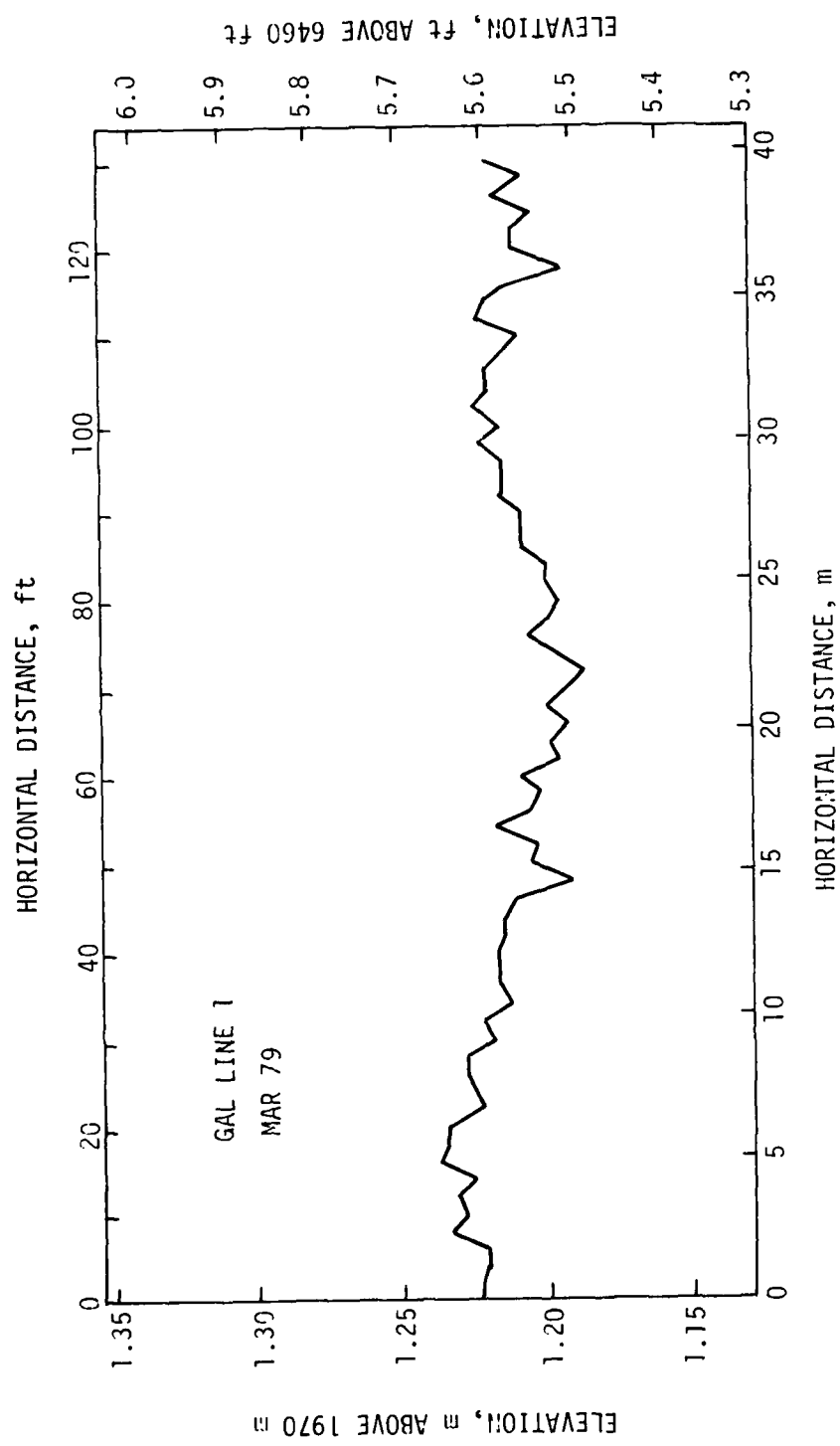


FIGURE 5-4. ELEVATIONS ON SOIL SURFACE AT GAL.

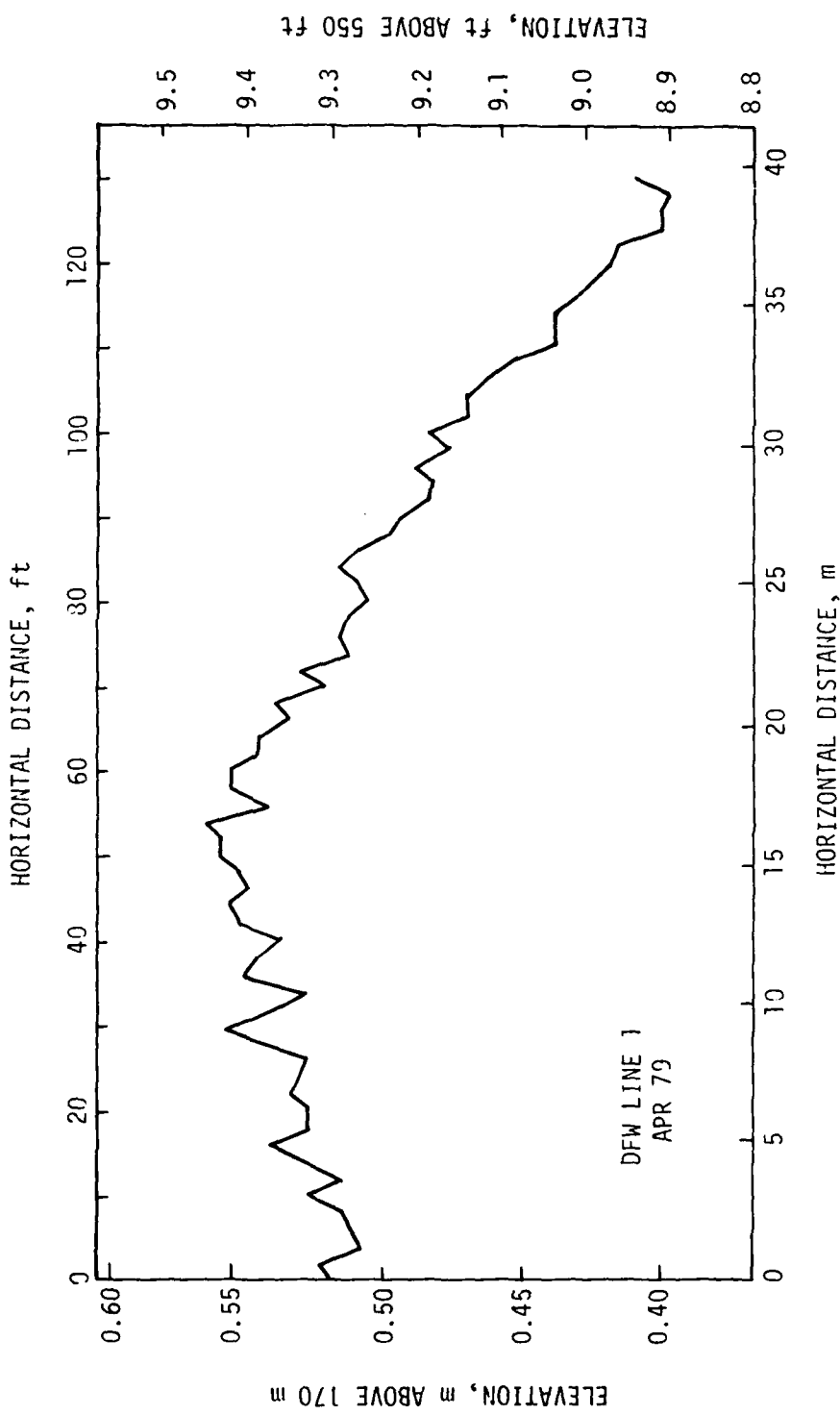


FIGURE 5-5. ELEVATIONS ON SOIL SURFACE AT DFW.

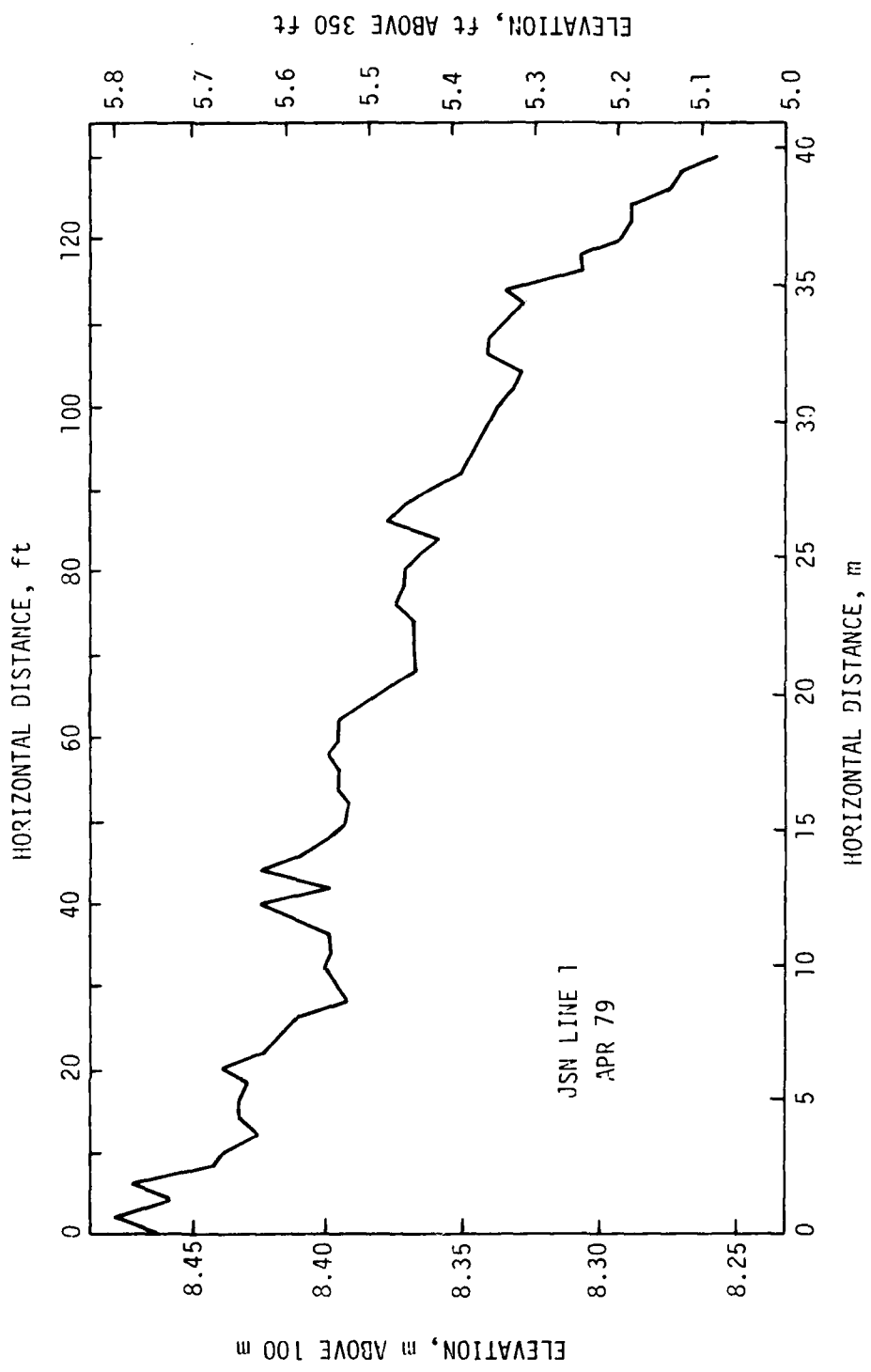


FIGURE 5-6. ELEVATIONS ON SOIL SURFACE AT JSN.

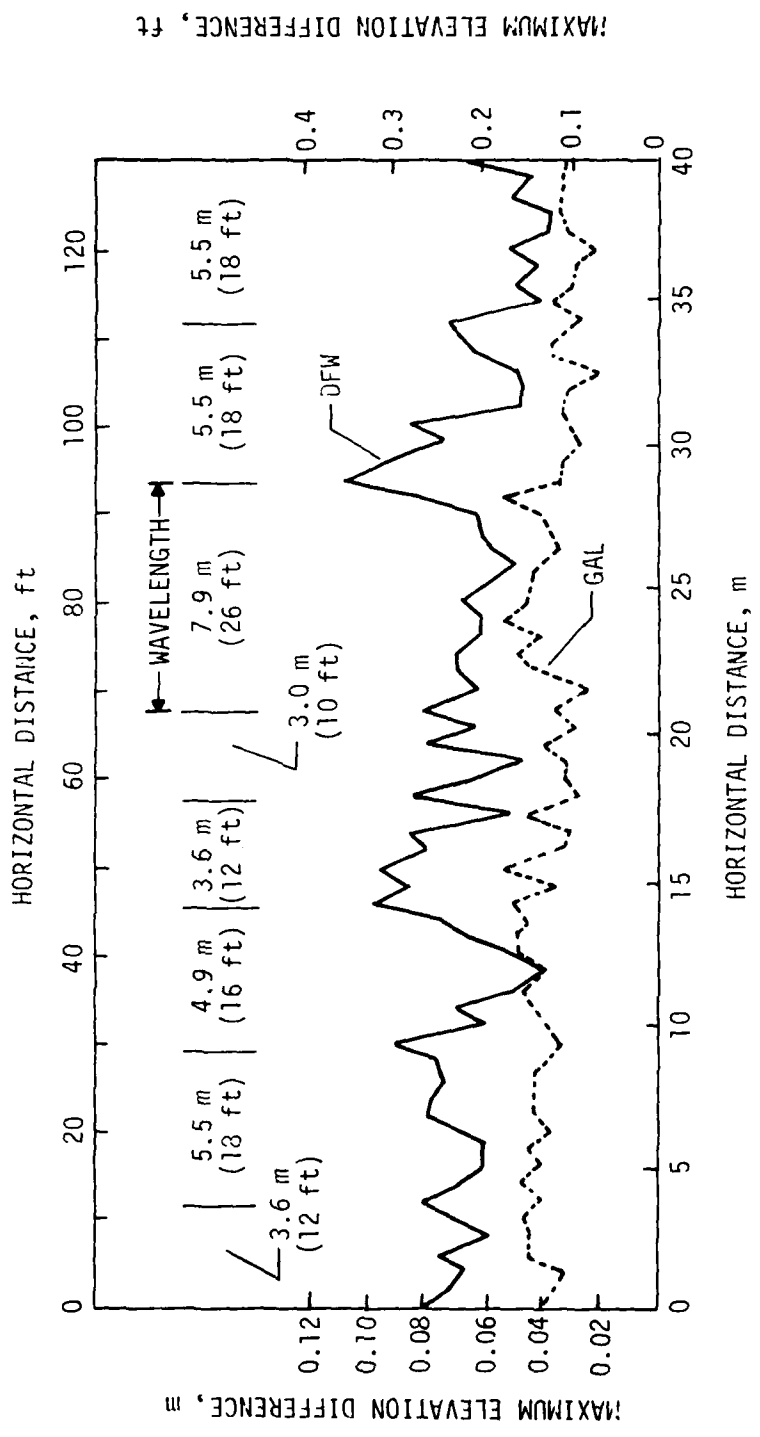


FIGURE 5-7. RANGE OF ELEVATION CHANGES AT DFW AND GAL.

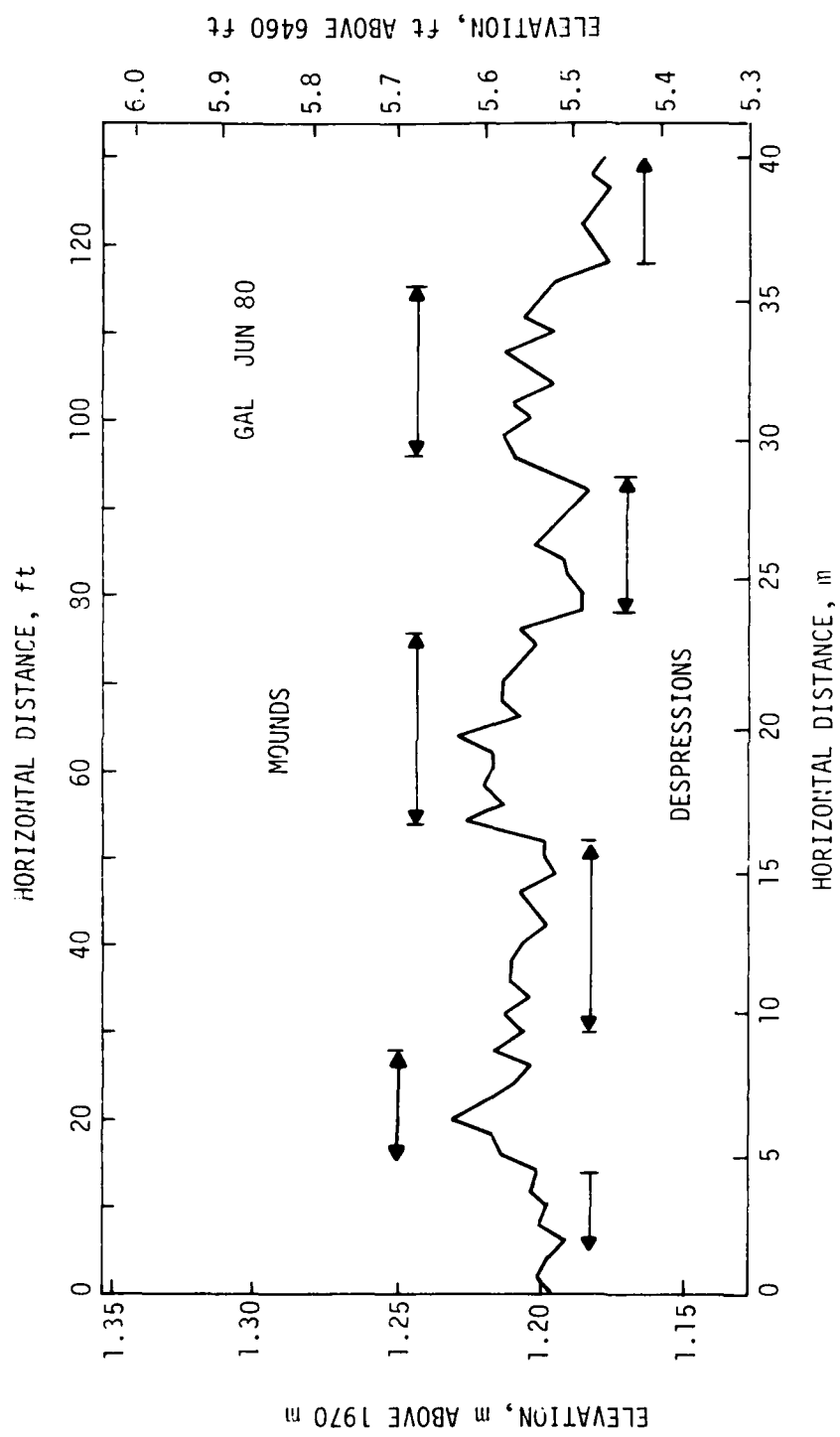


FIGURE 5-8. EVIDENCE OF SOIL DIFFERENTIAL RESPONSE AT GAL.

The fundamental idea presented in this report is that soil volume responds to soil moisture suction changes. If this is true, the field elevations should reflect this relationship. Figure 5-9 is a plot of change in elevation versus change in suction at the DFW and GAL field sites. Thirteen of the observed points were used to calculate a statistical relationship between elevation (measured at several points near the suction measurement) and the average suction in the top 1.5 m (5 ft) of the soil. Results yielded

$$\Delta H = 0.0164 - 0.2202 (\Delta h_a) \quad (5-1)$$

where

ΔH = elevation change, ft

Δh_a = average suction in the top 5 ft (1.5 m), pF

number of samples = 13

coefficient of determination (R^2) = 0.922

sample standard deviation = 0.032 ft

The two deviant points shown in Figure 5-9 indicate that the soil surface is subsiding as the soil is wetting. This behavior is contrary to the concept of the suction compression index previously presented. The complete model recommended, however, requires evaluation of the lateral restraint on the soil in the profile. This idea is illustrated in Figure 5-10. Figure 5-10a shows an uncracked, wet soil profile. When the soil dries, it cracks as shown in 5-10b at an interval H_c , to depth Z_c . Crack width at the surface is W_c ; and, assuming a triangular shape, the average crack width is $W_c/2$. It is proposed in 5-10c that, as the cracks fill with surface water, a process of horizontal swelling fills the cracks in the soil. This stress relaxation at the cracks also results in surface subsidence. Assuming that the volume of surface subsidence is equal to the volume of cracks filled, estimates of crack spacing and depth can be made. The problem is illustrated in Figure 5-11. From the information shown,

$$V_1 = (H_c - W_c) \Delta H \text{ per unit of crack length} \quad (5-2)$$

$$V_2 = \frac{W_c}{2} (Z_c - \Delta H) \text{ per unit of crack length} \quad (5-3)$$

where

ΔH = surface subsidence

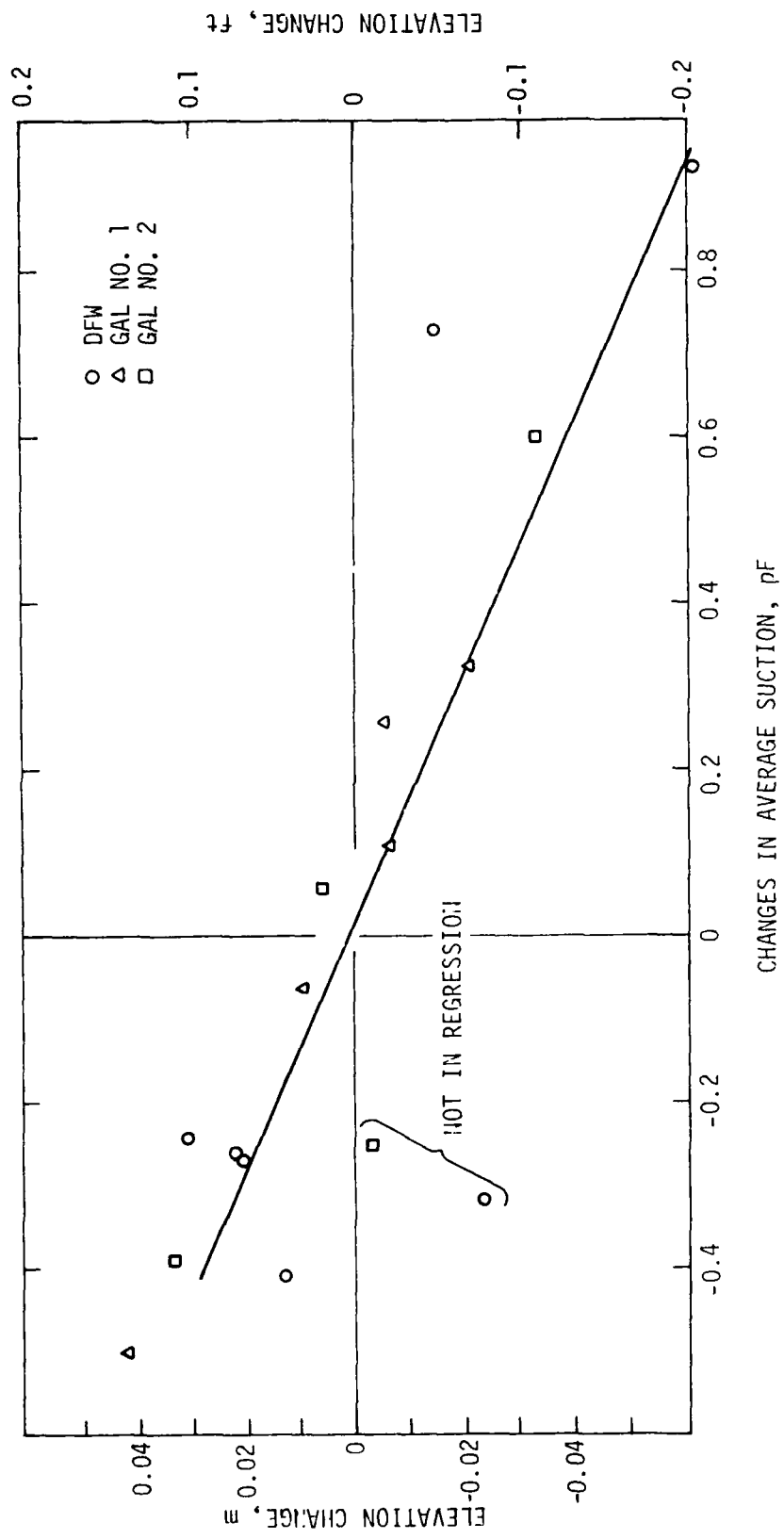
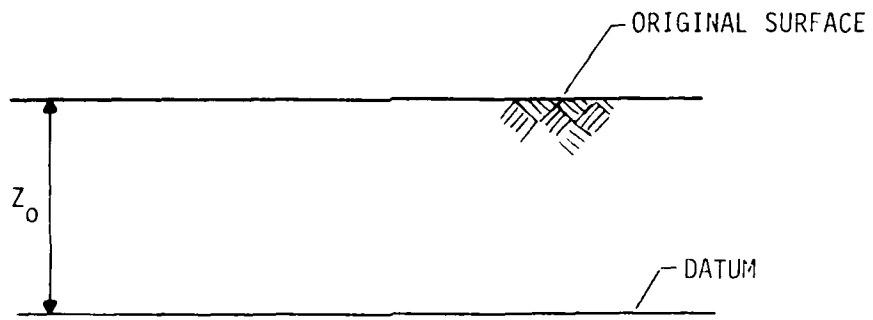
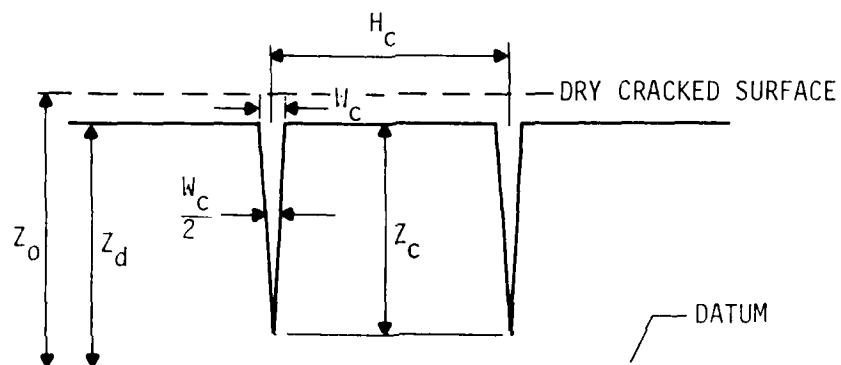


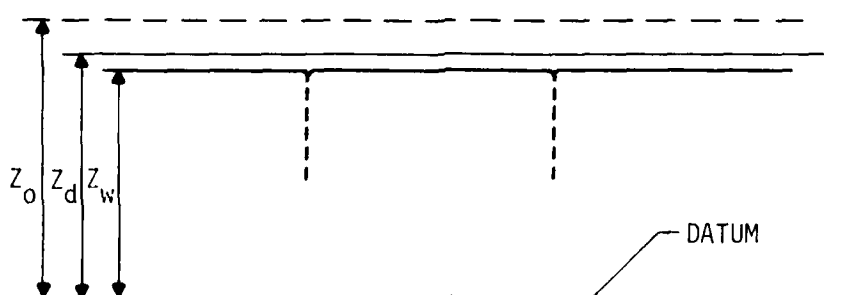
FIGURE 5-9. CORRELATION OF ELEVATION AND SUCTION CHANGES.



a. UNCRACKED, WET SOIL



b. DRIED SOIL



c. WETTING SOIL

H_c = CRACK SPACING

Z_c = CRACK DEPTH

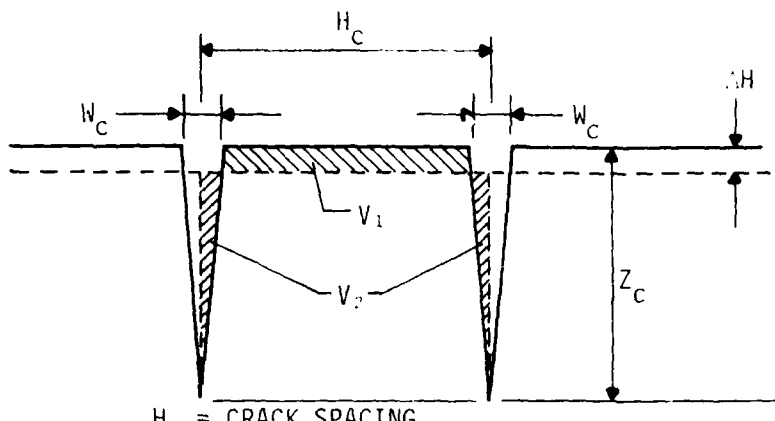
W_c = MAXIMUM CRACK
WIDTH

Z_0 = ORIGINAL DEPTH

Z_d = DEPTH AFTER DRYING

Z_w = DEPTH AFTER WETTING

FIGURE 5-10. SOIL SUBSIDENCE CAUSED BY WETTING.



H_c = CRACK SPACING
 Z_c = CRACK DEPTH
 W_c = MAXIMUM CRACK WIDTH
 ΔH = SURFACE SUBSIDENCE
 V_1 = VOLUME OF SOIL SUBSIDENCE
 V_2 = VOLUME OF SOIL TO FILL CRACKS

FIGURE 5-11. CRACK SUBSIDENCE PROBLEM.

Equating these volumes and solving for Z_c yields

$$Z_c = \Delta H \left[\frac{2H_c}{W_c} - 1 \right] \quad (5-4)$$

A comparison with observations at the sites studied is provided in Table 5-2. The results indicate that the calculated Z_c values are about twice those measured. These are interpreted as good estimates because the average crack depths were measured with a steel tape from the surface. Obviously the measurement could only be made to a depth at which the crack would not permit further penetration of the tape. The depths measured could easily be about half the actual distance.

These results show that a cracked expansive soil profile will undergo surface subsidence upon wetting. When the surface cracks are filled by slumping, swelling soil, then surface heaving occurs. The nature of cracking in an expansive soil profile very strongly influences its behavior. A method of accounting for this influence is needed.

TABLE 5-2. CRACKING CHARACTERISTICS COMPARED

	Observed values				Calculated
	H_c , m (ft)	ΔH , m (ft)	W_c , m (ft)	Z_c , m (ft)	Z_c , m (ft)
DFW Sep 79	0.9 (3.0)	0.023 (0.08)	0.051 (0.17)	0.46 (1.5)	0.79 (2.6)
GAL Nov 79	0.2 (0.8)	0.003 (0.01)	0.020 (0.07)	0.033 (0.13)	0.070 (0.23)

Notes: H_c = interval between cracks; W_c = crack width at surface; Z_c = depth of crack; ΔH = surface subsidence.

PAVEMENT SURFACE DATA ANALYSIS

Root-Mean-Square Profile Elevation

Observations of pavement surface elevations were made several times during the field experiment and coincided with determinations of soil moisture and suction. A variety of tools have been developed for analyzing roughness. In the present work, several specific methods were used. The RMS (root-mean-square) profile elevation and Δ RMS (root-mean-square elevation changes) were computed in accordance with Air Force roughness procedures (Seeman and Nielsen, 1976).

The following group of equations describe profile characteristics to be used and their interpretation.

$$\bar{y} = \frac{\sum_{i=1}^N y_i}{N} \quad (5-5)$$

where

\bar{y} = average elevation

y_i = individual elevation observation

N = total number of observations

Seeman, Douglas R., and Nielsen, John P., (1976) "Suggested Procedure to Isolate and Repair Runway Roughness," Letter Report CERF-11, University of New Mexico Civil Engineering Research Facility, Albuquerque.

$$\Delta RMS = \frac{\sum_{i=1}^{N-1} (y_{i+1} - y_i)^2}{N - 2} \quad (5-6)$$

where

ΔRMS = root-mean-square elevation change from point to point
 y_{i+1} , y_i = consecutive elevation observations
 N = total number of observations

If the ΔRMS is divided by the observation spacing of 0.61 m (2.0 ft), it then represents the RMS slope of the pavement profile.

Transform Method

Fast Fourier transforms are used widely in the analysis of signals. Their value is derived from the capability of obtaining the frequency content of a time-domain signal. Knowing the frequency content, the electrical engineer is in a much better position for solving signal analysis problems. In the present study, it has been proposed that expansive soil profiles exhibit microrelief of a periodic nature. It has also been stated that roughness of pavement structures founded on expansive soils is related to the soil microrelief. If these assertions are true, a frequency domain plot of the surface elevation data should exhibit the dominant frequency components characteristic of the soil-pavement system. Thus the fast Fourier transformation appears to be a viable analysis technique.

Pavement surface analysis involved calculating, from the space domain data, a discrete frequency domain function using a fast Fourier transform. Literally this transform expresses the data in terms of a complex Fourier series in the space domain. The Fourier coefficients are calculated using a least squares technique. In the frequency domain, half of the amplitude components are plotted versus frequency for use in the analysis. Each component also has a phase angle associated with it.

The first step in the procedure is to obtain a space domain function representing the observed data set as a complex Fourier series. The observed data can be fitted exactly using a Fourier series.

$$y(x_n) = \frac{a_0}{2} + \sum_{n=0}^{N-1} \left(a_n \cos \frac{2\pi mn}{N} + b_n \sin \frac{2\pi mn}{N} \right) \quad (5-7)$$

where

$y(x_n)$ = the observed elevation at x_n
 x_n = horizontal station of elevation measurement

$m, n = 0, 1, 2 \dots N$

N = number of observations

a_n, b_n = Fourier coefficients

Equivalent forms for this equation are given by Stearns (1975):

$$y(x_n) = \frac{A_0}{2} + \sum_{n=0}^{N-1} A_n \cos (nf_0 x_n + \alpha_n) \quad (5-8)$$

$$y(x_n) = \sum_{n=-N/2}^{+N/2} C_n \exp(jnf_0 x_n) \quad (5-9)$$

Frequency components of the function are expressed using a discrete Fourier transform (DFT):

$$\bar{F}(jw) = \sum_{n=0}^{N-1} y(x_n) e^{-j2\pi mn/N} \quad (5-10)$$

$$= \sum_{n=0}^{N-1} y(x_n) \cos\left(\frac{2\pi mn}{N}\right) - j \sum_{n=0}^{N-1} y(x_n) \sin\left(\frac{2\pi mn}{N}\right) \quad (5-11)$$

where

$\bar{F}(jw)$ = complex Fourier transform of $y(x_n)$

$y(x_n)$ = observed elevation at x_n

m, n = same as above

$j = \sqrt{-1}$

Some features of this technique are illustrated in the following example. Figure 5-12a is a space domain plot of 64 elevation observations taken on the surface of an aircraft parking apron at the JSN site. The data are properly

Stearns, Samuel D., (1975) *Digital Signal Analysis*, Hayden Book Company, Rochelle Park, N.J.

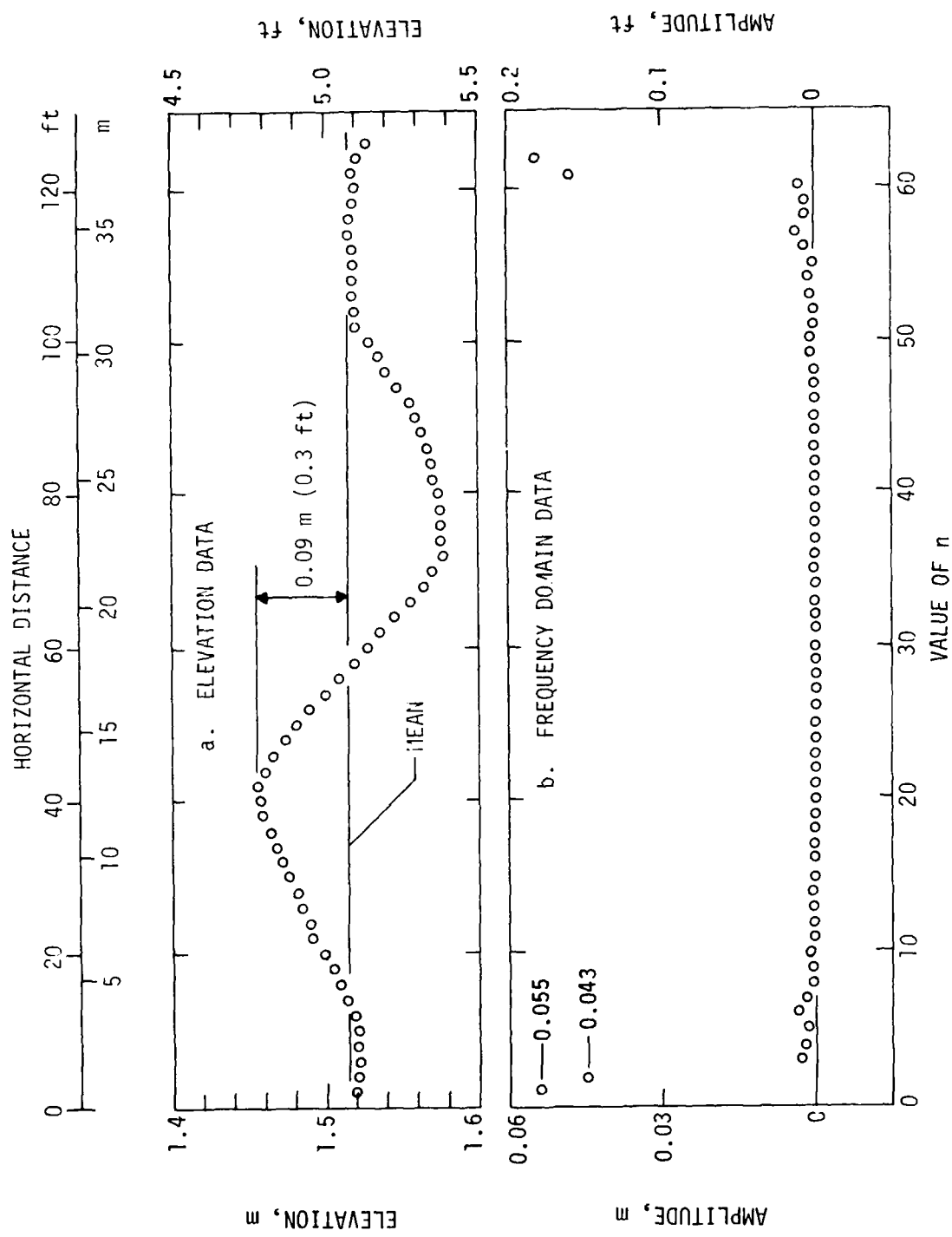


FIGURE 5-12. ILLUSTRATION OF FOURIER TRANSFORMATION OF A PROFILE.

represented here as discrete points rather than a continuous function. In Figure 5-12b the amplitude versus frequency data calculated using the DFT are shown. Because the Fourier series is complex, each frequency component also has a phase angle associated with it which is not shown. Notice that the data in Figure 5-12a appear to be periodic with a half-amplitude of 0.09 m (0.3 ft) and a wavelength (or period) of about 30.5 m (100 ft). In the frequency domain, the surface is expressed at discrete frequency components. The frequencies are determined by the sampling interval and overall length. Thus,

$$f_n = \frac{n}{L} = \frac{1}{\lambda_n} \quad (5-12)$$

f_n = spatial frequency of the nth component, cycles per unit length

$n = 1, 2, 3 \dots N$

L = overall sampling length

λ_n = wavelength of the nth component

Therefore, the frequencies with estimates are

$$f_1 = \frac{1}{128 \text{ ft}} = 0.0078 \text{ ft}^{-1} (0.26 \text{ m}^{-1})$$

$$f_2 = \frac{2}{128 \text{ ft}} = 0.0156 \text{ ft}^{-1} (0.0513 \text{ m}^{-1})$$

• • •

• • •

• • •

$$f_{32} = \frac{32}{128 \text{ ft}} = 0.250 \text{ ft}^{-1} (0.820 \text{ m}^{-1})$$

These have corresponding wavelengths, λ_n , as follows:

$$\lambda_1 = \frac{1}{f_1} = 128 \text{ ft} (39.0 \text{ m})$$

$$\lambda_2 = \frac{1}{f_2} = 64.0 \text{ ft} (19.5 \text{ m})$$

• • •

• • •

• • •

$$\lambda_{32} = \frac{1}{f_{32}} = 4.0 \text{ ft} (1.2 \text{ m})$$

Only half of the computed frequency components are unique. Thus, for 64 data points in the space domain, only 32 points in the frequency domain are determined. The data folds at the midpoint (called the *foldover* or *Nyquist frequency*) and subsequent points are a mirror image of the first half. The sampling procedure used in the present study yielded frequency components from 0.026 m^{-1} (0.0078 ft^{-1}) to 0.82 m^{-1} (0.25 ft^{-1}). The computed frequency components are at discrete frequencies determined by the sampling procedure. Because the real profile contains components at different frequencies from the calculated components, the real frequency components are distributed to those calculated. In the above example (Figure 5-12a), the wavelength was about 30.5 m (100 ft). The frequency domain represents this as two components at wavelengths of 39.0 m (128 ft) and 19.5 m (64 ft). Note that the sum of the amplitudes of these components is about equal to the space domain half-amplitude; i.e., $0.055 \text{ m} + 0.043 \text{ m} = 0.097 \text{ m}$ ($0.18 \text{ ft} + 0.16 \text{ ft} = 0.34 \text{ ft}$). The overestimate of amplitude results from phase differences in the components.

Appendix B contains frequency domain data for the pavements studied. Regression lines were fitted through the data. Equations are of the following form:

$$a_n = c(f)^b \quad (5-13)$$

a_n = half-amplitude, ft

f = spatial frequency, ft^{-1}

c, b = regression constants

Velasco (1980) has computed statistical relationships between these regression coefficients and a number of factors involved in the swelling soil problem for highway pavements. Table 5-3 shows the factors considered in the regression. The results of his study yielded regression equations for the prediction of c and b for a particular profile. These could then be related to the Present Serviceability Index of a highway pavement surface built on the soil.

Velasco, Manuel O., (1980) "Pavement Roughness on Expansive Clays," Thesis at Texas A & M University, College Station, Texas.

TABLE 5-3. VELASCO'S INDEPENDENT VARIABLES

DEPTH = effective depth of pavement, inches

TH = mean value of Thornthwaite moisture index for a 20-year period

RANGE = range of values of Thornthwaite moisture index for a 20-year period

TIME = time since construction or last rehabilitation before the roughness was measured, years

CLAY = percent clay (grain size less than 0.002 mm)

AC = activity $\left(\frac{\text{Plasticity Index}}{\text{CLAY}} \right)$

CEC = cation exchange capacity, $\frac{\text{me}}{100 \text{ g}}$

CEAC = cation exchange activity $\left(\frac{\text{CEC}}{\text{CLAY}} \right)$

COLE = coefficient of linear extensibility

ESP = exchange sodium percentage

Velasco, 1980

Other Methods

Stone and Dugundji (1965) studied microrelief of a variety of surfaces for the purpose of developing a quantitative method of expressing the surface characteristics. Their approach involved using a cosine series representation of the profile and determining a number of quantitative characteristics of the profile. A group of similar characteristics were obtained in the present study as shown in Table 5-4. Data computed for the pavements in this study are shown in Appendix C.

An important pavement characteristic for the study of roughness is the stiffness of the pavement structure itself. The approach taken by Velasco (1980) used an effective depth of the pavement structure to characterize it for study. The same approach was followed to characterize the pavements studied in the present work.

TABLE 5-4. ADDITIONAL PROFILE CHARACTERISTICS

Symbol	Method of determination	Interpretation
Σa_n	$\Sigma a_n = \sum_{n=1}^{N/2} a_n$	Maximum height of microrelief features possible
M	$M = \frac{1}{2} \sum_{n=1}^{N/2} (a_n)^2$	Maximum level of change expected as the profile is traversed
P	$P = \frac{N/2}{\sum_{n=1}^{N/2} n^2 a_n^2}$	Average steepness of microrelief features encountered
K	$K = \frac{1}{2} \left[\sum_{n=0}^{N/2} a_n^4 : \left(\sum a_n^2 \right)^2 \right]$	A measure of the periodicity of the microrelief
\bar{A}	$\bar{A} = \frac{N/2}{\sum_{n=1}^{N/2} a_n} \cos \frac{2\pi n}{N}$	A weighted amplitude

Stone, R. O., and Dugundji, T., (1965) "A Study of Microrelief--Its Mapping, Classification, and Quantification by Means of a Fourier Analysis," *Engineering Geology*, Vol. 1, No. 2:39-187.

VI. AIRCRAFT SIMULATIONS

TAXI COMPUTER CODE

The TAXI computer code was developed to determine the dynamic response of an aircraft to runway roughness during takeoff and constant-speed taxi. The mathematical model has been programmed for a CDC 6600 digital computer, and results to date indicate good agreement with results of runs using instrumented aircraft. The procedures involved are fully described by Gerardi and Lohwasser (1973 and 1974). A summary of this description is provided here from Gerardi (1978).

The general mathematical model is represented as an asymmetrical body with a nose and a right and a left main landing gear. Each landing-gear strut is assumed to have point contact with the profile, and it is assumed that each landing gear traverses a different profile. The model has aerodynamic lift and drag and thrust applied at the center of gravity of the aircraft.

The aircraft is free to roll, pitch, plunge, and translate horizontally down the runway, and each landing-gear unsprung mass is free to translate vertically. In addition to these rigid-body degrees of freedom, there are up to 30 flexible modes of vibration. This aircraft motion is controlled by the landing-gear strut forces and the lift, drag, thrust, and resisting parameters of aircraft mass and inertia.

The landing-gear struts are nonlinear, single- or double-acting, oleopneumatic energy-absorbing devices and are represented in the model as the sum of the three forces--pneumatic, hydraulic, and strut bearing friction....

The runway elevation data are input into the model in 0.61-m (2-ft) long increments. The profile is made continuous by fitting the following polynomial through three points and the slope at the end of the previous profile segment:

$$y(x) = a_1 + a_2x + a_3x^2 + a_4x^3 \quad (6-1)$$

Gerardi, Anthony G., (1978) "Dynamic Response of Aircraft to Pavement Unevenness," in *Research in Airport Pavements*, Special Report 175, Transportation Research Board, Washington, DC, pp. 91-96.

Gerardi, Anthony G. and Lohwasser, Adolph K., (1973) *Computer Program for the Prediction of Aircraft Response to Runway Roughness, Volume I, Program Development*, U. S. Air Force Flight Dynamics Laboratory, Technical Report No. AFWL-TR-73-109, Vol. I, Wright-Patterson AFB, Ohio.

Gerardi, Anthony G. and Lohwasser, Adolph K., (1974) *Computer Program for the Prediction of Aircraft Response to Runway Roughness, Volume II, Sample Manual*, U.S. Air Force Flight Dynamics Laboratory, Technical Report No. AFWL-TR-73-109, Vol. II, Wright-Patterson AFB, Ohio.

where a_1 , a_2 , a_3 , and a_4 = coefficients derived from elevation and slope data. This is done for each of the three lines of runway-profile data.

Several factors involved in the present study affect the use of this simulation. The data were gathered on the basis of anticipated roughness patterns caused by swelling soil. Wavelengths expected were in the range 3.0 to 15.0 m (10 to 50 ft). The longest wavelength obtained was the sampling interval (the total length sampled): 39.0 m (128 ft).

Previous studies investigated the effect of filtering out long wavelength components (Seeman and Nielsen, 1976). These results indicate that at the 39.0 m (128 ft) cut-off the accelerations are about 96 percent of those for the unfiltered data for the B727-100 aircraft. It was concluded that the predicted accelerations were satisfactory for roughness evaluation in this study. Results reported are averaged over four runs on the same pavement segment, where the segments were placed head to toe.

A single profile was available for each observation made. Thus, all of the landing gear was assumed to traverse the same profile.

Another factor not simulated is the flexural movement of the pavement structure. The TAXI code considers the surface of the pavement to be rigid; the pavement is not allowed to deflect under aircraft loads. Some of the roughness encountered on airport pavements results from the elastic deflection of the pavement under aircraft loads. These deflections are particularly important for large aircraft and light pavements. In this study all pavements are treated as rigid structures in the aircraft simulations.

Four aircraft were used in the simulation: the B727-100, B727-200, DC-9-40, and the TriJet Composite. Input aircraft characteristics and initial conditions are in Appendix D. All aircraft simulations consisted of constant-speed taxi runs over the pavement profiles under study.

RESULTS OF SIMULATIONS

Results of aircraft simulations are presented in Table 6-1. The results shown are RMS and peak accelerations at the pilot station. The date column in

TABLE 6-1a. RESULTS OF AIRCRAFT SIMULATIONS

Line	Date	Aircraft	Pilot station acceleration, g	
			RMS	Peak
Gal 2	Mar 79	727-100	0.0126	0.046
	Mar 79	DC-9-40	0.0136	0.049
	Mar 79	727-200	0.0103	0.042
	Mar 79	Wide body	0.0151	0.063
	Jun 80	727-100	0.0111	0.046
Gal 3	Mar 79	727-100	0.0219	0.059
	Mar 79	DC-9-40	0.0136	0.045
	Mar 79	727-200	0.0080	0.026
	Mar 79	Wide body	0.0203	0.056
	Jun 80	727-100	0.0174	0.047
DFW 2	Apr 79	727-100	0.0147	0.049
	May 79	727-100	0.0164	0.050
	Jul 79	727-100	0.0161	0.057
	Sep 79	727-100	0.0157	0.052
	Nov 79	727-100	0.0149	0.054
	Mar 80	727-100	0.0162	0.057
	Jun 80	727-100	0.0161	0.058
	Apr 79	DC-9-40	0.0144	0.053
	Apr 79	727-200	0.0198	0.074
	Apr 79	Wide body	0.0213	0.081
DFW 3	Apr 79	727-100	0.0113	0.035
	Apr 79	DC-9-40	0.0082	0.030
	Apr 79	727-200	0.0134	0.040
	Apr 79	Wide body	0.0143	0.049
DFW 5	Apr 79	727-100	0.1270	0.387
	May 79	727-100	0.1255	0.386
	Jul 79	727-100	0.1263	0.381
	Sep 79	727-100	0.1243	0.370
	Nov 79	727-100	0.1262	0.390
	Mar 80	727-100	0.1183	0.327
	Jun 80	727-100	0.1185	0.335
	Apr 79	DC-9-40	0.1201	0.821
	Apr 79	727-200	0.0905	0.344
	Apr 79	Wide body	0.1407	0.452
DFW 6	May 79	727-100	0.1056	0.300
	Jul 79	727-100	0.1050	0.290

TABLE 6-1b. RESULTS OF AIRCRAFT SIMULATIONS

Line	Date	Aircraft	Pilot station acceleration, g	
			RMS	Peak
DFW 7	Jun 80	727-100	0.0146	0.057
DFW 8	Jun 80	727-100	0.0324	0.108
DFW 9	Jun 80	727-100	0.0711	0.192
DFW 10	Jun 80	727-100	0.0557	0.147
DFW 11	Jun 80	727-100	0.1296	0.372
DFW 12	Jun 80	727-100	0.1330	0.390
	Jun 80	727-200	0.0974	0.397
	Jun 80	DC-9-40	0.0973	0.441
	Jun 80	Wide body	0.1452	0.561
DFW 13	Jun 80	727-100	0.0317	0.089
DFW 14	Jun 80	727-100	0.0243	0.068
	Jun 80	727-200	0.0179	0.060
	Jun 80	DC-9-40	0.0317	0.096
	Jun 80	Wide body	0.0261	0.076
NAS 1	Jun 80	727-100	0.1326	0.393
	Jun 80	727-200	0.1243	0.468
	Jun 80	DC-9-40	0.1071	0.450
	Jun 80	Wide body	0.1508	0.588
NAS 2	Jun 80	727-100	0.1495	0.431
	Jun 80	727-200	0.1069	0.422
	Jun 80	DC-9-40	0.1126	0.474
	Jun 80	Wide body	0.1651	0.642
NAS 3	Jun 80	727-100	0.0805	0.224
	Jun 80	727-200	0.0620	0.230
	Jun 80	DC-9-40	0.0844	0.564
	Jun 80	Wide body	0.1011	0.331
NAS 4	Jun 80	727-100	0.0772	0.199
GAL 4	Jun 80	727-100	0.0268	0.085
	Jun 80	727-200	0.0339	0.114
	Jun 80	DC-9-40	0.0398	0.131
GAL 5	Jun 80	727-100	0.0556	0.143
	Jun 80	727-200	0.0396	0.148
	Jun 80	DC-9-40	0.0412	0.215
GAL 6	Jun 80	727-100	0.0587	0.158
	Jun 80	727-200	0.0430	0.188
	Jun 80	DC-9-40	0.0512	0.374

TABLE 6-1c. RESULTS OF AIRCRAFT SIMULATIONS

Line	Date	Aircraft	Pilot station acceleration, g	
			RMS	Peak
JSN 2	Apr 79	727-100	0.0789	0.220
	Apr 79	727-200	0.0560	0.205
	Apr 79	DC-9-40	0.0707	0.468
	Apr 79	Wide body	0.0878	0.324
	Jun 80	727-100	0.0776	0.215
JSN 3	Apr 79	727-100	0.0825	0.232
	Apr 79	727-200	0.0615	0.236
	Apr 79	DC-9-40	0.0757	0.487
	Apr 79	Wide body	0.0927	0.352
	Jun 80	727-100	0.0814	0.242
JSN 4	Dec 79	727-100	0.1017	0.277
	Dec 79	727-200	0.0537	0.152
JSN 5	Jun 80	727-100	0.0934	0.249
JSN 6	Jun 80	727-100	0.0575	0.158
		727-200	0.0575	0.114
		DC-9-40	0.0427	0.226
		Wide body	0.0582	0.175
JSN 7	Jun 80	727-100	0.1007	0.244
		727-200	0.0772	0.286
		DC-9-40	0.0955	0.627
		Wide body	0.0962	0.449
JSN 8	Jun 80	727-100	0.0962	0.218
JSN 9	Jun 80	727-100	0.0440	0.102
JSN 10	Jun 80	727-100	0.0254	0.086
		727-200	0.0316	0.110
		DC-9-40	0.0392	0.212
		Wide body	0.0367	0.143
JSN 11	Jun 80	727-100	0.1465	0.387
JSN 12	Jun 80	727-100	0.1288	0.300
JSN 15	Jun 80	727-100	0.0991	0.281
		727-200	0.0698	0.220
		DC-9-40	0.1118	0.517
		Wide body	0.1041	0.285
JSN 16	Jun 80	727-100	0.0944	0.220

the table gives the date of the pavement profile observation. The pilot station acceleration was used for evaluation of roughness, and 0.4 g was the acceptable acceleration criterion initially used.

The acceptability of the pavement surface is clearly dependent on the aircraft under consideration. The same pavement may produce different responses in different aircraft. For example, at NAS 3, JSN 7, and JSN 15, the smaller aircraft, DC-9-40, exhibits higher peak acceleration response in the simulation.

Reports from users indicate that the stretched B727-200 has more trouble with roughness than the B727-100 model. No such consistent trend is evident in the data. It is believed the TAXI assumption of a rigid profile may contribute to this discrepancy. The TAXI simulation estimates are not as good for the B727-200 as for other aircraft. Peculiarities in the strut for this aircraft are not modeled properly in the TAXI program.

VII. ANALYSIS AND CONCLUSIONS

The current state of the art for characterizing expansive soils involves the mathematical description of a three-dimensional response surface. In this scheme, the soil volume is related to mechanical load and suction applied to the soil. Natural near-surface expansive clays contain other features, such as cracks and seams, that affect soil behavior significantly and must enter into the characterization process.

HEAVE PREDICTION

In Figure 5-9, surface elevation change is plotted against suction change. Several important facts were observed: (1) At two points the actual soil behavior was opposite to the behavior predicted by a suction model. (2) The error variance was apparently a function of the magnitude of suction change. (3) The elevation changes are serially correlated with the suction change, as indicated by the Durbin-Watson Test (Durbin and Watson, 1951). These observations clearly indicate that no simple model can describe field behavior of expansive soils adequately for pavement design.

The two deviant points in Figure 5-9 indicate that surface subsidence may accompany initial wetting in cracked expansive clays. This surface subsidence is attributed to heave caused by lack of lateral restraint on the soil at the cracks. Although it is a principal factor in soil behavior, lateral restraint is not accounted for in current state-of-the-art behavior models. These models either assume a fully restrained condition or arbitrarily assign a value of lateral restraint.

Lateral restraint may be thought of in terms of a factor, f :

$$f = \frac{(\Delta L/L)_z}{\Delta V/V_i} \quad (7-1)$$

where

f = lateral restraint factor

$(\Delta L/L)_z$ = vertical linear strain

$\Delta V/V_i$ = volumetric strain

Durbin, J., and Watson, G. S., (1951) "Testing for Serial Correlation in Least Squares Regression II," *Biometrika*, Vol. 38:159-78.

The f value will vary between 1, for fully restrained, and $1/3$, for unrestrained conditions.

However, roughness is the primary concern of the present research, and more accurate prediction of heave does not predict roughness. Therefore, it is reasonable to proceed toward a characterization of wavelength and amplitude rather than the prediction of heave.

PREDICTION OF WEIGHTED AMPLITUDE

Weighted amplitude, \bar{A} , represents a weighted value of the amplitudes of the frequency components calculated from the elevation data. The weights put more value on longer wavelength components. The calculation of the weighted amplitude was described in Table 5-4. The next step is to determine a method of predicting \bar{A} at a site.

Figure 7-1 shows the weighted amplitudes for the uncovered soil studied in the field experiment. The complexity of the behavior results from the soil cracking. Also, the suction values used in this plot were determined at discrete points, whereas the \bar{A} values are a function of data taken over a 39-m (128-ft) distance.

If the soil equilibrates normally beneath a newly constructed pavement, the soil volume changes only once. The associated suction change would represent the profile moving from a dry condition during construction to a condition of equilibrium beneath the pavement. For example, DFW reached 4.0 pF (10^3 kPa) at its driest point. At depth the suction is at 3.5 pF. Normal equilibrium would involve a change in suction of 0.5 pF. Some cases warrant a design based on saturated conditions. Previous work (McKeen and Nielsen, 1978) indicated an end suction of 2.5 pF would be appropriate for this case. The suction change would then be 1.5 pF.

The point is that initial and final suction profiles must be selected by the designer. With the profiles determined, the data in Figure 7-1 suggest the following relationships for predicting \bar{A} :

Site	Slope ($\Delta\bar{A}$)
DFW	0.021 m per pF (0.068 ft per pF)
JSN	0.023 m per pF (0.075 ft per pF)
GAL	0.015 m per pF (0.050 ft per pF)

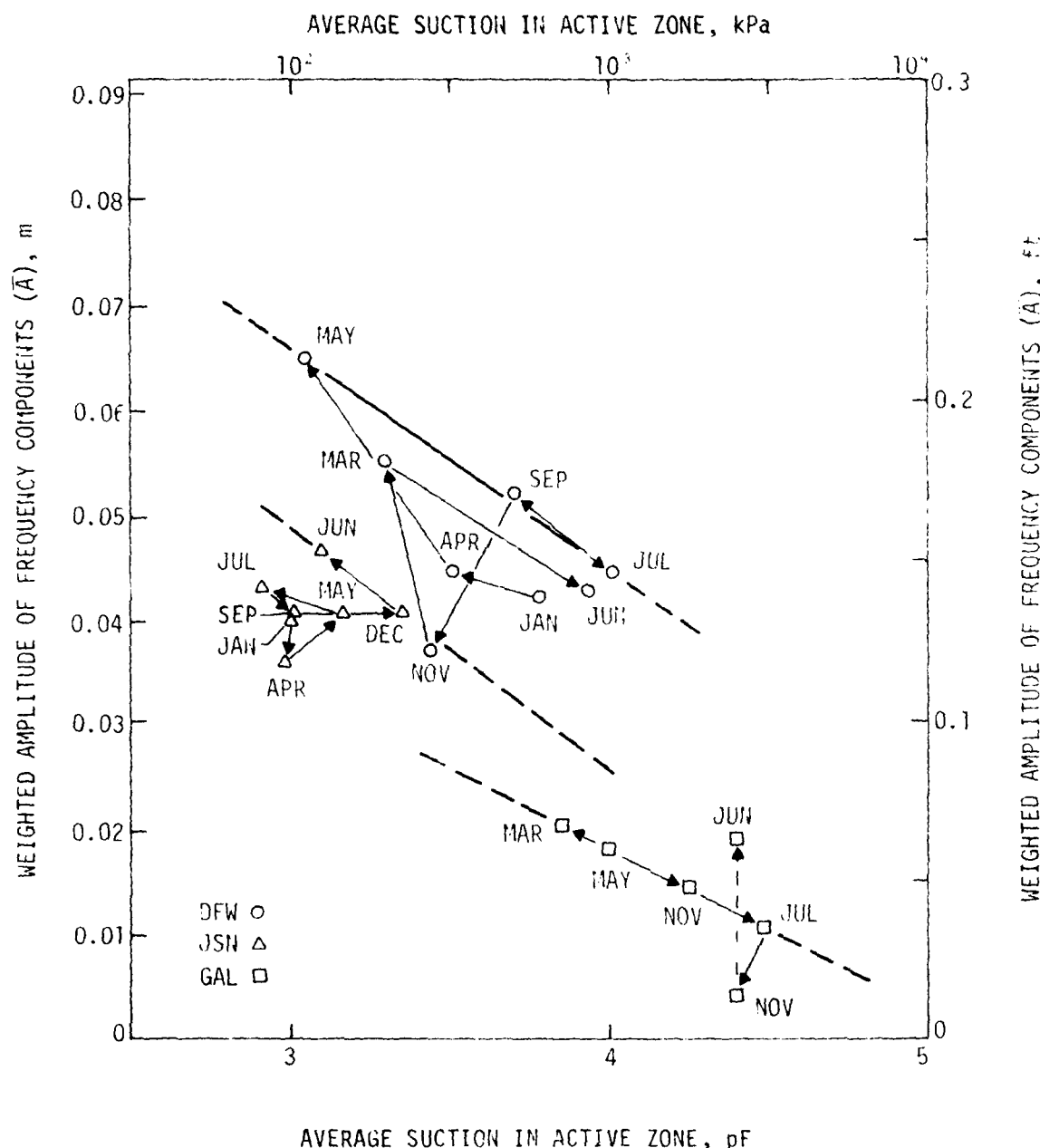


FIGURE 7-1. CHARACTERIZATION OF SOIL BEHAVIOR FOR PAVEMENT DESIGN.

The relationship between Δ and suction change depends on several factors. These include the depth of the active zone and the soil response to suction change as indicated by γ_h . The cracking fabric within the active zone as indicated by f is also very important.

The data shown in Figure 7-1 are the result of the field experiment conducted in this study. Clearly each of these sites exhibits distinctive features. Future work should be directed to obtaining more data of this type at a variety of sites.

WAVELLENGTH AND ROUGHNESS

The amplitudes must be accompanied by a horizontal distance in order to be useful in the study of roughness. To characterize the wavelength, the autocorrelation function for the elevation data was calculated. The horizontal distance at which the autocorrelation function goes to zero represents a characteristic of the cyclic nature of the surface. With this distance, it is possible to quantify the profile in terms of roughness parameters, an amplitude and a wavelength.

Wavelengths and amplitudes for the uncovered soil surfaces studied are given in Table 7-1. Note that the sites with deeper active zones (DFW, JSON) exhibit a more constant wavelength. The shallow active zone (GAL) shows more variation in wavelength. When a pavement is placed on these soils, this natural wavelength is changed. This change must be understood in order to proceed with the proposed approach to pavement design. Wavelength and amplitude data for the paved surfaces studied are presented in Tables 7-2 through 7-4. The layers in the pavements were converted into equivalent depths of asphalt concrete for ready comparison. The equivalent depth of each of these pavements is shown in Table 7-5.

The equivalent depth was calculated by first assuming modulus values as follows: portland cement concrete, 2.8×10^7 kPa (4×10^6 lb/in 2); asphaltic concrete, 3.5×10^6 kPa (5×10^5 lb/in 2); cement-treated base, 1.4×10^6 kPa (2×10^5 lb/in 2); lime-stabilized subgrade, 2.1×10^4 kPa (3×10^3 lb/in 2). Each layer thickness was then converted to an equivalent thickness of asphaltic concrete using the modular ratios. The sum of these thicknesses in the pavement is the equivalent depth.

TABLE 7-1. AMPLITUDE-WAVELENGTH FOR SOIL SURFACES

Pavement		Amplitude, m	(ft)	Wavelength, m	(ft)
DFW 1					
JAN	0.0421	(0.138)			
APR	0.0454	(0.149)	8.2	(27)	
MAY	0.0649	(0.213)	7.0	(23)	
JUL	0.0454	(0.149)	8.2	(27)	
SEP	0.0527	(0.173)	8.2	(27)	
NOV	0.0369	(0.121)	8.2	(27)	
MAR	0.0552	(0.181)			
JUN	0.0427	(0.140)			
JSN 1					
JAN	0.0399	(0.131)			
APR	0.0363	(0.119)	11.0	(36)	
MAY	0.0405	(0.133)	10.7	(35)	
JUL	0.0430	(0.141)	10.7	(35)	
SEP	0.0408	(0.134)	9.5	(31)	
DEC	0.0408	(0.134)	10.4	(34)	
JUN	0.0469	(0.154)			
GAL 1					
NOV	0.0146	(0.048)			
MAR	0.0204	(0.067)	7.0	(23)	
MAY	0.0183	(0.060)	4.6	(15)	
JUL	0.0110	(0.036)	7.0	(23)	
NOV	0.0046	(0.015)	3.1	(10)	
JUN	0.0189	(0.062)			

TABLE 7-2. AMPLITUDE-WAVELENGTH DATA FOR DFW PAVEMENTS

Pavement		Amplitude, m	Wavelength, m	(ft)
DFW 2				
NOV	0.014	(0.046)		
JAN	0.020	(0.064)		
APR	0.013	(0.044)	5.2	(17)
MAY	0.018	(0.058)	6.1	(20)
JUL	0.012	(0.040)	5.8	(19)
SEP	0.013	(0.043)	6.1	(20)
NOV	0.013	(0.042)	6.1	(20)
MAR	0.014	(0.046)		
JUN	0.015	(0.050)		
DFW 3				
NOV	0.0070	(0.023)		
JAN	0.0067	(0.022)		
APR	0.0085	(0.028)	9.1	(30)
MAY	0.0073	(0.024)	8.8	(29)
JUL	0.0076	(0.025)	9.1	(30)
SEP	0.0082	(0.027)	9.4	(31)
NOV	0.0070	(0.023)	9.1	(30)
MAR	0.0058	(0.019)		
JUN	0.0079	(0.026)		
DFW 5				
NOV	0.027	(0.087)		
JAN	0.020	(0.064)		
APR	0.023	(0.076)	4.6	(15)
MAY	0.018	(0.059)	3.7	(12)
JUL	0.022	(0.073)	3.7	(12)
SEP	0.025	(0.083)	3.7	(12)
NOV	0.024	(0.079)	3.7	(12)
MAR	0.024	(0.077)		
JUN	0.022	(0.073)		
DFW 6				
NOV	0.015	(0.049)		
JAN	0.014	(0.045)		
APR	0.014	(0.047)	10.4	(34)
MAY	0.014	(0.045)	10.1	(33)
JUL	0.014	(0.046)	9.1	(30)
SEP	0.018	(0.059)	9.8	(32)
NOV	0.014	(0.047)	10.1	(33)
MAR	0.015	(0.048)		
JUN	0.014	(0.046)		

TABLE 7-3. AMPLITUDE-WAVELENGTH DATA FOR JSN AND GAL

Pavement	Amplitude, m (ft)		Wavelength, m (ft)	
JSN 2				
JAN	0.0061	(0.020)		
APR	0.0024	(0.008)	11.0	(36)
MAY	0.0030	(0.010)	9.4	(31)
JUL	0.0052	(0.017)	10.1	(33)
SEP	0.0024	(0.008)	10.4	(34)
DEC	0.0018	(0.006)		
JUN	0.0021	(0.007)		
JSN 3				
JAN	0.0070	(0.023)		
APR	0.0055	(0.018)	5.5	(18)
MAY	0.0058	(0.019)	5.8	(19)
JUL	0.0043	(0.014)	4.3	(14)
SEP	0.0073	(0.024)	2.4	(8)
DEC	0.0070	(0.023)	7.9	(26)
JUN	0.0070	(0.023)		
GAL 2				
NOV	0.0134	(0.044)		
MAR	0.0122	(0.040)	3.7	(12)
MAY	0.0085	(0.028)	2.7	(9)
JUL	0.0088	(0.029)	2.4	(8)
NOV	0.0113	(0.037)	3.0	(10)
JUN	0.0119	(0.039)		
GAL 3				
NOV	0.0149	(0.049)		
MAR	0.0131	(0.043)	10.1	(33)
MAY	0.0131	(0.043)	10.1	(33)
JUL	0.0131	(0.043)	9.8	(32)
NOV	0.0134	(0.044)	10.1	(33)
JUN	0.0152	(0.050)		

TABLE 7-4. AMPLITUDE-WAVELENGTH DATA FOR ROUGH PAVEMENTS

Pavement		Amplitude, m (ft)	Wavelength, m (ft)
DFW	7	0.0314 (0.103)	2.7-3.7 (9-12)
	8	0.0250 (0.082)	9.1 (30)
	9	0.0454 (0.149)	7.9 (26)
	10	0.0469 (0.154)	5.8 (19)
	11	0.0600 (0.197)	8.2 (27)
	12	0.0393 (0.129)	7.3 (24)
	13	0.0351 (0.115)	5.9 (19.5)
	14	0.0344 (0.113)	7.3 (24)
NAS	1	0.0433 (0.142)	3.7-12.2 (12-40)
	2	0.0323 (0.106)	4.9 (16)
	3	0.0122 (0.040)	3.2-9.8 (10.5-32)
	4	0.0140 (0.046)	5.6 (18.5)
GAL	4	0.0527 (0.173)	4.0 (13)
	5	0.0223 (0.073)	6.2 (20.5)
	6	0.0143 (0.047)	11.3 (37)
JSN	4	0.1067 (0.350)	6.4 (21)
	5	0.0518 (0.170)	6.2 (20.5)
	6	0.0326 (0.107)	5.2 (17)
	7	0.0469 (0.154)	8.2 (27)
	8	0.0649 (0.213)	8.5 (28)
	9	0.0271 (0.089)	7.3 (24)
	10	0.0311 (0.102)	5.5 (18)
	11	0.0588 (0.193)	5.8 (19)
	12	0.1006 (0.330)	6.1 (20)
	15	0.1070 (0.351)	6.4 (21)
	16	0.0866 (0.284)	7.0 (23)

TABLE 7-5. PAVEMENT EFFECTIVE DEPTH

Pavement	Surface material	Equivalent depth, m (in)	
DFW 2	AC	0.115	(4.5)
DFW 3	PCC	0.820	(32.3)
DFW 5 through 14	AC	0.200	(7.9)
NAS 1,2	PCC	0.549	(21.6)
NAS 3,4	PCC	0.511	(20.1)
GAL 2 through 6	AC	0.400	(15.7)
JSN 2,3	AC/PCC	0.600	(23.6)
JSN 5-9	PCC	0.518	(20.4)
JSN 10	AC	0.257	(10.1)
JSN 11,12	PCC	0.628	(24.1)
JSN 4,15,16	PCC	0.305	(12.0)

Notes: AC is asphalt concrete; PCC is portland cement concrete.

A plot of equivalent depth versus wavelength for the pavements at GAL, DFW, and NAS is shown in Figure 7-2. Figure 7-3 is a similar plot for the JSN area. These data reveal that the wavelengths on the pavement edges and those in the interior differ markedly. In Figure 7-2, the edges contain shorter wavelengths whereas the interior lines exhibit wavelengths equal to or greater than the uncovered soil wavelength (λ_0). The data in Figure 7-3 show that the reverse is true of the pavements studied in the JSN area. This difference is interpreted as evidence of a fundamental difference in soil-pavement behavior at these test sites.

The shorter wavelengths exhibited at the pavement edges in Figure 7-2 result from climatic changes. The soil wet-dry sequence produces more movement near the edge than in the interior, resulting in shorter wavelengths. It is clear that the design condition should be the pavement edge, where cyclic movements occur and produce short-wavelength roughness.

In contrast, the JSN data reveal cyclic movements under the interior pavement areas. Three possible mechanisms are postulated: (a) moisture movement through the pavement surface, i.e., pavement permeability greater than

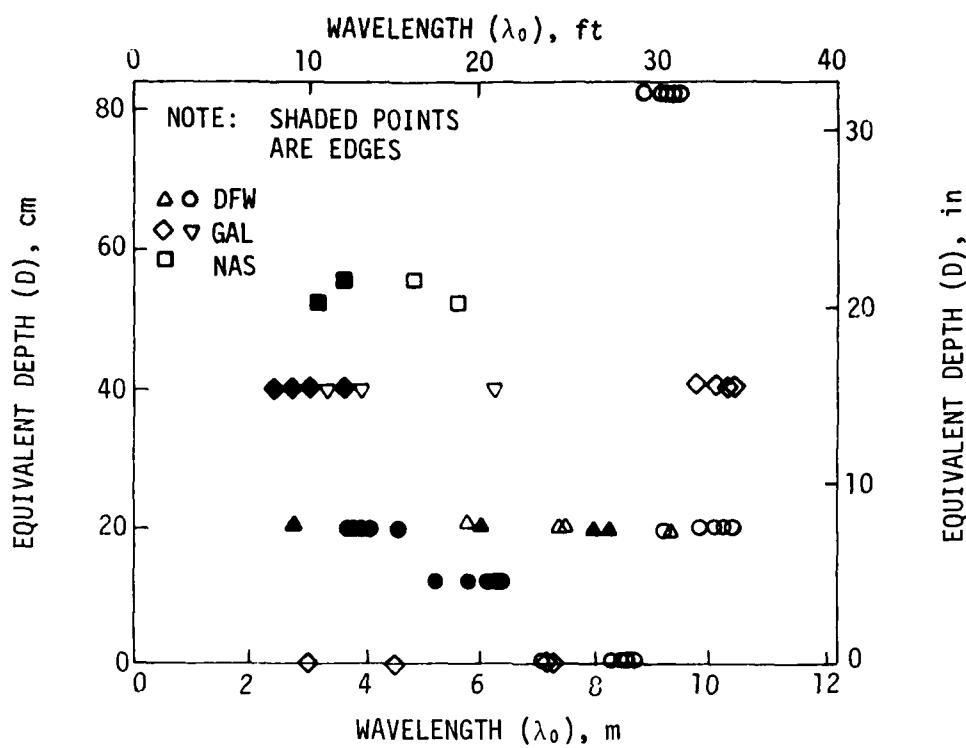


FIGURE 7-2. DEPTH-WAVELENGTH RELATIONSHIPS AT DFW, NAS, GAL.

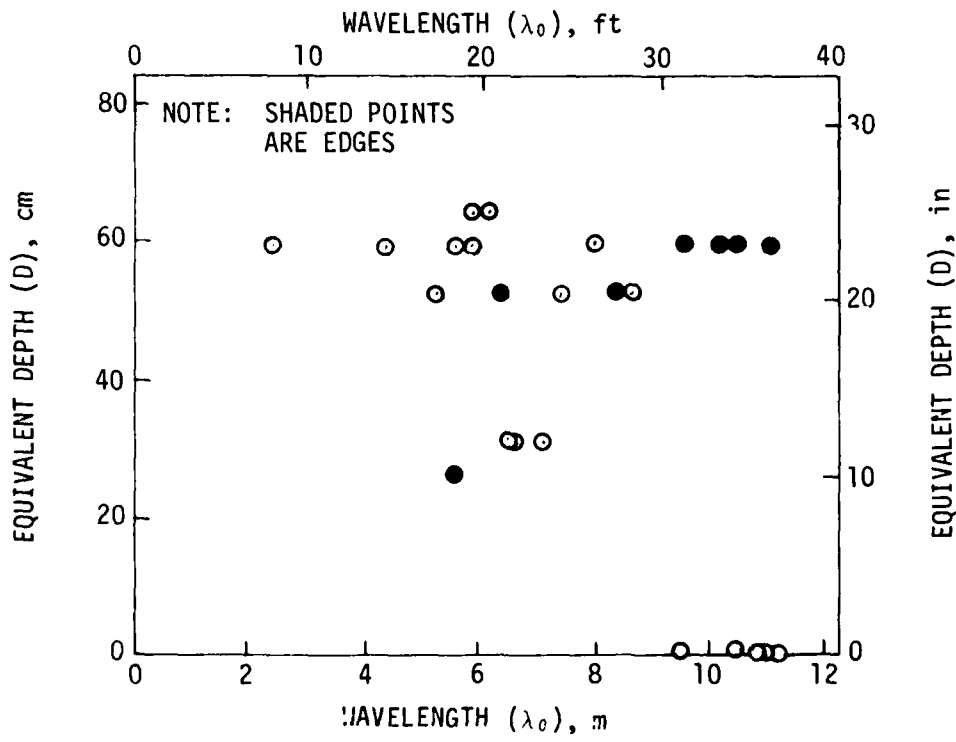


FIGURE 7-3. DEPTH-WAVELENGTH RELATIONSHIPS AT JSN.

subgrade permeability; (b) cyclic suction changes occurring via avenues within the profile such as seams and fissures; (c) changes in the osmotic suction in the profile which are not related to climatic variation.

Because shorter wavelengths produce more severe roughness, they are an attractive design parameter. The data in Figures 7-2 and 7-3 indicate that the design wavelength (λ_d) is about equal to half the soil wavelength (0.5') for airport pavements. This approximation will be applied in the next section.

ACCEPTABILITY CRITERIA

The use of wavelength and amplitude characteristics for the design of pavements requires the establishment of acceptability criteria. Acceptable pavement roughness depends on acceptable levels of aircraft response. Although no widely accepted aircraft criterion is available, a pilot station vertical acceleration of 0.4 g has been used most often. The TAXI computer code was first used to simulate aircraft response for the purpose of establishing acceptability quantitatively. The application of the 0.4-g criterion was not entirely satisfactory for the following reasons. (1) Each aircraft responds differently to a pavement surface; only four commercial aircraft were used in the simulation in this study. (2) As the gross weight of the aircraft varies, its response to the pavement surface varies. (3) The pavement deflection under aircraft loads contribute to the roughness encountered by real airplanes. TAXI does not model this behavior. (4) The 727-200 has not been modeled as well as other aircraft because the TAXI simulations do not properly model its specific strut characteristics.

In addition, several pavements clearly unacceptable to users and airport operators did not produce unacceptable accelerations in the aircraft simulations. This discrepancy may result from variations in the actual operating conditions, such as the gross weight and speed of the aircraft. Another factor involved in complaints by users is the appearance of the pavement profile.

The acceptability was therefore determined in two ways. First, an acceleration criterion of 0.3 g was used. It was reduced from 0.4 g because it is intended for design use. The reduction was made based on an examination

of the data in this study and on experience. The second criterion was subjectively determined and involved rating the acceptability of the pavement as expressed by users and operators. Visual inspection of the pavement and study of actual elevations were also used.

Acceptability data are shown in Figure 7-4 for B727-100 and -200 and in Figure 7-5 for the DC-9-40 and TriJet Composite. The lines on the graphs represent criteria for acceptability of the amplitude and wavelength combinations. The acceptability for the DC-9-40 and TriJet Composite was more conservative and was selected for further use in the present study.

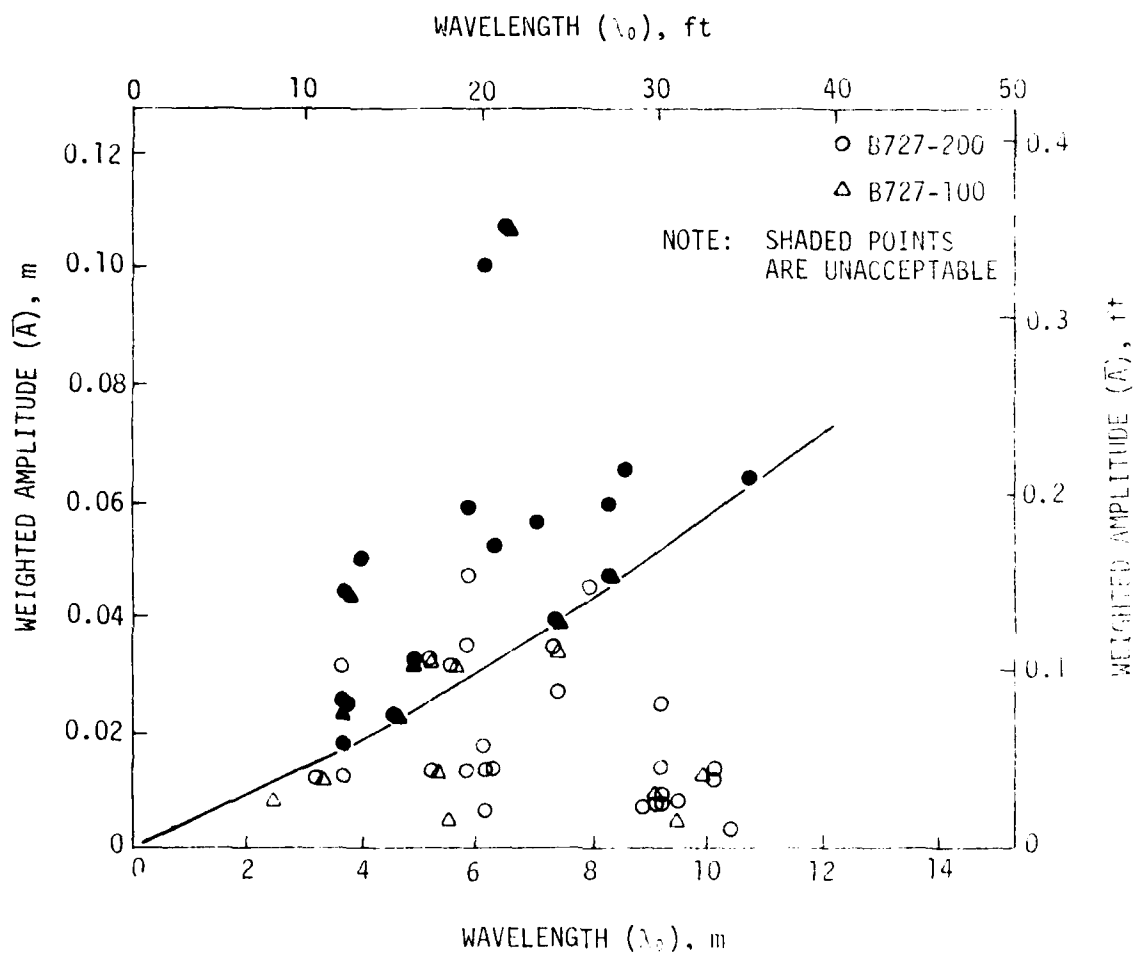


FIGURE 7-4. ACCEPTABILITY OF PAVEMENTS FOR THE B727-200 AND B727-100.

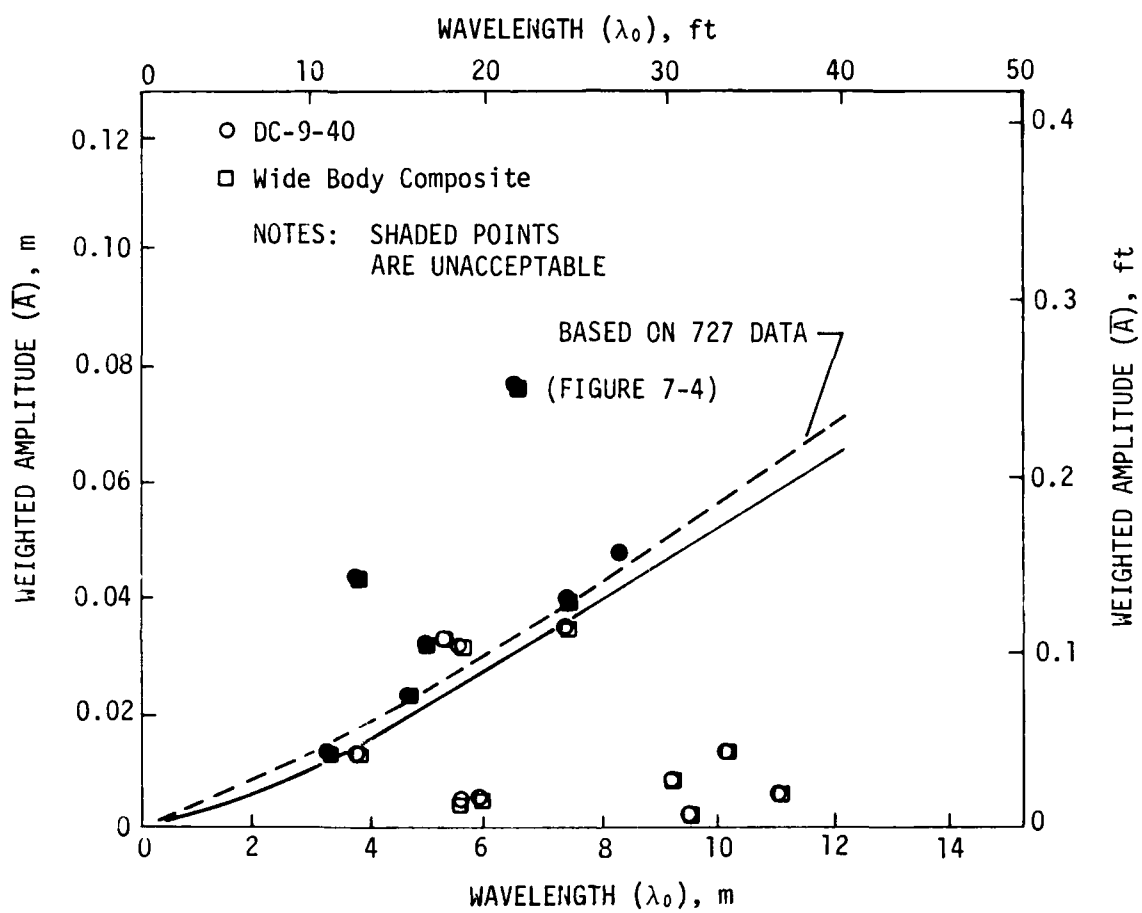


FIGURE 7-5. ACCEPTABILITY OF PAVEMENTS FOR THE DC-9-40 AND THE TRIJET COMPOSITE.

VIII. RECOMMENDATIONS

The findings of the field study provide a basis for recommendations for the design of airport pavements on expansive soils. A proposed design procedure was shown in Figure 4-2. In this section, the findings of the field experiment will be applied to this procedure.

INDICATOR TEST

An indicator test may be used to determine whether the soil requires special expansive soils design procedures. In many cases, this determination will not require a physical test, but will be made on the basis of experience or available data. In the absence of other evidence, the determination of undisturbed soil response to suction changes (e.g., provided by the ϕ_i) indicates of potential soil behavior. Suction tests provide different values depending on the lateral restraint imposed in the test:

$$\frac{(\Delta V/V_i)f}{\log_{10} \frac{h_f}{h_i}} \quad (8-1)$$

where

- r_h = suction compression index
- $\Delta V/V_i$ = volume change in terms of original volume
- h_f, h_i = final and initial suction in arithmetic units
- f = lateral restraint factor

The clod test and the COLE test, for example, provide values of r_h under no restraint ($f = 1/3$).

The values of ϕ_i shown in Figure 4-2 are for a lateral restraint factor $f = 1/3$. Either f value may be used in ϕ_i calculations as long as the lateral restraint factor is expressed explicitly. The values obtained from the chart in Figure 4-27 are for $f = 1.0$.

SOIL CHARACTERIZATION

The two steps shown in Figure 4-2 for swell evaluation and heave prediction should be combined into a single step called "soil characterization." Procedures for obtaining the six characteristics are described below.

Prediction of soil amplitude and wavelength is the first step. The wavelength λ is a direct function of the active zone depth for the sites studied (Figure 8-1). Active zone depth for JSN was inferred from the fact that interior pavement areas, rather than the edges, were undergoing movement. Interior movement suggests that the principal cause of distortion is not surface climatic variation; it is the movement of water via discontinuities in the soil. Data in Figure 4-11 indicate discontinuities at 3.7 m (12 ft) at the test site. The data in Figure 8-1 can be used for estimating λ for the soil at a site. Their use is not recommended outside of the given data range or in the presence of a water table. Wavelength may also be estimated by surveying the surface profile and calculating the decorrelation distance for the data. The decorrelation distance is the distance at which the auto correlation function goes to zero.

The other soil property required is the weighted amplitude A . The slope of A versus average active zone suction (Figure 7-1) is the best estimator for the sites studied. Thus, an estimate of initial and final suction profiles is required. With this estimate, the suction change can be used to predict the A . This prediction is for a one-time change from initial to final. If the suction profile fluctuates, the A will probably build up from cycle to cycle, resulting in a larger A .

For sites other than those studied, a method for prediction of A is desired. Measurement and estimation are alternative prediction procedures.

Measurement

With this procedure, elevation data are gathered and A computed at two or three times of the year. These data are plotted against suction, as shown in Figure 7-1, and the slope of the least square fit is determined. The following must be considered in using this method. During the initial swell of a cracked soil profile, decreases in A are likely. The area studied must be undisturbed soil in order to reflect the behavior of the active zone as it interacts with the climate. Preferably, the area should be relatively flat. These factors will combine to produce a worst-case or greatest amplitude soil for the study.

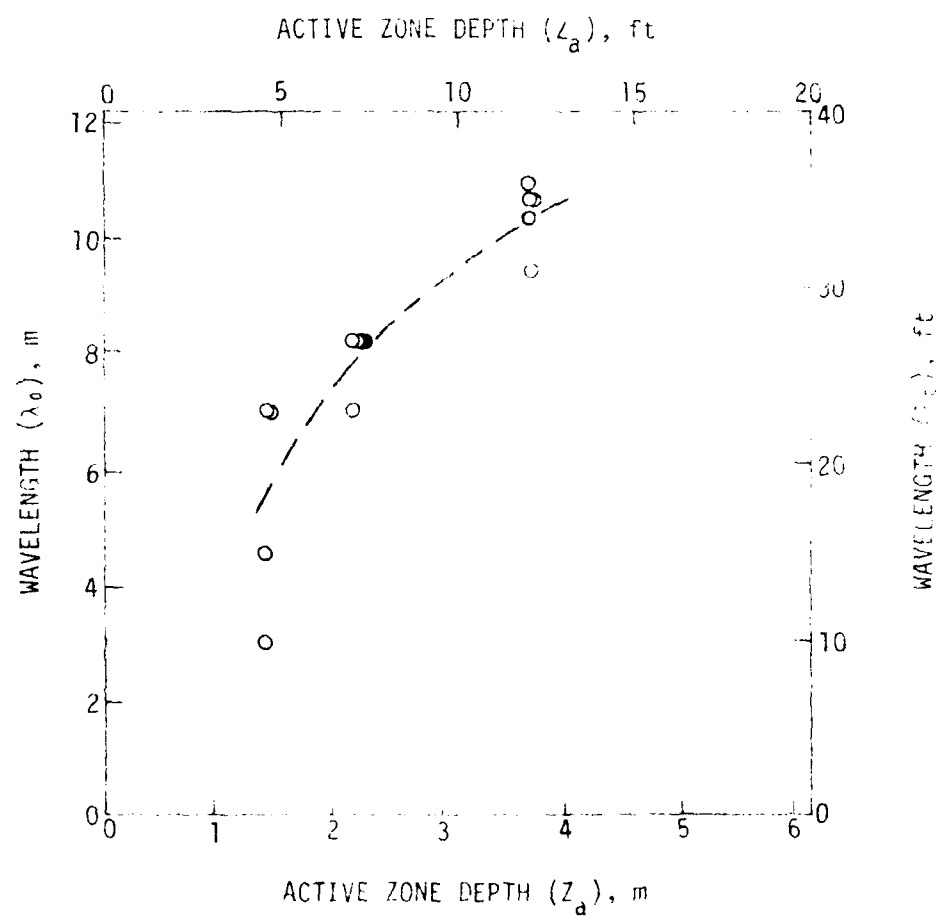


FIGURE 8-1. ESTIMATION OF SOIL WAVELENGTH.

Estimation

Soil properties may be used to predict the slope of the amplitude-suction relationship. On the basis of the factors involved in the swelling of a clay profile, \bar{A} is a function of

- suction compression index (i_h)
- active zone depth (Z_a)
- variation of suction compression index from point to point
- variation of suction profile from point to point (h_f , h_i)

The development of an estimate for a soil follows these steps:

$$\begin{aligned} [\Delta H]_{\max} &= i_{h_1} \log \left[\frac{h_f}{h_i} \right]_1 \cdot Z_a \\ [\Delta H]_{\min} &= i_{h_2} \log \left[\frac{h_f}{h_i} \right]_2 \cdot Z_a \\ \bar{A} &= 1/2 \left(\Delta H_{\max} - \Delta H_{\min} \right) = 1/2 \left[i_{h_1} \log \left[\frac{h_f}{h_i} \right]_1 - i_{h_2} \log \left[\frac{h_f}{h_i} \right]_2 \right] \end{aligned} \quad (8-2)$$

Now it is necessary to obtain a measure of the variability of i_h and h_f/h_i in the profile. So far it has been assumed that soil beneath pavement areas is in equilibrium after swell. Therefore, h_f/h_i will not vary, although the suction will vary at intermediate times. The case for no variation in suction was calculated and is illustrated in Figure 8-2.

SOIL-PAVEMENT INTERACTION MODEL

When a pavement is placed on an expansive soil, pavement stiffness can be expected to reduce the \bar{A} . In order to account for this effect, the following model is proposed.

The effect of pavement stiffness in smoothing expansive clay roughness is modeled using a beam on an elastic foundation (Figure 8-3). By summing vertical forces on the element, one obtains

$$Q - (Q + dQ) + kb(w - w')dx - qbdx = 0 \quad (8-3)$$

$$\frac{dQ}{dx} = kb(w - w') - qb \quad (8-4)$$

where

Q = shear

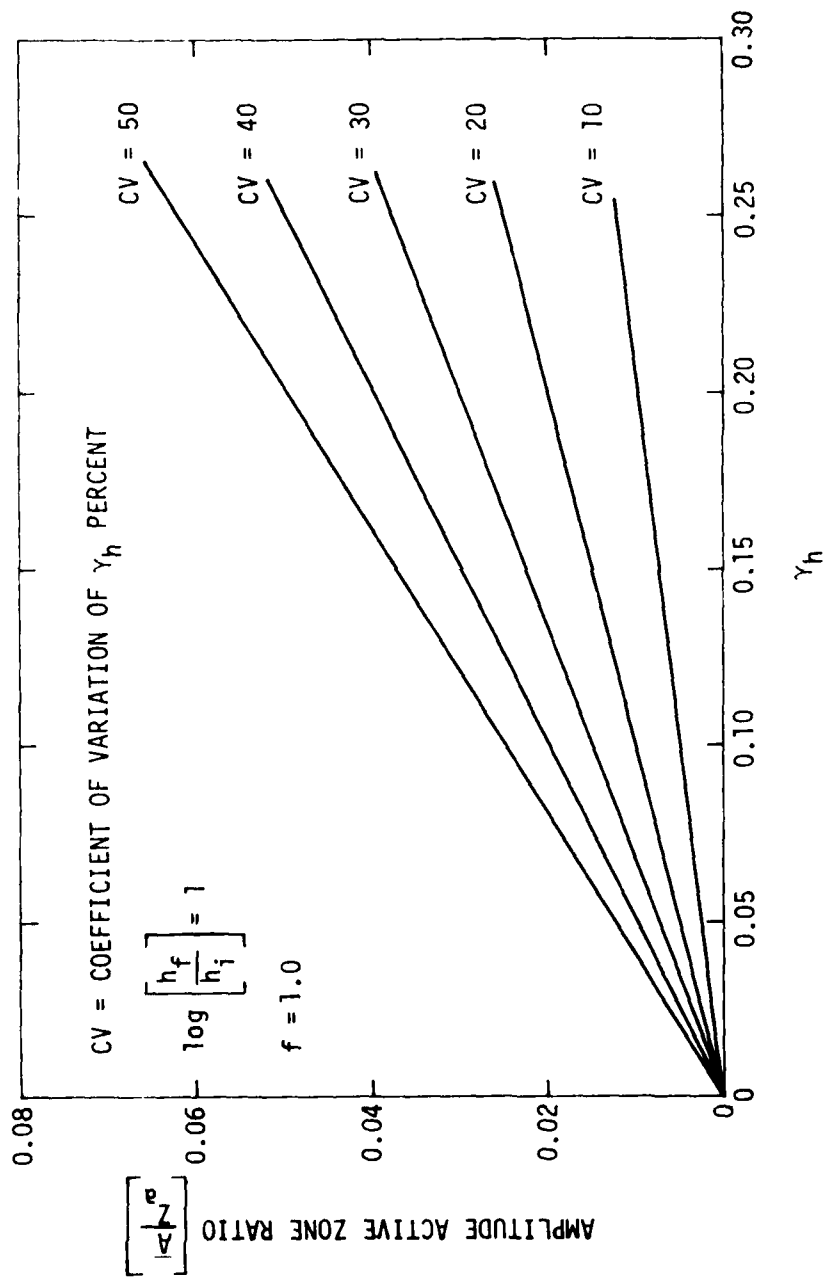
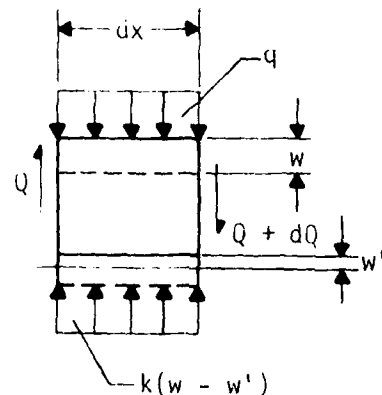
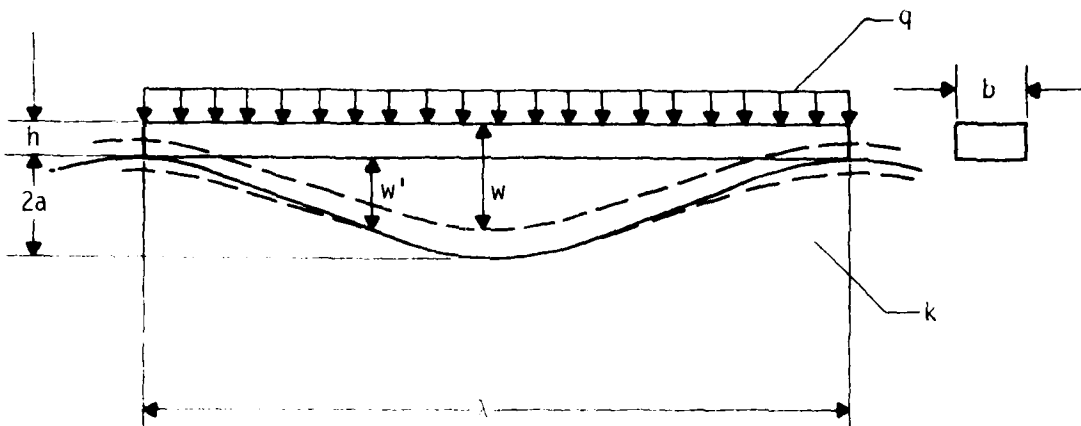


FIGURE 8-2. PREDICTION OF \bar{A} FROM γ_h AND ITS VARIATION.



- q = unit weight of beam material
- k = subgrade modulus
- b = width of beam
- a = half-amplitude of deformed soil
- h = thickness of beam
- w = deflection of beam
- w' = shape of soil surface
- Q = shear
- λ = wavelength
- dx = incremental length

FIGURE 8-3. BEAM ON DEFORMED ELASTIC FOUNDATION PROBLEM.

w = deflection of beam
 w' = shape of soil surface
 b = width of beam
 dx = incremental length
 k = subgrade modulus (explained below)
 q = unit weight of beam material

Because

$$\frac{dQ}{dx} = \frac{d^2M}{dx^2}$$

and

$$M = -EI \frac{d^2w}{dx^2}$$

where

E = modulus of elasticity of beam
 I = moment of inertia of the section
 M = moment

we can rewrite the expression as

$$\frac{dQ}{dx} = -EI \frac{d^4w}{dx^4} = kb(w - w') - qb \quad (8-5)$$

Now an expression for w is assumed:

$$w = Ae^{-\beta x} \cos \beta x + Be^{-\beta x} \sin \beta x + Ce^{\beta x} \cos \beta x + De^{\beta x} \sin \beta x + \frac{qb}{kb} + w'$$

where

A, B, C, D are constants

$$\beta = \left(\frac{kb}{4EI} \right)^{1/4} = \text{a characteristic stiffness} \quad (8-6)$$

Taking the necessary derivatives and substituting into Equation 8-5 yields

$$\begin{aligned} \frac{d^4w}{dx^4} &= -4A\beta^4 e^{-\beta x} \cos \beta x - 4B\beta^4 e^{-\beta x} \sin \beta x - 4C\beta^4 e^{\beta x} \cos \beta x \\ &\quad - 4D\beta^4 e^{\beta x} \sin \beta x + \frac{d^4w'}{dx^4} \end{aligned} \quad (8-7)$$

Then the following boundary conditions are imposed on the function w' :

$$\text{At } x = 0, w' = 0, \frac{dw'}{dx} = 0$$

$$\text{At } x = \frac{\lambda}{4}, w' = a$$

$$\text{At } x = \frac{\lambda}{2}, w' = 2a$$

$$\frac{d^4w'}{dx^4} = 0$$

a = the half-amplitude of the soil

Beginning with the last expression and integrating gives

$$w' = \frac{Ex^3}{6} + \frac{Fx^2}{2} + Gx + H$$

With the boundary conditions above, the constants (E , F , G , H) may be evaluated.

$$H = G = 0$$

$$\frac{E}{6}\left(\frac{\lambda}{4}\right)^3 + \frac{F}{2}\left(\frac{\lambda}{4}\right)^2 = a \quad (8-8)$$

$$\frac{E}{6}\left(\frac{\lambda}{2}\right)^3 + \frac{F}{2}\left(\frac{\lambda}{2}\right)^2 = 2a \quad (8-9)$$

Solving these equations simultaneously yields

$$w' = -32a\left(\frac{x}{\lambda}\right)^3 + 24a\left(\frac{x}{\lambda}\right)^2 \quad (8-10)$$

In solving the equation for the beam deflection, the following boundary conditions are imposed:

$$x = 0, \frac{dw}{dx} = 0 \quad (8-11)$$

$$x = 0, \frac{d^3w}{dx^3} = 0 \quad (8-12)$$

$$x = \frac{\lambda}{2}, \frac{dw}{dx} = 0 \quad (8-13)$$

$$x = \frac{\lambda}{2}, \frac{d^3w}{dx^3} = 0 \quad (8-14)$$

The boundary conditions 8-11 through 8-14 produce a system of four equations and four unknowns:

$$(-A + B)\beta + (C + D)\beta = - \left. \frac{dw'}{dx} \right|_{x=0} \quad (8-15)$$

$$2[A + B]\beta^3 + [-C + D]\beta^3 = - \left. \frac{d^3w'}{dx^3} \right|_{x=0} \quad (8-16)$$

$$(-A + B)\beta b_1 + (-A - B)\beta b_2 + (C + D)\beta b_3 + (-C + D)\beta b_4 = - \left. \frac{dw'}{dx} \right|_{x=\frac{\lambda}{2}} \quad (8-17)$$

$$(A + B)2\beta^3 b_1 + (-A + B)2\beta^3 b_2 + (-C + D)2\beta^3 b_3 + (-C - D)2\beta^3 b_4$$

$$= - \left. \frac{d^3w'}{dx^3} \right|_{x=\frac{\lambda}{2}} \quad (8-18)$$

where

$$b_1 = e^{-\frac{\beta\lambda}{2}} \cos \frac{\beta\lambda}{2}$$

$$b_2 = e^{-\frac{\beta\lambda}{2}} \sin \frac{\beta\lambda}{2}$$

$$b_3 = e^{\frac{\beta\lambda}{2}} \cos \frac{\beta\lambda}{2}$$

$$b_4 = e^{\frac{\beta\lambda}{2}} \sin \frac{\beta\lambda}{2}$$

This system of four equations and four unknowns may be solved by the use of matrix methods which provide values for A, B, C, and D. Then the maximum pavement elevation difference is

$$\Delta w \Big|_{\max} = w \Big|_{x=\frac{\lambda}{2}} - w \Big|_{x=0}$$

$$\frac{\Delta w}{2a} \Big|_{\max} = \frac{A}{a} (b_1 - 1) + \frac{B}{a} \left(\frac{b_2}{2} \right) + \frac{C}{a} \left(\frac{b_3}{2} - 1 \right) + \frac{D}{a} \left(\frac{b_4}{2} \right) + 1 \quad (8-19)$$

For ease of use, a plot of $\frac{\Delta w}{2a}$ versus $\beta\lambda$ was prepared for a variety of values of stiffness (Figure 8-4).

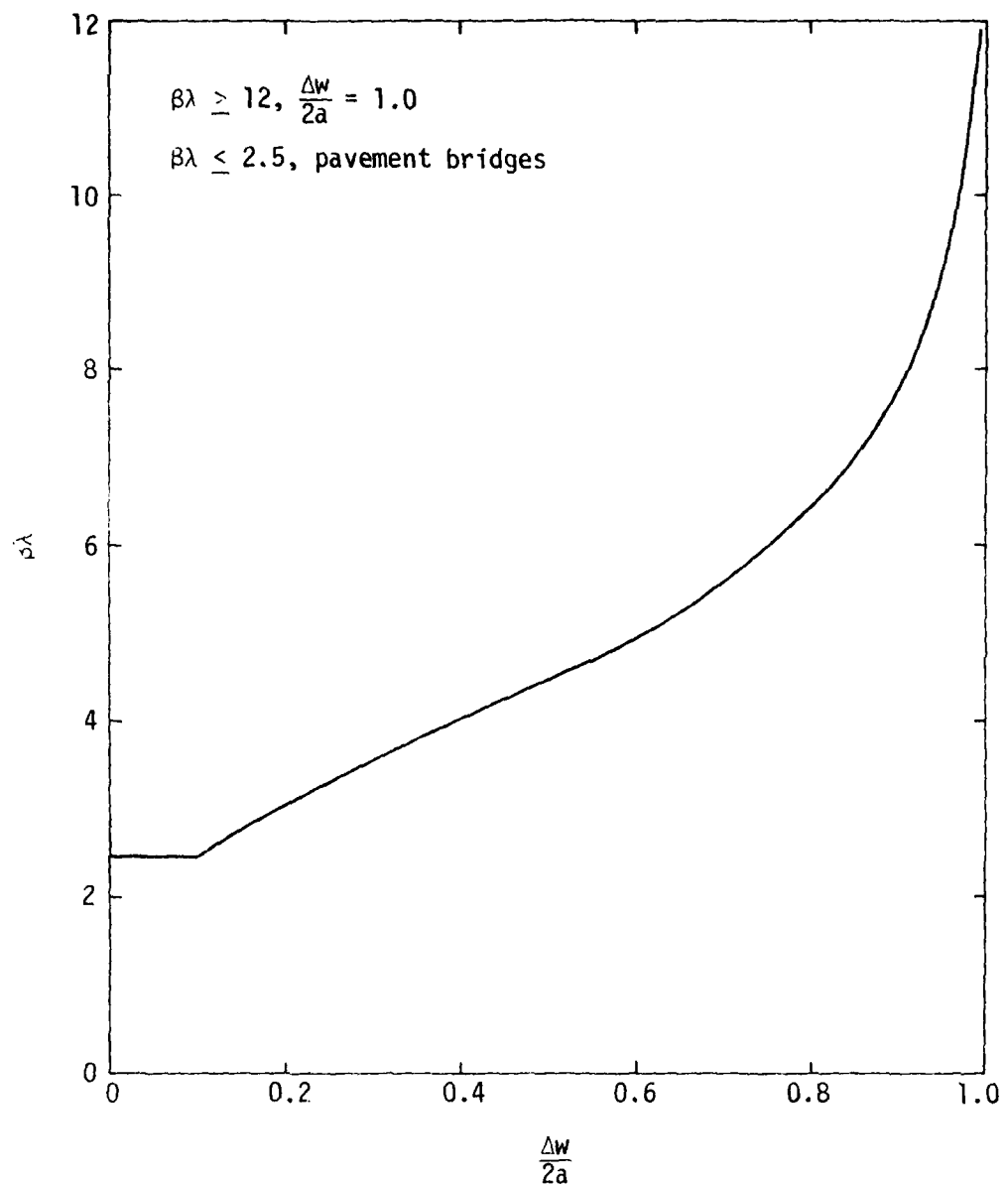


FIGURE 8-4. SOLUTION TO PAVEMENT MODEL EQUATION.

EXPANSIVE SOIL DESIGN PROCEDURE

Figure 8-5 outlines the revised design procedure for airport pavements on expansive soils. It may be viewed as a three-step procedure. Step 1 is the determination of the need for special expansive soil design. Step 2 is soil characterization in terms of parameters necessary for expansive soil design. Step 3 is a study of soil-pavement-aircraft interaction to arrive at a structurally adequate thickness for the pavement. These steps are described in detail below. Examples of numerical values for the sites studied are also provided. Important assumptions and limitations are listed.

Indicator Test

The suction compression index (γ_h) is recommended for use as an indicator of soil swell potential. In addition, the use of judgement and experience is necessary. In many cases, judgement and experience will eliminate the need for an objective system such as the γ_h rating criterion.

The γ_h for a particular site may be measured by any one of several tests, including the COLE, clod test, and standard consolidometer-swell test. A chart for indirect determination of γ_h has been developed and is presented in Figure 4-27. The data in Figures 4-25 (COLE) and 4-26 (clod) indicate very few γ_h values below 0.06, placing all of sites studied in the *high swell* category (Figure 8-5).

Soil Characterization

Once a soil is placed in the high category, special procedures are required. First, a number of soil parameters which are compatible with the interaction model are determined. Then these parameters are used to evaluate the soil-pavement interaction.

Active zone depth (Z_a)--The depth of soil that interacts with the surface climatic conditions is called the *active zone depth*. Its determination is not simple. The measurement of suction versus depth at several times of the year is probably the best indicator of Z_a . However, it should be clear that periods of extreme weather (wet or dry) may drive the seasonal influence to greater depths.

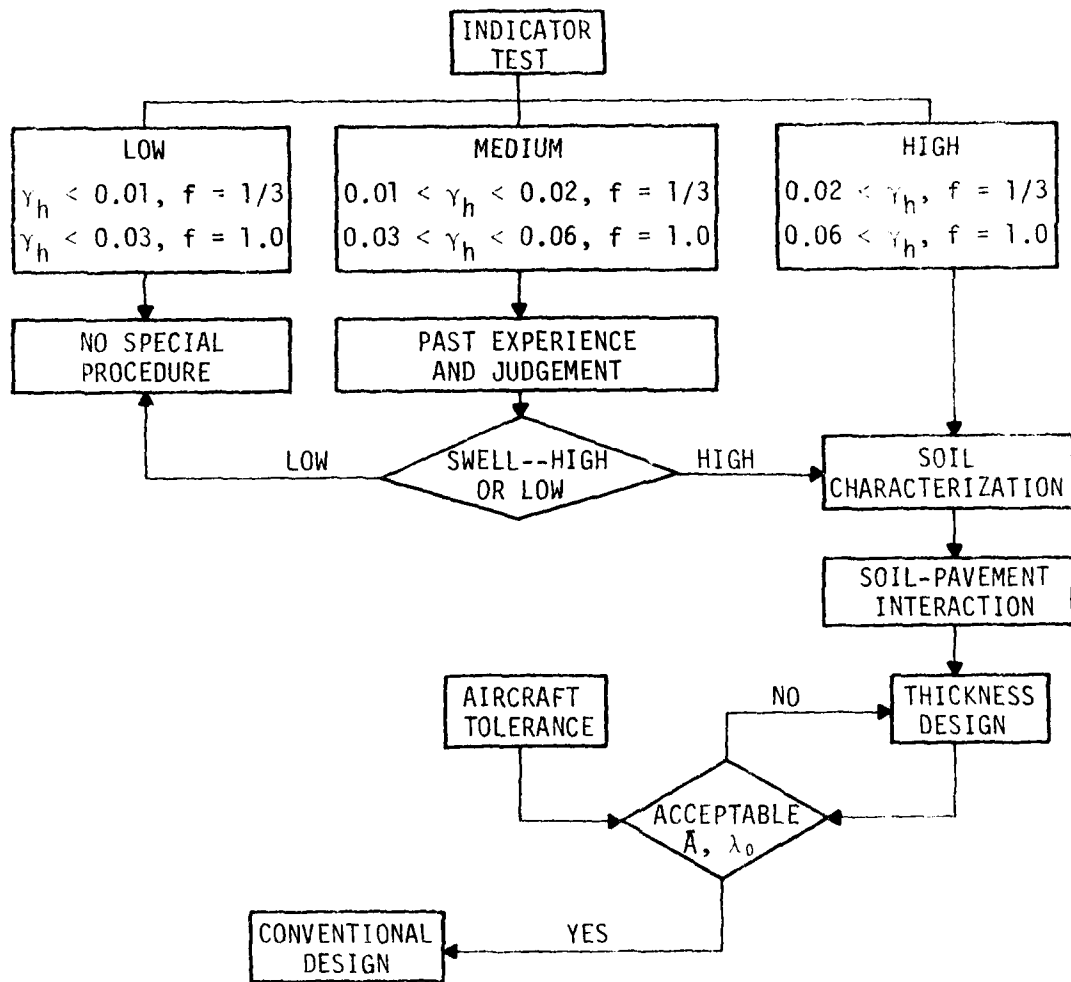


FIGURE 8-5. REVISED DESIGN PROCEDURE.

From the suction data in Figures 4-17 and 4-18, the active zone depth at DFW was estimated to be 2.1 m (7 ft). Data in Figure 4-19 for GAL indicate that the Z_a was 1.2 m (4 ft). The JSN site did not undergo a normal climatic cycle during this study; the soil profile remained wet for the duration of the observations. The approach taken was to determine the depth at which the suction profile reached a constant value. The data in Figures 4-20 and 4-21 indicate that a depth of 3.7 m (12 ft) is appropriate for the JSN active zone depth.

Subgrade modulus (k)--This modulus represents the reduction of swell by loads applied at the soil surface. Requirements for determining k are a swell value at little or no load and a swell value at loads approximately equal to the pavement load. It is the pavement dead load that will tend to reduce the swell of the underlying soil. Values of this modulus are not comparable to the conventional modulus of subgrade reaction. In the present study, k values were obtained by conducting consolidometer-swell tests at a token load and then consolidating the sample in normal increments. The modulus was calculated from the percent swell, sample height, and the load difference. Values obtained were as follows:

Site	k, kPa/m (lb/in^3)
GAL	1.65×10^5 (608)
DFW	3.56×10^5 (1310)
JSN	2.26×10^5 (537)

Suction change (Δh)--When expansive soils are covered, they no longer can interact with the climate at their surface. The normal result is moisture equilibration with the soil below the active zone. A water table or some other feature of the profile which influences water movement (e.g., seams and fissures) will alter the equilibration. The selection of the suction change during equilibration is not a well-defined procedure. Some workers recommend using saturated final conditions while others propose numerous alternatives, depending primarily on their particular climate and drainage conditions. In

the present work. the driest suction profiles are about 4.5 pF, and the wettest about 2.5 pF. These extremes were selected as initial and final profiles because there is, at present, no rational method for the selection of these values. Use of these extremes results in the greatest reasonable Δh . Therefore, for the present examples, Δh of 2.0 pF is used for design.

Soil amplitude (\bar{A})--Data from the field experiment were used to compute the weighted amplitude of the frequency components of the surface profile. These computations were discussed in Section V. The values of \bar{A} are plotted versus the change in suction in Figure 7-1. In some cases, because of cracking, the results do not follow a linear relationship. In each case, however, an estimate of the \bar{A} versus Δh slope ($\Delta \bar{A}$) was made. These values, together with estimated suction changes, were used to predict values of \bar{A} for each of the sites studied. Results of these computations are 0.030 m (0.100 ft) at GAL, 0.042 m (0.136 ft) at DFW, and 0.046 m (0.150 ft) at JSN.

Soil wavelength (λ_0)--A characteristic wavelength of the soil is required to complete the roughness characterization. The decorrelation distance of the autocorrelation function of the elevations measured was used. This distance may not be the actual fundamental wavelength of the soil, but it is some multiple of that wavelength and therefore serves the present purpose. Data were plotted versus active zone depth in Figure 8-1, and Z_a may be used to select a value of λ_0 for the soil. In Figures 7-2 and 7-3, values of λ_0 for pavement sections were plotted versus the equivalent depth of each pavement. It was recognized that pavement structures caused shorter wavelengths than those that occur on the uncovered soil. The design wavelength was determined to be half of the uncovered soil wavelength. Values of the design wavelength (λ_d) are therefore 2.7 m (9 ft) at GAL, 4.0 m (13 ft) at DFW, and 5.2 m (17 ft) at JSN. Results of the soil characterization for all sites is shown in Table 8-1.

Interaction Study

The next step is to determine the amount of stiffness required in a pavement section to resist the development of excessive pavement roughness caused by soil swelling. The pavement was modeled as a beam-on-elastic foundation with the foundation deformed. Through a combination of beam bending and soil compression, the amplitude of the soil deformation was reduced. The objective

TABLE 8-1. RESULTS OF SOIL CHARACTERIZATION

Parameter	GAL	DFW	JSN
Indicator test	High	High	High
Active zone depth (Z_a), m (ft)	1.2 (4)	2.1 (7)	3.7 (12)
Modulus (k), kPa/m (lb/in ³)	1.65×10^5 (608)	3.56×10^5 (1310)	1.45×10^5 (537)
Suction change (Δ_h), pF	2.0	2.0	2.0
Soil amplitude (\bar{A}_e), mm (ft)	30.5 (0.100)	41.5 (0.136)	45.7 (0.150)
Soil wavelength (λ_0), m (ft)	5.5 (18)	7.9 (26)	10.4 (34)
Design wavelength (λ_d), m (ft)	2.7 (9)	4.0 (13)	5.2 (17)

in design is, then, to reduce the amplitude in the pavement surface to a tolerable amount. Acceptable values of amplitude were determined from the TAXI computer code and are shown in Figure 7-5 for four aircraft (B727-100, B727-200, DC-9-40, TriJet Composite).

Results of the differential equation are plotted in Figure 8-4 in non-dimensional quantities $B\lambda$ and $\Delta w/2a$. In order to simplify the problem, the pavement is considered in terms of its equivalent depth D , where all pavement layers are converted to an equivalent thickness of asphaltic concrete with a modulus (E) of 1.95×10^6 kPa (5×10^5 lb/in²).

Acceptable values of amplitude were selected from the solid line in Figure 7-5 according to the design wavelength for each site. Results are in Table 8-2. Then the acceptable amplitude, \bar{A}_a , was divided by the estimated soil amplitude, \bar{A}_e , to provide the required $\Delta w/2a$. Using the model results

TABLE 8-2. RESULTS OF INTERACTION STUDY

Parameter	GAL	DFW	JSN
Design wavelength (λ_d), m (ft)	2.7 (9)	4.0 (13)	5.2 (17)
Acceptable amplitude, (\bar{A}_a), mm (ft)	9.1 (0.03)	15.2 (0.05)	22.9 (0.075)
Soil amplitude, \bar{A}_e mm (ft)	30.5 (0.100)	41.5 (0.136)	45.7 (0.150)
$\Delta w/2a = \bar{A}_a/\bar{A}_e$	0.30	0.37	0.50
$\beta\lambda$ (Figure 8-4)	3.6	3.9	4.5
Equivalent depth (D), mm (in)	384 (15.1)	699 (27.5)	643 (25.3)
Existing pavement equivalent depth mm (in)	400 (15.7)	820 (32.3)	518* (20.4)* 600** (23.6)**

*Original pavement.

**Includes recent overlay.

plotted in Figure 8-4, values of $\beta\lambda$ were obtained. Now using the k value and λ_d from Table 8-1 along with E, β and then D may be obtained. The results are shown in Table 8-2 along with the estimated equivalent depth of the existing pavement at the sites studied.

Table 8-2 shows the equivalent depth required by the expansive soils design and, for comparison, the existing depth at each site. At the GAL site, the existing pavement equivalent depth slightly exceeds that required. The original pavement at the site was structurally inadequate, and an overlay was placed in 1972 to upgrade the pavement. In June 1980, another overlay was constructed to upgrade the pavement. Distress in the pavement was attributed

to edge effects, utility locations improperly backfilled, and isolated areas of water infiltration. The design procedure provides a means of evaluating the pavement-soil interaction as the soil responds to pavement construction. It is assumed that the surface does not leak (e.g., through joints or cracks) and that the edges are isolated from wetting effects. From evaluation of the design and performance of the GAL pavement, it is concluded that these requirements were not adequately fulfilled.

Values in Table 8-2 for the DFW site indicate that the existing pavement is thicker than the requirement for expansive soils design. Pavement performance at DFW has been excellent. In this particular case, the final design resulted from extensive on-site study and monitoring of test sections. These results indicate that the expansive soils design may not be as demanding as the high volume, high gross weight traffic analysis used for the DFW pavement design.

Thickness requirements for the JSN site exceed the equivalent depth of the original pavement as well as the total depth after a recent overlay on the taxiway studied. This discrepancy indicates that the pavement originally constructed was inadequate for the expansive soil at the JSN site. Pavement performance has been unsatisfactory at JSN, and serious problems have been apparent. Existing pavements at the gates were originally thicker than the taxiway and runway structures. For example, the equivalent thickness for JSN 11 and 12 (Table 7-5) was 638 mm (25.1 in) which is about equal to the required thickness shown in Table 8-2. One would anticipate distinctly different pavement performance from an adequate pavement (JSN 11, 12) when compared to an inadequate pavement (JSN 5, 6). Study of the elevation profiles in Appendix A reveals that the inadequate pavement shows a continuous pattern of mounds and depressions. In contrast, the distortions are centered around a single joint on JSN 11 and 12, indicating surface moisture infiltration through the joint. Thus, JSN 5 and 6 evidence general structural distress because of insufficient pavement stiffness whereas JSN 11 and 12 show isolated distress caused by infiltration via surface discontinuities. Proper design must insure that provisions are made against both forms of distress.

Alternative designs were considered for adequate structural stiffness for the soil conditions at JSN. Two alternatives were computed following the procedures outlined previously and are shown in Table 8-3. Alternative 1 incorporated additional base and stabilized soil in the design. The required thickness was reduced by reducing the active zone depth and, thereby, the suction change. Thus, the required depth was 599 mm instead of 643 mm as shown in Table 8-2. Alternative 2 increased only the portland cement concrete thickness. Both alternatives produced equivalent depths which exceeded those required, resulting in structurally adequate pavements.

TABLE 8-3. ALTERNATIVE PAVEMENT DESIGNS FOR JSN

Material	Alternative 1 mm (in)	Alternative 2 mm (in)
Portland cement concrete	241 (9.5)	305 (12.0)
Cement-treated base	305 (12.0)	152 (6.0)
Lime-stabilized soil	254 (10.0)	---
Total equivalent depth of AC	615 (24.2)	663 (26.1)
Required equivalent depth	599 (23.6)	643 (25.3)

LIMITATIONS AND RECOMMENDATIONS

The method presented above provides a rational procedure for selecting a pavement thickness sufficient to mitigate the effects of swelling soil behavior. Several aspects of this method are important and cannot be ignored in applications to real problems.

Localized areas of soil saturation cannot be overcome by the design thickness. If the pavement leaks or seepage beneath the pavement occurs (e.g., along a utility installation), additional swelling and pavement distress may be expected. Therefore, maintenance of joints and cracks and the protection of shoulders from water are essential design features. Drainage must be adequate and properly maintained.

The presence of a near-surface water table or a perched water table complicates the evaluation of suction conditions in the soil profile. The present state-of-the-art is inadequate for establishing the initial and final suction profiles. Additional work is needed to better define equilibrium conditions.

An additional complication is the presence of a significant osmotic suction component. This portion of the total suction may vary dramatically while the water content remains fixed. It also may change very slowly with time. A rapid method is needed to evaluate the osmotic suction component and determine its change potential.

Follow-on work is needed to compile a data base for the comparison of predicted pavement requirements with performance data of existing structures. This type of validation is a necessary step in developing the concepts presented into useful procedures. The results shown in Figure 8-4 should also be converted into a design chart format for various values of $\frac{\Delta w}{2a}$, β , λ , and k .

At this time it is recommended that values of $\Delta w/2a$ be between 0.1 and 0.8. If $\Delta w/2a$ is larger than 0.8, special procedures for expansive soils are probably not required. If $\Delta w/2a$ is less than 0.1, the pavement will probably bridge or lose contact with the soil. This situation may result in serious pavement damage and should be avoided in design.

REFERENCE LIST

Aitchison, G. D. and Woodburn, J. A., (1969) "Soil Suction in Foundation Design," *Proceedings, 7th International Conference on Soil Mechanics and Foundation Engineering*, Vol. 2:1-8, Mexico City.

Aitchison, G. D., (1961) "Relationships of Moisture Stress and Effective Stress Functions in Unsaturated Soils," in *Tensile Pressure and Suction in Soils*, Butterworths, London.

Baughman, Wilbur T., (1971) "Rankin County Geology and Mineral Resources," *Bulletin 115*, Mississippi Geological, Economic and Topographical Survey, Jackson, Mississippi.

Baum, Neal P., and Stough, Trudey, (1975) *Evaluation of Inertial and Laser Profilometer Systems*, Report No. FAA-RD-74-188, Federal Aviation Administration, Washington, DC.

Beckman, G. G., Hubble, G. D., and Thompson, C. H., (1970) "Gilgai Forms, Distribution, and Soil Relationships in North-Eastern Australia," in *Proceedings, Symposium on Soils and Earth Structures in Arid Climates*, Institution of Engineers, Adelaide, Australia.

Bingham, G. E., Johnson, M. N., and Lemon, E. R., (1972) "Influence of Heat Sink Design on Thermocouple Psychrometer Response," in *Psychrometry in Water Relations Research*, Utah Agricultural Experiment Station, Utah State University.

Compton, Phil V., (1970) *A Study of the Swelling Behavior of An Expansive Clay as Influenced by the Clay Microstructure, Soil Suction, and External Loading*, AFWL-TR-70-26, Air Force Weapons Laboratory, Kirtland Air Force Base, New Mexico.

Design and Construction of Post-Tensioned Slabs-on-Ground, Post-Tensioning Institute, Phoenix, Arizona, October 1978.

Dowling, J. and Franco, R., (1974) "Evaluación de Terrenos y Deslizamientos," Second Columbian Geotechnical Symposium, Columbia Geotechnical Society, Bogotá, Columbia.

Durbin, J. and Watson, G. S., (1951) "Testing for Serial Correlation in Least Squares Regression II," *Biometrika*, Vol. 38:159-78.

Eckardt, F. E., (1960) "Eco-physiological Measuring Techniques Applied to Research on Water Relations of Plants in Arid and Semi-arid Regions, in *Arid Zone Rev.*: XV. UNESCO, New York.

Escario, Ventura, (1969) "Swelling of Soils in Contact with Water at a Negative Pressure," *Proceedings, 2nd International Research and Engineering Conference on Expansive Clay Soils*, College Station, Texas, pp. 207-217.

Fawcett, R. C., and Collis-George, N., (1967) "A Filter Paper Method of Determining the Moisture Characteristics of Soil," *Australian Journal of Experimental Agriculture and Animal Husbandry*, V. 7:162-167.

Footings and Foundations for Small Buildings in Arid Climates, edited by Faragher, Phillip J., Woodburn, John A., and Selby, Jonathan, The Institution of Engineers, Australia, South Australia Division, Adelaide, June 1979.

Fredlund, D. G., and Morgenstern, N. R., (1977) "Stress State Variables for Unsaturated Soils," *Journal of the Geotechnical Engineering Division*, ASCE, Vol. 103, No. GT5:447-466.

Fredlund, D. G., Hasan, J. U., and Filson, H. L., (1980) "The Prediction of Total Heave," *Proceedings*, 4th International Conference on Expansive Soils, ASCE, Vol. 1:1-17.

Gardner, R., (1937) "A Method of Measuring the Capillary Tension of Soil Moisture over a Wide Moisture Range," *Soil Science*, Vol. 43:277-283.

Gardner, W. R., (1956) "Calculation of Capillary Conductivity from Outflow Data," *Soil Science Society of America, Proceedings*, Vol. 20:317-320.

Gerardi, Anthony G. and Lohwasser, Adolph K., (1973) *Computer Program for the Prediction of Aircraft Response to Runway Roughness, Volume I, Program Development*, Technical Report No. AFWL-TR-73-109, Vol. I, U.S. Air Force Flight Dynamics Laboratory.

Gerardi, Anthony G. and Lohwasser, Adolph K., (1974) *Computer Program for the Prediction of Aircraft Response to Runway Roughness, Volume II, User's Manual*, Technical Report No. AFWL-TR-73-109, Vol. II, U.S. Air Force Flight Dynamics Laboratory.

Gerardi, Anthony G., (1978) "Dynamic Response of Aircraft to Pavement Unevenness," in *Research in Airport Pavements*, Special Report 175, Transportation Research Board, Washington, DC, pp. 91-96.

Gradmann, H., (1934) "Über die Messung von Bodensaugwerten" (About the measurement of soil suction), *Ab. Wiss Bot.* 80:92-111.

Hallsworth, E. G., (1968), "The Gilgai Phenomena," Chapter X, in *A Handbook of Australian Soil*, Rellion Technical Publications, Glenside, South Australia.

Hansen, H. C., (1926) "The Water Retaining Power of the Soil," *Journal of Ecology*, Vol. 14:111-119.

Holt, J. H., (1969) "A Study of Physico-Chemical, Mineralogical, and Engineering Index Properties of Fine-Grained Soils in Relation to Their Expansive Characteristics," Dissertation, Texas A & M University, College Station.

Horn, A., "Swell Test on Expansive Soils," *Mitteilungen der Deutschen Forschungsgesellschaft für Bodenmechanik* (degebo), No. 32:81-87.

Horta da Silva, J. A., (1975) "Solos Expansivos-Comportamento, Identificação, Quantificação da Instabilidade Volumétrica e Projectos de Fundações (1 Parte)," *Geotécnica*, No. 13:29-63, Portugal.

Houbolt, John C., (1961) "Runway Roughness Studies in the Aeronautical Field," *Journal of the Air Transport Division*, ASCE, Vol. 87, No. ATI:11-31.

Johnson, L. D., (1974) *An Evaluation of the Thermovigil Peacock Type Device for the Measurement of Suction in Clay Soils*, Technical Report No. S-74-1, U.S. Army Engineer Waterways Experiment Station, Vicksburg, Mississippi.

Loudon, P. A., (1972) "Recommendations for Pavements on Expansive Subgrades," *Internal Report RSS/72*, National Institute Road Research, Pretoria, South Africa.

Low, Phillip, (1977) "The Mechanisms of Clay Swelling," Presentation at the Symposium on Water Movement and Equilibrium in Swelling Soils, American Geophysical Union, San Francisco, California.

Lytton, R. L., (1977) "The Characterization of Expansive Soils in Engineering," Presentation at the Symposium on Water Movement and Equilibrium in Swelling Soils, American Geophysical Union, San Francisco, California.

Lytton, R. L., Boggess, R. L., and Spotts, J. W., (1976) "Characteristics of Expansive Clay Roughness of Pavements," *Engineering Geology, Transportation Research Record No. 568*:9-23, Washington, DC.

McKeen, R. G., (1977) "Characterizing Expansive Soils for Design Purposes," Presentation at the Joint Meeting of Texas, New Mexico, and Mexico Sections, American Society of Civil Engineers, Albuquerque, New Mexico.

McKeen, R. G., (1976) *Design and Construction of Airports Pavements in Expansive Soils*, FAA-RD-76-66, Federal Aviation Administration, Washington, DC.

McKeen, R. G., (1969) "Shrinkage-Cracking Characteristics of Structural Light-weight Concrete," Thesis, Texas A & M University, College Station.

McKeen, R. G. and Nielsen, J. P., (1978) *Interpreting Hygrometric Data for Airfield Pavement Design*, FAA-RD-78-59, Federal Aviation Administration, Washington, DC.

McQueen, I. S., and Miller, R. F., (1977) "The Wide-Range (Filter Paper) Method for Measuring the Forces of Moisture Retention," personal correspondence.

McQueen, I. S.. and Miller, R. F., (1974) "Approximating Soil Moisture Characteristics from Limited Data: Empirical Evidence and Tentative Model," *Water Resources Research*, Vol. 10, No. 3:521-527.

McQueen, Irene S., and Miller, R. F., (1968) "Calibration and Evaluation of a Wide-Range Gravimetric Method for Measuring Moisture Stress," *Soil Science*, Vol. 106 No. 3: pp. 225-231.

Meyn, R. L. and White, R. S., (1972) "Calibration of Thermocouple Psychrometers: A Suggested Procedure for Development of a Reliable Predictive Model," in *Agrometeorology in Water Management*, Utah Agricultural Experiment Station, Utah State University, Logan, Utah, pp. 56-64.

Michurin, B. N., and Lytayev, I. A., (1971) "Relationship between Moisture Content, Moisture Tension, and Specific Surface Area in Soil," *Soil Physics*, Vol. 8:1093-1103.

Mitchell, Peter W., (1980) "The Structural Analysis of Footings on Expansive Soil," in Kenneth W. G. Smith and Associates, *Ground Movement* N. 1, Second Edition, Newton, South Australia.

Nnyamah, Joe U., and Black, T. A., (1977) "Field Performance of the Dew Point Hygrometer in Studies of Soil-Root Water Relations," *Plant, Soil, and Water*, Vol. 57:437-444.

Nunez, E., and Carrillo, A., (1977) "Suelos Especiales: Colapsibles, Expansivos, Preconsolidados por Desecacion," *Boletin de la 5th Panamerican Conference on Soil Mechanics and Foundation Engineering*, Buenos Aires, Argentina, Vol. IV, Gen. Rep. 11:43-105.

O'Neill, Michael W. and Ghazzaly, Osman I., (1977) "Swell Potential Related to Building Performance," *Journal of the Geotechnical Engineering Division, ASCE*, Vol. 103, No. GT 12:1363-1379.

Parkinson, J. J., and Fenoux, G. Y.,(1976) "Soulevement de Fond de Fouille en Site Urban," *Proceedings, 6th European Conference on Soil Mechanics and Foundation Engineering*, Vienna, Austria, Vol. 1.2:641-646.

Pearring, J. R., (1968) "A Study of Basic Mineralogical, Physical-Chemical, and Engineering Properties of Laterite Soils," Dissertation, Texas A & M University, College Station.

Pore Pressure and Suction in Soils, Conference organized by the British National Society of the International Society of Soil Mechanics and Foundation Engineering, Butterworths, London, 1961.

Potter, Loren D., Reynolds, Robert C., and Louderbough, Ellen T., (1979) *Properties of Mansos Shale Soils and Effects on Plant Communities*, Final Report, U.S. Forest Service, Contract No. 16-729-GR, University of New Mexico, Albuquerque.

Rawlins, S. L., (1966) "Theory for Thermocouple Psychrometers Used To Measure Water Potential in Soil and Plant Samples," *Agricultural Meteorology*, Vol. 3:293-310.

Richards, L. A., and Ogata, G., (1958) "Thermocouple for Vapor Pressure Measurement in Biological and Soil Systems at High Humidity," *Plant Physiol.*, 128:1089-1090.

Riggle, F. R., (1978) "Soil Water Potential Determinations with Thermocouple Psychrometers," Master of Agriculture Integrating Paper, University of Minnesota, St. Paul.

Ritchie, J. T., Kissel, D. E., and Burnett, E., "Water Movement in Undisturbed Clay Soil," *Proceedings*, Soil Science Society of America, Vol. 36, No. 6:874-879.

Rodrigues, M. M., (1975) "Las Arcillas Expansivas: Su Estudio y Tratamiento," Laboratorio del Transporte y Mechanica del Suelo, *Bol. Inv. T. 1*, pp. 3-30.

Russam, Kenneth, and Coleman, J. D., "The Effect of Climatic Factors on Sub-grade Moisture Conditions," *Geotechnique*, Vol. III, No. 1:22-28.

Seeman, Douglas R., and Nielsen, John P., (1976) "Suggested Procedure To Isolate and Repair Runway Roughness," Letter Report CERF-11, University of New Mexico, Albuquerque.

Slack, D. C., (1975) "Modeling the Uptake of Soil Water by Plants," Dissertation, University of Kentucky, Lexington.

Snethen, D. R., and Johnson, L. D., (1980) *Evaluation of Soil Partition from Filter Paper*, Miscellaneous Paper GL-80-4, U.S. Army Waterways Experiment Station, Vicksburg, Mississippi.

Snethen, D. R., Johnson, L. D., and Patrick, D. M., (1977) *An Identification of the Natural Microscale Mechanisms that Cause Volume Change in Expansive Clays*, FHWA-RD-77-75, Federal Highway Administration, Washington, DC.

"Soil Survey Laboratory Data and Descriptions for Some Soils of Arizona," *Soil Survey Investigations Report No. 28*, Soil Conservation Service, U.S. Department of Agriculture, August 1974.

"Soil Survey Laboratory Data and Descriptions for Some Soils of California," *Soil Survey Investigations Report No. 24*, Soil Conservation Service, U.S. Department of Agriculture, June 1973.

"Soil Survey Laboratory Data and Description of Some Soils of Texas," *Soil Survey Investigations Report No. 30*, Soil Conservation Service, U.S. Department of Agriculture, January 1976.

Sonnenburg, Paul N., (1976) *Analysis of Airfield runway roughness criteria*, Report No. FAA-RD-75-110, Federal Aviation Administration, Washington, DC.

Sorocan, E., (1974) *Stroizdatoo sovremennoi na Naukach i Prakticheskikh issledovaniyakh*, Stroizdat Publ., Moscow.

Spanner, D. C., (1951) The Peltier Effect and Its Use in the Measurement of Suction Pressure, *Journal of Experimental Botany*, Vol. 11:145-168.

Spotts, J. W., (1974) "The Role of Water in Gilgai Formation," Dissertation, Texas A & M University, College Station.

Statement of the Review Panel: *Engineering Concepts of Soil-water Equilibrium and Moisture Changes in Soils*, Symposium in Print, Butterworths, 1965.

Stearns, Samuel D., (1975) *Digital Signal Analysis*, Hayden Book Company, Rochelle Park, N.J..

Stocker, O., (1930) "Über die Messung von Bodensaughkräften und ihren Verhältnis zu den Wurzelsaughkräften," *Z. Bod.* 23:27-56.

Stone, R. O., and Dugundji, T., (1965) "A Study of Microrelief--Its Mapping, Classification, and Quantification by Means of a Fourier Analysis," *Engineering Geology*, Vol. 1, No. 2:39-187.

Teng, T. C. Paul, Mattox, Robert M., and Clisby, M. Barrett, (1972) *A Study of Active Clays as Related to Highway Design*, Final Report, MSHD-RD-72-045, Vol. 1 and Vol. 2, Mississippi State Highway Department, Vicksburg.

Tetens, O., "Über einige meteorologische Begriffe," *Z. Meteorol.* 6:297-309.

Thornthwaite, C. W., (1948) "An Approach Toward a Rational Classification of Climate," *Geographical Review*, Vol. 38, No. 1:54-94.

Velasco, Manuel O., (1980) "Pavement Roughness on Expansive Clays," Thesis at A & M University, College Station.

Verbrugge, J. C., (1974) "Contribution A La Mesure De La Suction Et De La Pression Interstitielle Dans Les Sols Non Satures," Brussels Free University, School of Applied Sciences, Jacques Verdoyen Laboratory. (USACRREL, Draft Translation No. 529).

"Water in Roads: Prediction of Moisture Content of Road Subgrades," Organization for Economic Cooperation and Development, Paris, France, 1973.

Williams, O. E., and Sedgley, R. M., "A Simplified Filter Paper Method for Determining the 15-Atmosphere Percentage of Soils," *Australian Journal of Experimental Agriculture and Animal Husbandry*, Vol. 5:201-202.

ASCE, (1975) *Road Structures, A Design Guide and Commentary*, Structural Division, New York.

Wray, W. K., (1978) "Development of a Design Procedure for Residential and Light Commercial Slabs-on-Ground Constructed over Expansive Soils," Dissertation, Texas A & M University, College Station.

SYMBOLS AND ABBREVIATIONS

\bar{A}	Weighted amplitude of frequency components
AC	Asphalt concrete
Ac	Clay activity
C	Percent clay
CEC	Cation exchange capacity
CEAc	Cation exchange activity
COLE	Coefficient of linear extensibility
CV	Coefficient of variation
D	Equivalent depth of pavement in terms of asphalt concrete
DF	Deficit, Thornthwaite method
DFW	Dallas/Fort Worth airport field experiment site
DP	Depletion, Thornthwaite method
E	Modulus of elasticity
FP	Filter paper
GAL	Gallup airport field experiment site
ΔH	Elevation change
HC	Water holding capacity, Thornthwaite method
JSN	Jackson airport field experiment site
L	Overall sampling length
LL	Liquid limit
$\Delta L/L_d$	Linear strain relative to dry dimensions
$\Delta L/L_z$	Linear strain in the vertical direction
NAS	Dallas Naval Air Station survey site
NMERI	New Mexico Engineering Research Institute
PCC	Portland cement concrete
PE	Potential evapotranspiration, Thornthwaite method
PI	Plasticity index
R	Rainfall, Thornthwaite method
R^2	Coefficient of determination
RC	Recharge, Thornthwaite method
S	Degree of saturation; surplus, Thornthwaite method
TAXI	Computer code used to calculate aircraft accelerations

TCP	Thermocouple psychrometer
TI	Thorntwaite moisture index
$\Delta V/V$	Volumetric strain
$\Delta V/V_d$	Volume change with respect to dry volume
$\Delta V/V_i$	Change of volume with respect to initial volume
WES	U. S. Army Waterways Experiment Station
a_n	Half-amplitude of the nth frequency component
e	Void ratio
emf	electromotive force
f	Lateral restraint factor
f_n	Spatial frequency of the nth component
h	Suction
Δh_a	Average suction in the top 1.5 m
k	Subgrade modulus
m	Moisture characteristic
h_f, h_i	Final and initial suction
pF	Logarithmic unit for suction
w	Water content of soil
$\Delta w/2a$	Ratio of pavement amplitude to uncovered soil amplitude
$\beta\lambda$	Nondimensional stiffness characteristic
$\Delta \bar{A}$	Slope of the \bar{A} versus Δh relationship (Figure 7-1)
γ_d	Soil sample dry unit weight after oven drying
γ_h	Suction compression index
γ_w	Soil sample dry unit weight at 2.53 pF
γ_o	Total stress compression index
λ	Wavelength
λ_d	Characteristic wavelength for design
λ_n	Wavelength of nth component
λ_0	Characteristic wavelength of uncovered soil

APPENDIX A
ELEVATION PROFILES

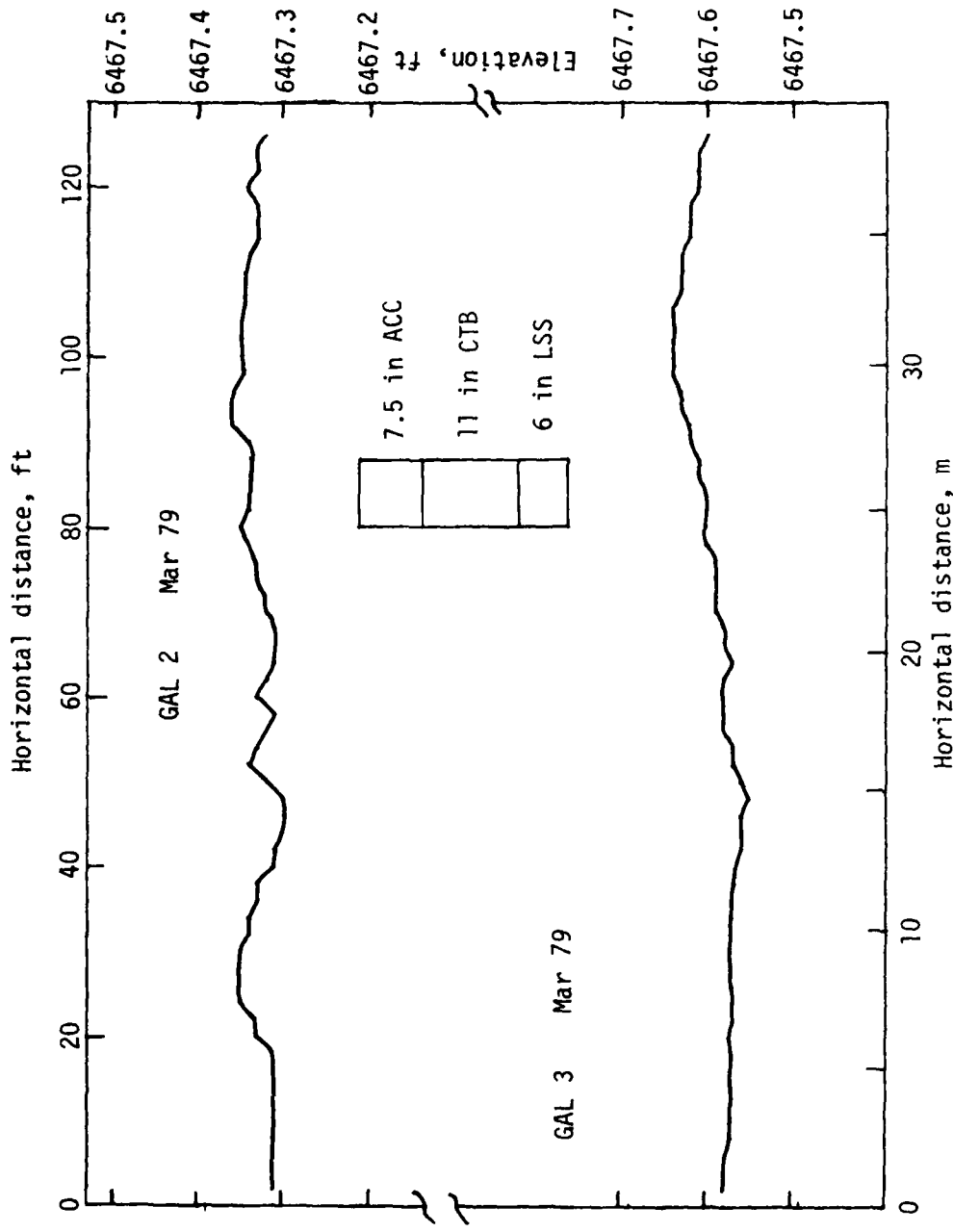


Figure A-1. Elevations along profiles at GAL.

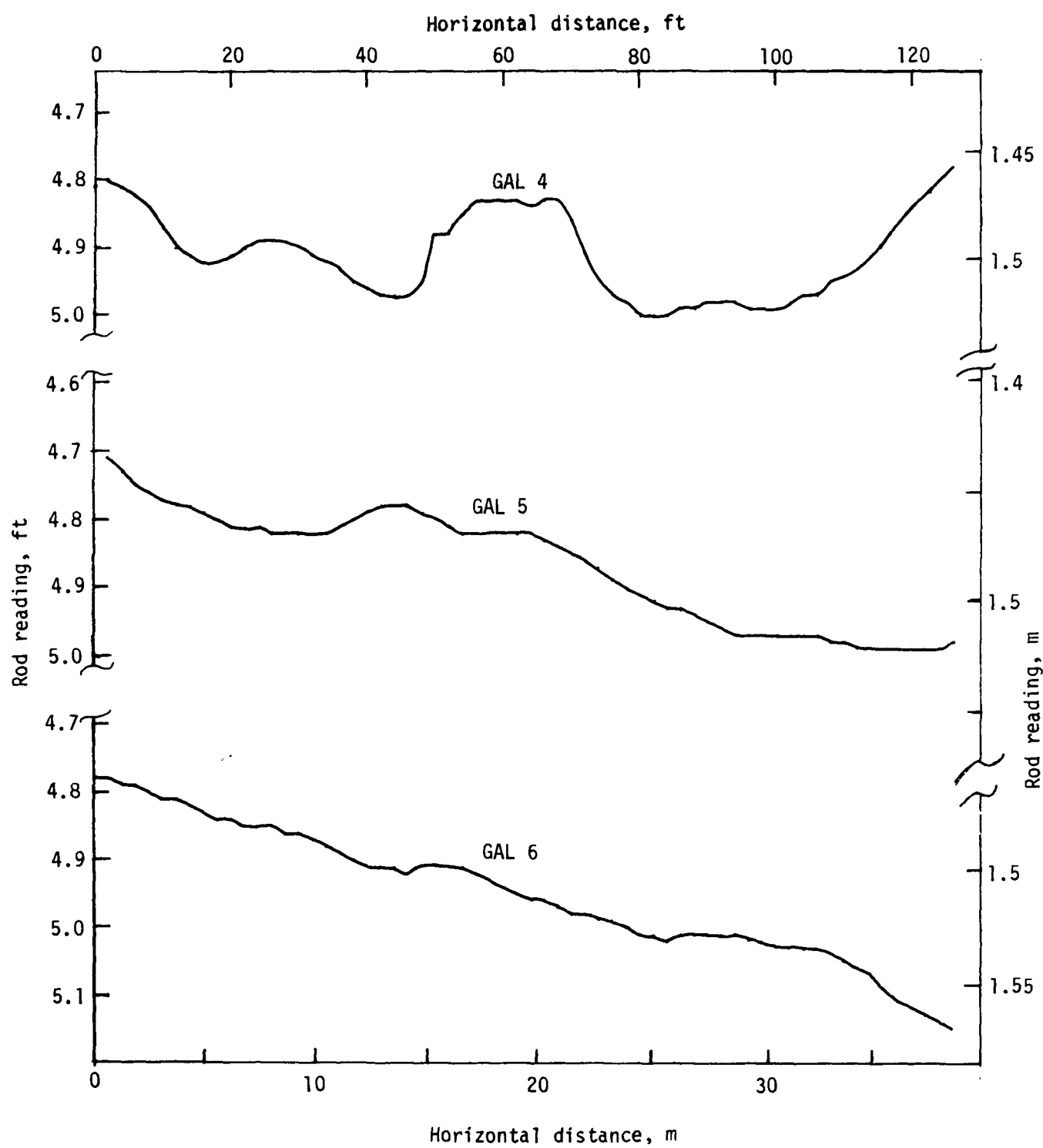


Figure A-2. Elevation data along Gallup runway.

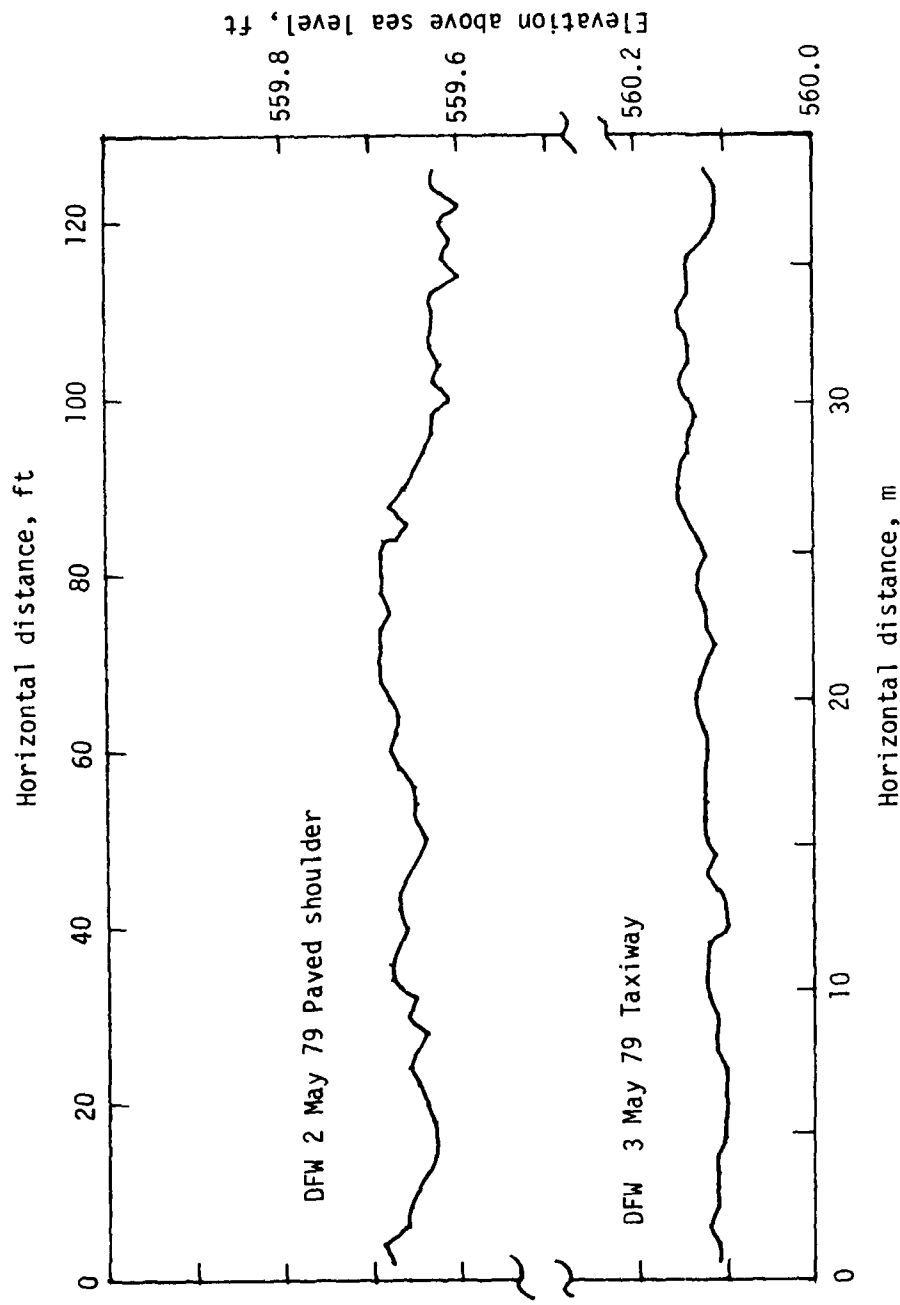


Figure A-3. Typical elevation data on Dallas/Ft. Worth taxiway.

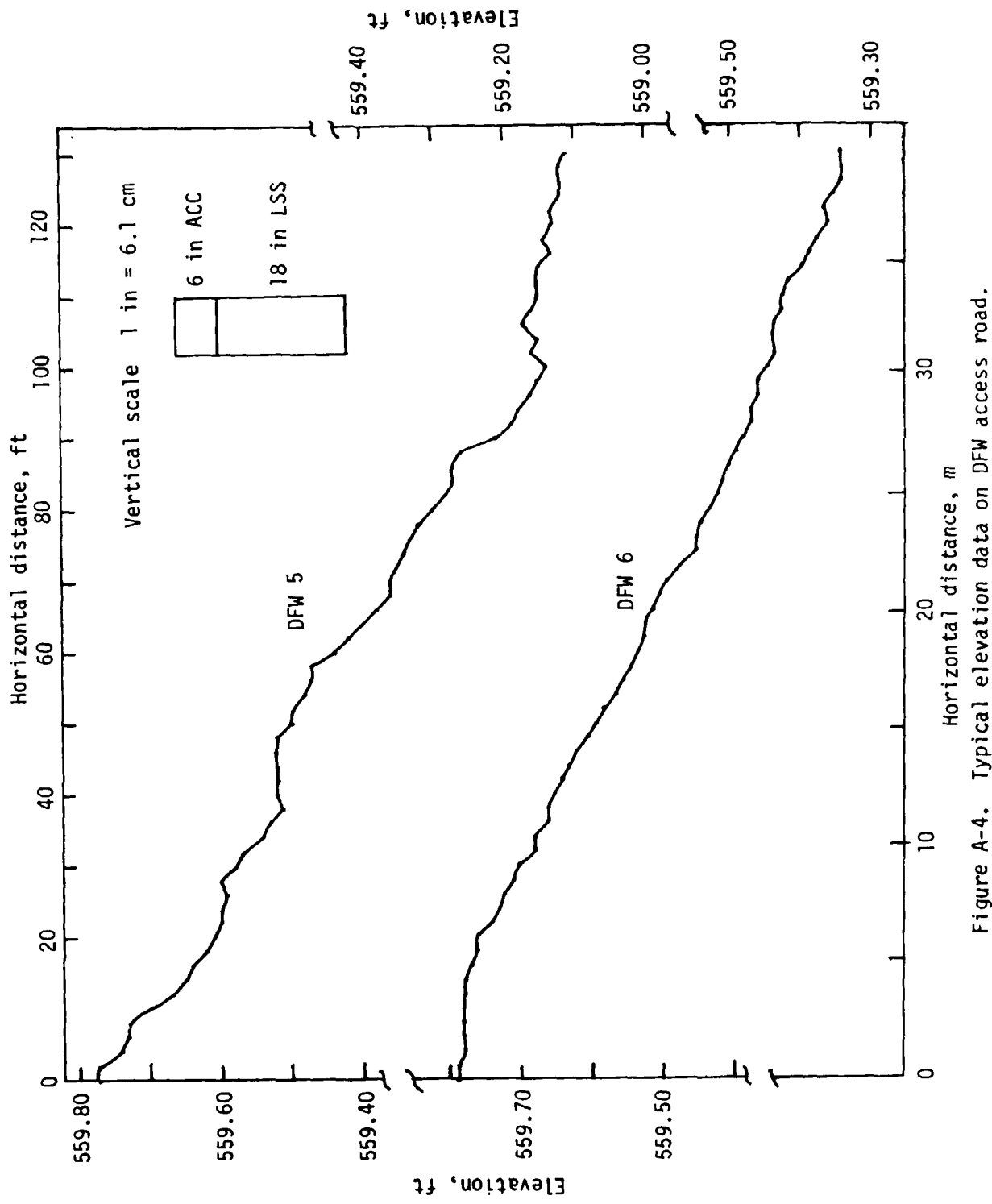


Figure A-4. Typical elevation data on DFW access road.

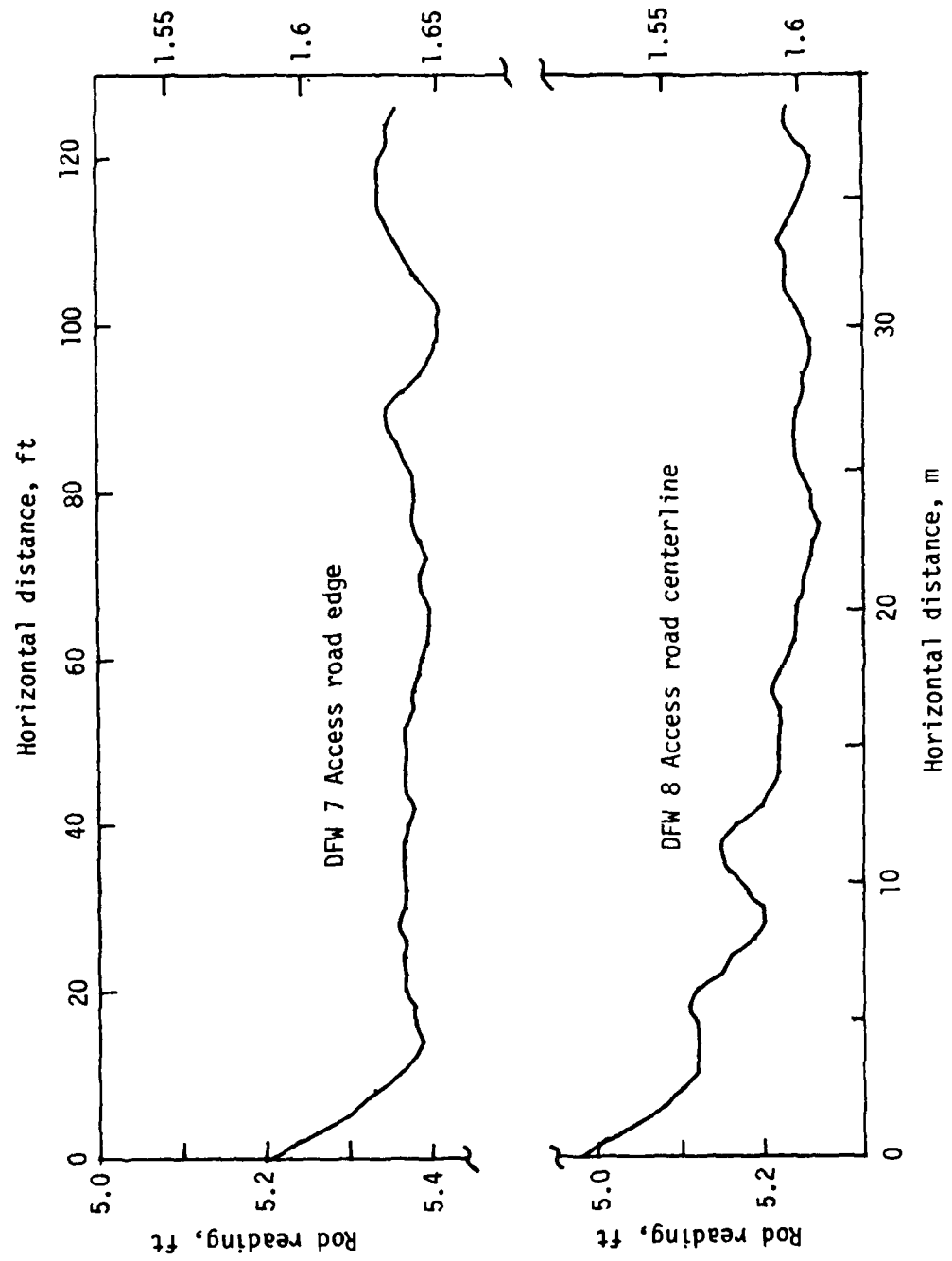


Figure A-5. Elevation profile on DFW access road.

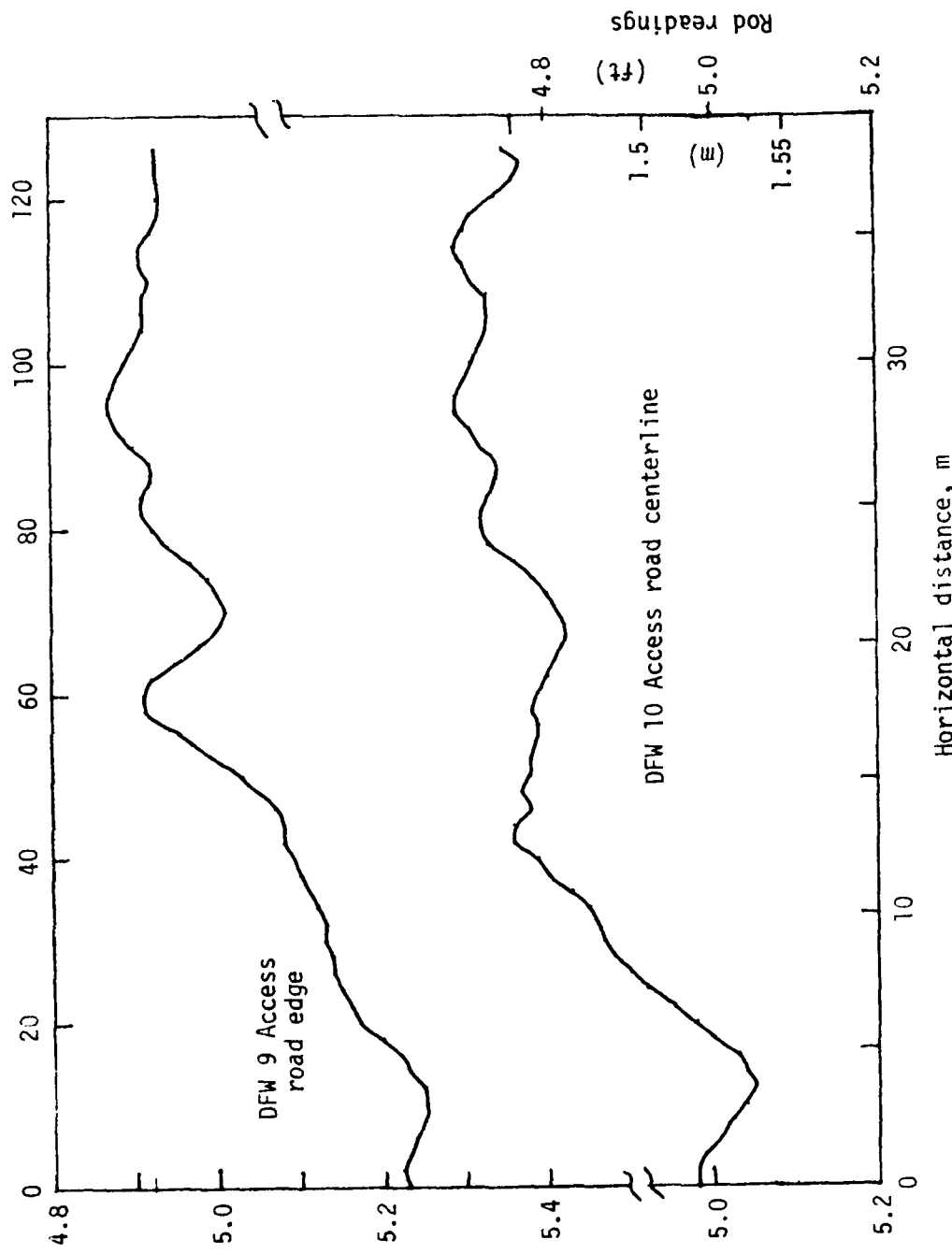


Figure A-6. Elevation profile on DFW access road.

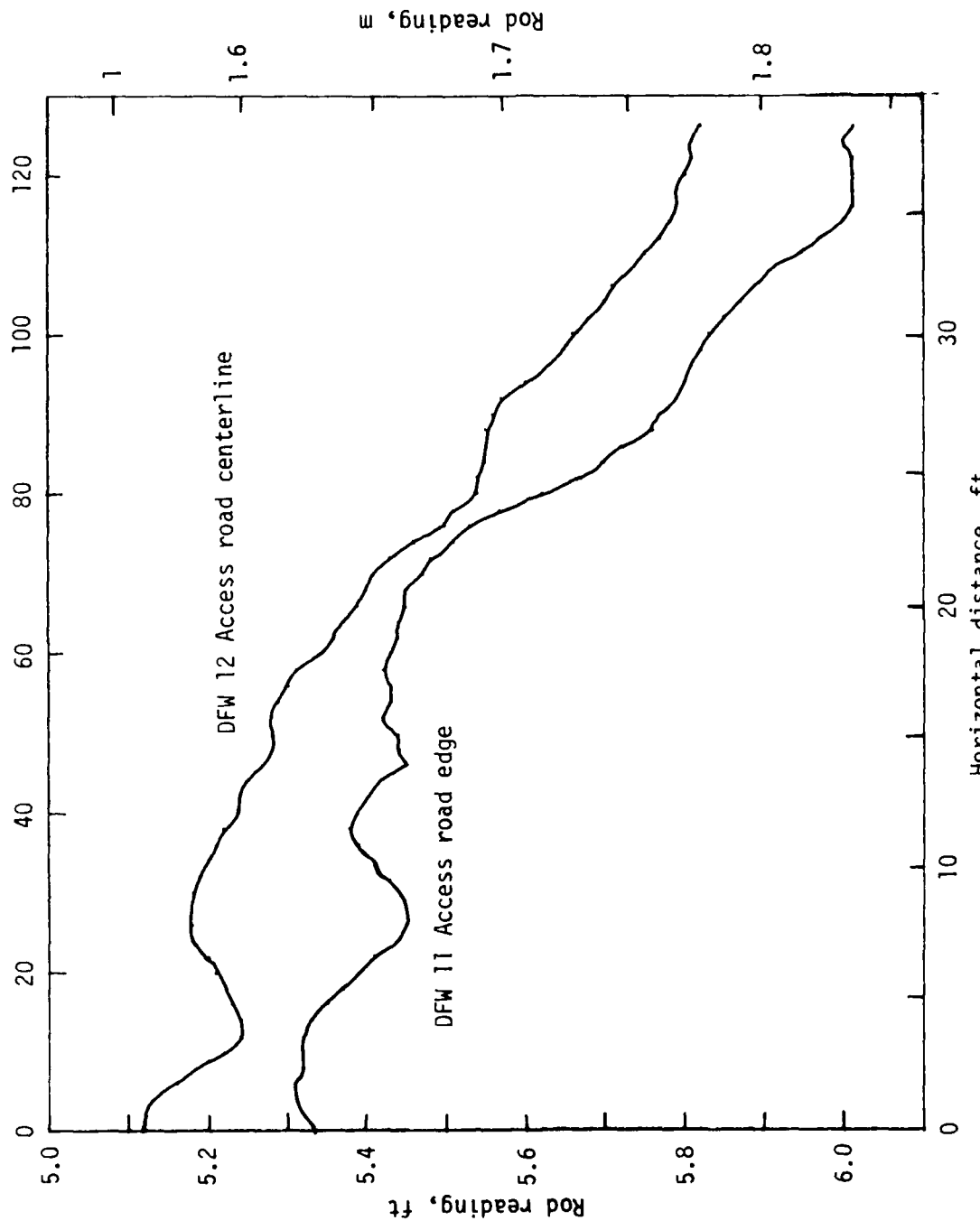


Figure A-7. Elevation profiles on DFW access road.

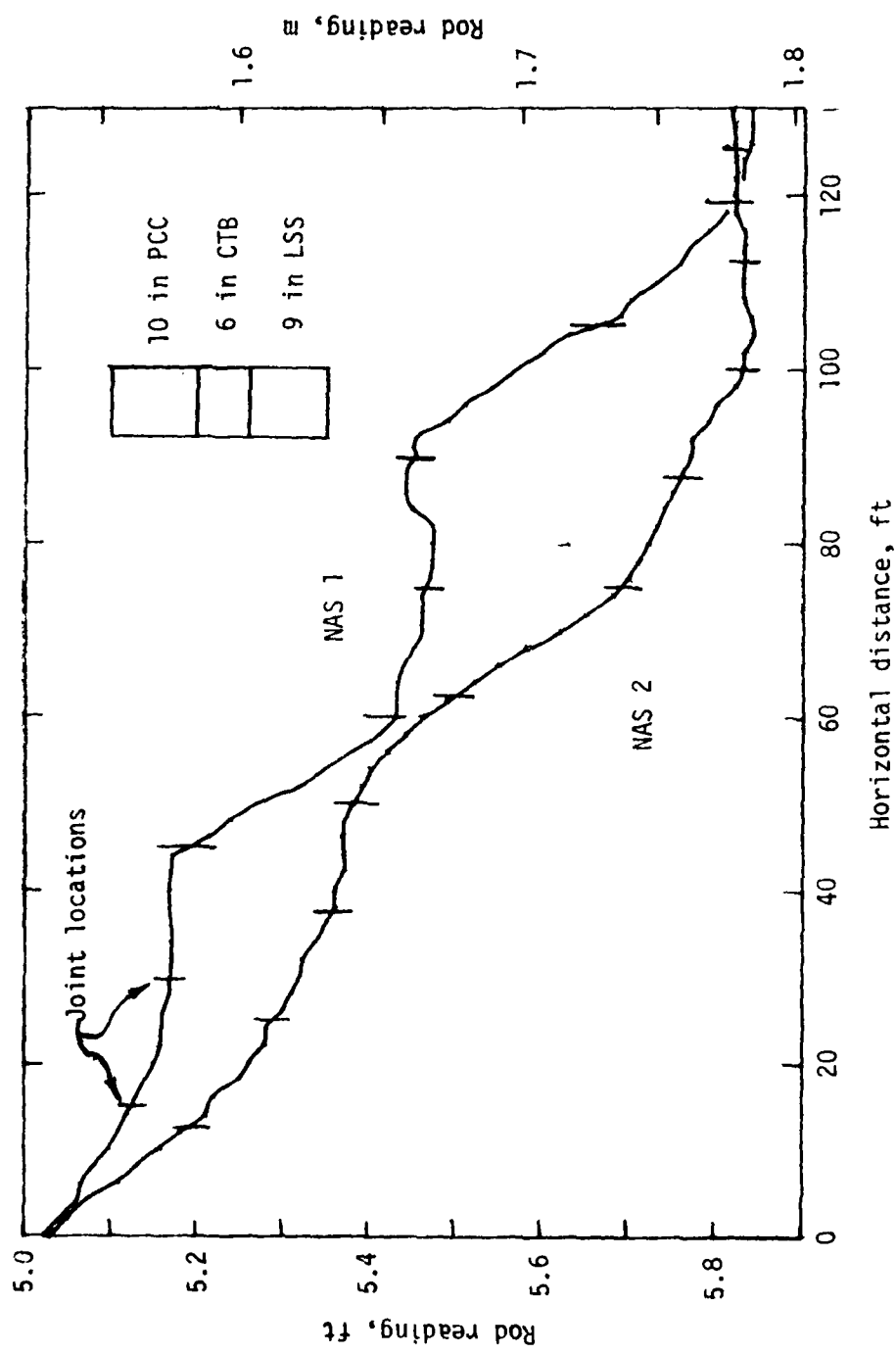


Figure A-8. Actual profile of Dallas Naval Air Station.

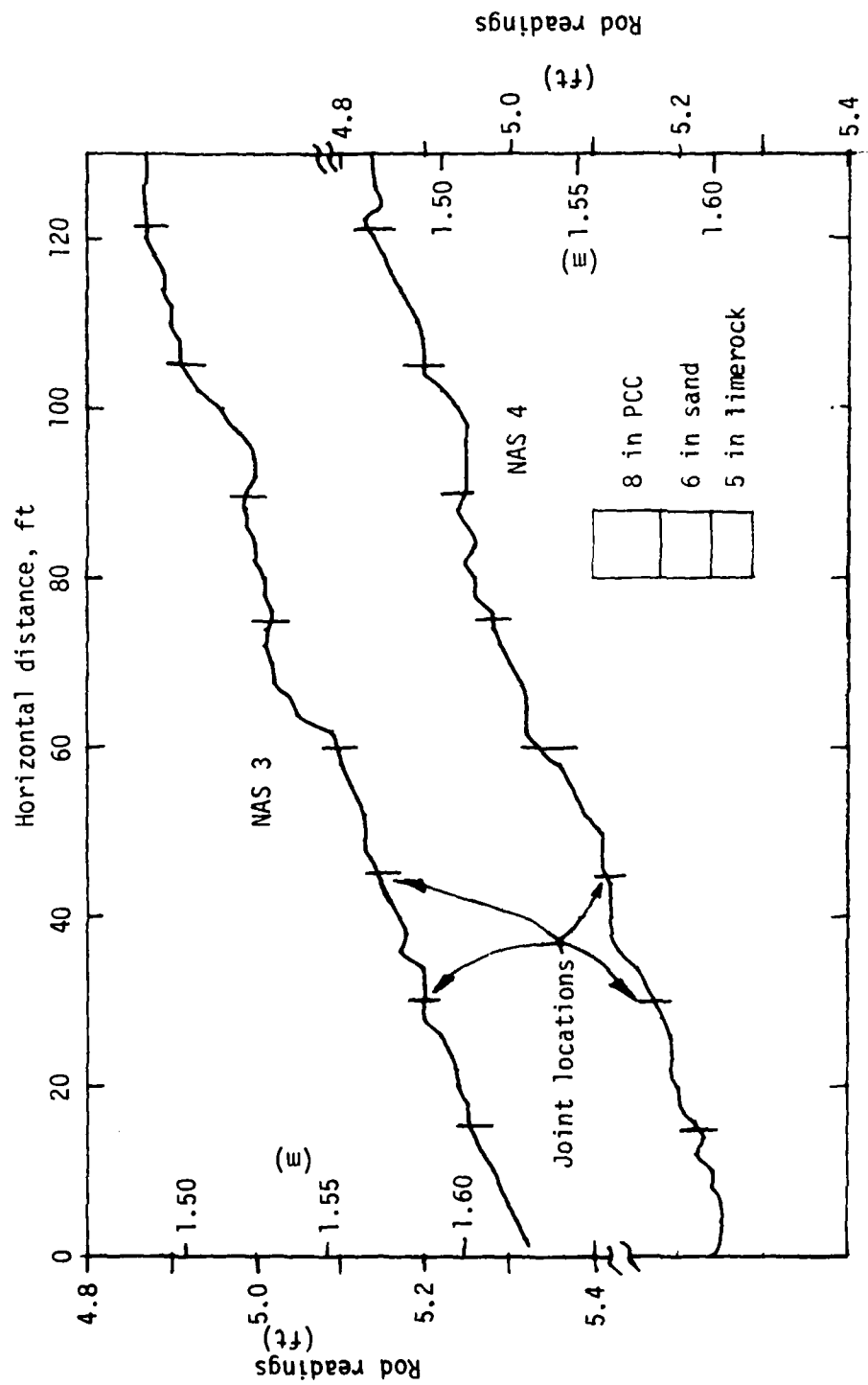


Figure A-9. Actual profile, Dallas Naval Air Station.

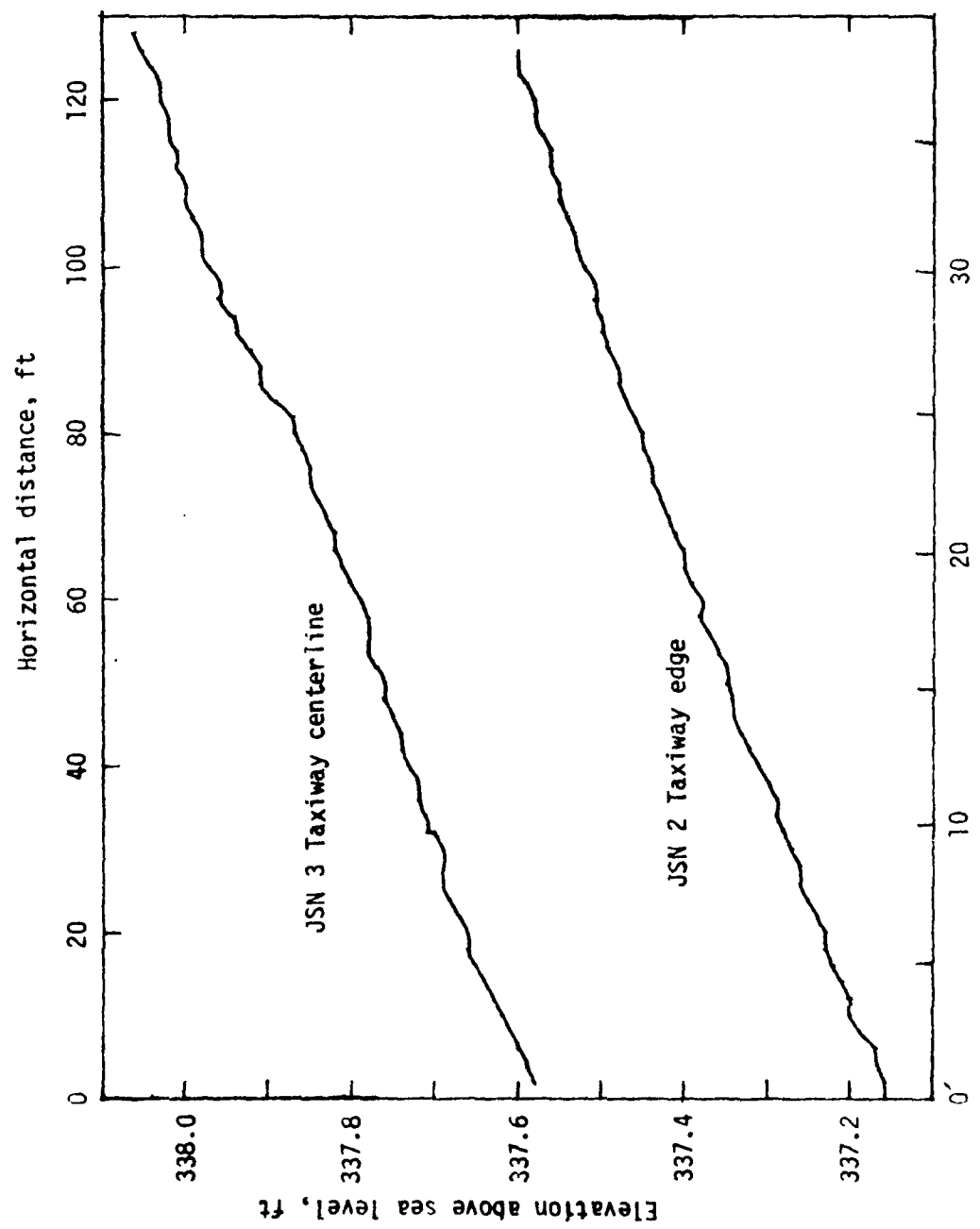


Figure A-10. Elevations along JSON taxiway.

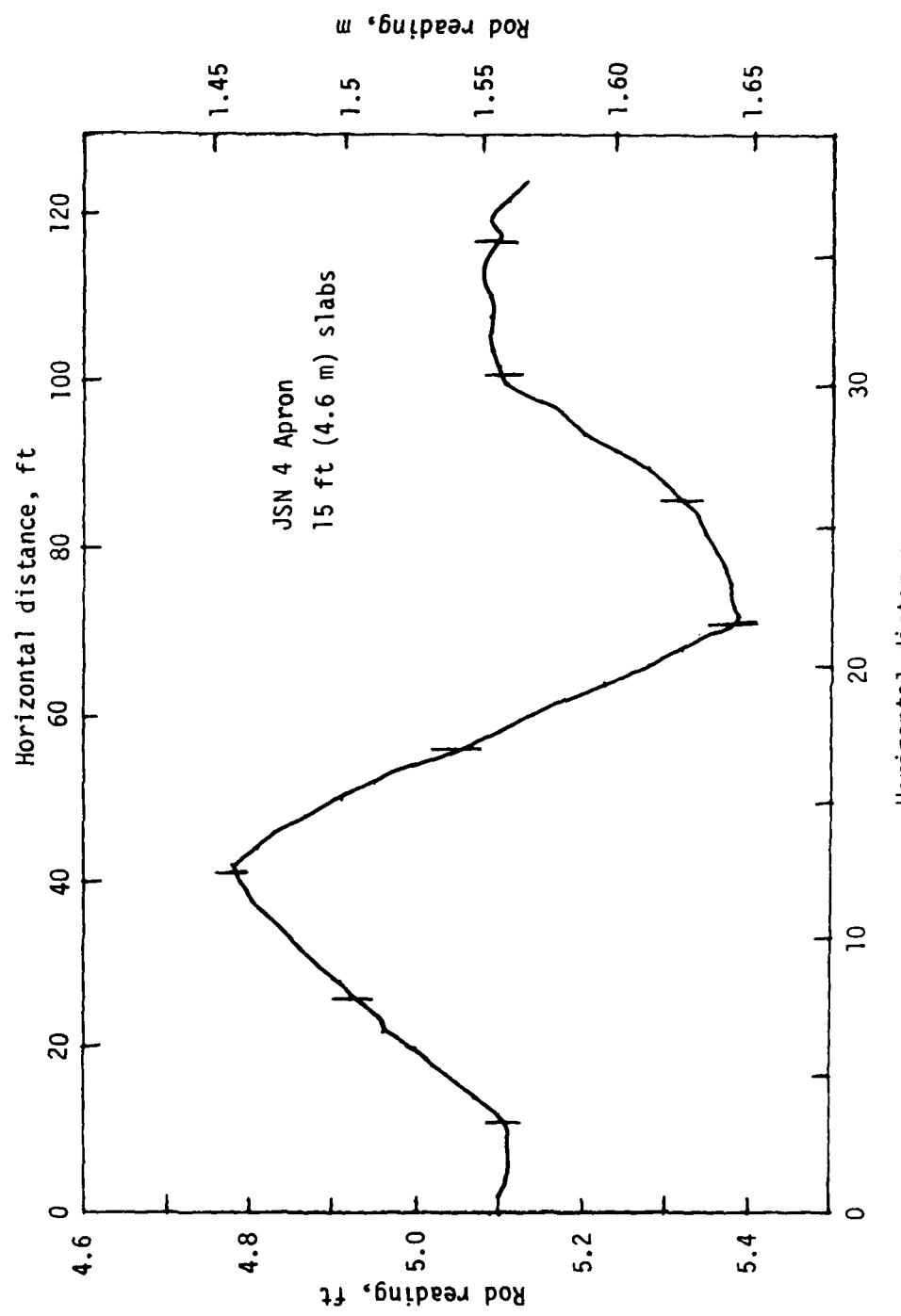


Figure A-11. Elevation profile along apron.

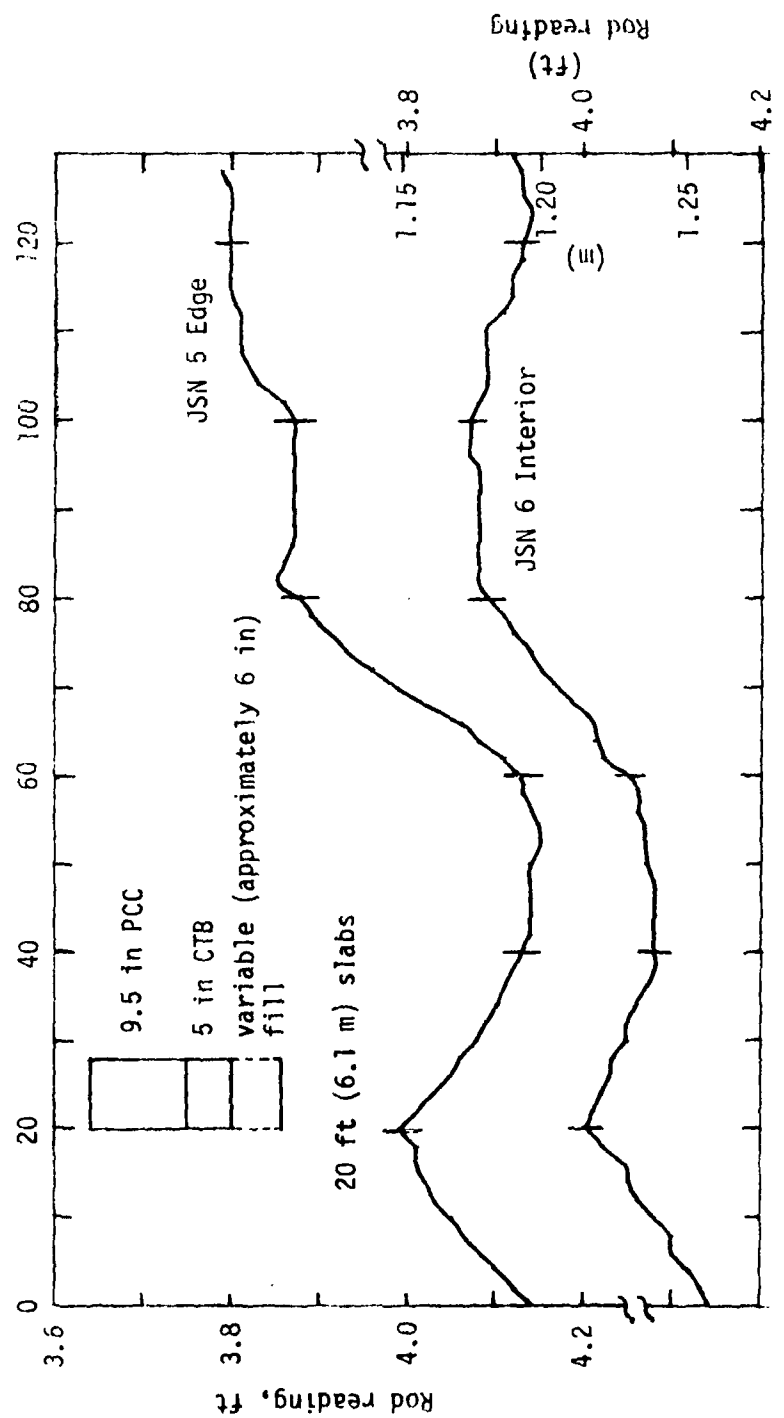


Figure A-12. Actual profiles, west taxiway Jackson airport.

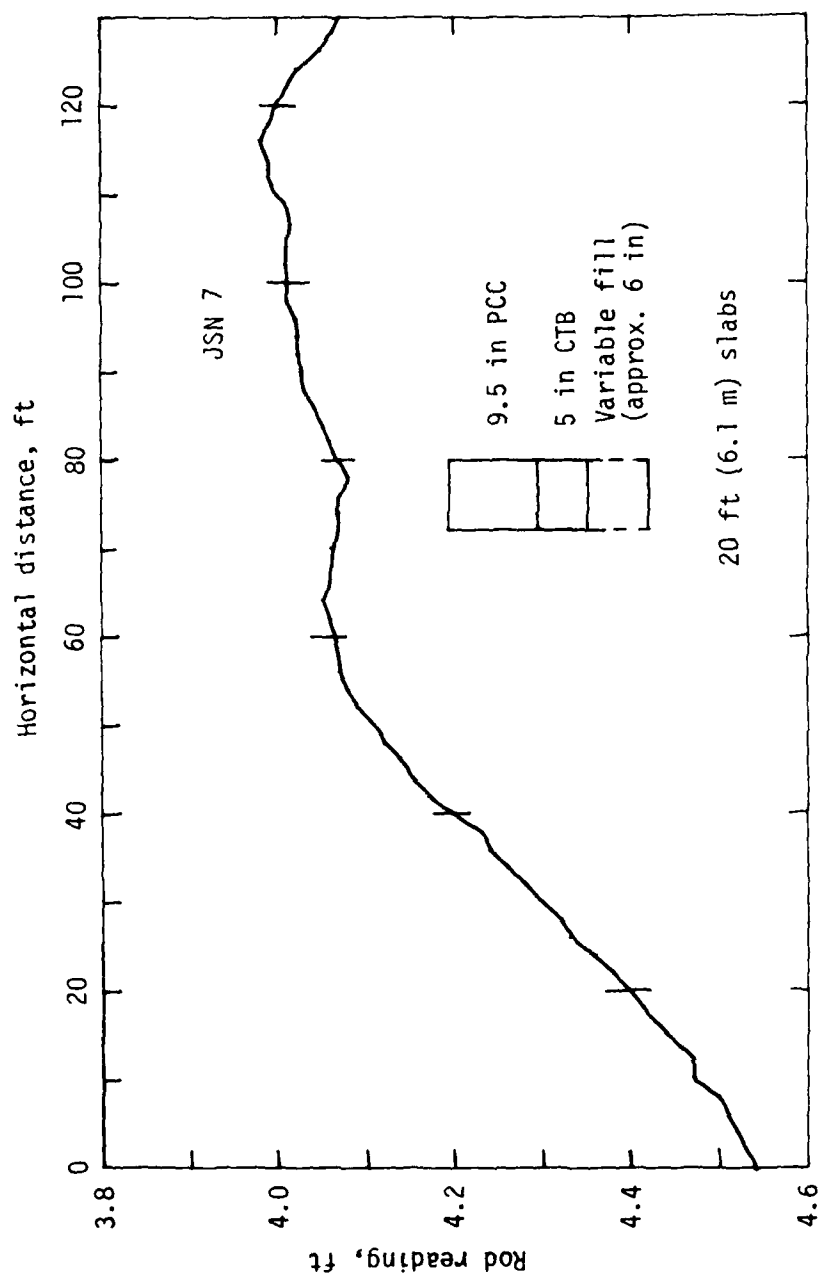


Figure A-13. Actual profiles, west taxiway Jackson airport.

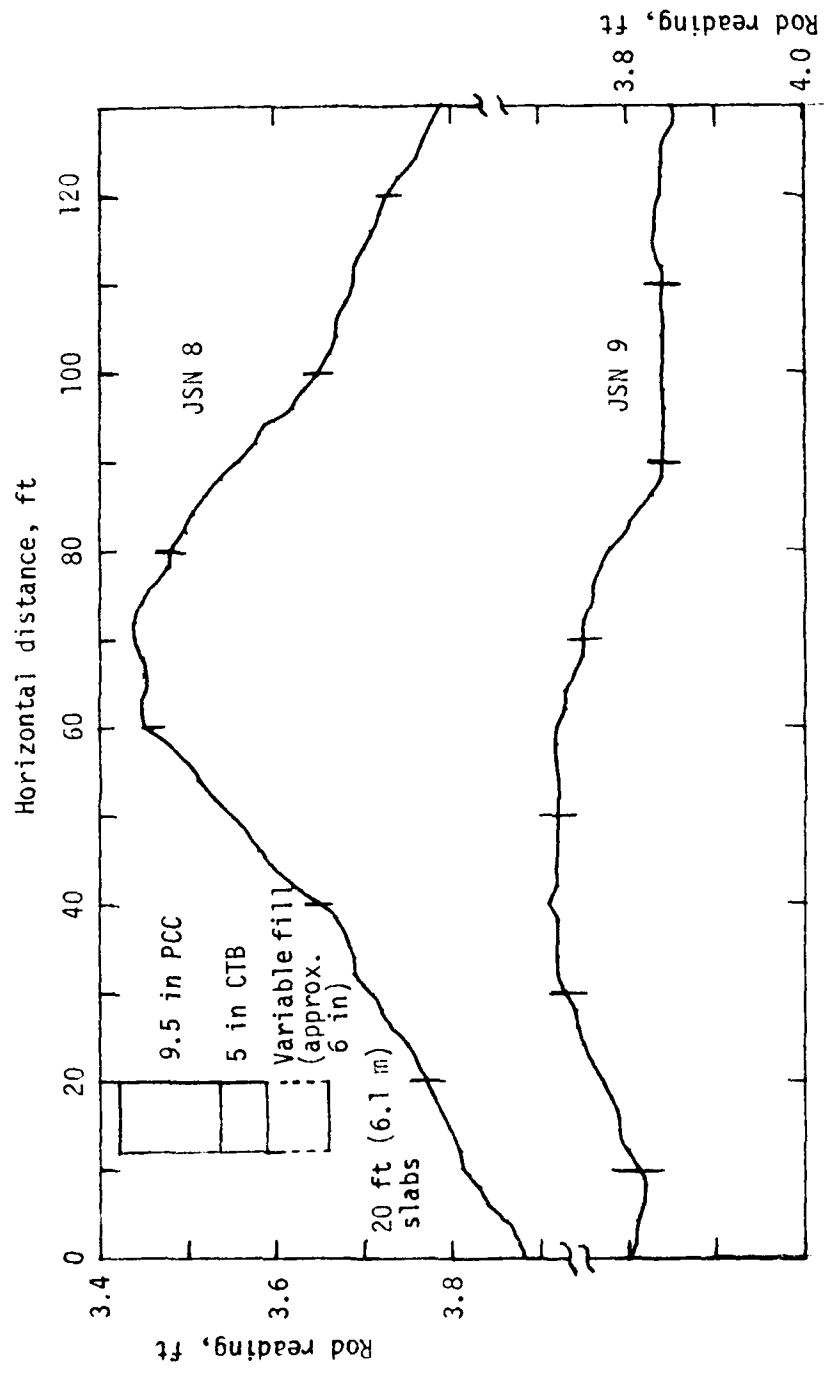


Figure A-14. Actual profiles, west taxiway Jackson airport.

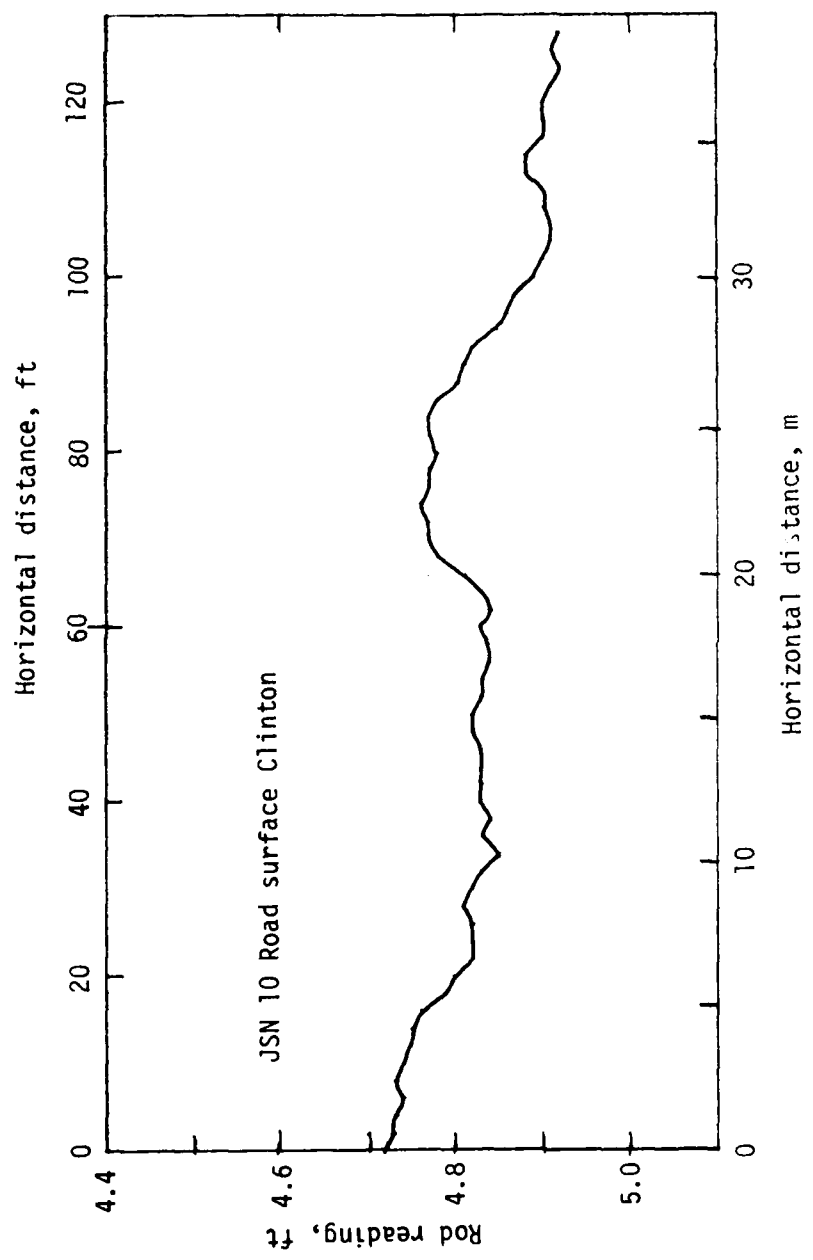


Figure A-15. Elevation profile on road at Clinton, MS.

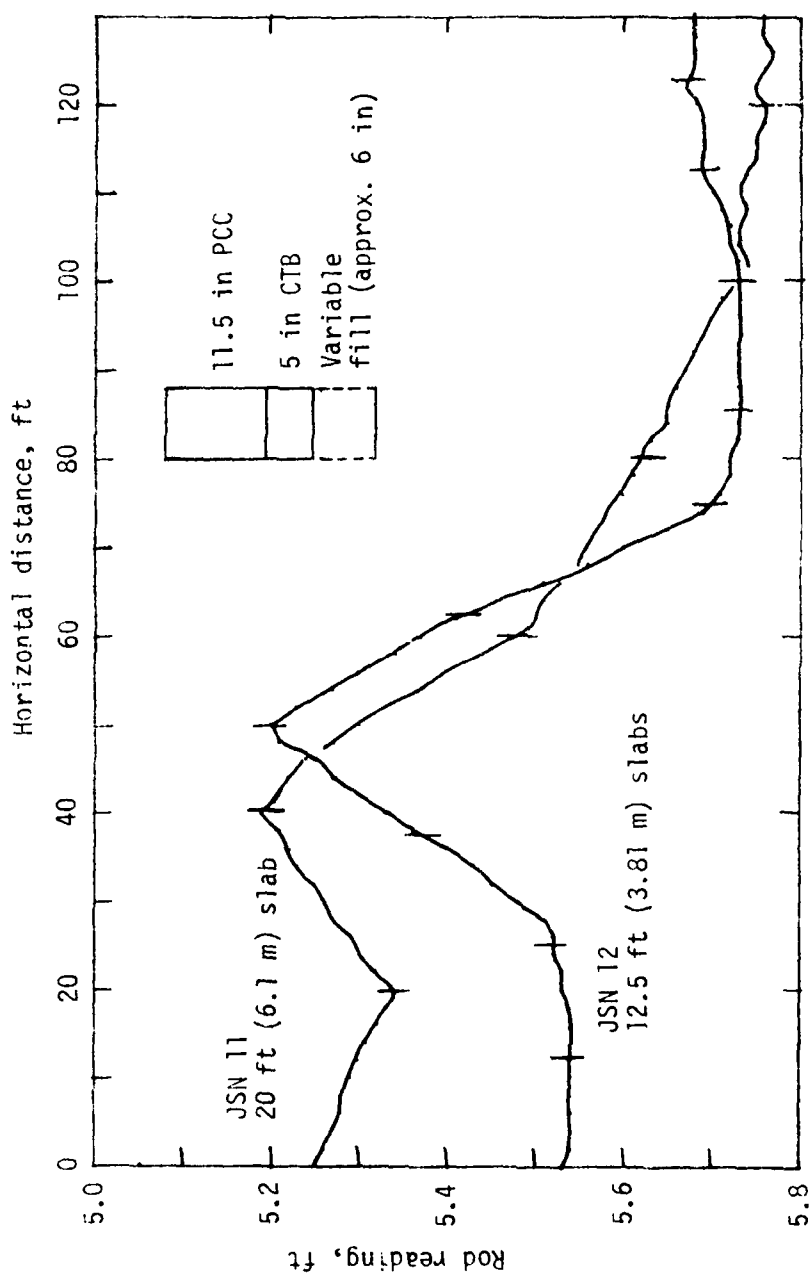


Figure A-16. Actual profiles, Jackson airport apron.

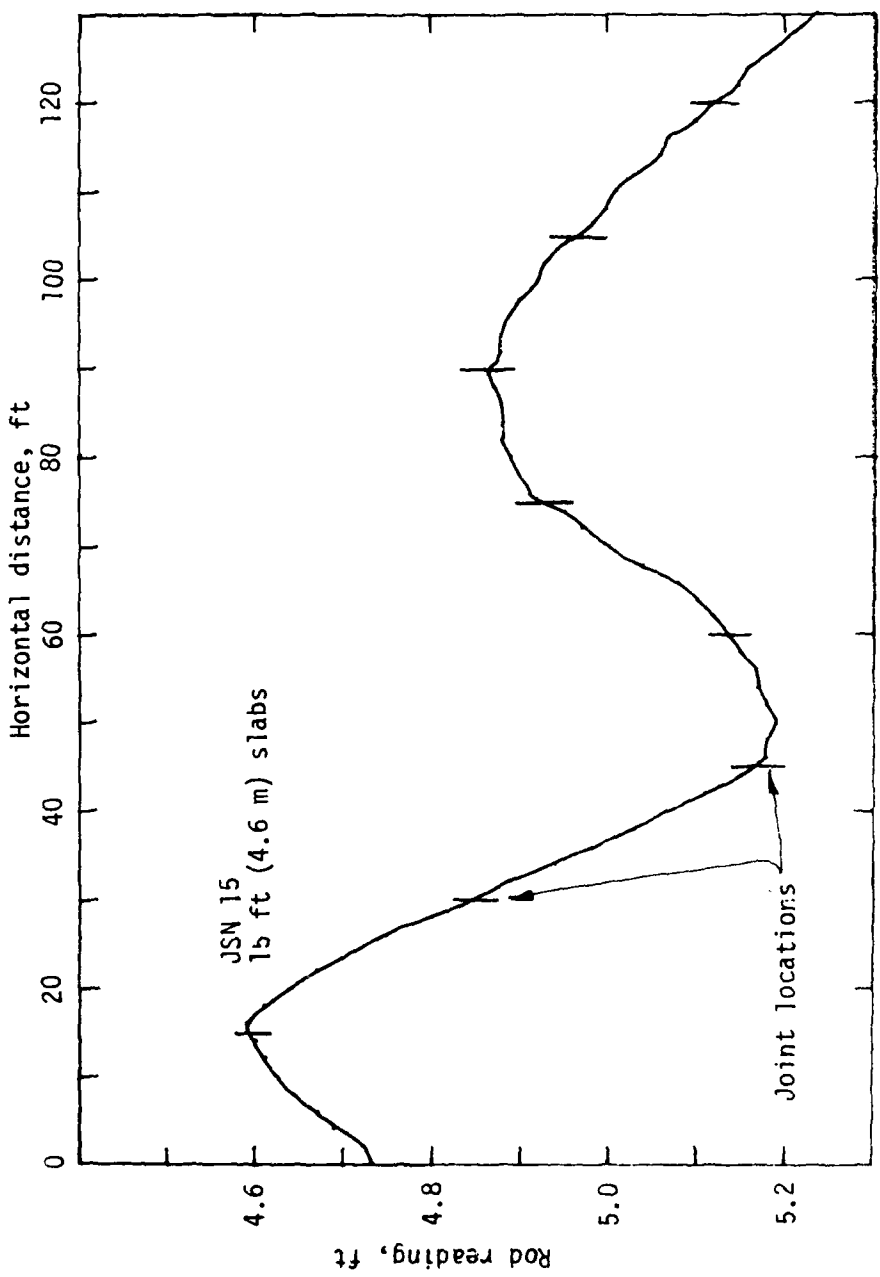


Figure A-17. Actual profile, Jackson airport General Aviation Apron.

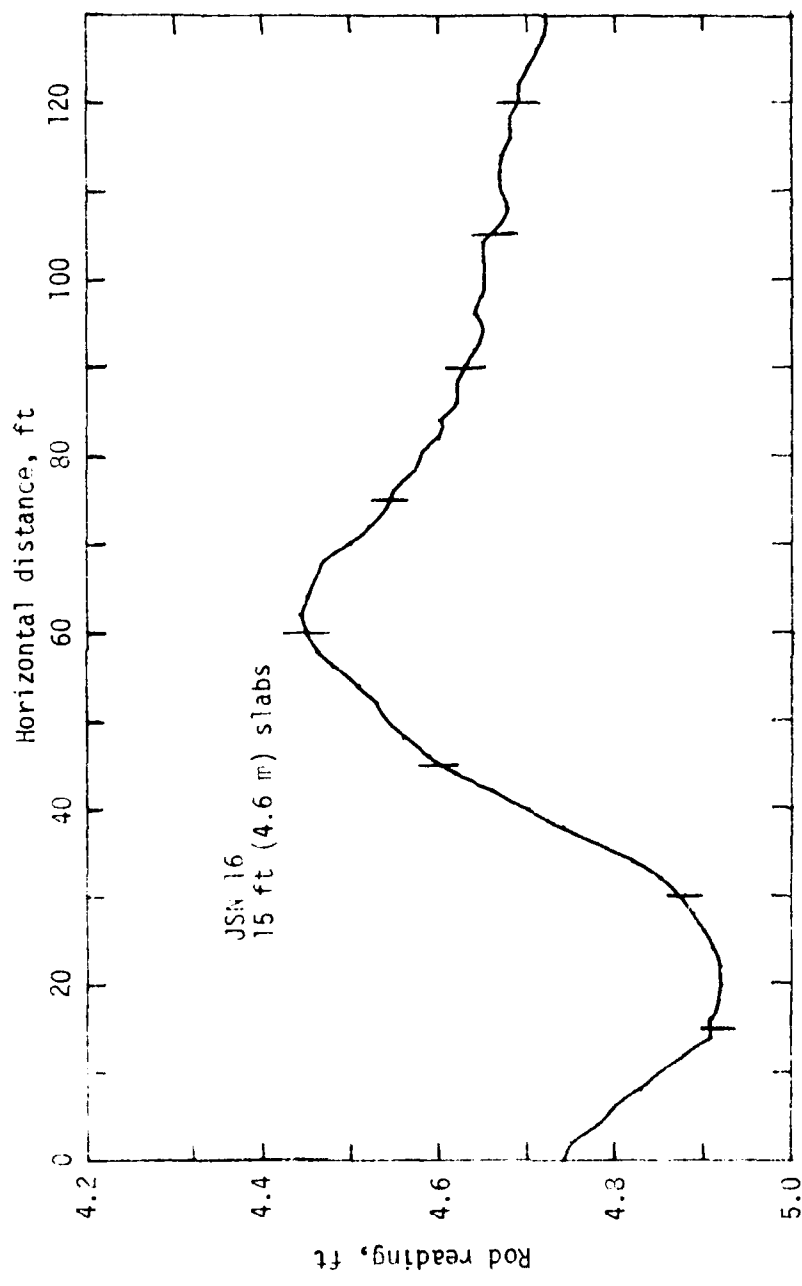


Figure A-18. Elevation profile on apron.

APPENDIX B
FREQUENCY DOMAIN DATA

The following data are given for the regression coefficients c, b in the regression equation

$$a_n = c(f)^b$$

where

a_n = half amplitude of frequency components
 f = frequency

The tabulated coefficients were calculated by least squares for the frequency domain data generated by the Fast Fourier Transform used in this study. The coefficients were determined for data a_n in feet and f in cycles per foot.

Profile	$c \times 10^4$	b
GAL 2 AVG	1.240	-1.067
GAL 3 AVG	0.305	-1.368
GAL 4	1.051	-1.337
GAL 5	0.834	-1.285
GAL 6	0.242	-1.476
DFW 2 AVG	2.162	-0.891
DFW 3 AVG	2.378	-0.778
DFW 5 AVG	2.446	-1.092
DFW 6 AVG	1.339	-1.054
DFW 7	0.254	-1.646
DFW 8	0.424	-1.409
DFW 9	0.308	-1.684
DFW 10	0.426	-1.586
DFW 11	0.353	-1.647
DFW 12	0.574	-1.447
DFW 13	0.652	-1.516
DFW 14	0.806	-1.379
NAS 1	0.120	-2.007
NAS 2	0.242	-1.760
NAS 3	0.180	-0.917
NAS 4	1.822	-1.061
JSN 2 AVG	1.926	-0.594
JSN 3 AVG	1.299	-0.864
JSN 4	0.154	-1.882
JSN 5	0.450	-1.585
JSN 6	1.340	-1.087
JSN 7	0.243	-1.662

Profile	c × 10 ⁴	b
JSN 8	0.220	-1.724
JSN 9	0.201	-1.593
JSN 10	0.297	-1.712
JSN 11	0.013	-1.872
JSN 12	0.191	-1.942
JSN 15	0.120	-2.027
JSN 16	0.173	-1.860

APPENDIX C
CALCULATED PROFILE CHARACTERISTICS

THIS PAGE IS BEST QUALITY PRACTICABLE
FROM COPY FURNISHED TO DDC

LINE	DATE	SJMAN	M
GAL 1	JUN 1980	.3473373E+00	.77086754E-12
GAL 2	JUN 1980	.3654367E+01	.1109410E-12
GAL 3	JUN 1980	.1177100E+01	.22929753E-13
GAL 4	JUN 1980	.1150562E+01	.1775707E-12
GAL 5	JUN 1980	.5382528E+01	.47126979E-13
GAL 6	JUN 1980	.3742244E+01	.1775707E-12

P	K	F	APAR
.514428867E+00	.147823100E+00	.3838148E+00	.514428867E+00
.5643130E+02	.115926300E+00	.4725740E+00	.115926300E+00
.108278388E+02	.334797581E+00	.1031000E+00	.1031000E+00
.15411145E+01	.195355777E+00	.1521400E+00	.1521400E+00
.59506145E+02	.133630738E+00	.24571201E+00	.24571201E+00
.59440328E+01	.111724000E+00	.4883578E+00	.4883578E+00

LINE	DATE	SJMAN	M
GAL 1C	MAR 1979	.98937923E-01	.76941261E-03
GAL 1C	MAY 1979	.93069200E-01	.55242337E-03
GAL 1C	2 JUL 1979	.83553377E-01	.33403838E-03
GAL 1C	NOV 1979	.81202680E-01	.29058824E-03
GAL 2C	MAR 1979	.39454208E-01	.11891488E-03
GAL 3C	MAR 1979	.33711798E-01	.22360853E-03
GAL 2C	MAY 1979	.32888693E-01	.78716031E-04
GAL 3C	MAY 1979	.32763855E-01	.22393735E-03
GAL 2C	2 JUL 1979	.30490595E-01	.74926038E-04
GAL 3C	2 JUL 1979	.35541881E-01	.20798450E-03
GAL 2C	NOV 1979	.34440166E-01	.93814268E-04
GAL 3C	NOV 1979	.32220036E-01	.19595573E-03

P	K	F	APAR
.62004513E-01	.17828088E+00	.47707054E-04	.33430693E-01
.54185899E-01	.12710974E+00	.29933557E-04	.29841558E-01
.53176061E-01	.61041713E-01	.17760846E-04	.17808649E-01
.70672102E-01	.40271966E-01	.20536482E-04	.73692433E-02
.55402894E-02	.11726244E+00	.65882283E-06	.20131312E-01
.22693450E-02	.37650554E+00	.50744490E-06	.21261430E-01
.45629235E-02	.12883280E+00	.35917522E-06	.14132159E-01
.20098496E-02	.33249119E+00	.45008038E-06	.21568845E-01
.35831219E-02	.14214900E+00	.26846913E-06	.14542539E-01
.26290747E-02	.34313812E+00	.54680678E-06	.21569821E-01
.37983192E-02	.10809975E+00	.35633653E-06	.13676955E-01
.15291694E-02	.35524239E+00	.29964951E-06	.22064449E-01

LINE	DATE	SUMAN	M
DFW 1	APR 1979	.15512261E+00	.428950215-02
DFW 1	* MAY 1979	.24487681E+00	.62527541E-02
DFW 1	JUL 1979	.24670949E+02	.551-02164E-02
DFW 1	SEP 1979	.26095025E+02	.53366747E-02
DFW 1	4 NOV 1979	.19954371E+00	.37880285E-02
DFW 2	26 APR 197	.53847869E-01	.18566-231-03
DFW 2	31 MAY 19	.58866771E-01	.264761231-03
DFW 2	27 JUL 197	.51919271E-01	.235704155E-03
DFW 2	27 SEP 197	.53320689E-01	.211215201-03
DFW 2	14 NOV 19	.53150731E-01	.17862389-03
DFW 3	APR 1979	.31829631E-01	.51691463E-04
DFW 3	* MAY 1979	.30724622E-01	.656253304E-04
DFW 3	JUL 1979	.314460525E-01	.82720993E-04
DFW 3	SEP 1979	.311271152E-01	.79300875E-04
DFW 3	4 NOV 1979	.30922571E-01	.64639374E-04
DFW 5	APR 1979	.65337707E-01	.45184843E-03
DFW 5	* MAY 1979	.66685250E-01	.38033831E-03
DFW 5	JUL 1979	.56910722E-01	.354205937E-03
DFW 5	SEP 1979	.68585367E-01	.47741724E-03
DFW 5	4 NOV 1979	.63932482E-01	.4145-472-03
DFW 6	26 APR 197	.70438292E-01	.21462575E-03
DFW 6	31 MAY 19	.37751523E-01	.21706593E-03
DFW 6	27 JUL 197	.42156620E-01	.1-387743E-03
DFW 6	27 SEP 197	.44554121E-01	.36359368E-03
DFW 6	14 NOV 19	.37178750E-01	.36221142E-03
DFW 13	APR 1979	.19530971E+00	.24355232E-02
DFW 13	JUL 1979	.27260510E+00	.55249445E-02

P	K	AFA
.3433830E-01	.49163638E+00	.36177142E-13
.12309206E+02	.33882364E+00	.74966759E-13
.34057512E+02	.28934772E+00	.1979700E-12
.75699161E+00	.22956459E+00	.1-1847-1,-12
.24146676E+00	.26570168E+00	.68081161E-23
.13132306E-01	.14937363E+00	.24321628E-23
.141194661E-01	.14674254E+00	.373303402E-25
.13632167E-01	.15338170E+00	.27941273E-25
.13807771E-01	.13422986E+00	.29130495E-25
.13438327E-01	.11475228E+00	.24114-3E-25
.39719722E-02	.25597427E+00	.36292214E-20
.42400665E-02	.14267556E+00	.77309476E-20
.44011354E-02	.21955114E+00	.1-4-17111,-10
.39497999E-02	.19013597E+00	.36927228E-20
.43381242E-02	.10099993E+00	.1951-1022E-20
.111011175E-01	.16585274E+00	.50160454E-15
.19274452E-01	.17367857E+00	.74022827E-25
.32659544E-02	.16658149E+00	.12449305E-15
.11757873E-01	.16491964E+00	.50987053E-20
.90164517E-02	.17841740E+00	.77771-2E-25
.26676138E-02	.32236041E+00	.67257-52E-25
.32198142E-02	.32483046E+00	.39831195E-16
.40882894E-02	.26943229E+00	.70472901E-20
.32335763E-02	.32922743E+00	.11918772E-03
.29427052E-02	.35548580E+00	.77164874E-06
.16174170E+00	.10081545E+00	.40360113E-03
.53548437E+00	.24750437E+00	.34691988E-27

ANSWER TO THE COMPUTER FOR THE EQUATIONS

LINE	DATE	SIMAN	M
NAS 1	JUN 1980	.94127646E-01	.15245746E-02
NAS 2	JUN 1980	.71972982E-01	.10869810F-02
NAS 3	JUN 1980	.40478820E-01	.13147522E-03
NAS 4	JUN 1980	.49851356E-01	.20230519E-03

P	K	E	ABAR
.12850250E-01	.17511117E+00	.19591164E-04	.71156834E-01
.91310421E-02	.30807089E+00	.99252692E-05	.52845970E-01
.61177849E-02	.11275971E+00	.80433711E-06	.20119757E-01
.90007798E-02	.14592777E+00	.18209045E-05	.23142614E-01

LINE	DATE	SIMAN	M
DFW 1	JUN 1980	.59672998E+00	.52394842E-01
DFW 2	JUN 1980	.54493959E-01	.21967951E-03
DFW 3	JUN 1980	.70495312F-01	.74531033E-04
DFW 5	JUN 1980	.70682134E-01	.51281241E-03
DFW 6	JUN 1980	.38457720E-01	.21468322E-03
JSN 1	JUN 1980	.53192795E+00	.36975612E-01
JSN 2	JUN 1980	.15455882E-01	.12469273E-04
JSN 3	JUN 1980	.27783458E-01	.58577478E-04

P	K	E	ABAR
.12684035E+01	.36389307E+00	.66457801E-01	.53659519E+00
.11396294E-01	.12611389E+00	.26030765F-05	.25371189F-01
.328784685E-02	.21461928E+00	.28956854E-06	.12763219E-01
.15537358E-01	.21823276E+00	.78123763E-05	.46443311E-01
.336203721E-02	.37857533E+00	.71976322E-06	.23088841F-01
.76440834E+00	.26002786E+00	.28088156E-01	.63966552F+01
.18831145E-02	.71309260E-01	.22765485E-07	.55221927E-02
.27644398E-02	.17765601E+00	.11472630E-06	.11447747F-01

LINE	DATE	SIMAN	M
DFW 7	JUN 1980	.61134111E-01	.11673311E-01
DFW 8	JUN 1980	.64437511E-01	.10201331E-01
DFW 9	JUN 1980	.54457132E-01	.11741141E-01
DFW 10	JUN 1980	.50016473E-01	.11777141E-01
DFW 11	JUN 1980	.10126236E-01	.10701147E-01
DFW 12	JUN 1980	.14422602E-01	.11147438E-01
DFW 13	JUN 1980	.14412511E-01	.10777111E-01
DFW 14	JUN 1980	.70523130E-01	.7714721E-01

.71156834E-01	.17131247E+00	.11147438E-01	.11147438E-01
.91156834E-02	.70523130E+00	.10777111E-01	.10777111E-01
.11147438E-01	.11147438E+00	.11147438E-01	.11147438E-01
.11147438E-01	.11147438E+00	.11147438E-01	.11147438E-01
.11147438E-01	.11147438E+00	.11147438E-01	.11147438E-01
.11147438E-01	.11147438E+00	.11147438E-01	.11147438E-01
.11147438E-01	.11147438E+00	.11147438E-01	.11147438E-01
.11147438E-01	.11147438E+00	.11147438E-01	.11147438E-01

LINE	DATE	SUMAN	M
JSN 4	06 DEC 197	.19846089E+00	.13820863E-01
JSN 1	APR 1979	.14346797E+00	.18926889E-02
JSN 2	19 APR 197	.17875657E-01	.20317200E-04
JSN 3	APR 1979	.22407545E-01	.37559900F-04
JSN 1	MAY 1979	.14034626E+00	.20200759E-02
JSN 2	31 MAY 197	.16910389E-01	.25115532E-04
JSN 3	MAY 1979	.23429580E-01	.43258840E-04
JSN 1	JUL 1979	.14955439E+00	.22402853E-02
JSN 2	27 JUL 197	.20954442E-01	.55220003E-04
JSN 3	JUL 1979	.18621460E-01	.23126644E-04
JSN 1	8 SEP 1979	.14220493E+00	.20524116E-02
JSN 2	28 SEP 19	.16327225E-01	.16466753E-04
JSN 3	8 SEP 1979	.31453024E-01	.56597235E-04
JSN 1	DEC 1979	.15119069E+00	.23052287E-02
JSN 2	06 DEC 197	.13608983F-01	.84182689E-05
JSN 3	DEC 1979	.23452169E-01	.52131608E-04

P	K	E	ABAR
.37886948E-01	.25538817E+00	.36479221E+00	.17516989E-02
.84367611E-01	.24269042E+00	.22433833E-01	.59328451E-01
.24015198E-02	.17413622E+00	.84601424E-02	.41307473E-01
.27381297E-02	.11784093E+00	.13717356E-01	.88698754E-02
.73056388E-01	.24964165E+00	.27650912E-01	.66638260E-01
.18245302E-02	.27425319E+00	.13765479E-01	.48656613E-02
.23976148E-02	.11834539E+00	.18042448E-01	.97233634E-02
.75800167E-01	.26541265E+00	.29555150E-01	.70611536E-01
.18818905E-02	.36550579E+00	.29342838E-01	.86749575E-02
.17690850E-02	.11780810E+00	.13072658E-01	.68407317E-02
.76184055E-01	.28070799E+00	.26948173E-01	.66910597E-01
.19083511E-02	.15161569E+00	.36287858E-02	.41159255E-02
.53472558E-02	.76337665E-01	.10584351E-01	.12117036E-01
.80085619E-01	.27508295E+00	.28734552E-01	.69951273E-01
.16433379E-02	.49211165E-01	.51226646E-02	.22074095E-02
.19108419E-02	.17209369E+00	.27282010E-01	.11336490E-01

LIN#	DATE	SJMAN	M
JSN 5	JUN 1980	.14547027E+00	.26416571E-02
JSN 6	JUN 1980	.73272325E-01	.10344613E-02
JSN 7	JUN 1980	.96610486E-01	.27511851E-02
JSN 8	JUN 1980	.12346096E+00	.72640783E-02
JSN 9	JUN 1980	.56750451E-01	.94921542E-03
JSN 10	JUN 1980	.75581455E-01	.81397903E-03
JSN 11	JUN 1980	.11585075E+00	.33800288E-02
JSN 12	JUN 1980	.18436389E+00	.99141126E-02
JSN 15	JUN 1980	.19914074E+00	.11501396E-01
JSN 16	JUN 1980	.16189373E+00	.91438853E-02

P	K	F	ABAR
.11631383E-01	.22220362E+00	.30262170E-04	.85115264E-01
.74994418E-02	.44834277E+00	.77578861E-05	.50617391E-01
.82153653E-02	.38101221E+00	.22691991E-04	.27188453E-01
.11248326E-01	.47754066E+00	.81708721E-04	.14645745E+00
.31396787E-02	.41326937E+00	.29802314E-05	.4424788E-01
.96178507E-02	.21087674E+00	.77998753E-05	.50795412E-01
.12073825E-01	.27989651E+00	.41829876E-04	.96572585E-01
.26555911E-01	.25943971E+00	.26301274E-03	.16579229E+00
.34437655E-01	.23932922E+00	.39667341E-03	.17466418E+00
.21036397E-01	.30786319E+00	.10217734E-03	.14211316E+00

APPENDIX D
AIRCRAFT DATA FOR TAXI SIMULATION

FORMAT FOR PRINTOUT OF AIRCRAFT DATA

AIRCRAFT MODEL	GROSS WEIGHT				
W	A	B			
PSARM	TAILRM				
SPEED	THRUST	TAKOFF			
CL	AREA	CD			
WM	WN	SXM	SXN		
AHN	AAN	AHM	AAM		
PAON	PAOM	VON	VOM	OAM	OAN
SLM	SLN				
TSM	TSN				
STROKE NOSE	PIN DIAMETER				
STROKE MAIN	PIN DIAMETER				
SIMAIN	SINOSE	SICG	SITAIL	SIPS	
GEN MASS	OMEGA				

***** * TAXI
 READ AND PRINT INPUT CATA TAXI
 W=VEHICLE WEIGHT AT CG (POUNDS) TAXI
 A=DISTANCE MAIN GEAR TO CG (INCHES) TAXI
 B=DISTANCE NOSE GEAR TO CG (INCHES) TAXI
 MM=MASS MOMENT OF INERTIA (LB IN SEC SQ) TAXI
 PLANE=AIRPLANE BEING SIMULATED AND GROSS WEIGHT TAXI
 PSARM=DISTANCE OF PILOT STATION TO CG TAXI
 TAILRM=DISTANCE OF TAIL STATION TO CG TAXI
 TAKOFF=TAKE-OFF SPEED (FEET/SEC) TAXI
 SPEED=INITIAL VEL OF AIRPLANE TAXI
 THRUST=TOTAL AIRPLANE THRUST TAXI

CL=LIFT COEFF. TAXI
 AREA =WING AREA TAXI
 CD=DRAG COEFF. TAXI
 WM=WEIGHT OF MAIN GEAR (EACH) TAXI
 WN=WEIGHT OF NOSE GEAR TAXI
 SXM=NUMBER OF MAIN GEAR STRUSS TAXI
 SZN=NUMBER OF NOSE GEAR STRUTS TAXI
 AHN=HYDRAULIC PISTON AREA NOSE SQ INCHES TAXI
 AAN PNEUMATIC POO TAXI
 AHN HYDRAULIC PISTON AREA NOSE SQ INCHES TAXI
 AAN PNEUMATIC PISTON AREA NOSE SQ INCHES TAXI
 AHM HYDRAULIC PISTON MAIN SQ INCHES TAXI
 AAM PNEUMATIC PISTON AREA MAIN SQ INCHES TAXI
 PAON NOSE STRUT PRELOAD PRESSURE PSI TAXI
 PAOM MAIN STRUT PRELOAD PRESSURE PSI TAXI
 VON NOSE STRUT INITIAL VOLUME CU. IN. TAXI
 VCM MAIN STRUT INITIAL VOLUME CU. IN. TAXI
 OAM ORIFACE AREA MAIN TAXI
 OAN ORIFACE AREA NOSE TAXI
 SLM=MAIN GEAR STRUT LENGTH UNLOADED INCHES TAXI
 DISTANCE FROM CL CF AXLE TO CG LINE TAXI
 SLN=NOSE GEAR STRUT LENGTH UNLOADED INCHES TAXI
 DISTANCE FROM CL OF AXLE TO CG LINE TAXI
 TSM MAIN TIRE SPRING CONSTANT PER STRUT TAXI
 TSN NOSE TIRE SPRING CONSTANT PER STRUT TAXI
 DX=TIME STEP SIZE TAXI
 READ METERING PIN DESCRIPTION STARTING AT ZERO STROKE TAXI
 NSCN= OF METERING PIN CHANGES NOSE GEAR TAXI
 NSCM= OF METERING PIN CHANGES MAIN GEAR TAXI
 NFM=NUMBER OF FLEXIBLE MODES TAXI
 SIXXXX(I)=MODE SHAPE DEFLECTION (NON DIM.) TAXI
 GM(I)=GENERALIZED MASS (POUNDS-SEC/IN) TAXI
 OMEGA(I)=MODAL FREQUENCIES (RAD/SEC) TAXI
 ***** * TAXI

WIDE BONDED TRI-JET COMPOSITE

391500.0	68.0	787.0	1300000000.0
1035.00	568.00		
120.0	115000.0	249.20	
0.227	5500.0	0.070	
5000.0	584.0	2.0	1.0
26.4	33.0	24.0	100.0
151.50	320.00	597.30	2630.00
183.0	173.0		2.00
55000.0	20000.0		0.57

3.0	0.0
10.0	0.364
17.0	0.752
50.0	0.752

0.0	0.0
15.0	1.2
25.0	1.2
50.0	1.2

-0.25	-1.25	-0.50	-0.30	-2.17
-1.25	-2.58	-0.39	-0.13	-2.34
-3.42	1.53	-0.23	0.50	2.52
1.20	1.13	-1.01	0.00	2.16
-0.19	0.17	-0.47	-0.19	0.53
-0.05	-0.54	0.06	0.63	-1.54
0.08	1.10	-0.35	-0.35	0.38
0.19	-1.42	0.41	-0.72	-1.24
0.42	0.50	0.01	1.39	1.99
1.41	-1.15	7.15	-1.26	-0.72
0.12	0.16	-0.54	0.40	1.47
0.47	-0.74	0.37	0.65	2.76
1.61	0.0	-0.27	-0.10	0.62
-1.00	1.74	-1.22	1.60	-3.16
-1.35	-0.19	4.64	-1.24	3.94

2000.0	7.63
2000.0	12.94
2000.0	15.12
2000.0	18.19
2000.0	22.37
2000.0	25.10
2000.0	27.34
2000.0	29.17
2000.0	35.95
2000.0	39.26
2000.0	39.96
2000.0	47.73
2000.0	52.27
2000.0	61.93
2000.0	71.33

AD-A104 660

NEW MEXICO ENGINEERING RESEARCH INST ALBUQUERQUE
DESIGN OF AIRPORT PAVEMENTS FOR EXPANSIVE SOILS.(U)

F/G 8/13

JAN 81 R G MCKEEN

F29601-76-C-0015

UNCLASSIFIED

NMERI-AP-37

FAA/RD-A1/25

NL

3 OF 3
AU A
104660

END
DATE
FILED
10-81
DTIC

BOEING 727-200 160000 POUNDS

160000.	35.7	717.5	62300000.
833.9	330.2		
170.	39900.	752.	
.91	1562.	.025	
1363.	495.	?	1.
14.10	19.	40.3	50.2
113.	267.	229.9	722.8
112.5	104.2		1.737
22742.	3594.		.95

2.	.976
2.45	.973
10.97	1.04
11.82	1.34
11.82	1.72
12.02	1.09

2.	1.48
2.	1.65
10.	1.3
12.75	1.39
14.	1.49

.709497	-.0942	.011204	-.032315	-1.22646
-.093893	.152547	-.092404	-.05057	.218125
.747948	-.131416	.059629	-.074921	-.210563
.708144	.002867	-.011620	.054756	.42227
-.007372	.008713	-.009566	.013297	.122697
.742956	-.005042	.045564	.052440	-.616221
-.365634	-.053043	-.063439	.223	-.140604
-.007325	-.013918	.015636	-.156446	-.229465
-.073625	.149478	-.061228	-.035077	.653536
-.01926	.050909	-.012772	-.012472	.255926
8.97	15.205			
3.55	18.72			
4.94	23.21			
16.26	44.02			
5.98	46.75			
5.73	47.75			
4.92	59.88			
18.51	72.45			
398.7	87.96			
27.79	94.71			

ARMING 727-160 14-070 POUNDS

1460000.	70.5	367.7	34450000.
645.9	211.1		
180.	181.0	252.	
.91	132.1	.025	
1353.	455.	2.	1.
14.10	19.	43.3	50.2
250.	255.	229.9	722.8
112.7	161.7		1.767
20740.	2624.		.05

2.72	.471			
7.45	.973			
10.87	1.34			
11.32	1.44			
11.92	1.75			
12.82	1.85			
7.	1.75			
13.	1.3			
13.75	1.33			
14.	1.43			
-.127	-.022	-.323	-.037	-.034
-.733	.024	-.089	-.060	.275
.201	-.476	.015	-.022	-.104
.295	-.130	.125	.024	-.230
-.010	.016	-.009	-.024	.015
.030	.136	.071	.020	.260
-.140	-.673	-.040	.030	-.145
-.095	.135	-.115	-.035	.300
-.352	.032	-.051	-.027	.078
-.370	-.028	-.060	-.055	-.254
6.72	14. 92			
2.01	22.372			
2.74	32.752			
10.84	44.657			
3.82	43.997			
4.35	59.16			
8.26	75.555			
170.26	32.025			
26.17	57.542			
11.55	90.740			

DC-9-40 114000 POUNDS GROSS WEIGHT 35 % MAC
 114000. 24.43 652.43 21540000.
 662.5 513.
 100. 2300. 285.
 .69 1820.7 .365
 1074. 164. 2. 1.
 6.321 2.276 20.609 25.922
 120.3 222.3 126.66 462.2 .6524 .422
 27.93 23.7
 25.82. 12320.0

.375
 .545 .639
 6.325 .654
 12.425 .713
 15.025 .722
 15.147 .723

.421
 .3 .421
 1.5 .569
 3.5 .641
 8.1 .76
 12.5 .826
 17.0 .826

-.211	-.269	-.2267	-.2747	-.2627
-.228	-.291	-.2263	.0246	.2261
.115	-.378	.1026	-.1170	-.3222
.315	-.113	.3112	-.2720	-.1213
.337	-.242	.337	-.0110	-.0467
-.329	.110	-.0321	.1152	.1200
-.203	-.236	.0130	-.0456	-.2396
.213	.225	-.3151	.0690	.2510
-.207	-.210	-.0030	-.0240	-.7113
-.244	.078	-.3101	-.0564	.0917
.032	-.262	-.0399	.2030	-.2703

4.28	19.5
1.38	23.1
8.64	33.9
3.52	43.9
1.07	53.6
32.7	56.9
5.27	57.3
7.21	71.6
1.79	95.5
3.43	111.
3.68	113.

APPENDIX E
CLOD TEST PROCEDURE

Clod Test Procedures and Data Reduction

General Description

1. Clods weighing 120 ± 20 grams are separated from undisturbed samples and placed in 4 ounce moisture cans; usually seven for the initial test.
2. Three are wetted, one remains at natural moisture and three are dried to achieve a variety of moisture conditions. For example:

18, 20, 22, 24 (natural), 26, 28, 30 percent
3. When the desired moisture condition is achieved, a sensor is placed in the container and allowed to equilibrate. The sensor may be filter paper or a thermocouple psychrometer. Separate procedures for each are used.
4. The containers with the sensor and the sample are placed in an insulated chest to equilibrate. After equilibration, the suction sensor is removed and the procedures for the remainder of the clod test are independent of sensor type.
5. Clods are weighed (W_1), followed by preparation of the clod for bulk density measurement. A wire, tag, and possibly a hair net are attached to provide a means of handling the sample. These tare items may be added before adjusting the moisture content if desired in order to prevent difficulty in the wetter region. Experience has shown that many clods crumble when wet if handled at all. Following this installation, a weight is taken (W_2).
6. The clod is then coated with saran resin. Solutions of 1:7 or 1:4, saran: methyl ethyl ketone are used. The 1:4 is used only for very porous materials. Sequence for coating is as follows:
 - a. For 1:4 Solution--dip in liquid, dry five minutes; dip again, dry fifty-five minutes.
 - b. For 1:7 Solution--dip in liquid, dry five minutes; dip again, dry eight minutes; dip again, dry fifty-five minutes. (This is patterned after the SCS, NSSL COLE procedure.)
7. Immediately weigh the clod in air and water at the end of the drying period. These weights are W_3 and W_4 , respectively. In this test procedure, the buoyant force on the clod is measured rather than the submerged weight.
8. Clods are then dried in air until they reach a constant weight. A weight in air and water is determined as before. These are W_5 and W_6 respectively.
9. Clods are placed in a cold oven which is started and raised to 105°C ; they are dried for 48 hours.

10. The clods are removed and cooled until easy to handle. Weights are taken in air and water again (W_7 and W_8). The weights taken in water (W_4 , W_6 , W_8) are the buoyant force on the clod rather than clod weight while submerged.
11. The saran plastic coating used loses 10-20% by weight during oven drying. The Soil Conservation Service uses 15% weight loss in COLE calculations. NMERI tests using oven dried alumina blocks as samples indicated the average weight losses as follows:

BLOCK	COATING	WEIGHT LOSS g	%
A	None	0.01	0.01
B	7:1	0.14	16.7
C	4:1	0.26	16.7

In NMERI calculations, a 15% weight loss is assumed.

12. Sensor measurements involve the determination of water content of a filter paper or output measurement of a thermocouple psychrometer. In both cases, the quantity determined is compared to a calibration curve for the particular sensor involved. The calibration is used to convert the readings to suction in pf units.

SUMMARY OF MEASUREMENTS

A. Clod Samples

$$W_1 = W_s + W_w \text{ (Weight of wet clod)}$$

$$W_2 = W_s + W_w + T \text{ (Wet clod plus tare)}$$

$$W_3 = W_s + W_w + T + W_r \text{ (Wet clod, tare, saran coating)}$$

$$W_4 = \text{Buoyant force on submerged clod}$$

$$W_5 = W_s + (W_w)_a + T + W_r \text{ (Air dried to constant weight)}$$

$$W_6 = \text{Buoyant force on submerged clod}$$

$$T_6 = \text{Water temperature at which } W_6 \text{ was determined}$$

$$W_7 = W_s + T + 0.85 (W_r) \text{ (Oven dried)}$$

$$W_8 = \text{Buoyant force on submerged clod}$$

$$T_8 = \text{Water temperature at which } W_8 \text{ was determined}$$

B. Suction (Filter Paper)

See also suction measurement procedures.

$$W_{11} = W_f + W_w + T_c \text{ (Weight of filter paper, water, tare-cold)}$$

$$W_{12} = W_f + T_h \text{ (Weight of filter paper, tare-hot)}$$

$$W_{13} = T_c \text{ (Cold tare)}$$

$$W_{14} = T_h \text{ (Hot tare)}$$

Temperature at equilibrium (measured in the insulated chest).

C. Suction (Thermocouple Psychrometer)

See also suction measurement procedures.

E = Output in microvolts

T_{mv} = Temperature in millivolts

COMPUTATIONS

$$1. \quad W_s = W_7 - 0.85 (W_3 - W_2) - (W_2 - W_1)$$

$$2. \quad w = \frac{W_1 - W_s}{W_s}$$

$$3. \quad V_w = \frac{W_4}{\gamma_w} - \left(\frac{W_3 - W_2}{1.3} \right) (\gamma_r = \text{density of saran} = 1.3)$$

$$4. \quad (\gamma_d)_w = \frac{W_s}{V_w}$$

$$5. \quad e = \frac{G_s \gamma_w}{(\gamma_d)_w} - 1$$

$$6. \quad S = \frac{1}{e} \left[\frac{(1 + w)(\gamma_d)_w (1 + e)}{\gamma_w} \right] - G_s$$

$$7. \quad (V_t)_d = \frac{W_8}{\gamma_w} - \left[\frac{(W_3 - W_2)}{1.3} \right] 0.85$$

$$8. \quad (\gamma_d)_d = \frac{W_s}{(V_t)_d}$$

$$9. \quad \frac{\Delta L}{L_d} = \left[\frac{(\gamma_d)_w}{(\gamma_d)_d} \right]^{1/3} - 1.0$$

$$10. \quad (V_t)_a = \frac{W_6}{\gamma_w} - \left[\frac{W_3 - W_2}{1.3} \right]$$

$$11. \quad (\gamma_d)_a = \frac{W_s}{(V_t)_a}$$

$$12. \quad \frac{\Delta L}{L_a} = \left[\frac{(\gamma_d)_w}{(\gamma_d)_a} \right]^{1/3} - 1.0$$

DATE
LME